THE WAVEMAKING RESISTANCE OF SHIPS:
VERTICAL FORCE AND FORM RESISTANCE OF A HULL AT UNIFORM VELOCITY

Thesis presented for the Degree of Ph.D.

at the University of Glasgow

By

I.W. Dand, B.Sc.

Department of Naval Architecture.

1964 - 1967

ProQuest LLC.
789 East Eisenhower Parkway
P.O. Box 1346
Ann Arbor, MI 48106 – 1346

STATEMENT

Except where reference is made to the work of others, this thesis is believed to be original.

TABLE OF CONTENTS

TABLES

FIGURES

PLATES

NOMENCLATURE

Forces and Moments

R_T - Total resistance

R_W - Wave resistance

R_{wp} - Wave pattern resistance

R_V - Viscous resistance

R_I - Interference resistance

R_f - Frictional resistance

R_{fo} - Flat plate friction resistance

R_{ff} - Friction form resistance

R_{VP} - Viscous pressure resistance

R_{Vf} - Viscous form resistance

Z - Vertical hydrodynamic force on model

Z_s - Vertical hydrodynamic force on equivalent spheroid

Z_B - Vertical hydrdoynamic force on bulb

Z_{BOW} - Measured vertical force at bow

Z_{STERN} - Measured vertical force at stern

T - Towing force

F_R - Resultant hydrodynamic force

M - Trimming moment on model

M_V - Trimming moment of vertical component of pressure force

M_H - Trimming moment of horizontal component of pressure force

M_s - Moment of body source distribution

Non-dimensional Coefficients

C_P - $p(x,y,z)/\rho V^2$, a general pressure coefficient

C_{PTOT} - Total linearised dynamic pressure coefficient

C_{PO} - Pressure coefficient arising from body sources and sinks

$C_{P\ell}$ - Pressure coefficient arising from local wave pressure system

C_{PW} - Pressure coefficient arising from free wave pressure syste

C_t - Total resistance coefficient = $R_T/\frac{1}{2}\rho SV^2$

C_W - Wave resistance coefficient = $R_W/\frac{1}{2}\rho SV^2$

C_{wp} - Wave pattern resistance coefficient = $R_{wp}/\frac{1}{2}\rho SV^2$

C_V - Viscous resistance coefficient = $R_V/\frac{1}{2}\rho SV^2$

C_{fo} - Flat plate friction resistance coefficient = $R_{fo}/\frac{1}{2}\rho SV^2$

C_Z - Vertical force coefficient = $Z/\frac{1}{2}\rho SV^2$

C_M - Trimming moment coefficient = $M/\frac{1}{2}\rho SLV^2$

r - Form factor = $C_V/C_{fo}-1 = R_V/R_{fo}-1$

r_{ff} - Friction form factor = $\delta R_{fo}/R_{fo} = R_{ff}/R_{fo}$

K_{ff} - Percentage form factor = $r_{ff} \times 100$

C_s - Mean sinkage coefficient = $\frac{1}{2}(s_B + s_S) \times 100/L$

C_{sB} - Bow sinkage coefficient = $100s_B/L$

C_τ - Trim coefficient = $(s_S - s_B) \times 100/L$

λ - $\mathrm{Tan}^{-1}\ (\mathcal{F}/R_n)$

Velocity

V - Steady velocity of model

V_M - Mean flow velocity over hull

q - Velocity of fluid particle

u, v, w - Perturbation velocities in x,y,z directions respectively

ϕ - Velocity potential, $u = \partial\phi/\partial x$, $v = \partial\phi/\partial y$, $w = \partial\phi/\partial z$

ϕ_s - Velocity potential of a simple source

ϕ_o - Velocity potential due to sources and image sinks

ϕ_ℓ - Velocity potential corresponding to local wave system

ϕ_w - Velocity potential corresponding to free wave system

Ψ - Stream function

K_o - Wave number = g/V^2

$\mathcal{F}$ - Froude number = $V/\sqrt{gL}$

F_H - Froude depth number = $V/\sqrt{gh}$

N - Bulb Froude number = $V/\sqrt{gl_s}$

R_n - Reynold's number = VL/ν

Λ - $(\log_{10}R - 2)^{-2}$

Fluid Properties

ρ - Density

ν - Kinematic viscosity

g - Acceleration of gravity

$p(x,y,z)$ - Linearised dynamic component of pressure

P - Uniform pressure acting on a streamline

Geometry

x,y,z - Co-ordinate axis system for model

x',y',z' - Co-ordinate axis system for fluid

ρ, ψ, z - Cylindrical co-ordinates for section 2.1.4.

$F(x,y,z,t)$ - Equation of bounding surface

$\pm\eta(x,z), \pm F(x,z)$ - Equation of hull surface

$\zeta(x,y)$ - Equation of free surface

l,m,n - Direction cosines of normal

$\partial / \partial n$ - Normal derivative

ζ_H - Hull wave system (part 3)

ζ_B - Bulb wave system (part 3)

L - Length of hull

ℓ - Local $\frac{1}{2}$ length of waterplanes. For waterplane 0 - 5, $\ell = \frac{1}{2}L$

l_s - Length of equivalent spheroid

d' - Distance of point of application of R_W below S.W.L.

h - Tank depth

S - Underwater surface area

ϵ - Model offset error = (offset from ref. 53) - (measured offset)

d_1 - Longitudinal distance of bulb centre from origin

A_R - Ram area ratio) see fig. 47 for definitions

A_B - Bulb area ratio)

f - Depth of immersion of axis of spheroid and bulb

β - Beam-length ratio of equivalent spheroid

γ - Ratio of bulb displacement volume to displacement volume of equivalent spheroid

s - Mean sinkage

s_B - Bow sinkage

s_S - Stern sinkage

$\delta_B, \delta_S, \delta_{Bw}, \delta_{Sw}, {}_S\delta_B, {}_B\delta_S, \delta_{BACT}, \delta_{SACT}, \delta_{BR}, \delta_{SR}$ - Proving ring deflections defined in appendix C.

τ - Trim angle (defined as positive for a bow up trim)

ψ - $\mathrm{Tan}^{-1}(R_W/Z)$

$\tilde{\omega}$ - $x \cos\theta + y \sin\theta$

θ - Elementary wave angle

α, β - Angles defined in figure A 1.

m - Source strength

σ - Surface source density

r - Length of position vector of source

Mathematics

B_ν - Bessel Operator

$\mathcal{H}_\nu[f(x,y), x \to \xi]$ - Hankel Transform, of order ν, of the function $f(x,y)$

$J_o(\xi)$ - Zero order Bessel function of the First Kind

$Y_o(\xi)$ - Zero order Bessel function of the Second Kind

$K_o(\xi)$ - Zero order modified Bessel function

$H_o(\xi)$ - Struve function of zero order

$\Gamma(\xi)$ - Gamma function

$Q_\nu(\xi)$ - Function defined by equation (B 20)

M_1, ϕ_1 - Amplitude and phase of free wave functions

$A(\xi), B(\xi)$ - Arbitrary parameters in Section 2.1.4

$A(\theta), B(\theta)$ - Inui's hull and bulb amplitude functions

F_1, F_2 - Wigley's hull and bulb amplitude functions

σ_s - Standard error of the mean

ρ_c - Correlation coefficient

Hydrostatic terms and some geometrical coefficients are defined in table 2.

SUMMARY

A mathematical model has been tested in calm water and total resistance, trim and vertical forces measured. Measurements are compared with calculations made using a linearised theory and it is concluded that neglect of non-linearities contributes more to the poor agreement between calculation and measurement than the neglect of viscosity.

A relation between vertical force, wave resistance and friction form resistance is proposed and it is suggested that there is a relation between trimming moment, wave resistance and viscous pressure resistance.

In order to test these deductions, a large ram bulb was designed to modify the flow over the hull. Total resistance, wave pattern resistance, sinkage, trim and vertical forces were measured after the addition of the bulb. This second series of tests showed that a ram bow can markedly alter the viscous pressure resistance and running trim of a model.

INTRODUCTION

The design of a ship must be a compromise between several conflicting requirements, most of which are initially determined by economic considerations.

One important requirement is that the ship should pass through the water at a given speed, carrying a given deadweight while expending the least possible energy in order to do so. This has led to the study of the hydrodynamic forces acting on a ship in motion. These forces, and the flow associated with them, largely govern the underwater shape of the hull so that a knowledge of their action is of prime importance in ship hull design.

The first systematic study of such forces was initiated by W. Froude in 1869 (1)* although work of this nature had been performed as early as 1761 (2). Froude's work laid the foundations of modern tank testing and many of his ideas and techniques have remained fundamentally the same to the present day.

After the initial impetus given by Froude, empiricism in ship hydrodynamics became the only means of predicting the powering requirements of full-size ships from the results of tank tests on geometrically similar models (geosims). Hull forms were developed on a 'cut and try' basis, which, with the advent of more refined instrumentation and equipment, has resulted in modern test tanks being large and expensive establishments dealing with large volumes of work.

It is thus becoming increasingly important to develop a reliable theory to describe the motion of a ship through water to supplement and finally, perhaps, to supplant tank tests. Such a theory could guide the experimenter towards the most fruitful areas of research, and, in some cases, predict results which would defy empirical determination. The foundations for such a theory must be laid on a sound and clear knowledge of the flow conditions (and the forces and moments arising therefrom) which obtain on a ship hull at steady speed both in still water and in waves.

---

* Numbers in parentheses refer to the list of references on page 239 et seq.

Unfortunately the complexity of hydrodynamics is such that a reliable theory for predicting the forces and moments on a ship in motion does not yet exist. However, an approximate theory has been developed to a fairly high degree over the last 70 years, and this, in spite of its shortcomings, has already been of considerable use in the design of hull forms.

When a ship advances into undisturbed deep water, observation shows that the resultant force and moment acting on the ship cause

(i) a resistance to motion,

(ii) a bodily settling of the model (sinkage) and

(iii) a rotation about a transverse axis (trim).

To date, theoretical studies have concentrated on the resistance to motion closely associated with the production of waves and viscous forces, whereas little interest has been shown in the vertical force causing sinkage and the moment causing trim.

The following investigation concentrates on the vertical force acting on a mathematical model. In Part 2 an attempt is made to reconcile calculation with observation, and the relation of the vertical force to a small but important component of the total resistance is deduced. In Part 3, conclusions obtained in Part 2 are used in the design of a bulbous bow.

1. HISTORICAL BACKGROUND

1.1 FUNDAMENTAL HYDRODYNAMICS

Theoretical ship hydrodynamics, for the steady state, uses concepts fundamental to all theoretical hydrodynamics.

The work of the Swiss mathematician Euler, published in 1755, (3) provided the basic equations governing fluid motion, based on his own investigations and earlier work of Bernoulli and d'Alembert. In this work, Euler enunciated concepts basic to the theory later developed to describe the steady motion of a body in undisturbed fluid. The idea of complex potentials for the source, sink and vortex were introduced by him, as were the concepts of the stream function and the material derivative.

After Euler, many mathematicians applied themselves to the analytical study of hydrodynamics and notable advances were made by Lagrange, who extended some of Euler's concepts, Green, who was the first to use the word 'potential' (although this idea had been used by both Euler and d'Alembert) and Stokes who formalised the equations of viscous fluid motion (The Navier-Stokes equations) and overcame the famous d'Alembert paradox in his solution for the drag of a sphere in slow motion through a fluid.

The starting point for the analytical study of wave motion is in famous memoirs by Cauchy and Poisson (4) to the Royal Academy of Sciences in 1816. Cauchy was able to obtain the velocity potential of two-dimensional wave motion making extensive use of the 'perfect' fluid potential flow concepts and a Fourier Transform solution of Laplace's Equation.

Wave theory was extended by the work of Stokes, Rayleigh, Green and others, but it was in 1887 that Lord Kelvin (5) first gave a satisfactory mathematical model of the characteristic three-dimensional wave disturbance which follows a moving object on the free surface of a fluid. By considering the moving object to be so small that it could be replaced by a point impulse (or point pressure disturbance) Kelvin obtained an expression for the three-dimensional

surface elevation using a Fourier Transform solution of Laplace's Equation. Numerical evaluation of this expression was troublesome due to the multiplicity of zeros of the integrand ., so Kelvin used an approximate method, known as the Method of Stationary Phase, for its determination.

The use made by Rankine in 1863 (6, 7) of discrete sources and sinks showed how streamline forms could be generated in two dimensions, this idea being developed by Taylor in 1894 (8). Taylor extended the source-sink pair concept to that of a distribution of sources and sinks along a line, and was thus able to generate streamline forms closely resembling ship waterlines.

No survey of analytical hydrodynamics, however brief, is complete without mention of the work of Sir Horace Lamb. His substantial contributions to the study of hydrodynamics culminated in his book 'Hydrodynamics' (9) first published in 1879. Many developments in analytical ship hydrodynamics have stemmed from this work and we shall often have recourse to it in the following investigation.

It is against this background of general hydrodynamics that wave resistance theory must be placed. Many of the concepts used are well-known, but the complexity of the subject is such that, in spite of the exertions of many eminent mathematicians, it still remains in many ways an inadequate and incomplete theory.

1.2 WAVE RESISTANCE THEORY.

1.2.1 Early Work

The theoretical study of the fluid flow past a ship and the forces and moments resulting therefrom has a long history beginning with a notable paper by J.H. Michell in 1898 (10). Dealing only with the steady state case, Michell obtained a velocity potential using a Fourier analysis, representing the hull surface as a Fourier Series. The resultant trigonometric potential was used to give the horizontal component of the resultant force acting on the ship - the wave resistance. The resultant expressions were cumbersome, but at that time it appeared that the wave resistance value calculated might agree quite well with the measured value.

Guilloton, in an examination of Michell's paper (11), points out that of the many important aspects of the analysis probably the most significant is the choice of arbitrary terms in the potential which make the surface waves trail aft of the hull. (It is unfortunate that the mathematical solution gives waves ahead as well as astern of the ship.)

Michell's work is fundamental to the theory of wave resistance and, apart from Havelock's concept of elementary waves, has not been fundamentally improved to the present day. His method of calculating pressures over the hull and then integrating them to obtain the wave resistance is used in the following investigation and is attractive for many reasons, not least of which is the simplicity of the basic concept.

Developments and improvements of this basic theory were made by Sir Thomas Havelock in a notable series of papers (12) beginning in 1908 with studies of groups of waves in dispersive media, progressing to ship wave resistance, heaving and pitching forces on submerged bodies, and ending in 1958 with a paper on the effect of the speed of advance on the damping of heave and pitch.

Of the many concepts introduced by Havelock, perhaps the most important were his use of sources and sinks to represent the body, thus generalising Michell's theory, and his determination of wave resistance from the energy in the free wave system trailing aft of the hull. (This latter idea, coupled with a suggestion of his in 1952 (13) has led to the present-day experimental determination of wave resistance.) Havelock's elegant results and lucid explanations undoubtedly have done much to bring the rather abstract world of wave resistance theory and the practical world of ship design closer together.

In parallel with Havelock's early work was the work of Lamb (14, 15) in which he calculated the wave resistance from the rate of dissipation of energy by a certain integral taken over the free surface. This approach was improved by Havelock in 1927 (12, p.279).

Wigley, in 1931 (16, 17) was the first to systematically study the wave profile alongside the hull both analytically and empirically. This led to a long series of papers by him using, in the main, the theories of Havelock in which calculation and experiment were compared. For some years previous to this calculations had been restricted to mathematical hull forms bearing only a slight resemblance to ship forms. Wigley tested these mathematical forms and found that agreement between the calculated wave resistance and that deduced empirically was poor except at high speeds. This led to renewed efforts both by Havelock and Wigley and by Weinblum who, in 1932 (18), tested mathematical forms bearing some resemblance to normal hull shapes.

Hogner studied 'flat' ships (as distinct from 'thin' ships) and proposed an 'interpolation formula' to determine the wave resistance (19). This formula was studied by Havelock who compared it with his own findings (12, p.374, 375). Hogner also studied the wave pattern of a point disturbance and obtained a result slightly different from Kelvin's due to a special treatment of the 'cusp' region. (20).

An entirely original approach to the wave resistance problem began in 1939 (21) when Guilloton attempted to determine the stream flow around a hull form by a geometrical method. Dividing the hull into elementary wedges, he calculated wave profiles and wave resistance from the known elementary values deduced for each wedge from Michell's theory and then invoked the principle of linear superposition. Although neither as mathematically elegent nor as rigorous as the work of Havelock and his contemporaries Guilloton's method gave good results and present-day applications of his theory (22) show encouraging agreement between calculation and experiment.

Although much of Guilloton's work is devoted to the calculation of wave resistance from measurements of the wave profile along the side of the hull, it was the concept of elementary free waves due to Havelock (12, p.377-397) that laid the foundations of a method for the experimental determination of wave resistance. Havelock considered the wave pattern of a ship to be composed of an infinite number of elementary waves augmenting and cancelling each other to form the characteristic transverse and diverging waves. By consideration of the rate of increase of energy in a control region surrounding the ship, an exceedingly simple and elegant expression for wave resistance was deduced.

It was then possible to discern two approaches to the wave resistance problem: The calculation of wave resistance from a knowledge of the hull shape only, and the calculation of wave resistance from a knowledge of the free wave pattern to the rear of the hull. These two approaches exist today, although the latter is at present more popular due to its applicability to the experimental determination of wave resistance. It is the former approach that is used in the following investigation.

1.2.2 Bulbous Bows and Minimum Resistance Forms

Apart from its intrinsic mathematical interest, wave resistance theory has at least one important practical application - the

analysis of the action of bulbous bows.

Beginning in 1935 with the work of Wigley (23) the theory has added materially to our knowledge of the action of the bulbous bow considered as a wave-cancelling device. Wigley's initial work studied the cancellation of the bow wave pattern of the hull using point doublets (to represent a spherical bulb) and a line source (to represent an ellipsoidal bulb). Havelock's free wave theory was used exclusively, and Wigley was able to demonstrate that the wave resistance of the hull/bulb configuration consisted of a superposition of the resistance of the hull on that of the bulb, and an 'interference' resistance due to the bulb. It was the sign of this interference resistance which determined the beneficial or otherwise effect of the bulb on the total resistance.

In Japan in the late 1950's Inui attempted to cancel the free wave system (24) using, once again, Havelock's elementary wave theory. These 'waveless hull forms' (Inui's term) were generated from known source-sink distributions, thus correctly satisfying one of the boundary conditions of the problem i.e., that at the hull surface (25, 26). Inui's work has had a profound effect on the hull shapes of many Japanese ships and has undoubtedly led to the adoption of larger bulbous bows.

Inui's ideas were extended by Pien (27), who used line distributions of doublets and sources to cancel waves, whereas Inui used point doublets exclusively. Though generated by streamline integration, Pien's hull forms were not of extreme shape and did not use exceedingly large bulbs; they also showed very large resistance reductions over conventional hull forms (28).

The general idea of a hull of minimum resistance was taken up by other Japanese workers, among whom Maruo has made the most significant contributions (29, 30). Using the Calculus of Variations and Weinblum's 'elementary ship' idea (i.e. a hull surface with equation $y = f(X(x)\,Z(z))$ with no coupling between the x and z

terms) he sought X(x) such that the wave resistance was a minimum for a given Z(z). The resultant waterline shapes were similar to those obtained by Karp, Kotik and Lurye for vertical struts of infinite draft (31) and by Weinblum, Wustrau and Vossers (32).

1.2.3 Higher Order Theories

The advent of the high-speed digital computer did much to relieve workers in this subject of the vast amount of tedious calculation and it soon became apparent that efforts should be directed toward minimising deficiencies in the theory.

Wave resistance theory is fundamentally deficient in two ways: It is a 'perfect fluid' theory and thus entirely neglects viscous effects; it is also a linearised theory. The mathematical problem involves a solution of Laplace's Equation with non-linear boundary conditions. In order to make this tractable analytically, Michell and Havelock 'linearised' the boundary conditions (see section 2.1.3) and in effect made it directly applicable to ships of very small beam in relation to the length, making waves of infinitesimal height.

Peters and Stoker (33) made a significant step forward when they introduced a completely general theory in 1954. Using a perturbation method they obtained a series solution to the problem, of which the Michell-Havelock result was the 'linear term' of the series and higher-order approximations could be obtained, at the expense of manipulative difficulties, by taking more terms. This extension of the theory to higher orders has been adopted by Maruo in Japan (34), and by Sisov (35) in Russia, who made use of a Green's Function in his derivation of the velocity potential. Wehausen (36) using a different Green's Function, developed a second-order term in the expression for wave resistance. Recently Eggers (37) corrected errors in Sisov's paper and in deviating slightly from Wehausen's approach, produced a slightly simplified higher order theory. A second-order theory has also been developed by Bessho (38, 39, 40) in Japan, again using a Green's Function approach.

Using slender body theory, i.e., considering a hull form of small

draft and beam compared to length, but of realistic beam/draft ratio, Vossers proposed a new formulation of the wave resistance problem (41). This theory was subsequently studied and corrected by Tuck (42) and Maruo (43), Tuck proposing certain second-order corrections. Lewison, using Tuck's theory to first and second orders, compared calculation and experiment for a semi-submerged axi-symmetric body (44).

A highly accurate method of determining the surface source distribution of arbitrary three-dimensional bodies, given by Smith and Hess (45), led Breslin and Eng to investigate its application to wave resistance calculation (46). Using Havelock's theory it was found that the accurate surface source distribution gave worse agreement with experimental results for a 0.60 block coefficient Series 60 form than the corresponding 'thin ship' result using a centreplane surface source distribution.

Higher order theories can be advanced to a greater degree when submerged bodies are considered, and mention may be made of the work of Havelock (ref. 12, p.420), Bessho (47, 48) and Tuck (49). The last paper contains an elegant extension of Havelock's early work on a submerged two-dimensional cylinder using complex potentials and the method of images.

1.2.4. Wave Pattern Analysis

With the increased interest in wave resistance theory there has been a corresponding increase in experimental methods for its determination. Wave resistance is notoriously difficult to define rigorously and measure accurately, so that comparison of higher order theories with experiment becomes difficult, if not meaningless, without a clear idea of what entities are being compared. It was stated above that Havelock's elementary free wave theory has been used extensively in both the empirical and analytical investigation of bulbous bows. The same experimental and analytical techniques are used in the comparison of calculated and measured wave resistance. In fact the problem of the

definition of wave resistance seems to have been resolved satisfactorily by such wave pattern analysis.

It is customary to define wave resistance in this case by considerations of energy and momentum flux and from measurement aft of the model, either of the wave pattern itself, or of forces on a vertical cylinder (50).

A great deal of work of this type has been done in Europe, U.S.A. and Japan. Reference 51 contains an extensive bibliography dealing with papers on wave pattern analysis. We propose only to dwell on one method, however, that of Eggers (52), experimentally verified by Sharma (53) and Gadd and Hogben (54). Eggers assumes an expression for the free wave system aft of the ship which has the amplitude and phase as two unknowns. By measuring the wave profile at two transverse or longitudinal vertical planes ('Eggers Cuts'), a Fourier analysis gives the amplitudes and phases. Using an assumed velocity potential in the form of an infinite series, Eggers deduced an expression for wave resistance involving the above amplitudes. Eggers' result is entirely general and is applicable to restricted fluid domains as well as infinite domains. As measurements are made well aft of the model, viscous wake effects are minimised, as are the 'local disturbance' effects, the only limitations being that linearisations are adopted in the derivation of the wave resistance expression.

Recently Kobus (55) has examined Eggers' relationship between transverse wave profiles and wave resistance, including the near-field 'local disturbance' terms. A two-dimensional vertical strut with a cross section obtained by conformal mapping of an ogive in an unbounded plane into a channel was tested. It was concluded that wave profiles downstream from a body cannot be predicted in more than a qualitative manner.

Ward (50) measured forces in two perpendicular directions on a vertical cylinder in the wave pattern. Using a simple and elegant relation between these forces and the energy in the wave pattern, he calculated the wave resistance. Eggers' and Ward's methods were compared (51) and good agreement was found between

the wave resistance measured for a mathematical model by both methods.

1.2.5 Other Experimental Methods

Ship hull pressure measurements by Laute (56), Hogben (57), Townsin (58) and Conn and Ferguson (59), enabled the horizontal pressure resistance of hull forms over a range of speeds to be deduced. The relationship of this pressure resistance to wave resistance measured as detailed in section 1.2.4. is not too clear, but such measurements have been of great value in demonstrating the undulatory nature of the deduced viscous resistance with speed. This has been confirmed by pitot traverse surveys of the viscous wake by Landweber and Wu (60) and Townsin (61).

A further investigation pertinent to this work is that of Steele and Pearce (62) who measured the distribution of skin friction over a model of a high-speed liner. Investigations of this type both supplement and complement the wave resistance investigations mentioned above.

1.3 VISCOSITY EFFECTS.

It was stated in section 1.2.3 that a deficiency of wave resistance theory is its complete neglect of viscosity effects. Some attempts to overcome this, both of a semi-empirical and theoretical nature, have been made.

1.3.1 Semi-empirical viscosity corrections

Havelock in 1935 (12, p.398) discussed the reduction in stern wave-making due to the viscous flow regime by using a 'reducing factor' over the aft body of the form. He obtained theoretical expressions for wave profiles and wave resistance involving this factor and was thus able to demonstrate that the wave resistance of a model going ahead was different to that going astern, a result not given by 'perfect' fluid reasoning.

Wigley in 1938 (63) used Havelock's idea and extended it to find values of the reducing factor for a family of models from experiments. By calculation of theoretical wave resistance and flat-plate friction resistance, as well as the theoretical wave resistance of the bow alone, he found a general expression for the reducing factor. It was found that an improvement was obtained in the agreement between calculated and measured resistance curves in all cases at low Froude numbers. The measured difference of resistance of an unsymmetrical model when moving in opposite directions was well reproduced by the calculated results.

It is worth noting that Wigley was in fact measuring the component of resistance known as 'viscous pressure' resistance and the accuracy of his semi-empirical factor was demonstrated in the interdependence study performed by Shearer, Cross and Lackenby (64, 65). Wigley also measured total form resistance and compared his results with those of Horn (66).

Wigley again demonstrated his viscosity correction in 1942 (67) and applied it to a different family of hulls. In general the conclusions were the same as those of his previous experiments except that discrepancies between measurement and calculation at

high speeds were attributed to the changing attitude of the model.

Guilloton in 1952 (68) proposed a correction resembling that of Horn's involving measured sinkage and trim which resulted in an adjustment to the calculated frictional resistance.

Emerson extended Wigley's approach by adopting his original idea of deducing two correction factors, independent of each other (69). One factor represented the viscous damping of the wave system while the other represented the reduction in the effective slope of the after-body lines due to the formation of a boundary layer. Very good agreement between measured and calculated resistances was obtained by Emerson in this manner.

By re-interpreting the work of Havelock and Wigley, Inui proposed an elaborate set of correction factors (25, p.205 - 215). Finite height corrections to bow and stern waves were proposed, as were hull self-interference corrections and a phase shift correction due to viscosity and other effects. These various factors were derived from experiments on streamline forms (as distinct from the mathematical models of Wigley) and complete agreement over the whole speed range was obtained between calculated wave resistance and a residuary resistance.

Sharma, in an extensive investigation (53), re-tested one of Inui's forms and again deduced correction factors. Unsatisfied with Inui's phase-shift correction, he proposed some improvements of his own and introduced a separation correction to the stern wave system. This last factor, prompted by observation, was an attempt to take into account the finite beam of the model. In spite of some scatter, Sharma was able to draw fair curves through his correction factors for a range of Froude Numbers and subsequent testing with wave pattern analysis (51) showed their general validity for this particular model.

A different approach has recently been tried by Breslin and Eng (70). Regarding the decisive effect of viscosity as stemming from the difference between the measured pressure distribution at

the stern and that predicted by inviscid-flow theory, they found a velocity potential to fit an experimental pressure distribution. This procedure was applied to a strut-like model with a symmetrical generalised Joukowski cross-section of which the pressure distribution in an infinite fluid was known both from calculation and measurement. The study did not support the authors' basic postulate. It was concluded that the pressure deficiency at the stern of the body had little or no effect in the determination of wave resistance.

1.3.2 Theoretical Approach

Many complexities arise when viscous effects are considered theoretically and only an approximate analytical approach to the problem has been attempted.

Havelock in 1948 (12, p.528) investigated the effect on calculated wave resistance of a modification of the waterlines near the stern. This modification, assumed to represent the effect of the boundary layer, had a marked effect in reducing the magnitude of the wave resistance. It was an important application of the theory, for it showed how a small modification to the hull form can have a comparatively large 'damping' effect on the resistance curve. Incidentally, this aspect has been exploited by Guilloton in his latest work on wave resistance (71).

A more fundamental approach was that adopted by Sretensky (72) in 1957. Beginning with the linearised form of the Navier-Stokes equations (Oseen's equations) and considering pressure distributions over the free surface, he proceeded in a manner similar to Havelock's early work on pressure disturbances (12, p.94 - 118) and obtained an elaborate expression for wave resistance, similar to the Michell-Havelock result. Expressions were obtained for various pressure distributions but no numerical results or experimental comparisons were given. In the discussion Graff stated that such an approach

was used at the Duisberg Tank and good agreement had been found between theoretical calculation and model results.

Wu and Messick also developed a linearised theory to investigate the viscous effects on two-dimensional waves generated by a system of external disturbances (73). This work was continued by Cumberbatch for the particular case of a ship wave system (74). Extending the study to the three dimensional case he found that the damping of the transverse waves varied little from the two-dimensional value and the infinite wave heights usually associated with the inviscid treatment were not obtained.

Work on this subject has also been done recently by Wigley (75) and Wu (76) but the problems of fully turbulent flow and separation cannot as yet be taken into account. Due to the complexity of the analytical treatment, an entirely numerical, finite difference scheme for two dimensional flows has been developed (77). By using finite difference forms of the complete Navier-Stokes equations and with the aid of a high-speed digital computer, solutions to basic fluid flow problems have been achieved, showing far better agreement with observations than those obtained by a purely analytical approach.

1.4 VERTICAL FORCES AND TRIMMING MOMENTS

1.4.1 Vertical Forces and Form Resistance.

Due to computational problems and the absence of any obvious practical applications, vertical forces have not been studied to the same extent as wave resistance. Early studies on submerged bodies discussed the vertical forces and moments acting thereon and their relationship to wave resistance.

It was not until 1932 that a practical use of these forces and the associated change in the position of the model appeared, when Horn (66 and 78) suggested a connection between mean sinkage and form resistance. Havelock in 1939 (12, p.458) calculated the vertical force and hence the mean sinkage for an ellipsoid at low speeds and deduced the form resistance from an application of Horn's expression. The calculated values of form resistance showed an encouraging agreement with observed values so that Havelock returned to this problem (12, p.609) and obtained an interesting relation between the form resistance of a spheroid and its virtual inertia coefficient for axial motion. A study was also made of the effect of tank boundary effect or 'blockage' for the same spheroid.

Saunders pointed out the effect of trim on resistance (79) and Havelock calculated the trimming moment for a simple, symmetrical form (12. p.520). It became apparent that mean sinkage and trim were of some importance in studies of the physics of ship resistance and it is pertinent to review some of the theoretical studies made for both the submerged and floating bodies.

1.4.2. Submerged Bodies

The vertical force on a cylinder submerged in a uniform stream was calculated by Havelock in 1928 (12. p.297) using the method of successive images to obtain the velocity potential and Blasius' Theorem to obtain the force. The vertical force coefficient was a positive constant at low speeds, whereas it had the same numerical value, but opposite sign, at high speeds. A more complete solution

was given by the same author in 1936 (12, p.420) when the condition at the surface of the cylinder was fulfilled exactly. Bessho (47) and Tuck (49) studied the same problem and attempted a solution using a non-linear free surface condition, the latter finding that the vertical force was significantly affected by the free surface non-linearities, a conclusion not reached by Bessho due to errors in his analysis.

Havelock extended his studies to submerged spheroids and ellipsoids giving expressions for wave resistance, vertical force and moments (e.g. 12, p.575). But no numerical examples were given and it was left to Wigley to provide these in an important paper (80). Calculating these forces and moments on a submerged spheroid for a range of Froude Numbers and immersions, he showed that the vertical force acted upwards at low Froude Numbers, rising to a maximum and decreasing until it acted downwards at high Froude Numbers. This was comparable to the earlier findings of Havelock for the submerged cylinder. Similar results were obtained by Bessho (47) to a higher degree of approximation and Pond (81) who considered the case of a Rankine ovoid.

Vertical forces on a submerged rectangular cylinder in time-dependent flow have been calculated numerically for low Reynold's Numbers by Harlow and Fromm (82) who obtained very good agreement between calculated and measured results.

Several of the above studies have considered not only the vertical force acting on the body but also the trimming moment. A comparison of various methods of computing trimming moment for a submerged prolate spheroid was made by Kinoshita, Abe and Okada in Japan (83).

1.4.3 Floating Bodies

As stated earlier, Havelock considered the sinkage of an ellipsoid and obtained expressions valid only for the low speed regime. He also deduced an expression for the vertical forces acting on two doublets abreast of each other in a uniform stream (12, p.417) but no numerical results were given.

Trim at high speeds was also calculated by Havelock in 1946 (12, p.520) for a simple symmetrical floating body. He deduced pressures over the hull from source-sink theory and gave expressions for the trimming moment due to the waves trailing aft of the form. It was found that the order of agreement between calculation and observation was much the same as that between calculated and measured curves of wave resistance.

When higher order theories of wave resistance are considered, a knowledge of mean sinkage and trim is important and it was with this in mind that Bessho studied vertical forces and trimming moments for floating bodies (84). Using a linearised theory and Lagally's Theorem (85) he calculated wave resistance, vertical force and trimming moment for a simple mathematical form and concluded that false results could be obtained with the injudicial use of Lagally's Theorem. Wave resistance values coincided when derived by both Lagally's Theorem and linearised theory but the same was not true of the vertical force and the trimming moment.

The higher order theories of Wehausen (37) and Sisov (35) give expressions for vertical force and trimming moment, Wehausen showing that second-order corrections involve sinkage and trim; Stoker (86) also derived an expression for vertical force and trimming moment but in linearised form.

Direct measurement of the vertical force causing mean sinkage and the moment causing trim was performed by Lewison (44) for a semi-submerged body. Comparisons were made between theoretical predictions (using Guilloton's method) and 'equivalent' forces and moments derived from measured mean sinkage and trim. Fair agreement was obtained between measurement and calculation for vertical force in spite of some scatter in the results, but poor agreement was obtained for the trimming moments.

Recently Tuck (87) studied mean sinkage and trim in shallow water of finite width, this being relevant to investigations of both blockage and squatting. A plotting was given which showed a unique curve for various hull shapes and enabled an estimate of the effect of blockage on sinkage and trim to be obtained. It was noted that the effect of finite width was far more serious for sinkage than for

In retrospect, it is seen that theoretical steady-state ship hydrodynamics consists almost exclusively of the study of wave resistance of simple mathematical forms. In general poor agreement between calculated and measured results has resulted from using an 'ab initio' approach, Guilloton's method showing most promise in this respect. Work with empirical correction factors has, on the whole, been unsatisfactory and efforts have been made to develop a consistent higher-order theory.

The technique of wave-pattern analysis has been developed into a useful tool for the research worker and the interdependence of wave-making and viscous resistance has been shown empirically.

A connection between form resistance and mean sinkage has been proposed ; a few theoretical and experimental studies of the vertical forces and moments acting on a floating body have been performed.

It is against this background that the following investigation is set.

2. HYDRODYNAMIC FORCES AND MOMENTS :

THEIR CALCULATION & MEASUREMENT FOR A MATHEMATICAL MODEL.

2.1 BASIC THEORY

The theoretical approach which follows is due to Havelock (12, p520 - 527.) A simplified pressure distribution over the hull is calculated and the resultant horizontal and vertical hydrodynamic forces and a trimming moment are obtained. It is pertinent to the discussion to derive the expressions ab initio which will be done after some preliminary definitions.

2.1.1 Definitions

Axis System

The Eulerian equations of motion are used throughout.

Before the problem can be stated mathematically an axis system must be defined relative to which all measurements may be referred. It is usual to assume that the axis system is fixed within the ship with the origin in the undisturbed free surface of the water on the centreline amidships. Axis oz is directed vertically upward, ox forward parallel to the direction of motion and oy is directed to one side as shown below

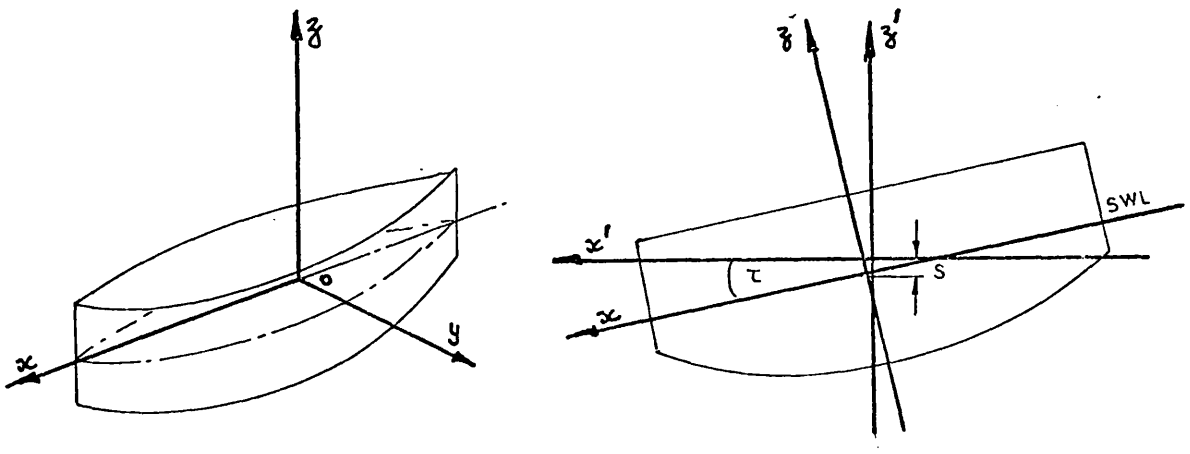

MODEL AXIS SYSTEM

FIG. 1

The free surface is defined as a surface in the fluid across which there is a marked density discontinuity. It is a surface upon which all fluid velocities are tangential and the pressure is constant (usually atmospheric).

Wave Resistance R_w in the following analysis is defined as the resistance experienced by a body moving at constant velocity, on or beneath, the free surface of a perfect fluid. It is caused by the generation of pressure forces over the hull which manifest themselves as waves on the free surface.

The vertical hydrodynamic force Z is defined as the vertical component of the pressure forces acting on the hull.

For equilibrium between the forces acting, the hull takes up a new attitude involving:

(a) Mean Sinkage s defined as the vertical movement of the midships position relative to a reference axis system ox',oy',oz'.

(b) Trim τ defined as the angle through which the axis ox moves relative to a reference system ox', oy', oz'. It is defined as negative if the bow sinks lower than the stern.

The resultant force F_R, is defined as the vector sum of R_W and Z

$$F_R = \sqrt{R_w^2 + Z^2} \qquad \ldots\ldots\ldots\ldots \text{(2.1.1a)}$$

and is assumed to act at an angle ψ to the oz axis where

$$\tan \psi = R_w / Z \qquad \ldots\ldots\ldots\ldots \text{(2.1.1b)}$$

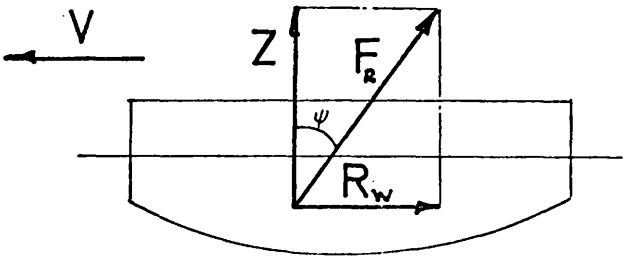

FIG. 2

There are two velocities to be considered:

(i) The steady velocity of the ship itself denoted by V.

(ii) Fluid velocities in each of the directions ox, oy, oz, induced by the motion of the ship. These perturbation velocities are termed u, v and w respectively.

By definition, the resultant velocity q, of a fluid particle is

$$q^2 = (V+u)^2 + v^2 + w^2 \qquad \ldots\ldots (2.1.2)$$

The fluid motion is assumed to be irrotational. This will be true in general except in the wake region. The fluid itself is assumed to occupy the half space $z<o$ and to be a perfect fluid i.e. it is incompressible, homogeneous and inviscid.

The shortcomings of the above definitions and assumptions will be discussed below.

2.1.2. Statement of the Problem

The problem may be formulated mathematically as the solution of an elliptic partial differential equation (Laplace's Equation) subject to non-linear boundary conditions. This problem has proved intractable analytically and certain simplifying assumptions have been introduced.

Virtually no attempt has been made to solve the problem using numerical methods exclusively e.g. finite difference techniques, and a combination of analytical and numerical methods has been employed below.

Laplace's Equation

A fundamental result of classical hydrodynamics is that the Principle of Continuity shall hold within the fluid.

This implies that

(i) The mass of fluid is conserved,

(ii) The flow is continuous.

For a fluid of constant density, this may be stated mathematically as

$$\frac{\partial u}{\partial x} + \frac{\partial v}{\partial y} + \frac{\partial w}{\partial z} = 0 \qquad z \leq 0 \qquad \ldots\ldots\ldots\ldots (2.1.3)$$

We have assumed the flow to be irrotational and this leads directly to the use of a velocity potential, ϕ, to describe the flow. (88, p67). Thus

$$u = \frac{\partial \phi}{\partial x}, \quad v = \frac{\partial \phi}{\partial y}, \quad w = \frac{\partial \phi}{\partial z} \qquad \ldots\ldots\ldots\ldots (2.1.4)$$

Substituting equations (2.1.4) into (2.1.3) we have

$$\frac{\partial^2 \phi}{\partial x^2} + \frac{\partial^2 \phi}{\partial y^2} + \frac{\partial^2 \phi}{\partial z^2} = 0 \qquad z \leq 0 \qquad \ldots\ldots\ldots\ldots (2.1.5)$$

This elliptical partial differential equation, known as Laplace's equation is fundamental to many steady-state fluid problems.

Boundary and Radiation Conditions.

The boundary conditions can be defined in three distinct regions:

a) On the underwater hull surface.

b) On the free surface.

c) At boundaries an infinite distance from the body.

At any fixed boundary within the fluid (we assume the free surface to act as such a boundary) the normal velocity must be zero, i.e., A Neumann boundary value problem exists.

If $F(x,y,z,t) = 0$ is the equation of the bounding surface, then at every point of it, the material derivative of F must vanish (9, p6-7) i.e.

$$\frac{DF}{Dt} = \frac{\partial F}{\partial t} + u\frac{\partial F}{\partial x} + v\frac{\partial F}{\partial y} + w\frac{\partial F}{\partial z} = 0 \qquad \ldots\ldots (2.1.6)$$

If the underwater hull surface is represented by an equation of the form

$$y = \eta(x,z) \qquad \ldots\ldots (2.1.7)$$

i.e. $F = y - \eta(x,z)$

substitution of equation (2.1.7) into (2.1.6) gives, remembering that the motion is invariant with time,

$$\left|(V+u)\frac{\partial \eta}{\partial x} - v + w\frac{\partial \eta}{\partial z}\right|_{y=\eta} = 0 \qquad \ldots\ldots (2.1.8a)$$

Inserting values from equation (2.1.4) gives the boundary condition (a) on the underwater hull surface as

$$\left|\left(V+\frac{\partial \phi}{\partial x}\right)\cdot\frac{\partial \eta}{\partial x} + \frac{\partial \phi}{\partial z}\cdot\frac{\partial \eta}{\partial z} = \frac{\partial \phi}{\partial y}\right|_{y=\eta} \qquad \ldots\ldots (2.1.8b)$$

In a similar manner we may deal with the boundary condition at the free surface in which case we assume

$$z = \zeta(x,y) \qquad \ldots\ldots (2.1.9)$$

i.e. $F = z - \zeta(x,y)$

which gives

$$\left|(V+u)\frac{\partial \zeta}{\partial x} + v\frac{\partial \zeta}{\partial y} - w = 0\right|_{z=\zeta} \qquad \ldots\ldots (2.1.10a)$$

or

$$\left|\left(V+\frac{\partial \phi}{\partial x}\right)\cdot\frac{\partial \zeta}{\partial x} + \frac{\partial \phi}{\partial y}\cdot\frac{\partial \zeta}{\partial y} = \frac{\partial \phi}{\partial z}\right|_{z=\zeta} \qquad \ldots\ldots (2.1.10b)$$

On the free surface not only are the velocities tangential but the pressure is constant. It is thus necessary to apply Bernoulli's equation:

$$\frac{P}{\rho} + \frac{q^2}{2} + g\zeta = \frac{P}{\rho} + \frac{V^2}{2} \qquad \ldots\ldots (2.1.11)$$

The L.H.S. of equation (2.1.11) refers to conditions on the free surface at and abaft the hull and the R.H.S. refers to steady conditions a great distance ahead of the hull. In this equation P is the uniform pressure acting on a streamline, ρ the mass density of the fluid and g the acceleration of gravity, both ρ and g being assumed constant throughout the half space $z<o$.

Substituting equation (2.1.2) into equation (2.1.11) and rearranging gives an expression for the surface elevation :

$$\zeta = -\frac{V}{g}.u - \frac{1}{2g}(u^2 + v^2 + w^2) \quad \text{AT } z=\zeta \qquad \ldots\ldots (2.1.12a)$$

or, in terms of the velocity potential,

$$\zeta = -\frac{V}{g}.\frac{\partial\phi}{\partial x} - \frac{1}{2g}\left[\left(\frac{\partial\phi}{\partial x}\right)^2 + \left(\frac{\partial\phi}{\partial y}\right)^2 + \left(\frac{\partial\phi}{\partial z}\right)^2\right]_{AT\, z=\zeta} \qquad \ldots\ldots (2.1.12b)$$

As both equations (2.1.10) and (2.1.12) must apply at the free surface, $z = \zeta$ they may be combined into one equation, defining what is usually known as the Free Surface Condition:

$$\frac{\partial^2\phi}{\partial x^2} + K_o\frac{\partial\phi}{\partial z} = -\frac{K_o}{g}\left[V\left(\frac{\partial\phi}{\partial x}.\frac{\partial^2\phi}{\partial x^2} + \frac{\partial\phi}{\partial y}.\frac{\partial^2\phi}{\partial x\partial y}\right)\right. \qquad \ldots\ldots (2.1.13)$$

$$+\left(V+\frac{\partial\phi}{\partial x}\right)\left(\frac{\partial\phi}{\partial x}.\frac{\partial^2\phi}{\partial x^2} + \frac{\partial\phi}{\partial y}.\frac{\partial^2\phi}{\partial y\partial x} + \frac{\partial\phi}{\partial z}.\frac{\partial^2\phi}{\partial z\partial x}\right)$$

$$\left.+\frac{\partial\phi}{\partial y}\left(\frac{\partial\phi}{\partial x}.\frac{\partial^2\phi}{\partial y\partial x} + \frac{\partial\phi}{\partial y}.\frac{\partial^2\phi}{\partial y^2} + \frac{\partial\phi}{\partial z}.\frac{\partial^2\phi}{\partial y\partial z}\right)\right]_{AT\, z=\zeta}$$

where

$$K_o = g / V^2$$

Conditions imposed upon the solution of equation (2.1.5) at the boundaries at $x = \pm \infty$ are known as the Radiation Conditions.

We have assumed the fluid to occupy the half space $z<o$ and imply that it is otherwise unbounded. All motions at $x = \pm\infty$ must vanish if the floating body is assumed to advance into undisturbed fluid. This implies that

$$\lim_{x \to +\infty} \phi = 0 \qquad \ldots\ldots \text{(2.1.14a)}$$

Similarly there must be no vertical component of flow a great distance below the body or

$$\frac{\partial \phi}{\partial z} = 0 \quad \text{AT} \quad z = -\infty$$

The condition at $x = -\infty$ is more difficult to impose as the position of the free surface and the type of motion at this point are not known in advance. We have assumed the fluid to be inviscid so we cannot expect attenuation of any motion due to viscosity. Stoker (86,p209) states that the steady-state problem postulated above is unrealistic and suggests re-formulation by considering time-variant flows.

The steady state case is then taken to be the limiting case as t tends to infinity, t being the time variable. He states that the limiting case as t tends to infinity would satisfy all necessary radiation conditions. This method was used by Havelock (12,p564) who derived the usual steady-state result obtained with the general radiation condition:

$$\lim_{x \to -\infty} \phi = \text{BOUNDED} \qquad \ldots\ldots \text{(2.1.14c)}$$

Stoker (86,p59) further adds that at $x = -\infty$ the wave system should behave like progressive waves moving away from the initial disturbance. This leads to a unique solution of the problem.

The condition at $x = -\infty$ is important if an entirely numerical approach is to be adopted for the solution of Laplace's equation with the relevant boundary conditions. A discussion of such a problem is given in ref. 77 where potential flow is discarded and the basic Navier-Stokes equations are solved making use of the equation of continuity (equation (2.1.3)) and basic velocity/pressure relationships for the fluid particles.

2.1.3 Solution by Linearisation

In section 2.1.2 the condition of a ship advancing into undisturbed fluid at a constant velocity was represented by an approximate mathematical model. Within the limitations of the assumptions of section 2.1.1 it was found that the flow was specified by Laplace's Equation subject to non-linear boundary conditions given by equations (2.1.8) to (2.1.14).

Such a problem has proved intractable analytically due to the non-linear nature of the boundary conditions. These obviate the use of simple super-position of solutions and bring additional problems concerning the uniqueness of any solution obtained.

It is therefore necessary to simplify the boundary conditions by linearisation. Superposition of solutions is then possible and conventional linear mathematics may be used. After linearisation (i.e. the neglect of squares and higher powers of small quantities such as $\partial\phi/\partial x$, $\partial\phi/\partial z$ etc.) the boundary conditions become

$$V\frac{\partial \eta}{\partial x} = \frac{\partial \phi}{\partial y} \quad \text{AT } y = \eta(x,z) \qquad \ldots\ldots (2.1.15)$$

from equation (2.1.8b)

$$\frac{\partial^2 \phi}{\partial x^2} + K_0 \frac{\partial \phi}{\partial z} = 0 \quad \text{AT } z = \zeta(x,y) \qquad \ldots\ldots (2.1.16)$$

from equation (2.1.13)

$$\zeta = -\frac{V}{g}\cdot\frac{\partial\phi}{\partial x}\Big|_{z=\zeta} \qquad \ldots\ldots (2.1.17)$$

from equation (2.1.12b)

We have stated that for linearisation the squares and higher powers of small quantities may be neglected. This implies that the perturbation velocities must be small and that the slopes $\partial\eta/\partial x$, $\partial\eta/\partial z$ of the body surface must also be small, as must the surface slopes $\partial\zeta/\partial x$, $\partial\zeta/\partial y$ of the free surface.

The following simplifications are made:

(i) the free surface condition is assumed to act at $z = o$ instead of $z = \zeta$.

(ii) the surface elevation ζ is assumed to be calculable from $\partial\phi/\partial x$ at $z = o$ instead of $z = \zeta$.

(iii) In what follows it will become apparent that the body surface condition is assumed to act at $y = o$ instead of $y = \eta(x, z)$.

These last conditions follow from the general linearisation. While not an essential part of the linearisation itself, they result therefrom and facilitate the mathematical analysis.

The result of linearisation is that from the physical conditions we have arrived at a mathematical representation in which the ship is replaced by a body whose surface slopes are everywhere small, advancing at constant velocity into an inviscid fluid, making waves of infinitesimal height. (see figure 3). Clearly this representation diverges from reality in two major aspects.

(i) Viscosity is neglected.

(ii) Non-linearities, which may be significant, are assumed to be negligible.

FIG. 3

THE WAVE RESISTANCE PROBLEM.

LINEAR SYSTEM

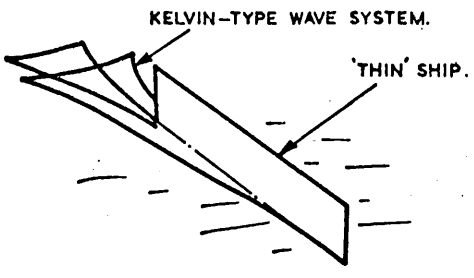

BASIC EQUATION

$$\frac{\delta^2\phi}{\delta x^2} + \frac{\delta^2\phi}{\delta y^2} + \frac{\delta^2\phi}{\delta z^2} = 0$$

BOUNDARY CONDITIONS

$$\frac{\delta\phi}{\delta y} = V\frac{\delta f}{\delta x} \quad \text{AT } y = 0$$

$$\frac{\delta^2\phi}{\delta x^2} + K_0\frac{\delta\phi}{\delta z} = 0 \quad \text{AT } z = 0$$

FREE SURFACE ELEVATION

$$\zeta = -\frac{V}{g}\frac{\delta\phi}{\delta x} \quad \text{AT } y = 0$$

RADIATION CONDITIONS

$$\lim_{x \to +\infty} \phi = 0$$

$$\lim_{x \to -\infty} \phi = \text{BOUNDED}$$

$$\frac{\delta\phi}{\delta z} = 0, \quad z \to -\infty$$

NON-LINEAR (PHYSICAL) SYSTEM

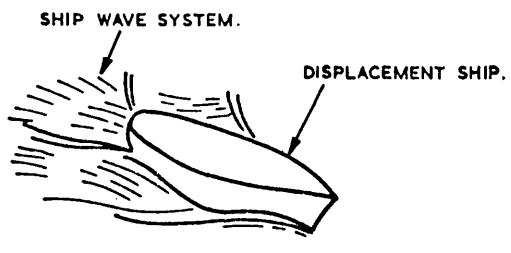

BASIC EQUATION

$$\frac{\delta^2\phi}{\delta x^2} + \frac{\delta^2\phi}{\delta y^2} + \frac{\delta^2\phi}{\delta z^2} = 0$$

BOUNDARY CONDITIONS

$$\frac{\delta\phi}{\delta y} = \left(V + \frac{\delta\phi}{\delta x}\right)\frac{\delta f}{\delta x} + \frac{\delta\phi}{\delta z}\cdot\frac{\delta f}{\delta z} \quad \text{AT } y = f$$

$$\frac{\delta^2\phi}{\delta x^2} + K_0\frac{\delta\phi}{\delta z} = -K_0\left[V\left(\frac{\delta\phi}{\delta x}\cdot\frac{\delta^2\phi}{\delta x^2} + \frac{\delta\phi}{\delta z}\cdot\frac{\delta^2\phi}{\delta x\delta z}\right)\right.$$

$$+\left(V + \frac{\delta\phi}{\delta x}\right)\left(\frac{\delta\phi}{\delta x}\cdot\frac{\delta^2\phi}{\delta x^2} + \frac{\delta\phi}{\delta z}\cdot\frac{\delta^2\phi}{\delta z\delta x} + \frac{\delta\phi}{\delta y}\cdot\frac{\delta^2\phi}{\delta y\delta x}\right)$$

$$\left. + \frac{\delta\phi}{\delta z}\left(\frac{\delta\phi}{\delta x}\cdot\frac{\delta^2\phi}{\delta x\delta z} + \frac{\delta\phi}{\delta z}\cdot\frac{\delta^2\phi}{\delta z^2} + \frac{\delta\phi}{\delta y}\cdot\frac{\delta^2\phi}{\delta y\delta z}\right)\right] \text{AT } y = \zeta$$

FREE SURFACE ELEVATION

$$\zeta = -\frac{V}{g}\frac{\delta\phi}{\delta x} - \frac{1}{2g}\left[\left(\frac{\delta\phi}{\delta x}\right)^2 + \left(\frac{\delta\phi}{\delta z}\right)^2 + \left(\frac{\delta\phi}{\delta y}\right)^2\right] \quad \text{AT } y = \zeta$$

RADIATION CONDITIONS

$$\lim_{x \to +\infty} \phi = 0$$

$$\lim_{x \to -\infty} \phi = \text{BOUNDED}$$

$$\frac{\delta\phi}{\delta z} = 0, \quad z \to -\infty$$

FLUID ASSUMED IRROTATIONAL, INCOMPRESSIBLE, HOMOGENEOUS & INVISCID.

Guilloton has estimated the magnitude of perturbation velocities and their contribution to equation (2.1.12) for a destroyer form (11). He found that at a speed-length ratio of 1.72 the $\left(\frac{\partial \phi}{\partial y}\right)^2$ term contributed some 26% of the term retained after linearisation. This calculation was performed at a station near the bow where $\partial\phi/\partial y$ was of appreciable magnitude. Similar investigations for a mathematical model are included in Appendix A.

It therefore appears that the neglect of non-linearities is unfortunate.

2.1.4 Derivation of the Velocity Potential

With the problem stated mathematically in terms of a velocity potential an expression for such a potential which satisfies Laplace's Equation and the various linearised boundary conditions must be derived. We adopt the approach of Havelock as described by Lunde (89), assuming the body to be capable of representation by some suitable surface source distribution. We shall derive the potential for a particular case and show its relationship to the potential of a simple source; this result will then be modified to fit the free surface condition and then generalised by integration.

An advantage arising from the use of source distributions is that the body surface conditions, given by equations (2.1.8) and (2.1.15) are automatically satisfied. This is discussed further in section 2.2.

We rewrite Laplace's equation in cylindrical co-ordinates,

$$\frac{\partial^2 \phi}{\partial \rho^2} + \frac{1}{\rho}\frac{\partial \phi}{\partial \rho} + \frac{1}{\rho^2}\cdot\frac{\partial^2 \phi}{\partial \psi^2} + \frac{\partial^2 \phi}{\partial z^2} = 0 \qquad \ldots\ldots\ldots (2.1.18)$$

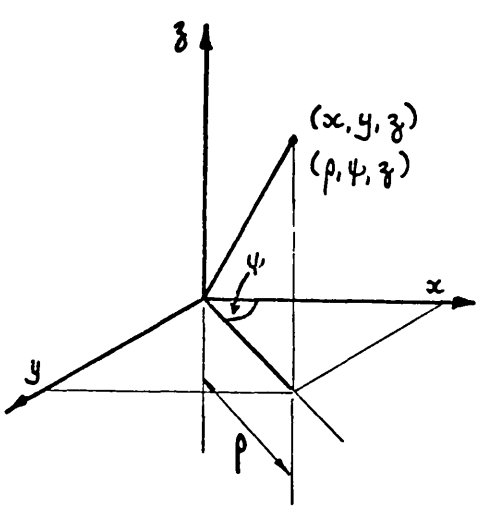

AXIS SYSTEM (CYLINDRICAL CO-ORDINATES)

FIG. 4

We define the 'Bessel Operator' B_ν as

$$B_\nu = \frac{\partial^2}{\partial\rho^2} + \frac{1}{\rho}\frac{\partial}{\partial\rho} - \frac{\nu^2}{\rho^2} \qquad \ldots\ldots (2.1.19)$$

and after using a 'separation of variables' technique to obtain a solution of equation (2.1.18) as

$$\phi(\rho, \psi, z) = \phi_1(\rho, z)\, e^{i\nu\psi} \qquad \ldots\ldots (2.1.20)$$

we find that equation (2.1.18) reduces to

$$e^{i\nu\psi}\left(B_\nu + \frac{\partial^2}{\partial z^2}\right)\phi_1(\rho, z)\Big|_{\nu=0} = 0 \qquad \ldots\ldots (2.1.21)$$

Following Sneddon (90, p291) the Hankel Transform of zero order ($\nu = 0$) is introduced.

$$\mathcal{H}_0\left[\phi_1(\rho, z),\ \rho \to \xi\right] = \int_0^\infty \rho\, \phi_1(\rho, z)\, J_0(\xi\rho)\, d\rho = \bar{\phi}_1 \qquad \ldots\ldots (2.1.22)$$

We note in passing that if a bounded fluid had been considered (e.g. the water in a test tank) it would have been appropriate to introduce a finite transform. This has been done by Eggers (52) who considered such a restricted fluid and added the further boundary condition :

$$\frac{\partial\phi}{\partial y} = 0 \quad \text{AT} \quad y = \pm b/2$$

where b = tank breadth.

This additional boundary condition causes an infinite sum (instead of an infinite integral) to appear in the velocity

potential expression due to infinite images reflected in the tank walls at $y = \pm b/2$

Returning to the case under consideration, on multiplying both sides of equation (2.1.21) by $\rho J_0(\xi\rho)$ and integrating from 0 to ∞ we have

$$\frac{d^2\bar{\phi}_1}{dz^2} - \xi^2\bar{\phi}_1 = 0 \qquad \ldots\ldots (2.1.23)$$

where we have used the known result (ref. 90, p61, Equation 32)

$$\mathcal{H}_\nu[B_\nu(\beta), \rho \to \xi] = -\xi^2 \bar{\beta}_\nu(\xi)$$

Equation (2.1.23) is now seen to be an ordinary differential equation in $\bar{\phi}_1$. Using the well-known D-operator method of solution and considering the case where $\bar{\phi}_1 \to 0$ as $z \to +\infty$

$$\bar{\phi}_1 = A(\xi)\, e^{-\xi z} \qquad z>0 \qquad \ldots\ldots (2.1.24a)$$

and

$$\bar{\phi}_1 = B(\xi)\, e^{\xi z} \qquad z<0 \qquad \ldots\ldots (2.1.24b)$$

where $A(\xi)$ and $B(\xi)$ are arbitrary parameters.

In what follows the case $z>0$ is considered remembering that the argument is valid for $z<0$ also, resulting in a simple change of sign in the final expression.

Applying the Hankel Inversion Theorem to equation (2.1.24a) gives

$$\phi_1(\rho, z) = \int_0^\infty \xi A(\xi) e^{-\xi z} J_0(\xi\rho)\, d\xi \qquad \ldots\ldots (2.1.25)$$

This is a general solution for a velocity potential satisfying Laplace's Equation, convergent for $z>0$, in which $A(\xi)$ may be chosen to suit the problem in hand.

We wish to represent the body by a certain distribution of sources and sinks. It is well known (9,p57) that the velocity potential at the origin due to a simple source at r is

$$\phi_s = \frac{m}{r}, \quad r^2 = x^2+y^2+z^2 \qquad \ldots\ldots (2.1.26)$$

where m is the source strength.

If we therefore choose $A(\xi) = m/\xi$ (where m is some constant) and make use of the known result of Lipschitz (91,p384):

$$\int_0^\infty e^{-at} J_0(bt)\, dt = \frac{1}{\sqrt{(a^2+b^2)}} \qquad \ldots\ldots (2.1.26a)$$

we have, from equation (2.1.25), as $\rho^2 = x^2+y^2$

$$\phi_s = \phi_1(\rho, z) = m \int_0^\infty e^{-\xi z} J_0(\xi\rho)\, d\xi$$

$$= \frac{m}{\sqrt{(\rho^2+z^2)}} = \frac{m}{r} \qquad \ldots\ldots (2.1.27)$$

It is convenient to replace $J_0(\xi\rho)$ by its integral representation:

$$J_0(\xi\rho) = \frac{1}{2\pi}\int_{-\pi}^{\pi} e^{i\xi\cos\theta.\rho}\, d\theta = \frac{1}{2\pi}\int_{-\pi}^{\pi} e^{i\xi\rho\cos(\theta-\psi)}\, d\theta \qquad \ldots\ldots (2.1.28)$$

(See 91,p20 and 52)

Substitution of equation (2.1.28) into (2.1.27) gives:

$$\phi_s = \phi_1 = \frac{m}{r} = \frac{m}{2\pi}\int_{-\pi}^{\pi} d\theta \int_0^\infty e^{-\xi z} e^{i\xi\rho\cos(\theta-\psi)}\, d\xi \qquad \ldots\ldots (2.1.29)$$

Using the fact that

$$\rho\cos(\theta-\psi) = \rho\cos\theta\cos\psi + \rho\sin\theta\sin\psi,$$
$$x = \rho\cos\psi, \quad y = \rho\sin\psi$$

equation (2.1.29) becomes:

$$\phi_s = \frac{m}{\sqrt{(x^2+y^2+z^2)}} = \frac{m}{2\pi}\int_{-\pi}^{\pi} d\theta \int_0^{\infty} e^{-\xi z}\, e^{i\xi\tilde{\omega}}\, d\xi \qquad \ldots\ldots (2.1.30a)$$

or, in Havelock's notation:

$$\phi_s = \frac{m}{r} = \frac{m}{2\pi}\int_{-\pi}^{\pi} d\theta \int_0^{\infty} e^{-\kappa z}\, e^{i\kappa\tilde{\omega}}\, d\kappa \qquad (z>0) \qquad \ldots\ldots (2.1.30b)$$

$$= \frac{m}{2\pi}\int_{-\pi}^{\pi} d\theta \int_0^{\infty} e^{\kappa z}\, e^{i\kappa\tilde{\omega}}\, d\kappa \qquad (z<0) \qquad \ldots\ldots (2.1.30b)$$

where

$$\tilde{\omega} = x\cos\theta + y\sin\theta$$

Equations (2.1.30) represent the velocity potential of a simple source in an unbounded fluid without a free surface. As soon as a free surface is introduced, some sort of image system in the free surface must exist (89). Havelock assumes this image system to take an arbitrary form and represents it by the function $F(\theta,K)$. This gives a velocity potential for the fluid motion of

$$\phi_s = \frac{m}{2\pi}\int_{-\pi}^{\pi} d\theta \int_0^{\infty} e^{-\kappa(z+f)}\, e^{i\kappa\tilde{\omega}}\, d\kappa + \int_{-\pi}^{\pi} d\theta \int_0^{\infty} F(\theta,\kappa)\, e^{\kappa z}\, e^{i\kappa\tilde{\omega}}\, d\kappa \qquad (2.1.31a)$$

where we have assumed the source to be situated at the point $(o,o,-f)$ and have taken the appropriate forms of equation (2.1.30).

The free surface condition is now modified by the addition of a term involving a small 'frictional' force proportional to the velocity. The resulting 'friction' coefficient, μ, is inserted merely to make the analytical wave system trail aft of the body. It is a purely artificial concept, is discarded once it has served it

purpose and is discussed in more detail in references 9, p.398-403; 51, Appendix 1; 89, Appendix 1.

The value of $F(\theta,K)$, found after substituting (2.1.31a) into the modified free surface condition:

$$\frac{\partial^2\phi}{\partial x^2} + \kappa_0 \frac{\partial\phi}{\partial z} - \mu \frac{\partial\phi}{\partial x} = 0$$

is given by

$$F(\theta,\kappa) = -\frac{m}{2\pi}\left[\frac{\kappa + \kappa_0 \sec^2\theta + i\mu\sec\theta}{\kappa - \kappa_0 \sec^2\theta + i\mu\sec\theta}\right] e^{-\kappa f} \quad \ldots\ldots \text{(2.1.31b)}$$

Substitution of (2.1.31b) into (2.1.31a) gives the velocity potential for a source at the point (o,o,-f):

$$\phi_s = \frac{m}{2\pi}\int_{-\pi}^{\pi} d\theta \int_0^\infty e^{-\kappa(z+f)} e^{i\kappa\tilde{\omega}}\, d\kappa - \frac{m}{2\pi}\int_{-\pi}^{\pi} d\theta \int_0^\infty \frac{\kappa+\kappa_0\sec^2\theta + i\mu\sec\theta}{\kappa-\kappa_0\sec^2\theta+i\mu\sec\theta} e^{-\kappa(z+f)+i\kappa\tilde{\omega}} d\kappa \quad \text{(2.1.32a)}$$

which becomes, after writing $F(\theta,K)$ in the form:

$$F(\theta,\kappa) = -\frac{m}{2\pi} e^{-\kappa f} - \frac{m}{2\pi}\frac{\kappa_0\sec^2\theta}{\kappa-\kappa_0\sec^2\theta+i\mu\sec\theta} e^{-\kappa f},$$

$$\phi_s = \frac{m}{r_1} - \frac{m}{r_2} - \frac{\kappa_0 m}{2\pi}\int_{-\pi}^{\pi} \sec^2\theta\, d\theta \int_0^\infty \frac{e^{-\kappa(f-z)} e^{i\kappa\tilde{\omega}}}{\kappa-\kappa_0\sec^2\theta+i\mu\sec\theta} d\kappa \quad \ldots\ldots \text{(2.1.32b)}$$

where

$$r_1^2 = x^2+y^2+(z+f)^2 \; ; \quad r_2^2 = x^2+y^2+(z-f)^2$$

This potential is completed by the addition of a term representing the uniform stream, as shown by Lunde (89).

The expression given by equations (2.1.32) has been derived in some detail as it is a fundamental result of Havelock's work and is the foundation upon which the following analysis is built. It is important to have a clear idea of what it represents, as terms which do not contribute to the wave resistance are important when vertical forces are considered ; limiting cases, as $K_0 \to 0$ and $K_0 \to \infty$ are also of importance.

2.1.4a. The limiting case as Ko → o

As the wave number Ko tends to zero, the speed of advance tends to infinity. It is readily seen from equation (2.1.32b) that, as Ko → o, the potential assumes the form :

$$\lim_{K_o \to 0} \phi = \frac{m}{r_1} - \frac{m}{r_2} \qquad \ldots\ldots (2.1.33a)$$

which is immediately interpreted as the potential of a source at the point (o,o,-f) and an equal sink (due to the negative sign) at the image point (o,o,f).

This is an example of the 'inverse image' occurrence at a free surface at high speed. (see ref. 88, p.251).

If we consider the free surface condition given by equation (2.1.16) we have, as Ko → o,

$$\frac{\partial^2 \phi}{\partial x^2} = o \quad , \quad \frac{\partial \phi}{\partial x} = u = \text{CONSTANT.}$$

i.e., the free surface acts as a 'rigid wall' without gravitational effects.

2.1.4.b. The limiting case as Ko → ∞

As Ko → ∞, V → o and Lunde (89) has shown that a series expansion of the second term in equation (2.1.32a) gives, as Ko → ∞,

$$\lim_{K_o \to \infty} \phi = \frac{m}{r_1} + \frac{m}{r_2} \qquad \ldots\ldots (2.1.33b)$$

This is the potential of a source at (o,o,-f) with its corresponding image source at (o,o,f). Similarly the free surface condition gives as Ko → ∞.

$$\frac{\partial \phi}{\partial z} = o$$

in which case the free surface is acting simply as a rigid wall. If the source strength m were generalised to a surface source distribution, equation (2.1.33b) would represent the potential

of a double or reflex model.

Inspection shows that the potential has finite and unequal values at the two limiting values of Ko. This observation will be of significance later in the analysis.

We may now attempt a physical interpretation of equation (2.1.32). Taking equation (2.1.32b) as an example, the first two terms represent the potential of a source, (or, in the general case, a body) and its reflection in the free surface, assumed to remain plane. The wave motion caused by this body is represented by the third term, which is composed of both monotonic and oscillatory parts.

It is important to remember that for a complete solution of the problem, we should apply the method of images and add to this potential a term representing the influence of the ship on the wave motion. This would require the addition of further terms to maintain the boundary conditions and would give a potential in the form of an infinite series. Havelock has pursued this method for a submerged circular cylinder, as stated above, and it is pertinent to any discussions of total or partial non-linear treatments.

2.1.5 Calculations of Pressures, Forces and Moments

From Bernoulli's Equation the total pressure in the fluid is given by

$$p' = p - p_0 = -\frac{\rho}{2}\left[(V+u)^2 + v^2 + w^2\right] - \rho g \zeta + \frac{\rho}{2} V^2$$

Linearising the dynamic pressure term gives

$$p(x,y,z) = -\rho u.V = -\rho V.\frac{\partial \phi}{\partial x} \qquad \ldots\ldots (2.1.34)$$

We may now calculate the linearised pressure distribution over the hull surface and resolve it in appropriate directions to obtain the wave resistance, the vertical force and the trimming moment:

$$R_w = \iint p(x,y,z)\, dy\, dz \qquad \ldots\ldots(2.1.35a)$$

$$Z = \iint p(x,y,z)\, dy\, dx \qquad \ldots\ldots(2.1.35b)$$

$$M = \iint p(x,y,z)\, x\, dy\, dx - \iint p(x,y,z)\, z\, dy\, dz \qquad \ldots\ldots(2.1.35c)$$

The calculation of the linearised pressure from equations (2.1.32b) and (2.1.34) is now considered.

Lunde has shown (89) that after integration over suitable contours, the third term of equation (2.1.32b) degenerates into monotonic and oscillatory terms. Following Bessho (84) we denote these terms as follows:

$$\phi = \phi_o + \phi_\ell + \phi_\omega \qquad \ldots\ldots (2.1.36)$$

where ϕ_o is the potential due to the source and image sink

ϕ_ℓ is the potential due to the monotonic term

ϕ_ω is the potential due to the oscillatory term.

We assume that the simple source strength m may be generalised to a surface source distribution of density σ :

$$m = \int_S \sigma\, dS \qquad \ldots\ldots (2.1.37)$$

Defining a pressure coefficient C_p as

$$C_p = p(x,y,z)/\rho V^2 \qquad \ldots\ldots (2.1.38a)$$

and noting in passing that the dynamic pressure head is given by

$$\zeta(x,y,z) = C_p/K_o \qquad \ldots\ldots (2.1.38b)$$

we may write, from equations (2.1.36) and (2.1.38a)

$$C_{P_{TOT}} = C_{Po} + C_{P\ell} + C_{PW} \qquad \ldots\ldots (2.1.39)$$

where

C_{PO} = pressure coefficient arising from the body sources and sinks i.e. the zero wave pressure system

$C_{P\ell}$ = pressure coefficient arising from a local, symmetrical disturbance around the body, i.e. the local wave pressure system

C_{PW} = pressure coefficient arising from an oscillatory disturbance about the body, i.e. the free wave pressure system. (See fig. 5).

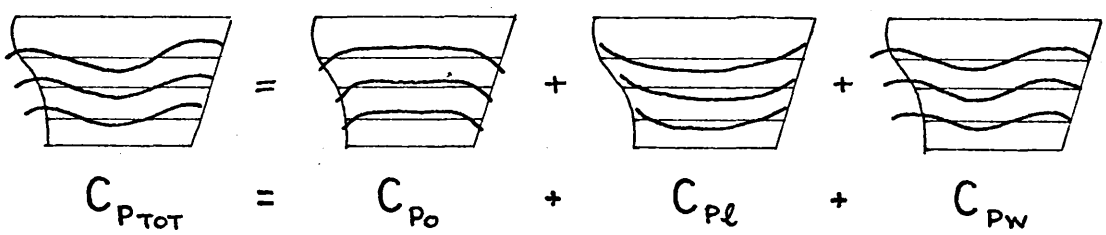

FIG. 5

It may be shown (12, p.520) that only C_{PW} contributes to R_W and, if the vessel is symmetrical about the plane x = o, C_{PW} is the only contribution to the trimming moment. All three components of the pressure system contribute to the vertical force, Z. i.e.

$$C_W = \frac{R_W}{\frac{1}{2}\rho S V^2} = \frac{2}{S}\iint C_{PW}(x,y,z)\,dy\,dz \qquad \ldots\ldots (2.1.40a)$$

$$C_Z = \frac{Z}{\frac{1}{2}\rho S V^2} = \frac{2}{S}\iint C_{P_{TOT}}(x,y,z)\,dy\,dx \qquad \ldots\ldots (2.1.40b)$$

$$C_M = \frac{M}{\frac{1}{2}\rho S L V^2} = \frac{2}{SL}\left\{\iint C_{P_{TOT}}(x,y,z)\,x\,dy\,dx - \iint C_{P_{TOT}}(x,y,z)\,z\,dy\,dz\right\}$$

$$= \frac{2}{SL}\left\{\iint C_{PW}(x,y,z)\,x\,dy\,dx - \iint C_{PW}(x,y,z).z\,dy\,dz\right\}$$

IF $y(-x,z) = y(x,z)$

$\ldots\ldots (2.1.40c)$

where S is a representative area (taken as the surface area of the body) and L is a representative length (taken as the length of the body)

Therefore as $Ko \rightarrow o$ and as $Ko \rightarrow +\infty$, C_W and $C_M \rightarrow o$ for a symmetrical model, whereas C_Z tends to a <u>finite</u> value both as $Ko \rightarrow o$ and $Ko \rightarrow \infty$. This follows from the discussion of the limiting values of the potential derived in section 2.1.4. Also, as $V \rightarrow o$ ($Ko \rightarrow \infty$) the pressure distribution corresponds to that of a double or reflex body in an infinite fluid.

Thus we may calculate the hydrodynamic force and moment coefficients from equations (2.1.40), using the linearised pressure/velocity potential relation (2.1.34) and the linearised velocity potential (2.1.32). Before we can do this for any specific body, it is necessary to find some means of representing the body in the flow.

2.2 REPRESENTATION OF THE BODY IN THE FLOW.

We assume the body to be representable by some distribution of singularities (usually sources, sinks or doublets) and distinguish between two approaches to the problem : One attempting to find a singularity distribution from a knowledge only of the shape of the body (the Direct Method), the other starting with a known singularity distribution and then deducing the body which this represents (the Inverse Method).

2.2.1. The Direct Method

It is usual to assume a surface source distribution of density σ distributed over the body surface. All that is known about the body is the shape of its surface and this seems the obvious place upon which to distribute sources.

If the total outward normal flow from the body surface S be denoted by $\partial\phi/\partial w$ the following condition must hold on S :

$$\frac{\partial\phi}{\partial w} = l\frac{\partial\phi}{\partial x} + m\frac{\partial\phi}{\partial y} + n\frac{\partial\phi}{\partial z} \qquad \ldots\ldots (2.2.1)$$

where l,m,n are the direction cosines of the normal.

From equations (2.1.26) and (2.1.37) we find the fundamental relationship for the potential of a surface source distribution :

$$\phi = \int_S \frac{\sigma}{r}\, dS \qquad \ldots\ldots (2.2.2)$$

We may now derive an integral equation for σ by finding the normal derivative of equation (2.2.2) and substituting it in equation (2.2.1). It has been shown (92) that as S is approached the integral (2.2.2) becomes singular and its principal part, $-2\pi\sigma$ must be extracted. Physically this corresponds to the contribution of the two-dimensional source density to the local normal velocity. The contribution of the remainder of the surface to the local normal velocity is given by the derivative of an integral of the form (2.2.2) evaluated on S. Hence on the body

surface the condition is

$$\frac{\partial \phi}{\partial n} = -2\pi\sigma + \int_S \frac{\partial}{\partial n}\left[\frac{1}{r}\right]\sigma \, dS \qquad \ldots\ldots (2.2.3)$$

Inserting this in equation (2.2.1) gives the integral equation for σ :

$$-2\pi\sigma + \int_S \frac{\partial}{\partial n}\left[\frac{1}{r}\right]\sigma \, dS = l\frac{\partial \phi}{\partial x} + m\frac{\partial \phi}{\partial y} + n\frac{\partial \phi}{\partial z} \qquad \ldots\ldots (2.2.4)$$

A numerical scheme for solving equation (2.2.4) is given by Smith and Hess in ref. 45 in which the body surface is approximated by a large number of plane elements over each of which σ is assumed to be constant.

We summarise the Direct Method by noting :

i) The body surface S is given.

ii) A surface source distribution of density σ is distributed on this surface.

iii) An integral equation in σ is formed from consideration of the boundary conditions on S (The Kinematic Boundary Condition).

Thus we have ensured that the velocity distribution over the body is correct and all stream particles remain tangential to S.

2.2.1.a. <u>The Michell - Havelock Approximation to the Direct Method</u>.

We assume a complete linearisation of the problem and distribute the sources over the plane y = o. By doing this we have

$$\frac{\partial \phi}{\partial n} = \frac{\partial \phi}{\partial y}$$

and from equation (2.1.15)

$$\frac{\partial \phi}{\partial w} = V \frac{\partial \eta}{\partial x} \qquad \ldots\ldots (2.2.5)$$

on $y = o$

Substitution of equation (2.2.5) into equation (2.2.3) gives

$$\sigma = -\frac{V}{2\pi} \frac{\partial \eta}{\partial x}\bigg|_{y=o} \qquad \ldots\ldots (2.2.6)$$

where $y = \pm \eta(x, z)$

Linearisation is now complete. The linear boundary condition (2.1.15) is satisfied and we have distributed sources over the centreline plane. (As stated above, this last is a consequence of linearisation.) Because of this, expression (2.2.6) is only valid for very fine bodies where $\frac{\partial \phi}{\partial z} \cdot \frac{\partial \eta}{\partial z}$ may be neglected and is only exact when $\frac{\partial \phi}{\partial y} = \frac{\partial \phi}{\partial w}$ i.e. a plank of zero beam. However, $\frac{\partial \phi}{\partial z} \cdot \frac{\partial \eta}{\partial z}$ is in general fairly small, except near the bow where it may become appreciable.

2.2.1.b. Havelock's Approximate Method.

Havelock showed (12. p.500) that it was possible to represent the body using a number of discrete sources instead of continuous distribution. Subdividing the body lengthwise, sources were located on the centreline plane. The depth and longitudinal position of each source were determined from a consideration of the relevant transverse areas and volumes. Consideration of the outflow of fluid from the sources through elementary areas of the hull surface gave the appropriate source strengths.

Lunde (93) extended this method by transverse as well as longitudinal subdivision of the body (in this case the hull of a destroyer) and found very good agreement between calculated wave resistance and the wave resistance deduced from tests at high speed. It is worth noting in passing that this method is ideal for determining the source distributions for non-mathematical forms ; with

greater subdivision, the distribution will become approximately continuous.

2.2.2. The Inverse Method.

Inui (25,P.186-192) investigated the Michell-Havelock approximation to $\sigma(x)$ in great detail. After a lengthy investigation he concluded, as might have been inferred, that it was unsatisfactory.

Assuming a polynomial surface source distribution on the plane $y = o$, he was able to calculate polynomial coefficients from relationships between the body surface streamline $\Psi = 0$ (where Ψ is the stream function of the flow) and the shape of the waterplane. Two-dimensional bodies were investigated and Inui's principal findings for one such form were :

i) The Michell-Havelock value of $\sigma(x)$ was numerically greater at the bow and stern than Inui's value.

ii) Inui's $\sigma(x)$ was curved compared to the straight line of the Michell-Havelock approximation.

iii) The Michell-Havelock value of $\sigma(x)$ is much smaller as the midsection is approached.

These findings are shown in fig. 6.

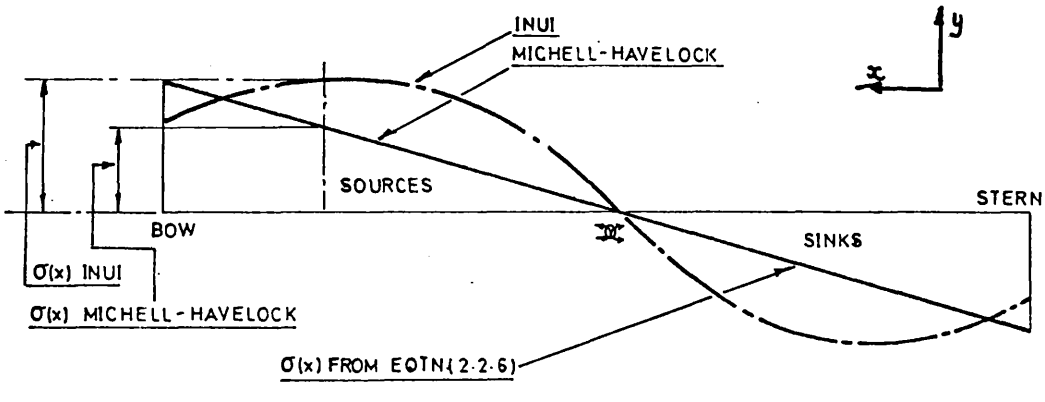

INUI'S INVESTIGATION OF THE SOURCE DISTRIBUTION $\sigma(x)$ APPROPRIATE TO THE FORM $y = b(1 - x^2)$

FIG. 6

Waterlines were calculated from the two different source distributions for the body and they were found to differ as a consequence of the findings listed above. The waterlines calculated

using Inui's values of $\sigma'(x)$ were deficient in beam amidships compared to the Michell-Havelock model (from (iii) above). Inui's waterlines were also fuller at bow and stern (from (i) above).

Wave resistance was calculated for the Inui and Michell-Havelock approximations and it was noted that, at high Froude Numbers, Inui's approximations gave the greater values, this trend being reversed at low Froude Numbers.

It is interesting to note that the smaller the beam-length ratio of Inui's forms, the nearer is his approximation to that of Michell-Havelock. This is to be expected, as the Michell-Havelock approximation to the source distribution becomes increasingly accurate as the beam tends to zero, as shown in section 2.2.1.a.

After this investigation Inui embarked upon the Inverse Method of relating a given hull to a surface source distribution, using streamline tracing techniques.

2.2.2.a. Streamline Tracing

A surface source distribution over a plane (which will lie within the resultant hull surface) is chosen at the outset. Streamlines corresponding to this distribution in a uniform flow V are then calculated from a numerical solution of the differential equations :

$$\frac{dx}{V+u} = \frac{dy}{v} = \frac{dz}{w} \qquad \ldots\ldots (2.2.7)$$

(ref. 9, p19) where u, v and w are related to a velocity potential as in equation (2.1.4).

Inui made an assumption regarding the velocity potential ϕ which is fundamental to the remainder of his reasoning. It is readily

seen (and has been shown in practice - ref. 94) that if equation (2.1.32) is taken for the velocity potential, any body generated from a solution of equations (2.2.7) will have a shape which is dependent on Froude Number. To overcome this, Inui assumed the velocity potential to be given by the limiting case (2.1.33 b) as $Ko \rightarrow \infty$ i.e., as the Froude Number tended to zero. This made the body shape independent of Froude Number at the cost of tacitly assuming the free surface to remain plane and obey the condition

$$\left.\frac{\partial \phi}{\partial z}\right|_{z=0} = 0$$

as discussed in section 2.1.4 b.

Equations (2.2.7) were solved by the Runge-Kutta method on a high-speed digital computer and the resultant streamlines plotted. A lines plan was then drawn as an envelope of these streamlines. Bodies derived in this way are termed Inuids.

2.2.2.b. The Inuid S 201

The body which is the object of the following investigation is a particular form of Inuid generated from the following straight-line source distribution :

$$\sigma = \frac{a_1 V}{4\pi} \cdot \frac{x}{\ell} \qquad -1 \leq x/\ell \leq +1 \qquad \ldots\ldots (2.2.8)$$

$$= 0 \qquad \text{ELSEWHERE.}$$

where the hull has length 2ℓ. For the Inuid S201, $a_1 = 0.8$ and is related to the beam-length ratio (25, p.194).

Details of the numerical procedures for generating this body are given by Inui in reference 25 and Sharma in reference 53.

2.2.3. The Validity of the Direct & Inverse Methods when used with the Linearised Wave Resistance Integrals.

The Direct and Inverse methods discussed above are summarised in fig. 7 and compared in Table 1.

FIG. 7.

DIRECT METHOD.

SMITH AND HESS.

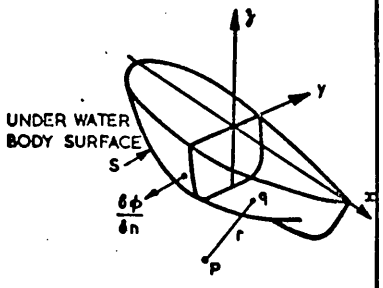

SOURCES DISTRIBUTED OVER S

SOLVE:

$$\frac{\delta\phi}{\delta n} = -2\pi\sigma(q) + \int_S \frac{\delta}{\delta n}\left[\frac{1}{r(P,q)}\right]\sigma(q)\,dS$$

ON S

MICHELL-HAVELOCK

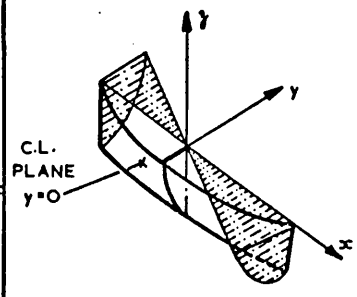

SOURCES DISTRIBUTED OVER C.L. PLANE, $y = 0$

SOLVE: $\sigma(x) = -\frac{V}{2\pi}\frac{\delta f}{\delta x}$ ON $y = 0$

(HALF HULL, $y = f(x, z)$ SHOWN FOR CLARITY.)

HAVELOCK

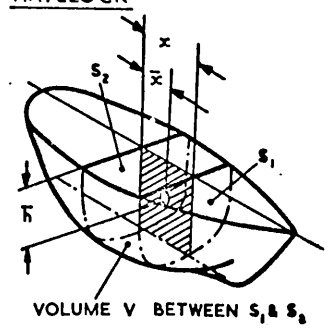

SOURCES DISTRIBUTED THROUGHOUT SUBDIVIDED HULL

SOLVE: $\sigma(\bar{x}) = \pm\frac{(S_2 - S_1)V}{4\pi}$

$$\bar{x} = \frac{V - S_1 x}{S_2 - S_1}$$

$\bar{h}$ = CENTROID OF AREA S_2-S_1

SEE REF. 12 P. 500.

INVERSE METHOD.

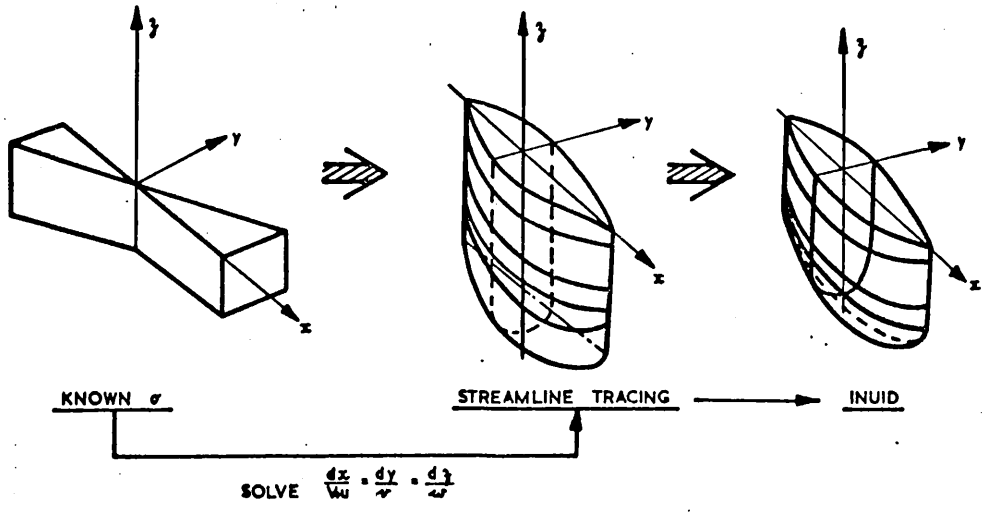

DIRECT AND INVERSE METHODS OF RELATING HULL FORMS AND SURFACE SOURCE DISTRIBUTIONS.

DIRECT METHOD	INVERSE METHOD
1. BODY SURFACE S KNOWN INITIALLY	1. BODY SURFACE S UNKNOWN
2. SOURCE DISTRIBUTION UNKNOWN INITIALLY	2. SOURCE DISTRIBUTION KNOWN INITIALLY
3. SOURCES DISTRIBUTED ON S BODY SURFACE	3. SOURCE DISTRIBUTION NOT ON S IN GENERAL
4. BODY SURFACE CONDITION FULFILLED	4. BODY SURFACE CONDITION FULFILLED
5. BODY STREAMLINES $\Psi = 0$ ON SAME SURFACE AS σ	5. BODY STREAMLINES NOT ON SAME SURFACE AS σ
6. STAGNATION POINT KNOWN	6. STAGNATION POINT CALCULATED
7. INTEGRAL EQUATION IN σ TO BE SOLVED	7. DIFFERENTIAL EQUATION IN σ TO BE SOLVED
8. CAN DEAL WITH DISCONTINUITIES - SHARP BOWS ETC.	8. GENERALLY CANNOT DEAL WITH DISCONTINUITIES WITHOUT INCREASE IN COMPLEXITY.

COMPARISON OF DIRECT AND INVERSE METHODS

OF RELATING SOURCE DISTRIBUTION AND HULL FORM

TABLE 1

It is important to note that when either the Inverse or Direct Methods are employed, the body surface condition (either linear or non-linear) is always completely satisfied. In other words, the flow is always wholly tangential to the body surface. In particular, the Inverse Method ensures that the full non-linear body surface condition - equation (2.1.8 b) is satisfied exactly.

However, Inui calculated the wave resistance for such a form from a linear theory and then applied semi-empirical correction factors to force theory and experiment into agreement. As stated by Tuck (49), there is no a priori reason why agreement between theory and experiment should be improved for a part non-linear/part linear treatment of the problem. In fact it would appear from reference 49 that complete fulfilment of the free surface condition is more important than complete fulfilment of the body surface condition. Moreover, Tuck found that when a higher order free surface condition was applied, a closed body was not generated when streamline tracing techniques were adopted.

Eng and Breslin (46) adopted the accurate Direct Method of Smith and Hess. Again they found that the combination of the exact, non-linear, body surface condition with approximate linear wave-resistance integrals gave poorer agreement between theory and experiment than the wholly consistent linearised Michell approach.

The writer therefore concluded that a wholly linear treatment of the problem was preferable to a partial non-linear one. This became apparent when calculations were performed for the vertical hydrodynamic force acting on the Inuid S201 (see section 2.3).

Nevertheless Inuid S201 was chosen for the following investigation because :

i) It was the subject of extensive investigations by both Inui (25) and Sharma (53).

ii) It was possible to complete a geosim series with Inui and Sharma's models by a suitable choice of model length.

iii) Prompted by wave resistance calculations for the Inuid S201 using the Michell-Havelock theory, (performed by Dr. G.E. Gadd of Ship Division, National Physical Laboratory,) it was felt it would be interesting to apply a wholly linear calculation to the form and compare it with Inui's partial non-linear treatments.

Unfortunately, the Inuid was subject to the following defects :

i) It has a pronounced 'rocker' to the keel.

ii) The bow and stern endings are rounded with infinite values of $\partial y/\partial x$ at $x = \pm \ell$. This fact was pointed out and investigated thoroughly by Sharma (53, p.220-224).

iii) There was pronounced flow separation at high Froude Numbers.

2.3. HYDRODYNAMIC FORCES ACTING ON INUID S201

Expressions for the hydrodynamic forces acting on Inuid S201 are now derived in more detail. Remembering the assumption that sources are distributed on the plane y = o with surface source density given by equation (2.2.6) we have from equations (2.1.32b) and (2.1.34) the pressure coefficient, C_{PTOT} at a point (x,o,z) due to a source at (h,o,-f) :

$$C_{PTOT}(x,o,z) = \frac{(x-h).m}{[(x-h)^2+(z+f)^2]^{3/2}} - \frac{(x-h).m}{[(x-h)^2+(z-f)^2]^{3/2}}$$

$$+ \frac{i\kappa_o m}{\pi}\int_{-\pi}^{\pi} \sec\theta\, d\theta \int_0^{\infty} \frac{e^{-\kappa(f-z)+i\kappa(x-h)\cos\theta}}{\kappa-\kappa_o\sec^2\theta+i\mu\sec\theta}\kappa\, d\kappa \qquad (2.3.1)$$

where, in (2.1.32b) (x-h) has been substituted for x. We now use equations (2.1.37) and (2.2.6) to obtain

$$m = \int_S \sigma\, dS = -\frac{V}{2\pi}\int_{-\ell}^{\ell} dh \int_0^d \frac{\partial\eta}{\partial h}\cdot df \qquad \ldots\ldots (2.3.2)$$

for a hull of length 2ℓ, draft d and surface equation $y = \pm\eta(x,z)$.

Lunde has shown (89) that the third term in equation (2.3.1) may be reduced to the following form after integration over suitable contours letting $\mu \to o$:

$$-8\pi\kappa_o\int_0^{\frac{\pi}{2}} e^{-\kappa_o(f-z)\sec^2\theta}\cos[\kappa_o(x-h)\sec\theta]\sec^3\theta\, d\theta$$

$$+ 8\int_0^{\frac{\pi}{2}} \sec\theta\, d\theta \int_0^{\infty} \frac{e^{-m|x-h|\cos\theta}[\kappa_o\sec^2\theta\sin m(f-z) - m\cos m(f-z)]\, m\, dm}{\kappa_o^2\sec^4\theta + m^2}$$

$\ldots\ldots$ (2.3.3)

The first integral in equation (2.3.3) arises from the pole of the integrand and the second integral from integration along the imaginary axis. Physically, the first integral in (2.3.3) is oscillatory and corresponds to the free wave disturbance whereas the second integral is monotonic in nature and corresponds to the local wave disturbance.

On substitution of equations (2.3.2) and (2.3.3.) into equation (2.3.1.) we have finally,

$$C_{P_{TOT}}(x,o,z) = C_{P_o}(x,o,z) + C_{P_\ell}(x,o,z) + C_{P_\omega}(x,o,z)$$

where

$$C_{P_o}(x,o,z) = \frac{1}{2\pi}\int_{-\ell}^{\ell} d\lambda \int_o^d \frac{\partial y}{\partial \lambda}\frac{(x-\lambda)}{[(x-\lambda)^2+(z+\beta)^2]^{3/2}}d\beta - \frac{1}{2\pi}\int_{-\ell}^{\ell} d\lambda \int_o^d \frac{\partial y}{\partial \lambda}\frac{(x-\lambda)}{[(x-\lambda)^2+(z-\beta)^2]^{3/2}}d\beta$$

$$C_{P_\ell}(x,o,z) = \frac{-4K_o}{\pi^2}\int_{-\ell}^{\ell}\frac{\partial y}{\partial \lambda}d\lambda\int_o^d d\beta\int_o^{\frac{\pi}{2}}\sec\theta\, d\theta\int_o^{\infty}\frac{e^{-m|x-\lambda|\cos\theta}\,[K_o\sec^2\theta\sin m(\beta-z)-m\cos m(\beta-z)]\,m\,dm}{K_o^2\sec^4\theta+m^2}$$

$$C_{P_\omega}(x,o,z) = \frac{4K_o^2}{\pi}\int_{-\ell}^{\ell}\frac{\partial y}{\partial \lambda}d\lambda\int_o^d d\beta\int_o^{\frac{\pi}{2}} e^{-K_o(\beta-z)\sec^2\theta}\cos[K_o(x-\lambda)\sec\theta]\sec^3\theta\, d\theta$$

..... (2.3.4)

The reduction of these integrals and their subsequent numerical calculation is given in Appendix B.

We now substitute these values for C_{PTOT} (x,o,z) into equations (2.1.40) and integrate over the centre plane thus :

$$C_\omega = \frac{2}{S}\int_{-\ell}^{\ell} dx\int_{-d}^{o} C_{P_\omega}(x,o,z)\frac{\partial y}{\partial x}\,dz \qquad \text{..... (2.3.5a)}$$

$$C_z = \frac{2}{S}\int_{-\ell}^{\ell} dx\int_{-d}^{o} C_{P_{TOT}}(x,o,z)\frac{\partial y}{\partial z}\,dz \qquad \text{..... (2.3.5b)}$$

$$C_M = \frac{2}{S.L}\left[\int_{-\ell}^{\ell} dx\int_{-d}^{o} C_{P_\omega}(x,o,z)\,x.\frac{\partial y}{\partial z}\,dz - \int_{-\ell}^{\ell} dx\int_{-d}^{o} C_{P_\omega}(x,o,z)\,z.\frac{\partial y}{\partial x}\,dz\right] \text{(2.3.5c)}$$

where we have utilised the symmetry of Inuid S201 about midships.

Values of $\partial\eta/\partial x$ and $\partial\eta/\partial z$ were obtained from the model offsets and values of $C_{PO}, C_{PW}, C_{P\ell}$ were calculated using the Glasgow University E.E.L.M. KDF 9 digital computer. These pressure coefficients were then integrated over the plane y = o to give the linearised force and moment coefficients.

The moment given by equation (2.1.35c) is made up of two parts, one representing the moment M_V of the vertical component of the pressure force. The second part represents the moment M_H of the horizontal pressure component and may be written

$$M_H = R_w . d' \qquad \ldots\ldots (2.3.6)$$

if R_W acts a small distance d' below the still waterline. It is thus possible to calculate d' from

$$d' = \frac{M_H}{R_w} = \frac{\int_{-\ell}^{\ell} dx \int_{-d}^{0} C_{pw}(x,0,z) . z \frac{\partial y}{\partial x} dz}{\int_{-\ell}^{\ell} dx \int_{-d}^{0} C_{pw}(x,0,z) \frac{\partial y}{\partial x} dz} \qquad \ldots\ldots (2.3.7)$$

It must be pointed out that the calculated moment coefficient C_M is only approximate and was expected to give only qualitative agreement with measurement. This is due to approximations adopted in the theory, and in the frictional contribution to the moment stressed in refs. 59 and 84.

It should be noted that, had the Inui source distribution (equation 2.2.8) for the Inuid S201 been adopted the wave resistance could have been calculated adequately as was done by Sharma and Inui (refs. 25 and 53). It would however, be difficult to calculate the vertical force and trimming moment without a prior knowledge of the body shape. This is because integration over the xy-plane, necessary in equations (2.1.40b) and (2.1.40c), would be impossible unless the values of $\partial\eta/\partial z$ were known in advance.

Using the Michell-Havelock approximation, Inui's source distribution (2.2.8) corresponds to that of a vertical strut with parabolic waterlines and rectangular cross section (see ref. 53 p.229, 238). The xy-surface is now specified. It is, in fact, the

waterplane area, the contribution to the vertical force from the sides of the strut being zero as $\partial\eta/\partial z = 0$ on the body surface (See fig. 8).

Thus the physical significance of Inui's method of relating source distribution and body shape is less obvious than that of the Michell-Havelock approximation. It only seems possible to calculate vertical forces and trimming moments by using Inui's theory in conjunction with Lagally's Theorem. The validity of Lagally's Theorem for surface-piercing bodies is by no means certain ; Bessho (84) found that its use gave results identical to the Michell-Havelock approximation for wave resistance but found large discrepancies between the two theories when vertical forces and trimming moments were considered.

When the vertical force Z and the moment M have been calculated, they may be related to an equivalent mean static sinkage s and trim τ in the usual manner :

$$s = \frac{Z}{\text{LBS TO CHANGE AT REST LEVEL BY 0·10 INCH}}$$

$$\tau = \frac{M}{\text{M.C.T. 1 INCH}} \qquad \ldots\ldots (2.3.8)$$

Values of s and τ were also calculated for a range of speeds.

(The sign convention in use with M and τ is that a positive moment gives a 'bow up' trim.)

FIG. 8

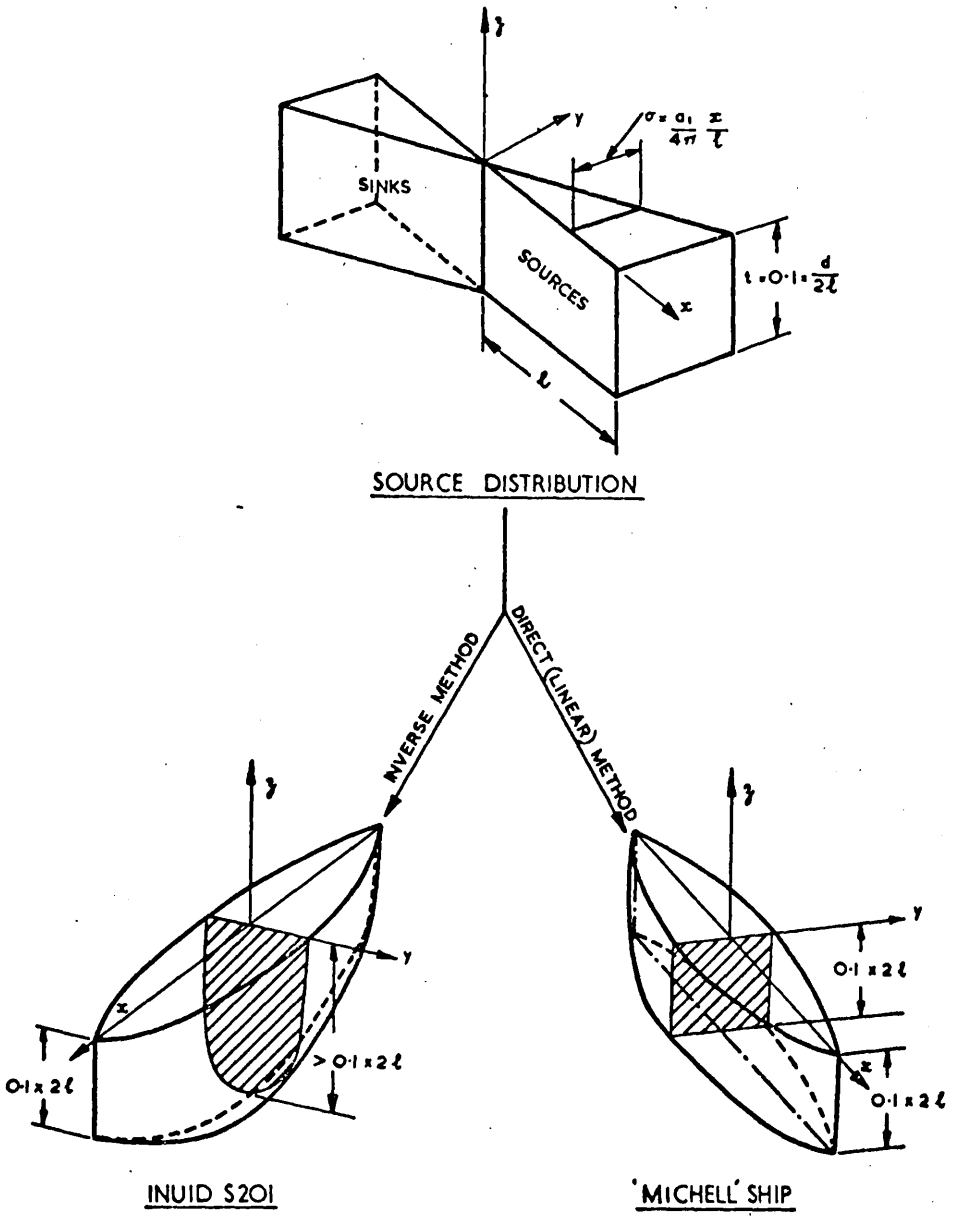

COMPARISON OF HULL FORMS PRODUCED FROM A LINEAR SURFACE SOURCE DISTRIBUTION.

2.4. VERTICAL HYDRODYNAMIC FORCE AND FORM RESISTANCE

2.4.1. Form Resistance

Form resistance for a surface-piercing hull making waves in a viscous fluid is made up of two components (refs. 64 and 65) :

i) Viscous pressure resistance, R_{VP} arising from an unbalance between normal fluid pressures on the forebody and aft body due to the development of a boundary layer.

ii) Friction form resistance R_{ff}. If a two-dimensional surface-piercing plate advances at steady speed V into undisturbed fluid there are tangential shearing forces between the fluid and the surface of the plate. If surface wavemaking is negligible, the local free stream velocity at a point (x,o,z) on the surface of the plate will equal the speed of advance V. The resultant frictional resistance is termed R_{fo}.

The local free stream velocity at a corresponding point (x,y,z) on the surface of a three-dimensional surface-piercing body of the same surface area of the plate will not in general equal V. It will be modified to $V^1 = V + \delta V(x,y,z,V)$ due to the shape of the body and the waves it creates. The tangential shearing forces on the body surface will therefore differ from those on the flat plate. A modification of R_{fo} follows and is called friction form resistance R_{ff}.

It is usual to assume that R_{VP} and R_{ff} are capable of linear supposition, thus :

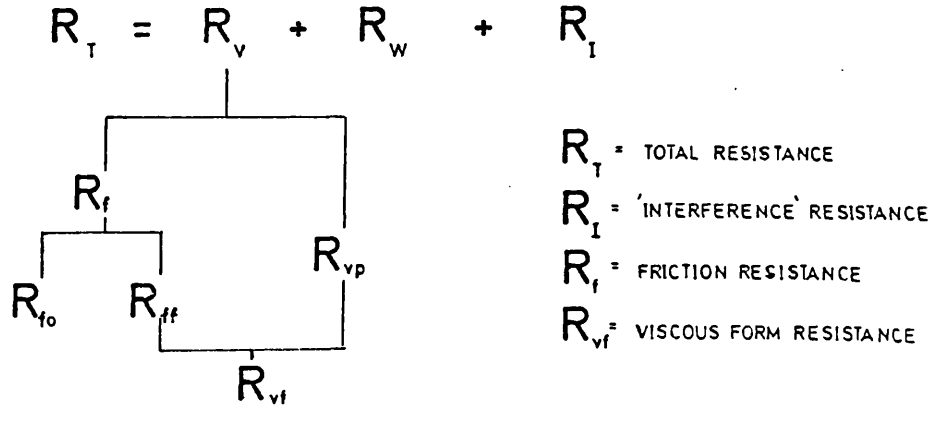

FIG. 9

This breakdown of total resistance into its component parts is an adequate, if simplified, picture. Surface wave-making accompanies a hull in steady motion and this must affect the components of viscous resistance ; the components cannot exist in isolation and their interactions will be important in the extrapolation of model results to full scale, particularly as the gap in size between model and ship increases.

Recent empirical investigations (refs. 59 to 62) have, at the expense of much experimental effort, shown viscous resistance to vary with Froude Number. No satisfactory theoretical explanation of this apparent interaction between viscous and wave-making resistance has been proposed ; form resistance of a surface-piercing hull possibly holds the key to the problem of interdependence and its theoretical study, no matter in how simple a form, would be of interest to corroborate experimental effort and to pave the way, ultimately, to the calculation of ship resistance ab initio. In this way the awkward problem of extrapolation from model to ship might be circumvented.

Investigations of the effect on wave resistance of a boundary layer were performed by Havelock (12. p.528) and more recently by Eng and Breslin (70). Boundary layers may now be calculated, albeit with difficulty, for some three-dimensional forms (95) and Tanaka (96) has studied the problem of form resistance for simple bodies.

The disadvantage of all these methods is that they involve complex numerical and analytical manipulations. A suggestion by Horn (66) that there was a relation between friction form resistance and mean sinkage, exploited later by Havelock (12. p458 and 609), had the advantage of simplicity and afforded a simple empirical (or theoretical) determination of this small but important component of resistance.

2.4.2. Horn's Analysis relating Mean Sinkage to Friction Form Resistance.

Horn's contention was that a value of the mean flow velocity V_M around the hull could be obtained from the mean sinkage s by an application of Bernoulli's Theorem :

$$\rho V^2/2 = \rho V_M^2/2 - \rho g s \qquad \ldots\ldots (2.4.1)$$

$$\therefore V_M = \sqrt{(V^2 + 2gs)} \qquad \ldots\ldots (2.4.2)$$

Assuming that

$$V_M = V + \delta V$$

he showed that

$$\frac{\delta V}{V} = \sqrt{1 + \frac{2gs}{V^2}} - 1 \qquad \ldots\ldots (2.4.3)$$

If it is assumed that the flat plate friction resistance, R_{fo} is given by

$$R_{f_o} = KV^n \qquad \ldots\ldots (2.4.4a)$$

or, more generally,

$$R_{f_o} = \sum_{i=0}^{m} R_i \quad , \quad R_i = K_i V^{n_i} \qquad \ldots\ldots (2.4.4b)$$

we have

$$\frac{\delta R_{f_o}}{R_{f_o}} = n \frac{\delta V}{V} \qquad \ldots\ldots (2.4.5a)$$

from equation (2.4.4a)

$$\frac{\delta R_{f_o}}{R_{f_o}} = \frac{\sum_{i=1}^{m} n_i R_i}{\sum_{i=1}^{m} R_i} \cdot \frac{\delta V}{V} \qquad \ldots\ldots (2.4.5b)$$

from equation (2.4.4b)

We define $\delta R_{fo}/R_{fo}$ as r_{ff} a friction form factor because $\delta R_{fo} = R_{ff}$.

Thus a knowledge of the mean sinkage of a surface-piercing hull enables part of the form resistance to be deduced. Moreover, an equation such as (2.4.5) may be used with theoretical or empirical values of mean sinkage ; an equivalent mean sinkage, calculated from equation (2.3.8) may be used to calculate friction form resistance ab initio.

It may be noted in passing that an important deduction may be made from such a simple analysis. It follows from equations (2.4.3) and (2.4.5) that if s is proportional to the square of the speed V, $\delta V/V$ will be a constant, thus implying a constant form factor r_{ff}. Havelock has shown that at low speeds ($\mathcal{F}<0.1$, $V/\sqrt{L}<0.336$), mean sinkage is in fact roughly proportional to the square of the speed of advance (12, p.458-461).

Nevertheless, such a simplified analysis of this complex problem must yield anomalies. For example

i) Equation (2.4.1) only applies to a single streamline or streamtube and ignores the stream flow over the hull as a whole. In this case s will represent the change in static head at a point on the hull surface and need not be equal to the mean sinkage.

ii) It is known that as speed is increased, mean sinkage will change in sign, being positive at low speeds and negative at high speeds as the pressure over the hull tends to lift it from the water. This implies that at the speed where $s = o$, $\delta V/V$ from equation (2.4.3) must also be zero with a subsequent zero value of friction form factor r_{ff}.

This may in fact happen.

iii) Equations (2.4.3) and (2.4.5) shed no light on possible interaction between wave resistance and viscous resistance.

It was therefore considered advisable to undertake an analysis basically similar to that of Horn's but in closer relationship to the physical causes.

2.4.3. An Extension of Horn's Analysis.

We consider a ship or model moving at steady speed in a free surface, and investigate the stream flow around the hull, as shown in fig. 10. (This stream flow will vary as the speed varies and the attitude of the hull changes but this is accounted for in the following analysis.)

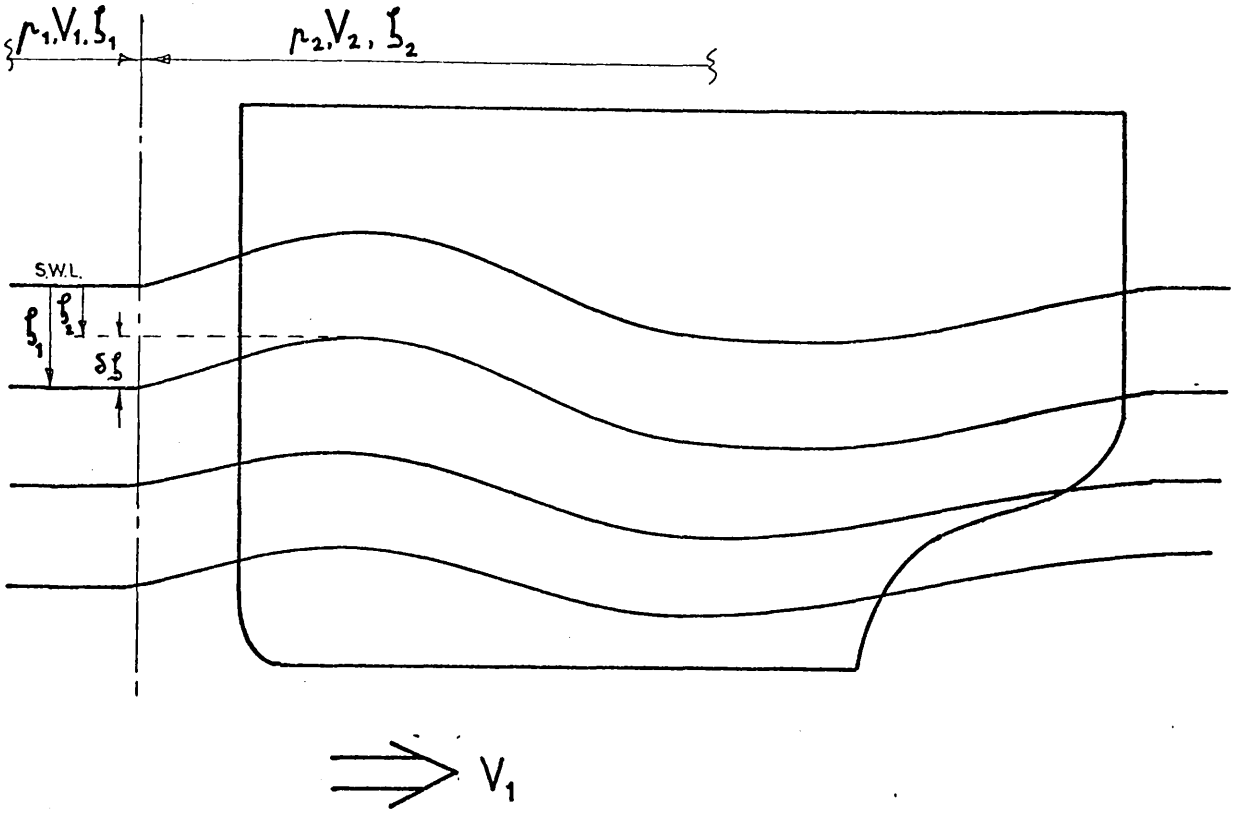

FIG. 10

We assume the vessel to be stationary in a uniform flow of speed V_1.

Applying Bernoulli's Theorem to an arbitrary stream-line we have :

$$\frac{p_1 - p_2}{\rho} + g(\zeta_1 - \zeta_2) = \frac{V_2^2 - V_1^2}{2} \qquad \ldots\ldots (2.4.6)$$

Where subscript 1 refers to the undisturbed flow, and subscript 2 to the disturbed flow. We may rewrite (2.4.6) as

$$\frac{\delta p}{\rho} + g\,\delta\zeta = \frac{(V_2 - V_1)(V_2 + V_1)}{2} \qquad \ldots\ldots (2.4.7)$$

Assuming that $V_2 = V_1 + \delta V_1$, we have

$$\frac{\delta p}{\rho} + g\delta\zeta = \frac{\delta V_1}{2}(2V_1 + \delta V_1) = \frac{\delta V_1}{V_1} \cdot \frac{V_1}{2} \cdot 2V_1\left(1 + \frac{\delta V_1}{2V_1}\right) \qquad \ldots\ldots (2.4.8)$$

We now define $\overline{\delta V_1}$, the mean value of the velocity increments over the hull surface S, as :

$$\overline{\delta V_1} = \frac{1}{S}\int_S \delta V_1 \, dS \quad \text{AND} \quad \overline{\delta V_1}^2 = \frac{1}{S}\int_S \delta V_1^2 \, dS$$

After multiplying equation (2.4.8) through by 1/S and integrating over the hull surface we have :

$$\frac{1}{\rho S}\int_S (\delta p + \rho g . \delta\zeta)\, dS = \frac{\overline{\delta V_1}}{V_1} \cdot \frac{V_1}{2} \cdot V_1 \left(1 + \frac{\overline{\delta V_1}}{2V_1}\right) \quad \ldots\ldots (2.4.9)$$

Clearly, the left hand side of equation (2.4.9) represents the integration over the hull surface S (modified by the wave profile) of the pressure differences due to motion. This will give rise to a resultant force F_R which may be resolved into its component parts : wave resistance R_w and vertical force Z. Re-writing and re-arranging equation (2.4.9) gives :

$$\frac{F_R}{\frac{1}{2}\rho S V_1^2} = \frac{(R_w^2 + Z^2)^{\frac{1}{2}}}{\frac{1}{2}\rho S V_1^2} = (C_w^2 + C_z^2)^{\frac{1}{2}} = \frac{\overline{\delta V_1}}{V_1}\left(1 + \frac{1}{2}\frac{\overline{\delta V_1}}{V_1}\right) \ldots\ldots (2.4.10)$$

Equation (2.4.10) may be further re-arranged to give the following quadratic equation in $\overline{\delta V_1}/V_1$

$$\frac{1}{2}\left(\frac{\overline{\delta V_1}}{V_1}\right)^2 + \frac{\overline{\delta V_1}}{V_1} - (C_w^2 + C_z^2)^{\frac{1}{2}} = 0 \quad \ldots\ldots (2.4.11)$$

which gives

$$\frac{\overline{\delta V_1}}{V_1} = \sqrt{1 + (C_w^2 + C_z^2)^{\frac{1}{2}}} - 1 \quad \ldots\ldots (2.4.12)$$

In the above analysis, the fluid has been assumed to be inviscid, homogenous and irrotational.

If C_w is neglected in equation (2.4.12) we have :

$$\frac{\overline{\delta V_1}}{V_1} = \sqrt{1 + \frac{2Z}{\rho S V_1^2}} - 1 \quad \ldots\ldots (2.4.13)$$

At low speeds

$$Z \simeq \rho g A_w s \qquad \ldots\ldots (2.4.14)$$

where A_w is the load waterplane area. Substitution of equation (2.4.14) into (2.4.13) gives

$$\frac{\overline{\delta V_1}}{V_1} = \sqrt{1 + \frac{2gs}{V_1^2} \cdot \frac{A_w}{S}} - 1 \qquad \ldots\ldots (2.4.15)$$

If equation (2.4.15) is compared with Horn's equation (2.4.3) it is seen that the two expressions differ by the factor A_w/S, the ratio of the water-plane area to the wetted surface area. It is seen that the two expressions are identical if $A_w = S$, i.e. if the "hull" degenerates into a horizontal flat plate.

We note that equations (2.4.12) and (2.4.5) demonstrate the possibility of friction form resistance interacting with wave resistance and vertical force.

The dependence of friction form resistance on vertical force is interesting. It suggests that an alteration of the mean sinkage of a ship or model by suitable hull design might have an effect on this component of resistance.

We note finally that no linearisations have been adopted in the derivation of equation (2.4.12). The only approximations involved are those arising from the assumption of a perfect fluid.

2.5. MODEL EXPERIMENTS.

In order to test the theories outlined in the sections above, model experiments were conducted on the Inuid S201 with the following aims :

i) Measurement of total resistance, mean sinkage and trim over the range of speeds quoted by Sharma (53) and Inui (25).

ii) Measurement of the vertical hydrodynamic force for subsequent comparison with the linearised calculation and mean sinkage measured in i) above.

iii) Measurement of the moment causing trim for subsequent comparison with the linearised calculation and trim measured in i).

iv) Deduction of form resistance from the completion of a three-model geosim series, using the results of Sharma and Inui. A comparison of this form resistance with the calculated values from equation (2.4.12) was also attempted.

The following secondary investigations were also undertaken :

v) A detailed error analysis of both the experimental techniques and the model itself.

vi) A study of the effect on measured trim of the towing point height in the model.

All experimental work was carried out in the Glasgow University Experiment Tank, a complete description of which is given in reference 59. The tank has dimensions 250 ft. by 15 ft. by 8 ft. and is equipped with a carriage spanning the tank carrying the necessary recording and propulsion equipment.

2.5.1. Description of the Model.

A detailed description of the Inuid S201 is given by Sharma in ref. 53, p.229-234.

Sharma re-analysed Inui's calculations to generate the hull (see section 2.2.) and gave a detailed offset table. These offsets were used for the Glasgow model which had a length of 8.60 feet.

This model length was chosen so that the results of the Glasgow model would plot approximately half-way between those of Inui and Sharma on a graph of C_t against $1/\ (\log_{10} R_n - 2)^2$ where

C_t = total resistance coefficient

R_n = Reynold's Number

In this way a three-model geosim series would result.

A body plan of the Inuid S201 is given in figure 11 and a comparison of the three models of the geosim series is given in table 2.

The model itself was constructed of glass-reinforced plastic (G.R.P.) using a wax female mould. After the surface had been finished with four coats of polyurethane yacht enamel, it was burnished to provide a smooth satin finish devoid of brush marks. A grid was drawn on the side of the model with 'Chinagraph' pencil to locate the stations (spaced at L/20), the at-rest water-line and other waterlines at $\frac{1}{4}$ inch intervals for the purpose of wave profile measurement.

Internally the model shell was strengthened by three G.R.P. bulheads, with intermediate ribs. Detachable wooden 'decks' supported ballast in the form of 10 lb. lead weights.

To allow for an anticipated large bow wave at high speeds, a raised forecastle was added to give a freeboard of 9.6 in. forward, there being a freeboard of 4.4 in. elsewhere. At a later stage detachable G.R.P. bulwarks were made to give a uniform 9.6 in. freeboard, these being necessary to prevent swamping of the model after a high speed run. (Plate 4 shows the model with bulwarks fitted.)

2.5.2. Total Resistance, Sinkage and Trim Measurements.

The model was towed from a position 20 inches forward of the aft perpendicular by a thin, high-tensile piano wire attached

FIG.11

INUID S201

LENGTH	8·600 ft.
BEAM	1·056 ft.
DRAFT	0·430 ft. (at perps.)
	0·842 ft. (midships)

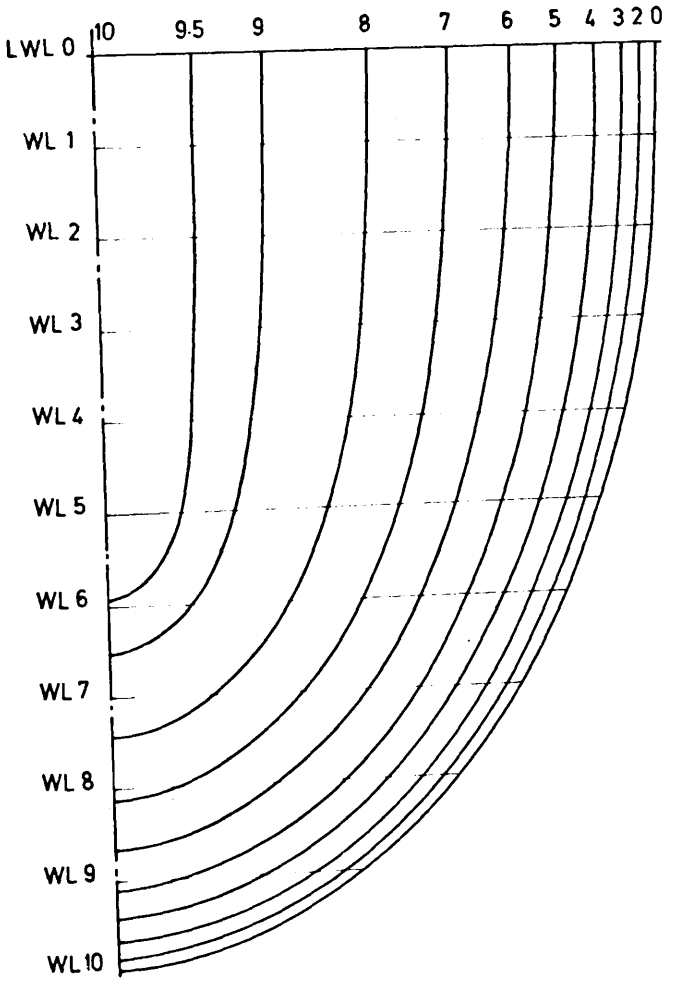

BODY PLAN

DIMENSION	TOKYO	GLASGOW	HAMBURG
L, Length, ft.	5.7400	8.6000	13.1200
B, Breadth, ft.	0.7052	1.0565	1.6118
d, Draft, ft. - at perpendiculars	0.2870	0.4300	0.6560
- amidships	0.5619	0.8415	1.2838
A_W, Load waterplane area, ft^2	-	6.6302	15.4420
A_M, Midship section area, ft^2	0.3152	0.7074	1.6383
∇ , Volume of displacement, ft^3	1.2224	4.1037	14.4870
V.C.B. below load water line, ft.	-	0.3285	0.5011
S , Wetted surface (exact) - ft^2	6.9891	15.7141	36.5330
S_o, " " (approximate) - ft^2	6.9891	15.5629	36.2209
Beam/length ratio	0.1229	0.1228	0.1228
Draft/length ratio - at perpendiculars	0.0500	0.0500	0.0500
- amidships	0.0979	0.0978	0.0978
C_W, Waterplane area coefficient	-	0.7297	0.7299
C_M, Midship section coefficient	0.7950	0.7958	0.7912
C_B, Block coefficient	0.5375	0.5367	0.5331
C_{PH} Horizontal - Prismatic coefficient - C_B/C_M	0.6761	0.6744	0.6738
C_{PV} Vertical - " " - C_B/C_W	-	0.7355	0.7304
$10^3\nabla/L^3$	6.463	6.4517	6.409
$S/\sqrt{\nabla L}$, Taylor surface area coefficient (exact)	2.637	2.645	2.650
$S_o/\sqrt{\nabla L}$, " " " " (approximate)	2.637	2.620	2.627
MCT1", Moment (lbs,ft.) to change trim one inch) at	-	16.578	-
Pounds per 0.1" immersion) L.W.L	-	3.438	-
L.C.B. at design draft	midships	midships	midships
Pitching period, secs.	-	0.860	-
I_L, Longitudinal moment of inertia of W' plane ft^4.	-	27.4954	-

INUID S201 - PRINCIPAL DIMENSIONS AND FORM PARAMETERS - COMPARISON OF TOKYO HAMBURG AND GLASGOW MODELS

TABLE 2

FIG.12.

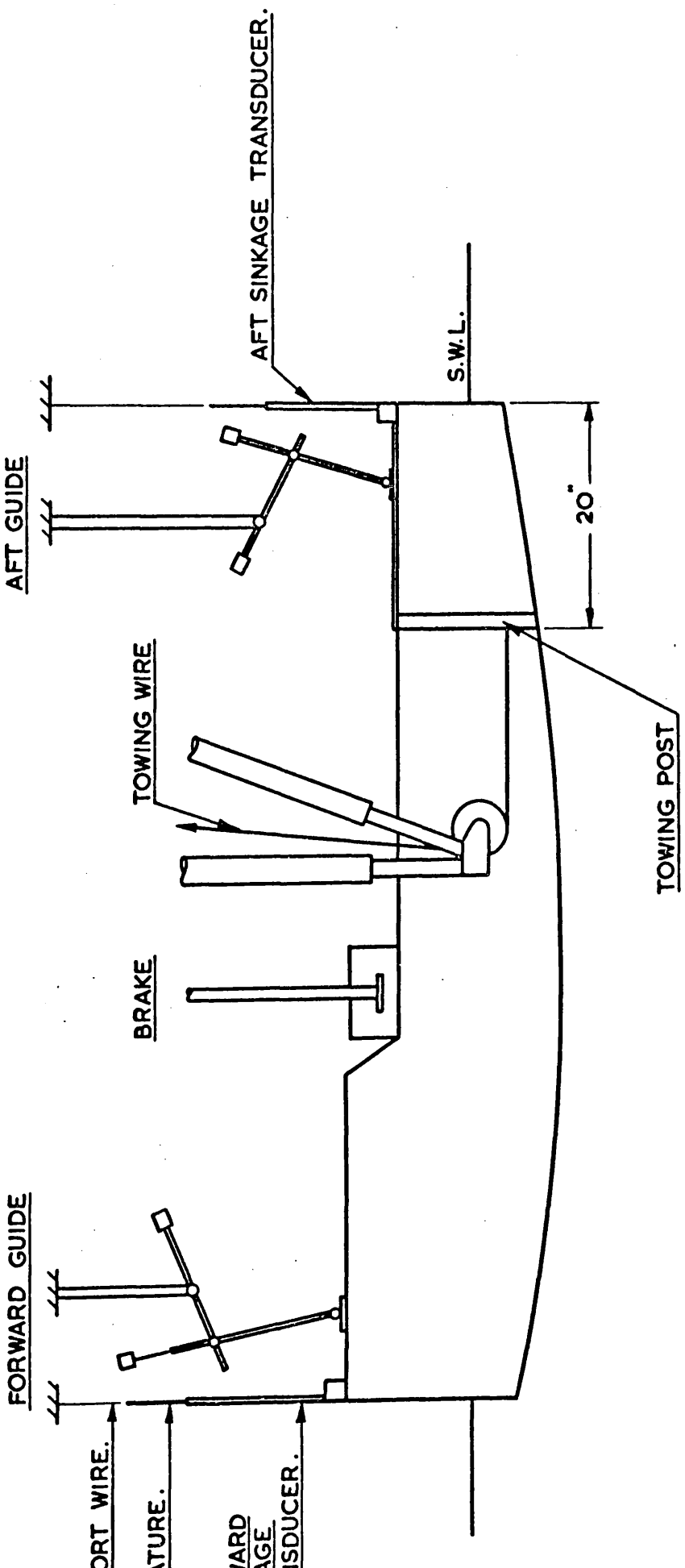

EXPERIMENTAL ARRANGEMENT FOR RESISTANCE, SINKAGE & TRIM TESTS

to the vertical duralumin towing post as shown in figure 12. The point of application of the towing wire was one inch below the at-rest water level.

Total resistance was measured on the standard dynamometer, the out-of-balance force being recorded by a pen on a rotating, paper-covered drum.

Sinkages at the fore and aft perpendiculars were measured by linear displacement transducers on the model, linked to an amplifier, the signal finally being displayed on an ultra-violet recorder.

Calibration of the sinkage transducers was effected by the use of a vernier height gauge attached to the carriage instrument rails as shown in figure 13. This calibration was checked periodically during the experiments and was found to have a negligible variation, being linear over most of the range.

FIG 13

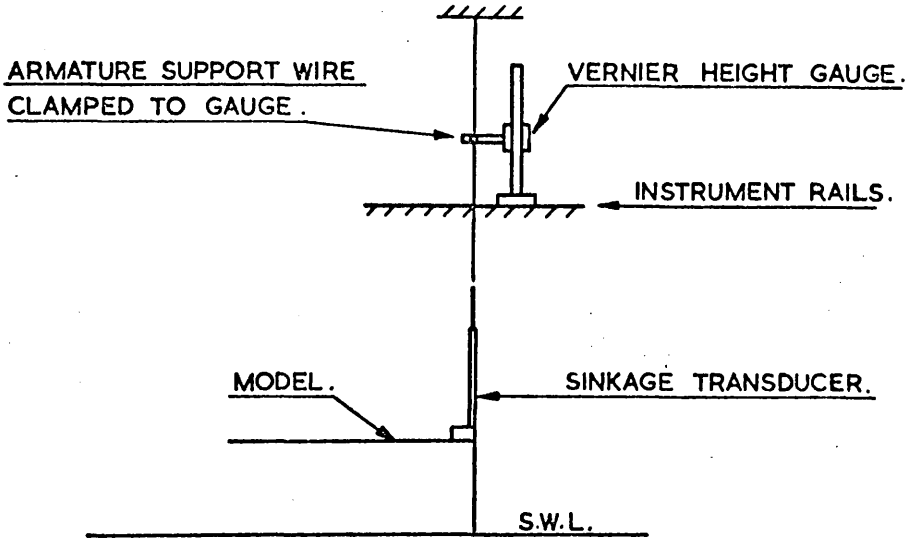

SINKAGE TRANSDUCER CALIBRATION ARRANGEMENT.

Ground speed was measured using an optical method (97) and was controlled by a Ward-Leonard speed control. Digital readings of speed, to three decimal places, were displayed on an electronic digital counter at intervals throughout the run. A mean speed was calculated for each run from the readings of the digital counter. This was an arithmetic mean and was taken over a period when resistance and towing force were well balanced and there was minimum model surge.

The following checks and precautions were also adopted:

i) At the start of each day's running the model surface was wiped to remove any small air bubbles.

ii) Periodic checks were carried out on the static draft and trim of the model.

iii) The standard procedure for measurement of water temperature at the Glasgow Tank was used, i.e., temperatures were measured three times a day at 1 inch intervals in depth down to 4 inches and then at 2 inch intervals to a depth of 12 inches. Interpolation then gave temperatures at one third of the midship draft of the model and further interpolation on a temperature/time-of-day graph gave the temperature for each run.

iv) The effects of temperature difference on water-movement and the resultant 'tide' have been discussed by Ferguson (98). Tide was therefore measured immediately prior to each run on the centreline of the tank at the half-length position. The distance travelled by a float in 100 seconds gave a value for the tide speed and the ground speed was adjusted accordingly to give the speed of the model through the water.

A range of Froude Number of $0.11 \leq \mathcal{F} \leq 0.68$ was chosen and the results are given in table 3 and figures 14 and 15. All the C_t values have been corrected to a standard temperature of $59^{\circ}F$, the speeds having being corrected for blockage using an equation due to Conn (99):

$$\left(\frac{V'}{V}\right)^3 \frac{F_M^2}{2} - \left[1 - \frac{A}{bh} + \frac{F_M^2}{2}\right] \cdot \frac{V'}{V} + 1 = 0 \qquad \ldots\ldots (2.5.1)$$

where

A = mean cross-sectional area of model.

F_H = Froude Depth number = $V/\sqrt{gh}$

b = tank breadth

h = depth of water

V^1 = model speed corrected for back flow δV or $V^1 = V + \delta V$

Wave profiles at various speeds throughout the range were recorded photographically using a camera with remote shutter release and electronic flash. The negatives were ultimately projected to approximately half- full-size and wave profile ordinates were measured to an accuracy of 0.0625 inch.

2.5.2. a. Turbulence Stimulation.

In order to stimulate a turbulent boundary layer, stimulation studs were fitted at 0.05L aft of the forward perpendicular, a practice adopted by Sharma and Inui. For the initial series of tests, studs in common use at the Glasgow Tank were adopted. These were cylindrical studs, 0.125 inches in diameter, projecting 0.1 inch above the surface of the model, spaced 15 mm apart.

Reference to figure 14 shows that the Glasgow total resistance coefficients were in general lower than would have been expected, after interpolation on iso-Froude lines, from the results of both Sharma and Inui. This was thought to be due to laminar flow resulting from a combination of two factors :

i) The Glasgow model was not fitted with the same 'plate' studs as those of Inui and Sharma.

ii) The Glasgow model was made from G.R.P. with an exceptionally good surface finish. Both Sharma and Inui's models were made of wood.

Tagori (100) studied the effect of various shapes of stimulators and provided graphs which enable a suitable stimulator to be designed.

FIG. 14

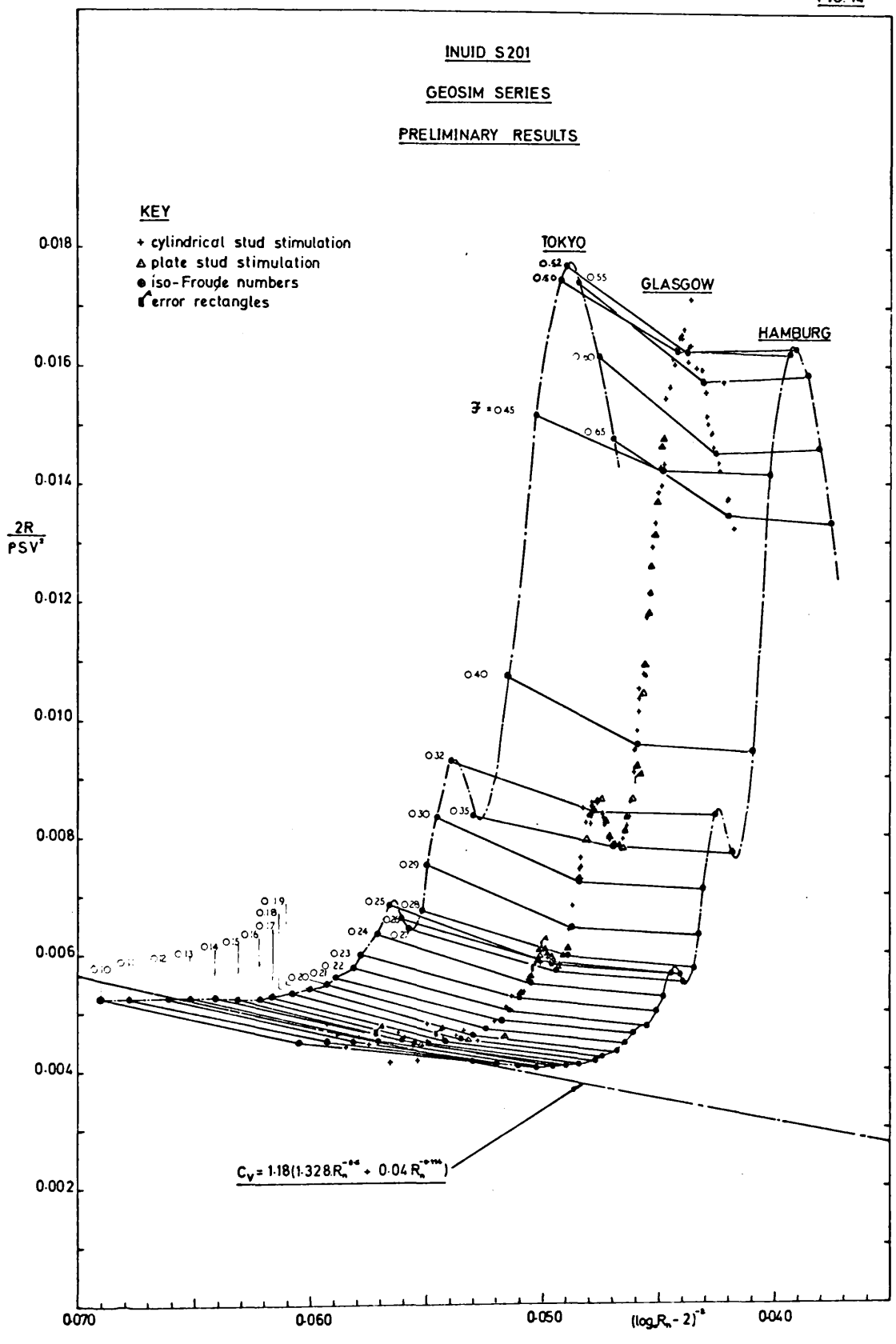
INUID S201
GEOSIM SERIES
PRELIMINARY RESULTS
KEY
+ cylindrical stud stimulation
△ plate stud stimulation
● iso-Froude numbers
error rectangles
TOKYO
GLASGOW
HAMBURG
0.018
0.016
0.014
0.012
0.010
0.008
0.006
0.004
0.002
2R/PSV²
0.070
0.060
0.050
0.040
(log R_n - 2)^-2
C_V = 1.18(1.328 R_n^-0.5 + 0.04 R_n^-0.175)

FIG. 15

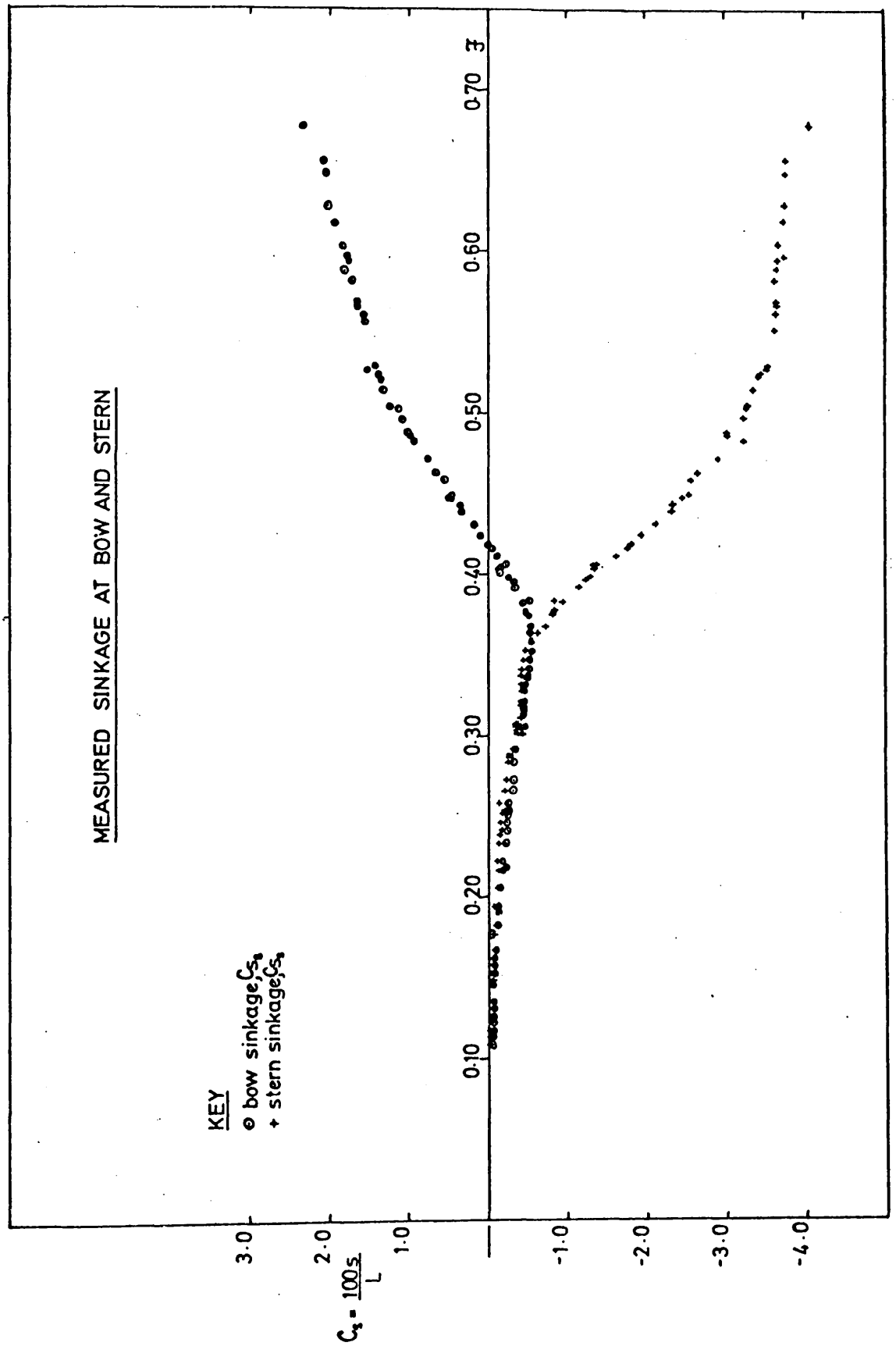
MEASURED SINKAGE AT BOW AND STERN
KEY
o bow sinkage, C_{s_a}
+ stern sinkage C_{s_s}
$C_s = \frac{100s}{L}$
3·0
2·0
1·0
-1·0
-2·0
-3·0
-4·0
0·10
0·20
0·30
0·40
0·50
0·60
0·70
F

Carriage Speed ft/sec	Tide ft./sec.	Resistance lb.	Temp. ^{o}F	Cs Bow	Cs Stern
3.177	-0.012	0.635	60.87	-0.126	-0.111
2.270	-0.010	0.321	60.93	-0.040	-0.046
2.475	-0.006	0.410	61.02	-0.060	-0.041
2.711	-0.013	0.510	61.11	-0.059	-0.060
3.430	-0.007	0.860	61.17	-0.140	-0.119
3.600	-0.002	1.000	61.23	-0.198	-0.133
3.680	-0.002	1.080	61.57	-0.198	-0.113
3.881	-0.010	1.210	61.65	-0.235	-0.159
4.280	-0.006	1.645	61.85	-0.257	-0.159
4.157	-0.002	1.530	61.92	-0.250	-0.192
4.717	-0.015	2.035	62.02	-0.329	-0.278
4.420	-0.017	1.708	61.55	-0.309	-0.206
4.540	-0.005	1.810	61.70	-0.316	-0.239
4.997	-0.005	2.825	61.40	-0.382	-0.318
4.840	-0.017	2.400	61.50	-0.319	-0.311
3.955	-0.017	1.305	61.63	-0.220	-0.151
2.780	-0.005	0.530	61.82	-0.051	-0.093
2.935	0	0.600	62.15	-0.051	-0.095
4.084	-0.005	1.475	62.17	-0.232	-0.154
3.216	-0.010	0.700	62.13	-0.129	-0.094
2.520	-0.003	0.400	62.12	-0.074	-0.040
1.818	-0.005	0.240	62.10	-0.029	-0.029
5.075	-0.006	3.310	62.05	-0.338	-0.331
4.768	-0.010	2.210	60.42	-0.294	-0.292
5.065	-0.007	2.910	60.58	-0.390	-0.404
4.975	+0.002	2.770	60.10	-0.360	-0.384
5.335	-0.002	3.712	60.52	-0.426	-0.431
5.154	-0.015	3.310	60.82	-0.389	-0.404
5.288	-0.012	3.600	61.11	-0.419	-0.424
5.510	-0.011	3.985	61.18	-0.472	-0.418

TOTAL RESISTANCE, SINKAGE AND TRIM RESULTS - CYLINDRICAL STUDS

TABLE 3A

Carriage Speed ft/sec	Tide ft/sec	Resistance lb	Temp. ^{o}F	C_s Bow	C_s Stern
5.407	0	3.810	61.57	-0.456	-0.404
5.270	0	3.460	61.70	-0.404	-0.411
5.850	-0.020	4.060	61.73	-0.559	-0.498
5.652	-0.015	3.950	61.81	-0.522	-0.429
5.758	0	4.000	61.84	-0.538	-0.448
6.026	+0.003	4.330	60.80	-0.538	-0.623
5.938	+0.001	4.194	61.30	-0.548	-0.558
5.579	+0.007	3.970	61.67	-0.509	-0.437
2.625	0	0.500	62.20	-0.096	-0.073
2.410	-0.007	0.400	62.22	-0.069	-0.060
6.366	-0.020	5.240	62.24	-0.529	-0.862
6.223	-0.026	4.735	62.25	-0.506	-0.802
2.017	+0.010	0.285	62.22	-0.053	-0.044
3.026	-0.010	0.631	62.20	-0.140	-0.114
6.110	-0.030	4.460	62.19	-0.547	-0.708
1.935	0	0.250	62.05	-0.057	-0.042
5.035	-0.025	2.908	62.02	-0.370	-0.392
1.900	-0.010	0.250	61.97	-0.053	-0.034
2.166	-0.002	0.331	61.95	-0.068	-0.054
4.202	-0.015	1.605	61.90	-0.272	-0.213
5.330	-0.007	3.668	61.88	-0.437	-0.418
2.120	-0.012	0.300	61.89	-0.066	-0.060
3.983	-0.005	1.332	61.90	-0.237	-0.192
5.576	-0.015	3.895	61.92	-0.507	-0.424
6.244	-0.010	4.819	61.94	-0.488	-0.850
6.336	+0.002	5.068	63.30	-0.450	-0.961
6.483	0	5.790	63.64	-0.351	-1.173
6.217	-0.012	4.725	60.92	-0.503	-0.817
6.548	-0.015	6.140	61.42	-0.331	-1.225
6.720	-0.017	7.178	61.76	-0.182	-1.326
6.615	-0.025	6.320	59.65	-0.279	-1.301

TABLE 3A CONT.

Carriage Speed ft/sec.	Tide ft/sec.	Resistance lb	Temp. ^{o}F	C_s Bow	C_s Stern
6.807	-0.011	7.565	60.00	-0.110	-1.627
7.022	-0.005	9.095	60.08	+0.095	-1.963
6.890	-0.005	7.745	60.16	-0.043	-1.770
6.929	-0.015	8.538	60.16	0	-1.812
7.125	0	9.983	60.12	+0.178	-2.121
7.262	-0.005	10.698	60.02	+0.317	-2.314
7.410	+0.005	11.695	60.24	+0.447	-2.560
7.400	+0.001	11.915	60.55	+0.450	-2.454
6.712	+0.002	7.092	61.13	+0.235	-1.384
7.595	-0.020	12.495	61.34	+0.522	-2.577
7.977	-0.005	15.679	61.74	+0.933	-3.243
7.325	-0.015	11.292	58.00	+0.338	-2.321
7.650	-0.001	13.780	58.00	+0.665	-2.656
8.016	+0.002	15.695	58.04	+0.985	-3.022
8.055	-0.015	16.050	58.21	+1.020	-3.089
8.508	-0.010	18.305	58.43	+1.317	-3.387
8.225	-0.025	16.890	58.17	+1.078	-3.243
8.295	+0.005	17.355	58.57	+1.124	-3.271
8.661	-0.005	18.620	58.77	+1.398	-3.448
8.961	-0.007	19.695	59.12	+1.509	-3.502
8.737	-0.010	18.960	57.69	+1.416	-3.539
9.105	-0.025	20.090	57.72	+1.550	-3.606
9.274	-0.025	20.510	57.77	+1.573	-3.661
9.363	+0.005	20.810	57.85	+1.660	-3.660
9.600	-0.003	21.290	57.94	+1.713	-3.612
9.803	-0.007	21.709	58.00	+1.776	-3.685
6.685	-0.022	6.851	58.06	-0.146	-1.387
7.790	-0.020	14.398	58.13	+0.764	-2.900
8.351	-0.018	17.428	58.22	+1.224	-3.296
9.963	-0.015	22.025	58.60	+1.840	-3.697
10.183	+0.005	22.709	58.77	+1.939	-3.721

TABLE 3A CONT.

Carriage Speed ft/sec	Tide ft/sec	Resistance lbs.	Temp. ^{o}F	C_s Bow	C_s Stern
10.360	-0.015	23.170	57.72	+2.015	-3.751
10.672	+0.025	23.933	57.93	+2.061	-3.764
11.137	+0.010	25.038	58.37	+2.369	-4.074
10.795	0	24.394	58.40	+2.091	-3.772
9.531	-0.010	21.209	58.64	+1.689	-3.660
9.732	-0.020	21.595	58.77	+1.817	-3.642
9.820	-0.007	21.790	58.46	+1.782	-3.757

TABLE 3A CONT.

Carriage Speed ft/sec	Tide ft/sec.	Resistance lbs.	Temp. ^{o}C	C_s Bow	C_s Stern
5.139	-0.001	3.265	12.70	-0.413	-0.418
2.070	+0.015	0.275	13.52	-0.013	-0.040
2.540	-0.001	0.445	13.70	-0.069	-0.072
3.085	-0.040	0.650	13.82	-0.106	-0.103
3.584	-0.021	0.900	13.90	-0.130	-0.187
4.143	+0.005	1.585	13.76	-0.269	-0.199
3.293	-0.010	0.760	13.65	-0.122	-0.126
3.870	-0.035	1.197	13.53	-0.224	-0.180
4.351	0	1.730	13.37	-0.330	-0.230
4.215	0	1.667	13.23	-0.278	-0.199
2.380	-0.014	0.395	12.94	-0.104	-0.107
4.257	-0.007	1.679	12.97	-0.300	-0.218
4.614	-0.011	1.963	13.03	-0.334	-0.262
4.526	-0.020	1.809	13.13	-0.326	-0.272
4.772	-0.001	2.268	13.26	-0.345	-0.322
4.944	-0.006	2.741	13.32	-0.369	-0.364
5.239	0	3.553	13.41	-0.426	-0.406
5.494	-0.011	3.923	13.52	-0.506	-0.387
5.384	-0.010	3.841	13.63	-0.471	-0.418

RESISTANCE, SINKAGE AND TRIM RESULTS - PLATE STUDS

TABLE 3B

Carriage Speed ft/sec	Tide ft/sec.	Resistance lbs.	Temp. ^{o}C	C_s Bow	C_s Stern
5.620	-0.007	4.030	13.75	-0.551	-0.429
5.496	-0.020	4.005	12.75	-0.597	-0.425
5.871	-0.020	4.150	12.85	-0.595	-0.525
5.761	-0.025	4.078	12.91	-0.586	-0.464
5.989	-0.016	4.337	13.10	-0.599	-0.560
6.177	-0.021	4.743	13.20	-0.543	-0.755
6.079	+0.011	4.484	13.40	-0.562	-0.613
6.337	-0.010	5.414	13.52	-0.452	-0.928
6.283	-0.010	5.063	13.62	-0.499	-0.832
6.534	+0.010	6.093	13.76	-0.356	-1.216
6.737	-0.007	7.295	13.81	-0.191	-1.492
6.627	0	6.606	13.91	-0.278	-1.343
6.816	0	7.867	13.91	-0.100	-1.630
7.025	-0.011	9.271	13.30	-	-
6.955	-0.015	8.804	13.32	-	-
7.291	0	11.282	13.33	-	-
7.174	-0.005	10.446	13.35	-	-
7.503	-0.001	12.774	13.41	-	-
7.523	-0.011	12.893	13.50	-	-
7.445	-0.005	12.509	13.67	-	-
7.066	-0.010	9.707	13.83	-	-
5.628	0	4.022	13.54	-0.569	-0.355
4.887	-0.007	2.575	13.57	-0.360	-0.303
4.417	-0.010	1.759	13.67	-0.313	-0.206
3.386	-0.011	0.853	13.72	-0.169	-0.093
3.256	-0.020	0.768	13.75	-0.148	-0.090
2.783	-0.005	0.542	13.76	-0.121	-0.067
2.289	-0.008	0.364	13.82	-0.069	-0.045
2.385	-0.020	0.392	13.84	-0.069	-0.052
1.936	-0.025	0.254	13.86	-0.039	-0.030
3.727	-0.020	1.093	13.87	-0.215	-0.119

TABLE 3B CONT.

FIG. 16

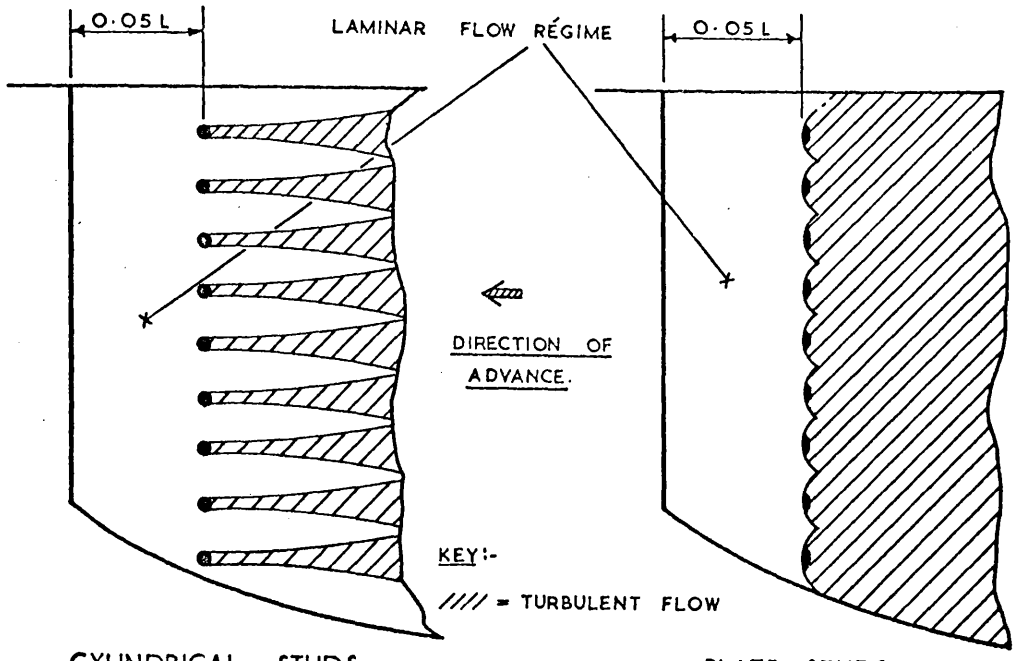

TURBULENCE STIMULATION BY CYLINDRICAL & PLATE STUDS.

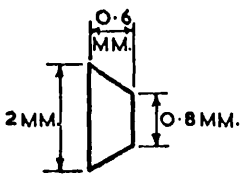

HEIGHT : 0·8 – 1·0MM.
PITCH : 5 – 10MM.

INUI

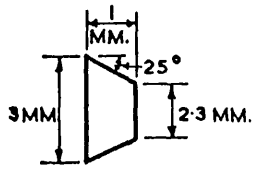

HEIGHT : 1·8 MM.
PITCH : 10 MM.

GLASGOW

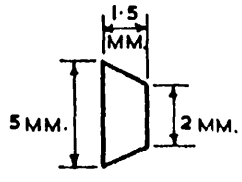

HEIGHT : 1·5MM.
PITCH : 15MM.

SHARMA

PLATE STUDS USED ON INUID GEOSIMS.

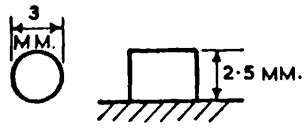

ORIGINAL GLASGOW STIMULATOR.

TURBULENCE STIMULATION.

He noted, moreover, that extensive areas of laminar flow could exist when cylindrical studs were used, these being minimised when other stimulators were adopted. (see fig. 16).

It was found, from Tagori's graphs, that plate studs of dimensions shown in fig. 16 were suitable for stimulating turbulence on the Glasgow model. The position of the studs aft of the bow could not be reconciled with a suitable stud pitch (Pi) from Tagori's recommendations. At this juncture it was appreciated that the problem was not necessarily to obtain complete stimulation, but to get stimulation similar to that of Inui and Sharma. The position of the studs aft of the forward perpendicular was thus fixed and a compromise pitch of 10 mm was chosen.

From ref. (100) the resistance due to these studs alone was 0.009 times the flat friction resistance, R_{fo}, at a Froude Number of 0.10 and 0.0035 R_{fo} at a Froude Number of 0.14. These resistance increments were considered negligible.

Plate studs of the dimensions shown in fig. 16 were made of xylonite and fixed to the model with an impact adhesive. Resistance tests were re-run over the speed range up to a Froude Number of 0.450 and the results are given both in table 3 and figure 14.

All subsequent experiments were run using these studs.

2.5.2. b. Towing Point Tests.

A secondary series of experiments was conducted to determine the effect of towing point height on resistance, sinkage and trim (101).

The towing post shown in figure 12 was modified by the addition of tapped holes, at the positions shown in figure 17,

giving a total variation of 10 inches in the height of the towing point.

FIG17

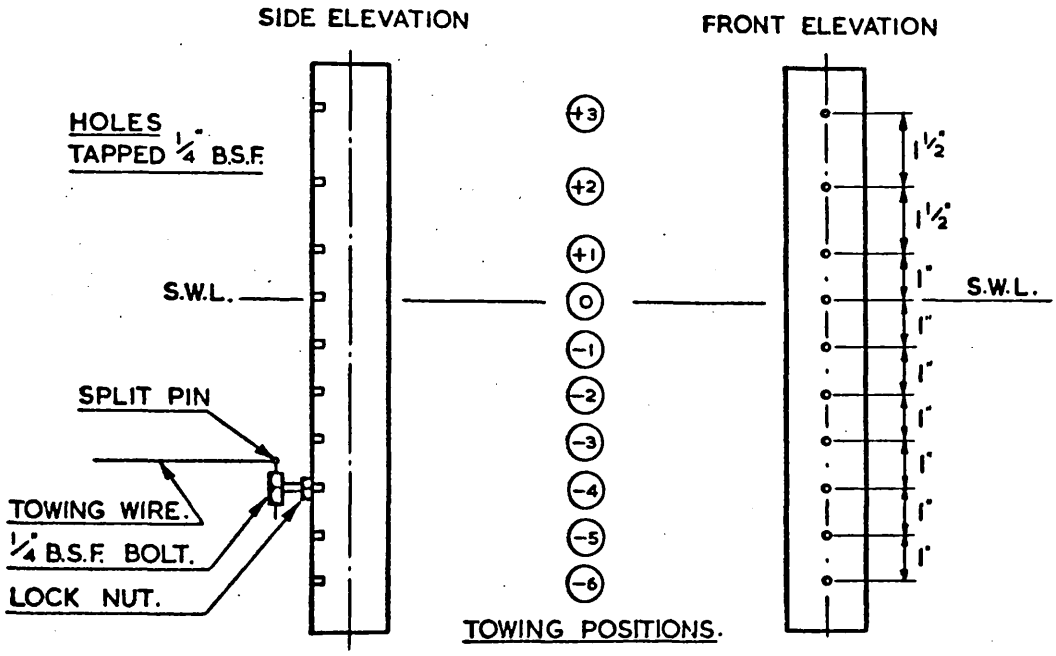

TOWING POST.

Tests were carried out as detailed above for resistance, sinkage and trim. Two speeds were chosen for the test viz. 4.46 ft./sec. (Froude Number of 0.268) and 5.75 ft./sec. (Froude Number of 0.345). These speeds corresponded to the 'flat' portions of the resistance-speed curve, to facilitate balance between applied towing force and resistance.

Tests at a higher speed corresponding to a Froude Number of 0.372 were attempted, but as resistance was changing very rapidly with speed at this point, it was found very difficult to maintain a balance between towing force and total resistance. Tests at this particular speed were abandoned.

Due to changes in the carriage speed calibration and the effect on speed of the 'tide', the model was towed at speeds above and below the desired value at each towing position, the results being interpolated at the appropriate speed. In order to obtain as accurate an interpolation as possible, one of the speeds was chosen

to be close to the desired speed.

A total of 67 runs were made of which 9 gave doubtful or unuseable results and so were rejected. The results of the remaining runs are shown in table 4 and figures 18A to 18D.

The changes in resistance due to varying the towing point height are shown in figures 18A and 18B. Figure 18A appears to have a turning value in the curve at approximately one inch below the still water level. This is not confirmed by results at the higher speed, shown in figure 18B. It is suggested that, as the scatter of experimental spots in Figure 18A is about $\pm 1\%$ of the maximum resistance, and this is the order of accuracy to which the experiments were conducted (See section 2.6), it would be erroneous to draw any firm conclusions from this plotting. If however fig. 18A does show a trend, it would appear that the resistance force vector acts a little below the still water level. This finding is substantiated by pressure measurements over model hulls (see for example, ref. 59).

Mean sinkage and trim results are shown in figures 18C and 18D. There is no significant change in mean sinkage at either speed.

A distinct reduction of trim by the head, corresponding to a lowering of the towing point, occurred at each speed, the reaons for this being well-known. (12, p.523).

From these observations it was concluded that trim measurements can be significantly in error if the wrong towing point height is used. It appeared that the towing height of about one inch below water level, adopted for all resistance, sinkage and trim tests, was probably correct.

2.5.3. Vertical Force Measurements.

Vertical forces at bow and stern were measured over the

MODEL SPEED THROUGH WATER : ft./sec

RESISTANCE : lbs

SINKAGE : inches

TEMPERATURE : °C.

TRIM(BY HEAD) : inches

EXPERIMENTAL RESULTS FOR $\mathcal{F}$ = 0.268

Towing Position	Water Speed	Resistance	Interpolated Resistance	Sinkage F.P.	Sinkage A.P.	Mean Sinkage	Trim By Head	Interpolated Mean Sinkage	Interpolated Trim	Temp.
0	4.278	1.725		0.333	0.215	0.274	0.118			11.28
0	4.551	1.880	1.807	0.354	0.260	0.307	0.094	0.302	0.102	11.28
0	4.370	1.760		0.346	0.235	0.290	0.111			11.29
+1	4.286	1.725		0.332	0.240	0.286	0.092			11.30
+1	4.646	2.038	1.800	0.367	0.285	0.326	0.082	0.291	0.117	11.32
+1	4.442	1.790		0.346	0.227	0.286	0.119			11.35
-1	4.304	1.725		0.324	0.215	0.270	0.109			11.40
-1	4.594	1.935	1.800	0.359	0.275	0.317	0.084	0.296	0.081	11.53
-1	4.446	1.790		0.330	0.260	0.295	0.070			10.73
-2	4.306	1.710		0.300	0.220	0.260	0.080			11.65
-2	4.613	2.030	1.795	0.335	0.305	0.320	0.030	0.293	0.066	11.97
-2	4.458	1.792		0.326	0.260	0.293	0.066			12.15
-3	4.372	1.735		0.315	0.260	0.267	0.055			11.35
-3	4.295	1.746	1.784	0.310	0.250	0.280	0.060	0.291	0.060	11.46
-3	4.525	1.853		0.320	0.265	0.292	0.055			11.46
-3	4.466	1.792		0.320	0.265	0.293	0.055			11.47
-4	4.372	1.752		0.310	0.260	0.285	0.050			12.28
-4	4.512	1.833	1.795	0.315	0.270	0.292	0.045	0.292	0.050	12.23
-4	4.327	1.739		0.315	0.235	0.275	0.080			11.33
-5	4.323	1.738		0.300	0.270	0.285	0.030			11.36
-5	4.526	1.846	1.778	0.310	0.280	0.295	0.030	0.283	0.033	11.37
-5	4.465	1.780		0.300	0.265	0.282	0.035			11.38
-6	4.365	1.760		0.290	0.250	0.270	0.040			11.45
-6	4.563	1.884	1.773	0.310	0.300	0.305	0.010	0.289	0.015	11.52
-6	4.470	1.775		0.300	0.285	0.292	0.015			11.62
+3	4.353	1.752		0.325	0.205	0.265	0.120			11.73
+3	4.563	1.894		0.350	0.240	0.295	0.110			11.86
+3	4.369	1.764	1.787	0.365	0.225	0.295	0.140	0.284	0.126	11.46
+3	4.403	1.769		0.335	0.220	0.277	0.115			11.60
+3	4.495	1.800		0.350	0.220	0.285	0.130			11.65

TOWING POINT TESTS

TABLE 4

EXPERIMENTAL RESULTS FOR $\mathcal{F}$ = 0.245

Towing Position	Water Speed	Resistance	Interpolated Resistance	Sinkage F.P.	Sinkage A.P.	Mean Sinkage	Trim By Head	Interpolated Mean Sinkage	Interpolated Trim	Temp.
0	5.805	4.091		0.600	0.440	0.520	0.160			12.21
0	5.835	4.109		0.575	0.430	0.502	0.145			12.17
0	5.825	4.111	4.077	0.600	0.430	0.515	0.170	0.515	0.150	12.06
0	5.674	4.051		0.565	0.385	0.475	0.180			11.81
0	5.783	4.083		0.530	0.515	0.522	0.015			12.30
0	5.717	4.080		0.582	0.463	0.522	0.119			12.53
+3	5.842	4.151		0.680	0.405	0.542	0.275			12.54
+3	5.720	4.068	4.076	0.550	0.351	0.450	0.199	0.495	0.298	12.54
+3	5.788	4.084		0.660	0.355	0.507	0.305			12.55
+3	5.637	4.050		0.644	0.330	0.487	0.314			12.58
-6	5.908	4.204		0.553	0.536	0.544	0.017			12.62
-6	5.790	4.090	4.072	0.553	0.483	0.518	0.070	0.508	0.073	12.69
-6	5.640	4.050		0.516	0.449	0.487	0.067			12.77
-3	5.932	4.220		0.599	0.511	0.555	0.088			12.82
-3	5.767	4.094	4.085	0.585	0.449	0.517	0.136	0.510	0.135	13.03
-3	5.657	4.042		0.545	0.408	0.476	0.137			13.15
-5	5.912	4.235		0.558	0.543	0.550	0.015			13.27
-5	5.604	4.042	4.074	0.555	0.472	0.513	0.083	0.480	0.080	13.40
-5	5.775	4.085		0.513	0.453	0.483	0.060			12.67
-1	5.884	4.220		0.615	0.474	0.544	0.141			12.67
-1	5.757	4.052	4.065	0.592	0.404	0.498	0.188	0.498	0.189	12.73
-1	5.609	4.033		0.562	0.385	0.473	0.177			12.77
+1	5.903	4.217		0.637	0.453	0.545	0.184			12.87
+1	5.779	4.092	4.076	0.623	0.394	0.508	0.229	0.501	0.230	13.55
+1	5.589	4.027		0.584	0.373	0.478	0.211			12.20

TABLE 4 CONTD.

FIG 18A.

VARIATION OF RESISTANCE WITH TOWING HEIGHT.

SPEED = 4.46 ft/sec., $\mathcal{F}$ = 0.268.

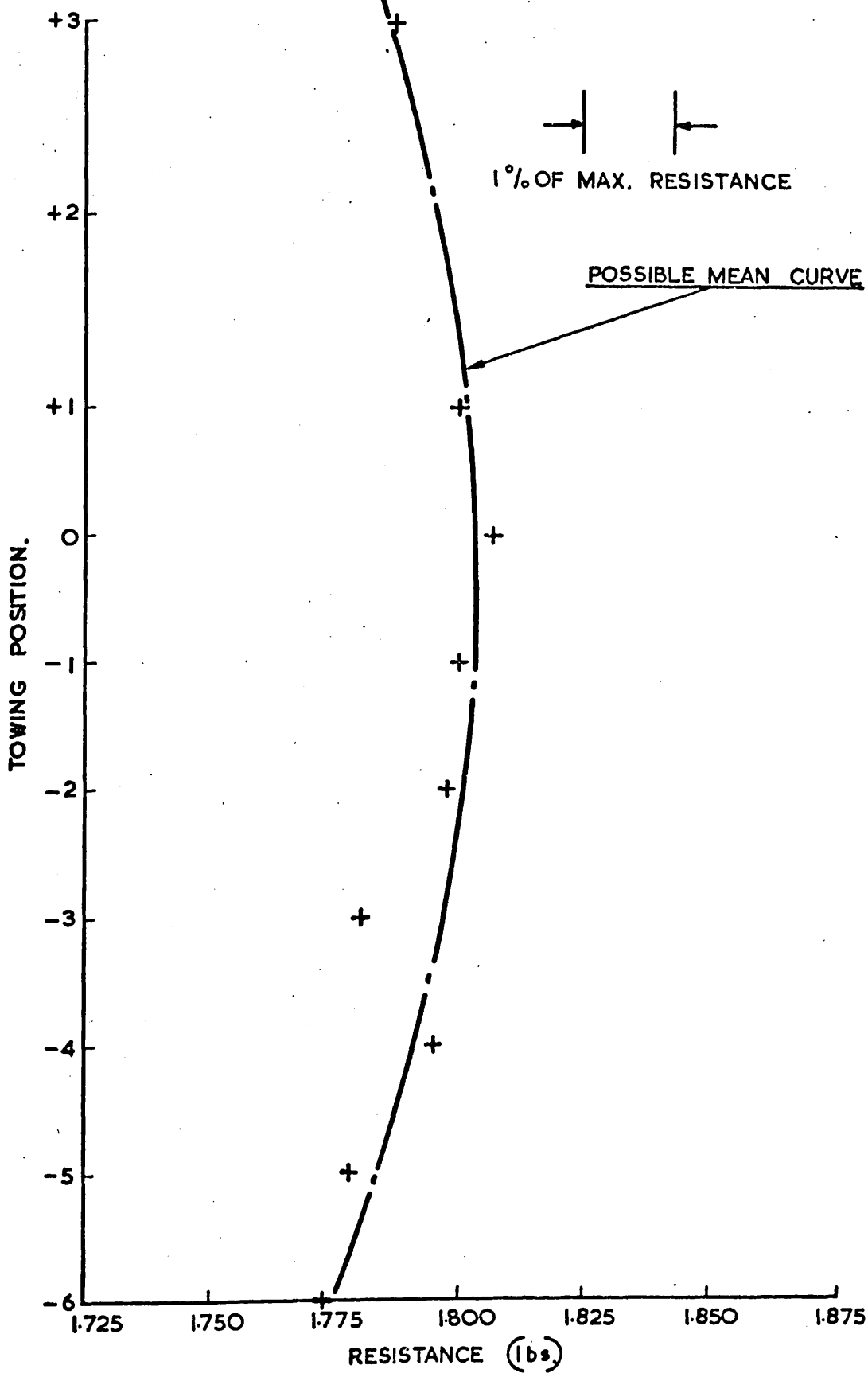

FIG 18B

VARIATION OF RESISTANCE WITH TOWING HEIGHT.

SPEED = 5.75 ft/sec., $\mathcal{F}$ = 0.345

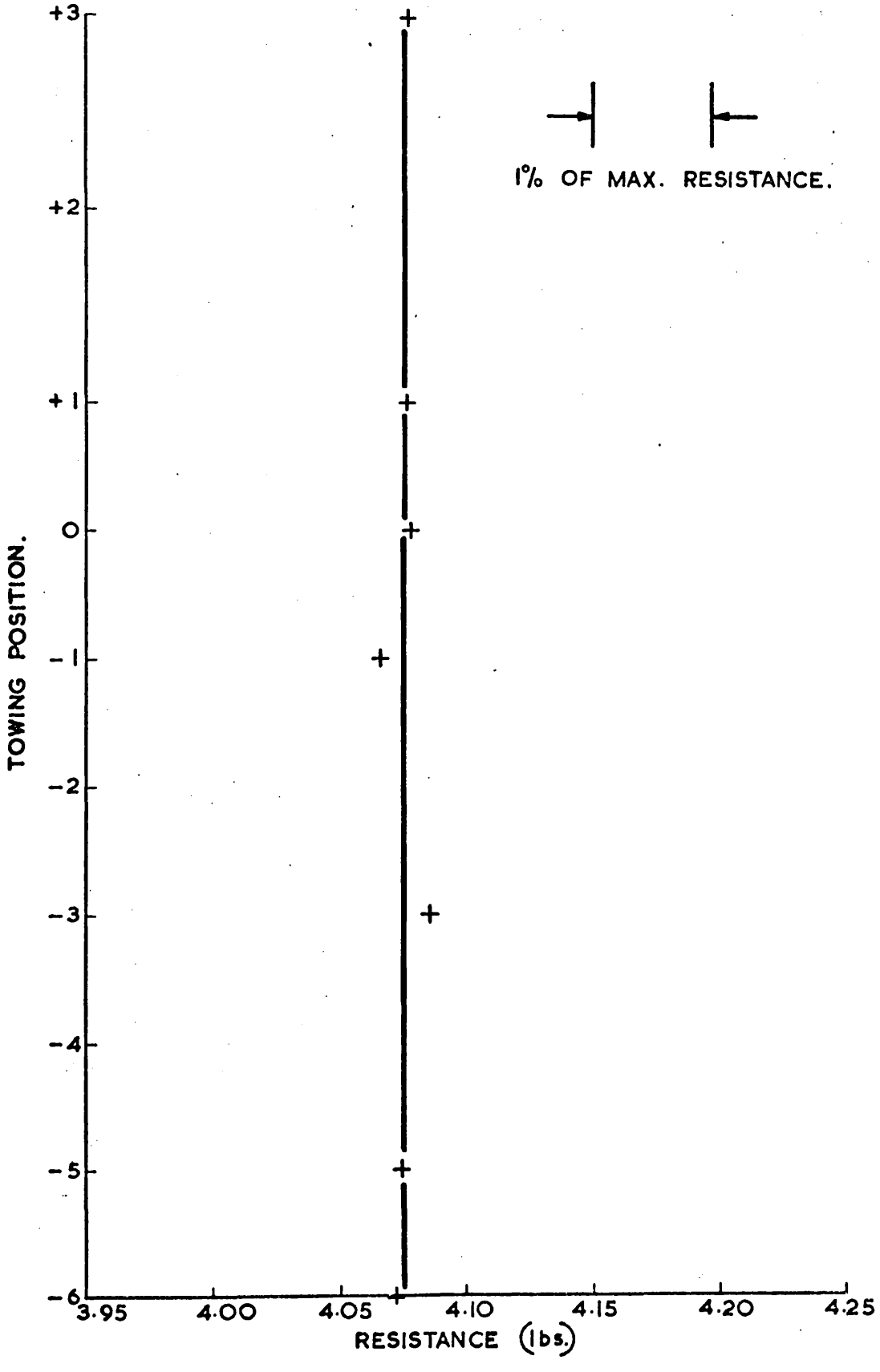

FIG 18C

VARIATION OF MEAN SINKAGE AND TRIM WITH TOWING HEIGHT.

SPEED = 4·46 ft/sec., $\mathcal{F}$ = 0·268,

TRIM BY HEAD POSITIVE

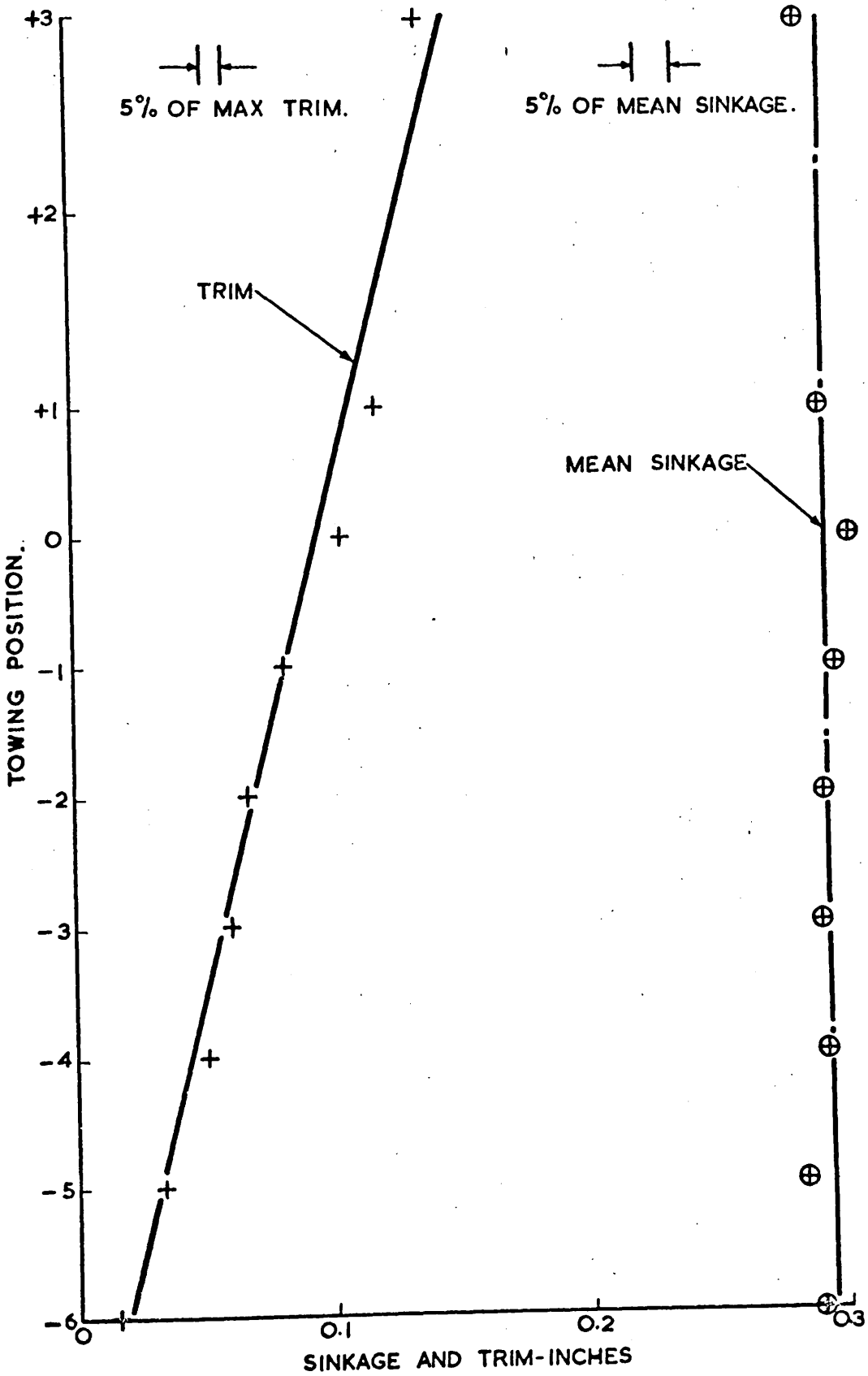

FIG 18D

VARIATION OF MEAN SINKAGE AND TRIM WITH TOWING HEIGHT.

SPEED = 5.75 ft/sec., $\mathcal{F} = 0.345$

TRIM BY HEAD POSITIVE.

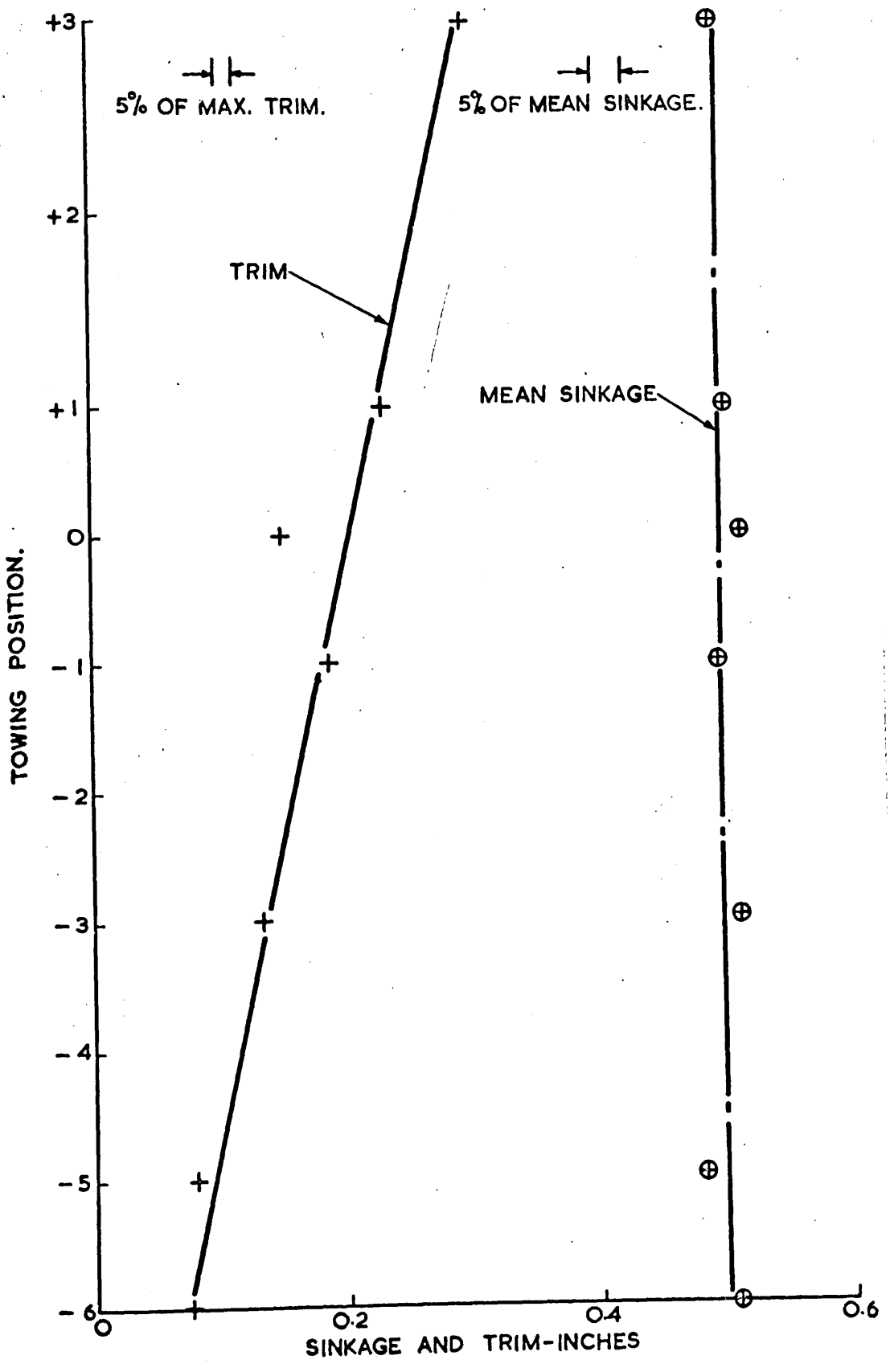

complete speed range. In order to do this the model had of necessity to be restrained from movement in any of its six degrees of freedom. Forces were thus measured with the model trimmed at the designed draft, the slight modification to the forces due to the inability of the model to sink or trim being ignored. When tested in this condition, the model corresponded to the linearised theoretical model where changes in underwater hull shape due to sinkage and trim are neglected.

Earlier work of this nature on a semi-submerged body had been carried out by Lewison (44). Unfortunately he did not measure bow and stern forces simultaneously and does not appear to have accounted for any cross-coupling between the two. Cross-coupling between the bow and stern forces and the total resistance was a major problem which had to be overcome. Empirical methods of assessing the degree of cross-coupling are described below and the subsequent analysis is given in Appendix C.

2.5.3. a. Apparatus.

Vertical forces at bow and stern were measured by two 'Clockhouse' Type 100 proving rings, suitably strain-gauged ; the signals from the gauges were amplified and displayed on an ultra-violet recorder. The proving rings were connected to the model by $1\frac{1}{4}$ inch bore tubes as shown in figs. 19 and 20. Rotating the tubes on their threaded lower mountings allowed adjustment of the model trim.

The lower mountings, shown in figure 20 and plates 1 and 3, were bolted to $\frac{1}{4}$ inch duralumin decks at bow and stern. Levelling screws enabled the tubes to be set up perpendicular to the still water surface.

The proving rings were attached to 2 in. x 2 in. mild steel angle bars clamped to the instrument rails on the carriage as shown in plate 2.

The model was towed from the standard towing space frame with the towing wheel removed. The towing link is shown in figure 20 and adjustment in a fore and aft direction was accomplished by

FIG. 19.

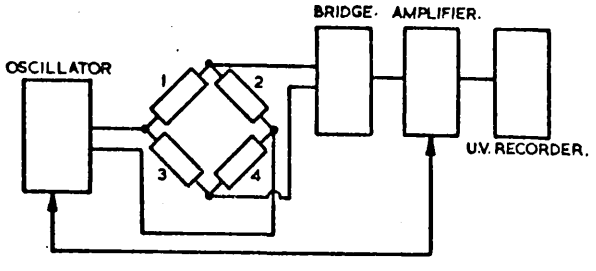

STRAIN GAUGE CIRCUIT.

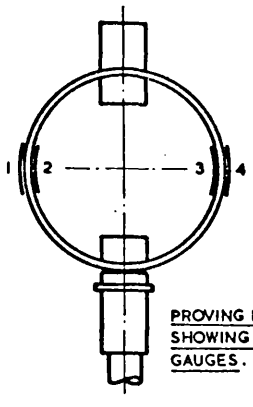

PROVING RING SHOWING STRAIN GAUGES.

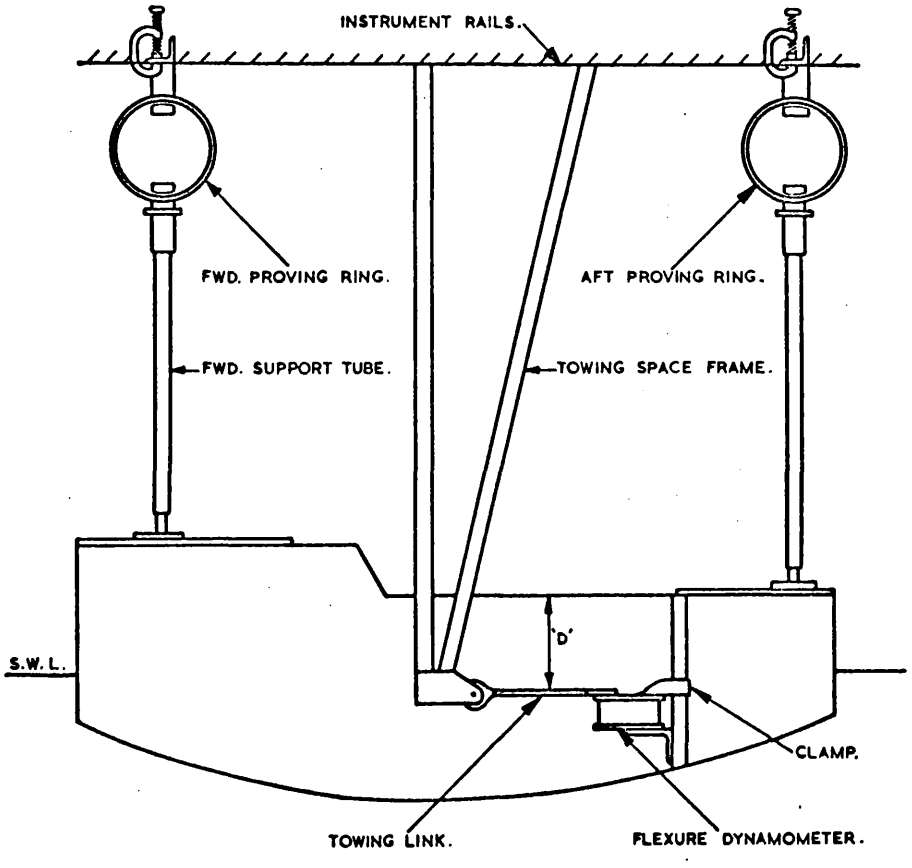

DRAWING NOT TO SCALE.

FOR DEFINITION OF 'D' SEE FIG. 22.

APPARATUS FOR VERTICAL FORCE MEASUREMENT.

FIG. 20.

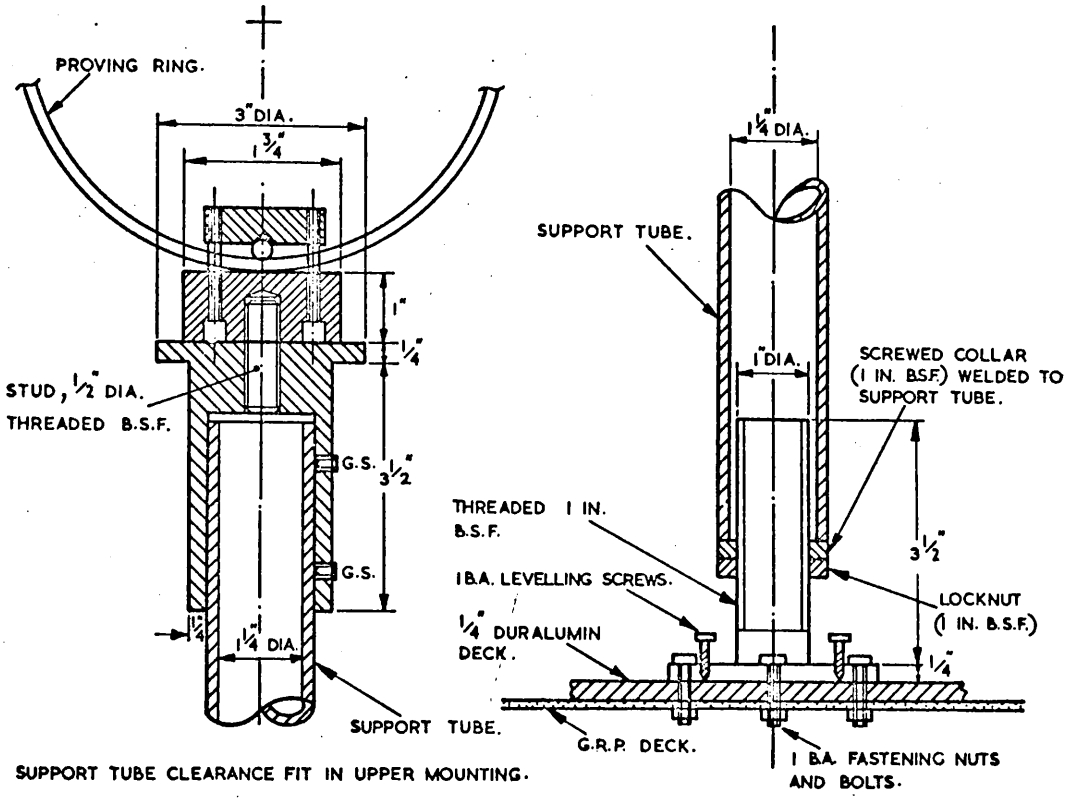

UPPER MOUNTING

LOWER MOUNTING

SUPPORT TUBE MOUNTINGS.

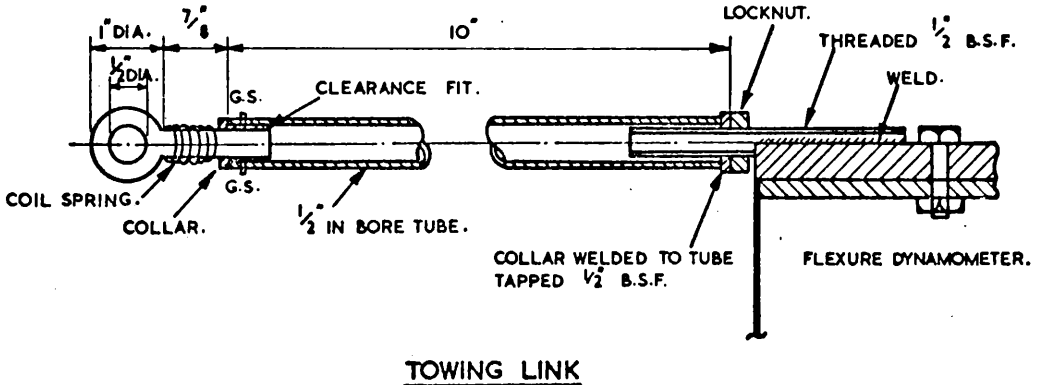

TOWING LINK

G.S.~GRUB SCREW.

ALL DIMENSIONS IN INCHES.

PLATE 1

PLATE 2

PLATE 3

PLATE 4

rotating the link about its longitudinal axis.

The link was attached to the $1\frac{1}{4}$ in. square cross-section duralumin towing post through a flexure dynamometer, as shown in plate 3, the original intention being to measure the resistance concurrently with the vertical forces. Unfortunately this proved impossible as any attempted heaving by the model during a run produced strains in the flexures far in excess of those produced by the resistance, with the result that the resistance strains were completely swamped by the heaving strains.

Furthermore, after a certain total resistance was reached any slackness in the rigid suspension system was taken up and further strains were not recorded by the flexures. This is illustrated in figure 21.

The measurement of resistance concurrently with the vertical forces was therefore abandoned. The flexure dynamometer was firmly clamped to the towing post, as shown in plate 3, for all subsequent tests.

Resistance with the model restrained from sinking or trimming, but not from surging, was measured approximately using a towing wire and suspending the model at bow and stern by piano wires as shown in figure 22. These tests entailed a recalibration of the resistance dynamometer-model system.

Other apparatus pertaining to the measurement of cross-coupling is described in Appendix C.

2.5.3. b. Experimental Procedure.

Bulwarks were added for all tests with the restrained model to minimise its being swamped at the end of a high-speed run.

The model was set up on the carriage as shown in plate 4. Alignment of the vertical tubes was checked and the model was trimmed to its at-rest position. The proving rings were pre-loaded by approximately 10 lbs to eliminate zero errors.

FIG. 21

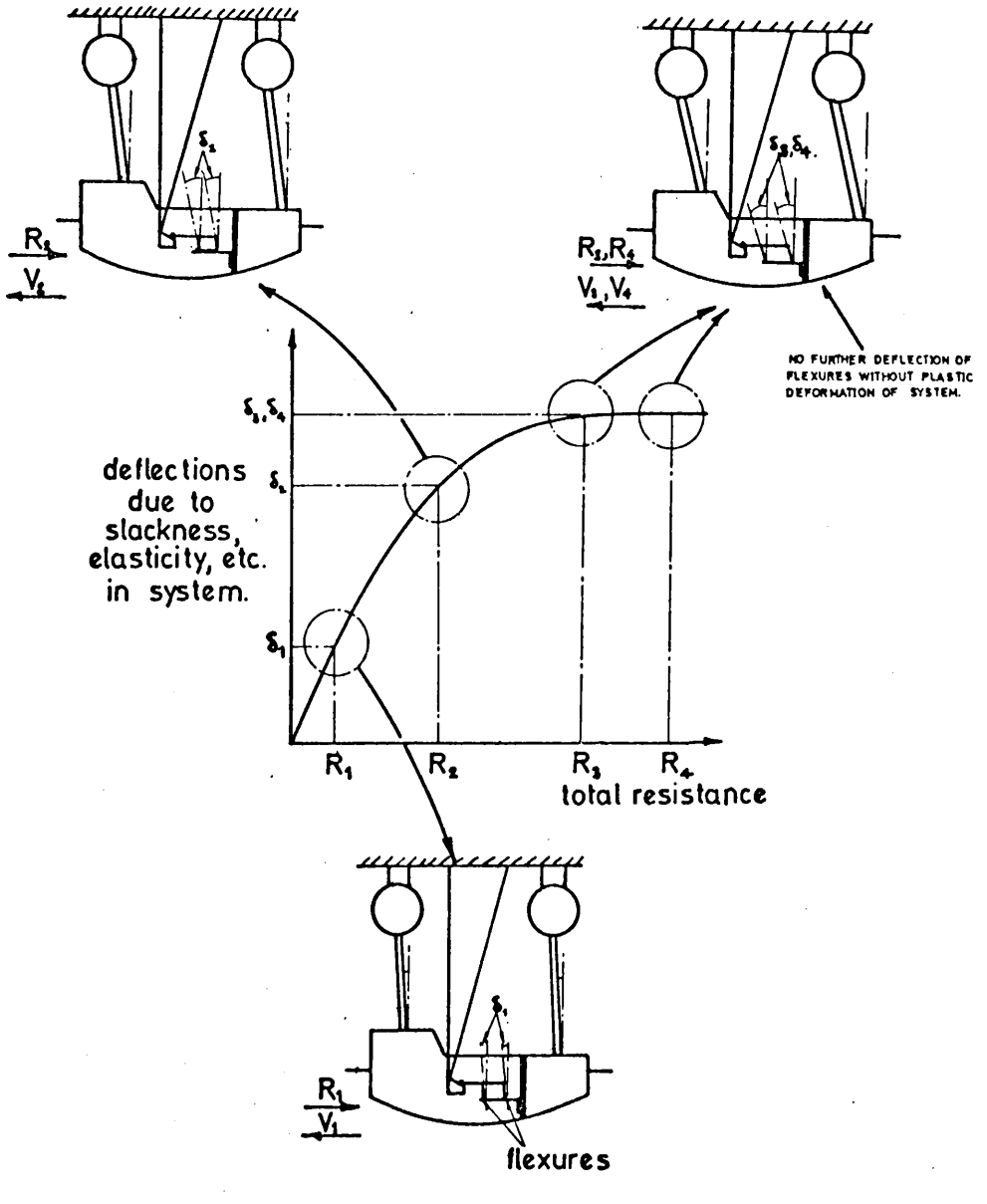

FLEXURE DYNAMOMETER BEHAVIOR

FIG. 22.

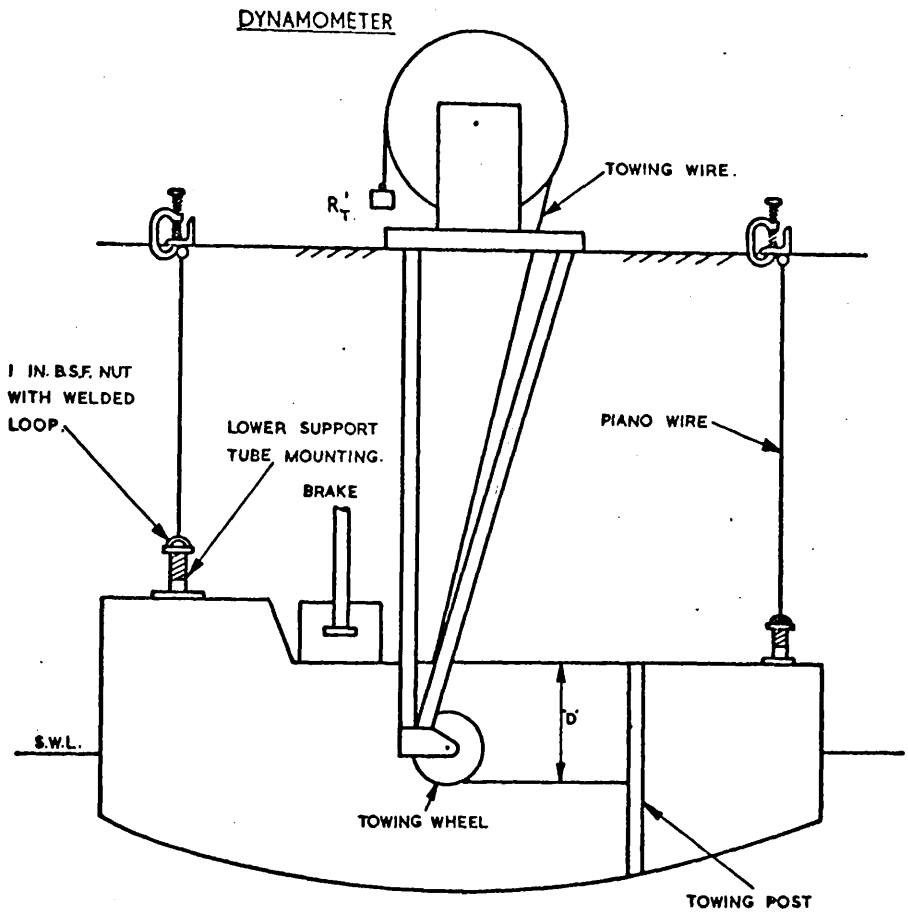

DEPTH 'D' = DISTANCE BELOW DATUM OF C.L. OF TOWING LINK AS IN FIG. 19 & FIG. C 2.

APPARATUS FOR RESISTANCE MEASUREMENT
— MODEL RESTRAINED FROM SINKING AND TRIMMING

Calibration of the proving rings was effected by placing known weights on the aluminium decks at a known position. All subsequent moment calculations were related to these 'calibration positions' and not to the fore and aft positions of the vertical tubes. Calibration checks were carried out each day before testing was begun and no drift was observed.

It was found during calibration of the proving rings that when one ring was loaded, a reading was observed on the other. This cross-coupling was quite repeatable and was of sufficient magnitude over the range of loadings to warrant removal.

Similarly the total resistance applied to the model gave rise to forces which could be measured at the bow and stern rings ; results from the resistance tests with the model restrained from sinking and trimming and with minimum surge, were used to eliminate this source of error as described in Appendix C. Wave profiles were also photographed during the restrained resistance tests.

Results of the vertical force tests, after correction for tide, blockage, cross-coupling, and temperature are given in table 5 and shown in figure 23.

Results of the restrained resistance tests are given also in table 5 and contrasted with those of the free model in figure 24.

FIG. 23

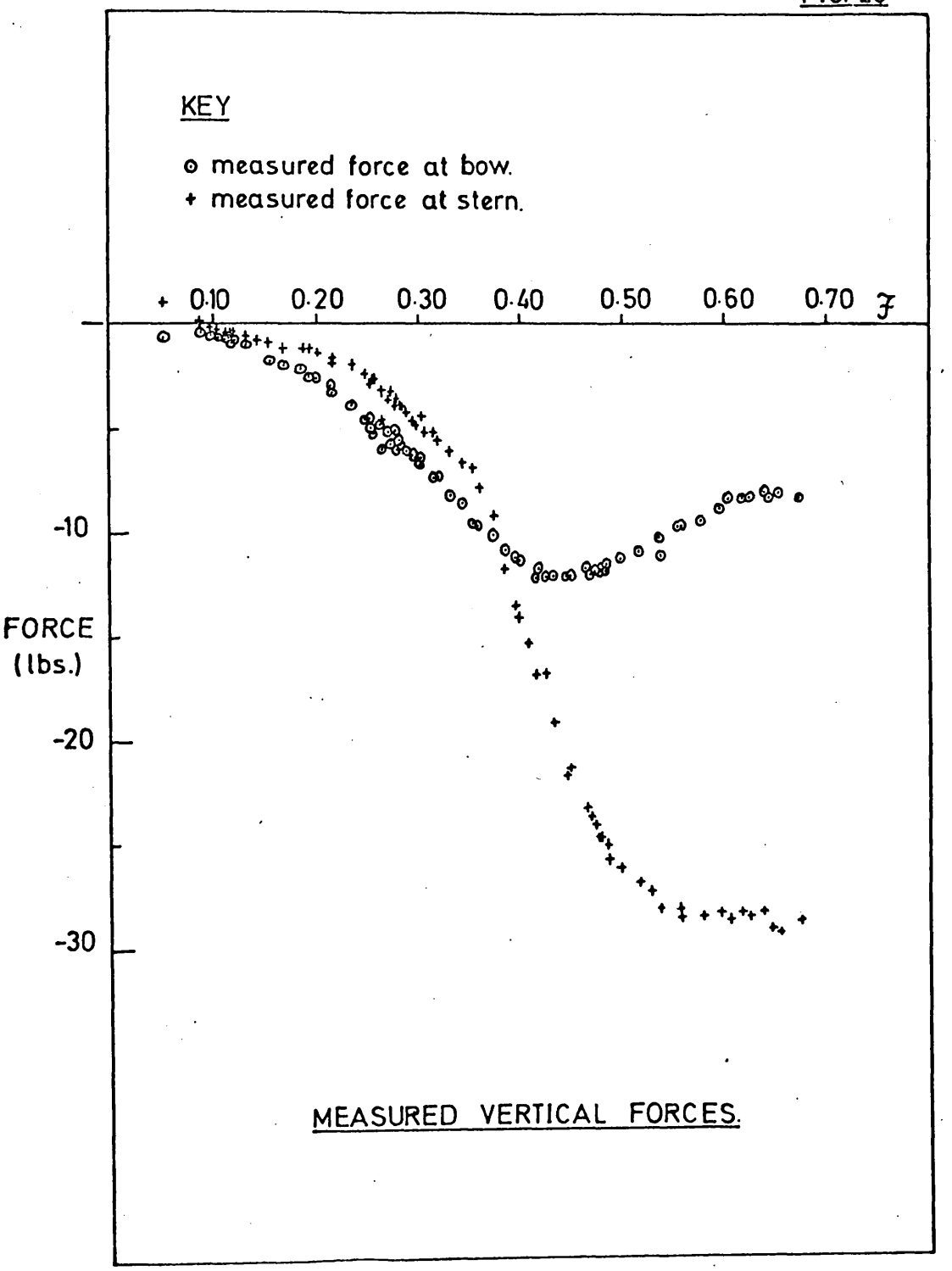

MEASURED VERTICAL FORCES.

$\mathcal{F}$	Z_{Bow} lbs.	Z_{Stern} lbs.	Z_{Total} lbs.	Trimming Moment, M lbs-ft.
0.250	-4.513	-2.706	-7.219	-7.412
0.247	-4.523	-2.399	-6.921	-8.446
0.305	-6.700	-4.443	-11.143	-9.618
0.118	-0.852	-0.421	-1.273	-1.694
0.130	-0.996	-0.529	-1.526	-1.858
0.156	-1.725	-0.810	-2.535	-3.564
0.141	-1.344	-0.717	-2.061	-2.497
0.169	-1.866	-1.085	-2.952	-3.175
0.424	-12.238	-16.976	-29.214	+11.265
0.187	-2.112	-1.118	-3.231	-3.951
0.200	-2.665	-1.488	-4.153	-4.735
0.216	-3.363	-1.690	-5.053	-6.582
0.234	-3.793	-1.928	-5.722	-7.357
0.261	-4.796	-3.124	-7.920	-7.069
0.216	-3.018	-1.868	-4.886	-4.767
0.273	-5.745	-3.395	-9.140	-9.594
0.289	-6.063	-4.369	-10.432	-7.569
0.320	-7.455	-5.569	-13.024	-8.663
0.330	-8.236	-6.058	-14.294	-9.880
0.343	-8.610	-6.621	-15.231	-9.393
0.306	-6.412	-5.147	-11.559	-6.289
0.270	-5.194	-3.544	-8.738	-7.132
0.295	-6.335	-4.567	-10.902	-7.900
0.265	-6.054	-4.666	-10.720	-6.570
0.281	-5.664	-3.947	-9.612	-7.509
0.299	-6.471	-4.719	-11.191	-7.895
0.088	-0.493	+0.255	-0.237	-2.602
0.098	-0.516	-0.088	-0.604	-1.570
0.102	-0.619	-0.205	-0.824	-1.559
0.111	-0.697	-0.339	-1.036	-1.400

FROUDE NUMBERS CORRECTED FOR BLOCKAGE AND TIDE EFFECTS
MEASURED VERTICAL FORCES AND TRIMMING MOMENT

TABLE 5A

$\mathcal{F}$	Z_{Bow} lbs.	Z_{Stern} lbs.	Z_{Total} lbs.	Trimming Moment, M lb.-ft.
0.120	-0.719	-0.425	-1.144	-1.200
0.052	-0.537	+1.060	+0.523	-5.379
0.277	-5.205	-3.615	-8.820	-6.937
0.281	-5.796	-3.994	-9.790	-7.828
0.193	-2.525	-1.220	-3.745	-5.106
0.360	-9.750	-7.992	-17.742	-9.028
0.373	-10.152	-9.348	-19.500	-6.056
0.387	-10.904	-11.747	-22.650	-0.955
0.400	-11.459	-14.049	-25.508	+4.541
0.396	-11.262	-13.954	-25.216	+4.937
0.280	-6.133	-3.928	-10.061	-9.255
0.432	-12.131	-19.366	-31.498	+19.429
0.354	-9.669	-6.936	-16.605	-12.172
0.415	-12.257	-16.869	-29.126	+10.849
0.409	-11.793	-15.409	-27.203	+7.766
0.314	-7.406	-5.201	-12.607	-9.688
0.445	-12.146	-21.751	-33.896	+27.136
0.464	-11.799	-23.306	-35.105	+33.444
0.477	-11.794	-24.737	-36.531	+38.119
0.483	-11.808	-25.797	-37.604	+41.516
0.637	-8.184	-28.427	-36.610	+63.096
0.528	-11.318	-27.519	-38.837	+48.879
0.470	-11.893	-24.096	-35.989	+35.675
0.498	-11.248	-26.250	-37.498	+45.005
0.450	-12.229	-21.428	-33.657	+25.787
0.479	-11.923	-24.836	-36.760	+37.977
0.516	-10.943	-26.956	-37.899	+48.392
0.556	-9.789	-28.554	-38.342	+57.742
0.253	-5.005	-2.668	-7.673	-9.299
0.535	-10.343	-28.206	-38.550	+54.618
0.553	-9.805	-28.235	-38.040	-56.647

TABLE 5A CONT.

$\mathcal{I}$	Z_{Bow} lbs.	Z_{Stern} lbs.	Z_{Total} lbs.	Trimming Moment M lb.-ft.
0.577	-9.584	-28.617	-38.202	+58.685
0.594	-8.986	-28.490	-37.477	+60.419
0.602	-8.437	-28.731	-37.168	+63.177
0.618	-8.453	-28.412	-36.865	+62.082
0.652	-8.399	-29.475	-37.875	+65.733
0.644	-8.421	-29.050	-37.471	+64.272
0.670	-8.432	-28.838	-37.269	+63.542
0.626	-8.448	-28.519	-36.966	+62.447
0.255	-5.212	-2.648	-7.860	-10.109
0.484	-11.578	-25.014	-36.592	+39.792
0.469	-12.044	-23.770	-35.814	+34.073

TABLE 5A CONT.

Carriage Speed ft/sec.	Tide ft./sec.	Resistance lbs.	Temp. ^{o}C
3.977	0	1.268	12.33
2.983	-0.010	0.513	12.38
5.123	-0.020	2.833	12.42
1.941	0	0.190	12.42
2.187	-0.028	0.225	12.41
2.490	-0.035	0.363	12.40
2.323	-0.008	0.305	12.38
2.735	-0.010	0.405	12.37
3.252	-0.035	0.590	12.36
3.566	-0.018	0.832	12.35
3.938	-0.020	1.090	12.33
3.684	+0.010	0.960	12.30
4.250	+0.015	1.455	12.27
4.094	+0.010	1.319	11.38
4.384	-0.007	1.525	11.70

MEASURED TOTAL RESISTANCE - MODEL RESTRAINED

TABLE 5B

Carriage Speed ft/sec.	Tide ft/sec.	Resistance lb.	Temp ^{o}C
4.276	-0.012	1.484	11.92
4.506	-0.020	1.590	12.10
4.435	0	1.505	12.32
4.382	-0.010	1.519	12.40
4.686	-0.010	1.733	12.43
4.880	-0.015	2.205	12.45
4.968	+0.005	2.475	12.43
5.023	-0.011	2.533	12.28
5.972	+0.010	3.645	12.75
5.281	-0.005	3.204	12.93
5.489	-0.010	3.433	13.05
5.454	-0.010	3.504	11.70
5.698	-0.015	3.583	11.71
5.099	-0.015	2.734	11.72
5.428	0	3.448	11.75
4.590	-0.012	1.675	11.76
4.254	-0.010	1.475	11.80
5.853	-0.010	3.755	11.84
5.521	-0.020	3.540	11.87
6.064	-0.005	3.986	11.91
6.772	0	6.208	11.97
6.235	+0.010	4.464	10.50
5.568	+0.022	3.559	10.60
6.474	-0.027	5.125	10.80
7.064	-0.005	8.238	10.92
7.400	-0.018	10.480	11.15
8.016	+0.005	13.540	11.33
7.350	-0.011	9.300	11.47
7.735	-0.022	11.695	11.60

TABLE 5B - CONT.

FIG. 24

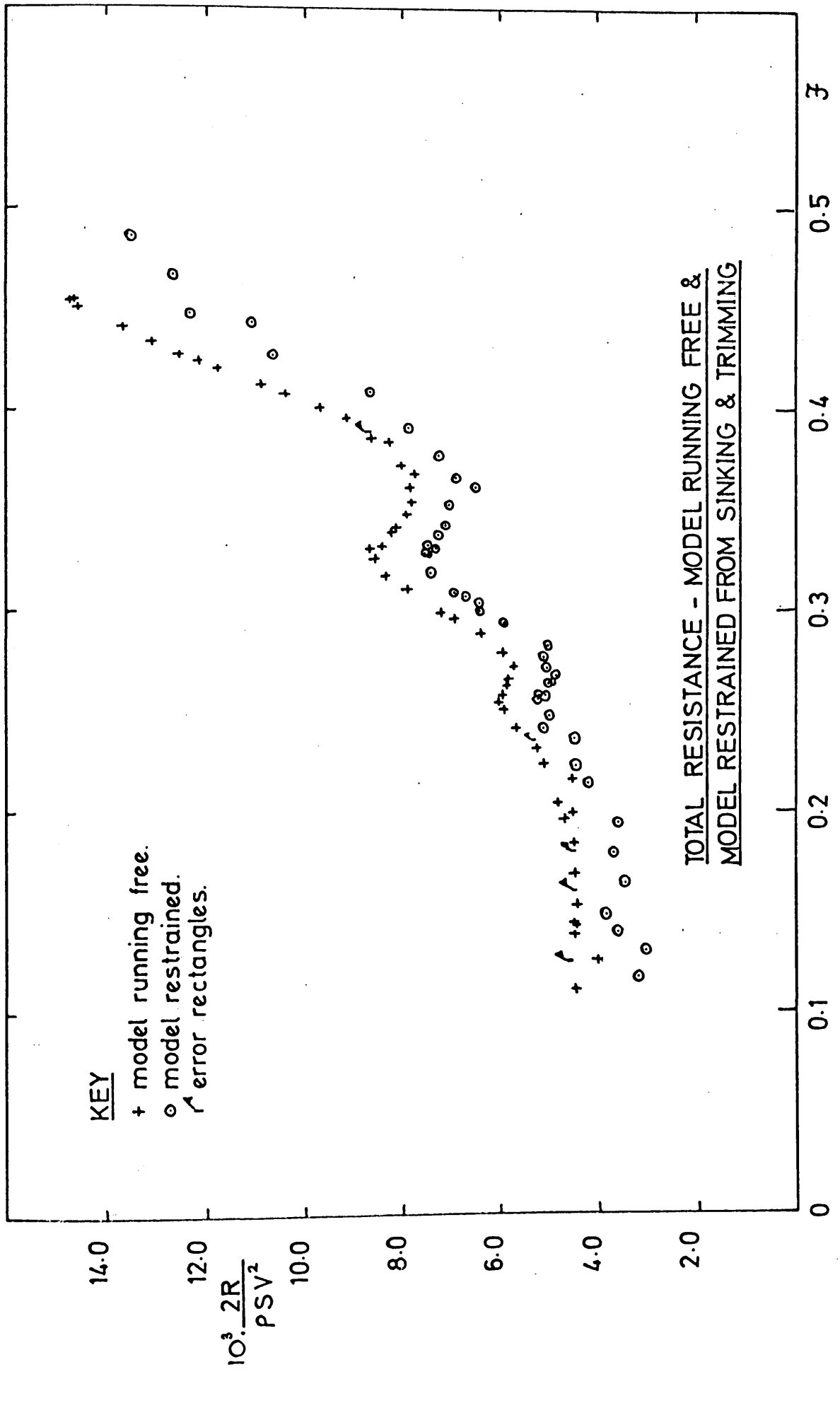
KEY
+ model running free.
⊙ model restrained.
error rectangles.
TOTAL RESISTANCE - MODEL RUNNING FREE &
MODEL RESTRAINED FROM SINKING & TRIMMING
$10^3 \cdot \frac{2R}{\rho S V^2}$
14.0
12.0
10.0
8.0
6.0
4.0
2.0
0
0.1
0.2
0.3
0.4
0.5
$\mathcal{F}$

2.6. ERROR ESTIMATION

One of the aims of the investigation was to study a small component of total resistance. This demanded accurate experimental work and made an estimation of the errors, both of the model itself and in the techniques of measurement, essential.

The treatment of errors of observation is well-known (102); Scott has made a study of them for the particular case of ship model resistance measurements (103).

2.6.1. Sources of Error

Sources of error, both random and systematic, abound in any experimental investigation. The principal causes of error in the experiments in question are listed below ; some are then considered in detail.

i) Blockage, tide and temperature.

Blockage was calculated and tide was measured and allowed for in all speed measurements. All density and viscosity values were corrected to a standard temperature of 59°F. The possible existence of thermocline conditions was noted (see ref. 98) and several temperature gradients were measured daily.

The corrections for blockage, tide and temperature have been discussed in detail in section 2.5.2.

ii) Turbulence stimulation.

Care was taken to ensure stimulation similar to that adopted by Sharma and Inui; it was not the intention to achieve more efficient stimulation. This has been discussed in section 2.5.2 a.

iii) Towing height position.

The empirical investigation of the effect of towing height position on resistance, sinkage and trim has been discussed in section 2.5.2. b.

iv) Equipment Errors

Scott concluded that, apart from errors in speed due to the presence of a tide, most remaining errors were probably due to limitations in the accuracy of the measuring equipment. These errors lend themselves to a statistical treatment and this is given in section 2.6.2. below.

v) Model Errors

The model as made will differ from the hull form derived in section 2.2. due to inaccuracies of manufacture. The consequence may be erroneous force measurements, wave patterns, boundary layers, etc. An attempt to investigate this and to relate the offset errors to the force and moment coefficients is made in section 2.6.3. below.

vi) Errors in experimental technique.

These are errors due to human errors such as the misreading of instruments etc. An attempt to overcome this is being made at Glasgow University Experiment Tank with the introduction of automatic data recording techniques. As far as possible, such techniques were used in this investigation.

vii) Stability of Flow Conditions.

This is intimately linked with the finish of the model, as noted in (v) above. Throughout the tests, sufficient time was allowed between runs for the tank water to return to an almost completely undisturbed state. At the start of each day's running the model was wiped down to remove any air bubbles clinging to its surface which might have had an adverse effect on the viscous flow over the hull.

2.6.2. Equipment Errors.

Equipment errors give rise to

a) Ground Speed measurement errors.

b) Force measurement errors.

c) Attitude (i.e. sinkage) measurement errors.

2.6.2a Ground speed measurement errors.

Ground speed was measured by counting the pulses from a radial diffraction grating on an electronic digital counter. This displayed a speed reading to three decimal places. The accuracy of the counter was given as ± 1 count, giving a speed accuracy to within ± 0.001 ft/sec. Moreover, the displayed speed was a mean speed over the time interval of the count, usually about 5 seconds. Speed throughout the run fluctuated in a regular manner about the mean (also having an accuracy of ± 0.001 ft/sec) due to deficiencies in the carriage speed control system. This is shown in fig. 25. But as the variation of speed throughout the run was not random, it did not seem justified to consider any value for the speed error other than ± 0.001 ft/sec in the range of speeds considered.

Speed fluctuations throughout any run were in general of a small order and a reasonable mean was easily obtainable.

2.6.2.b Force Measurement Errors.

Due to the speed fluctuations mentioned above, the carriage was continually accelerating and decelerating to a small degree throughout the run. This caused fluctuations in the out-of-balance resistance force shown in fig. 25.

The repeatability of the resistance readings and a subsequent error value was determined from the results of the towing point tests in table 4. These give a total of 9 readings at 4.46 ft/sec and 7 readings at 5.75 ft/sec. As the towing point variation had little or no effect on resistance measurement, it was decided to use these values and assume that they followed the

FIG. 25

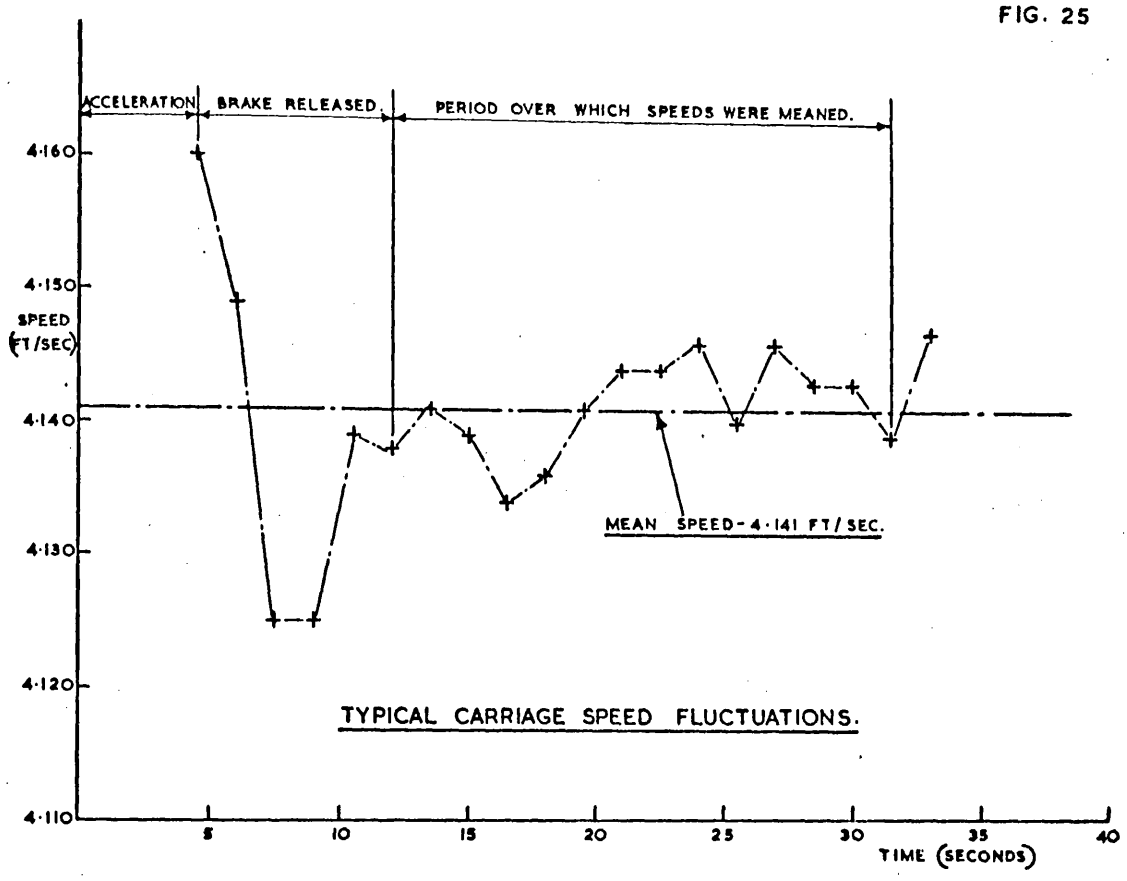

TYPICAL CARRIAGE SPEED FLUCTUATIONS.

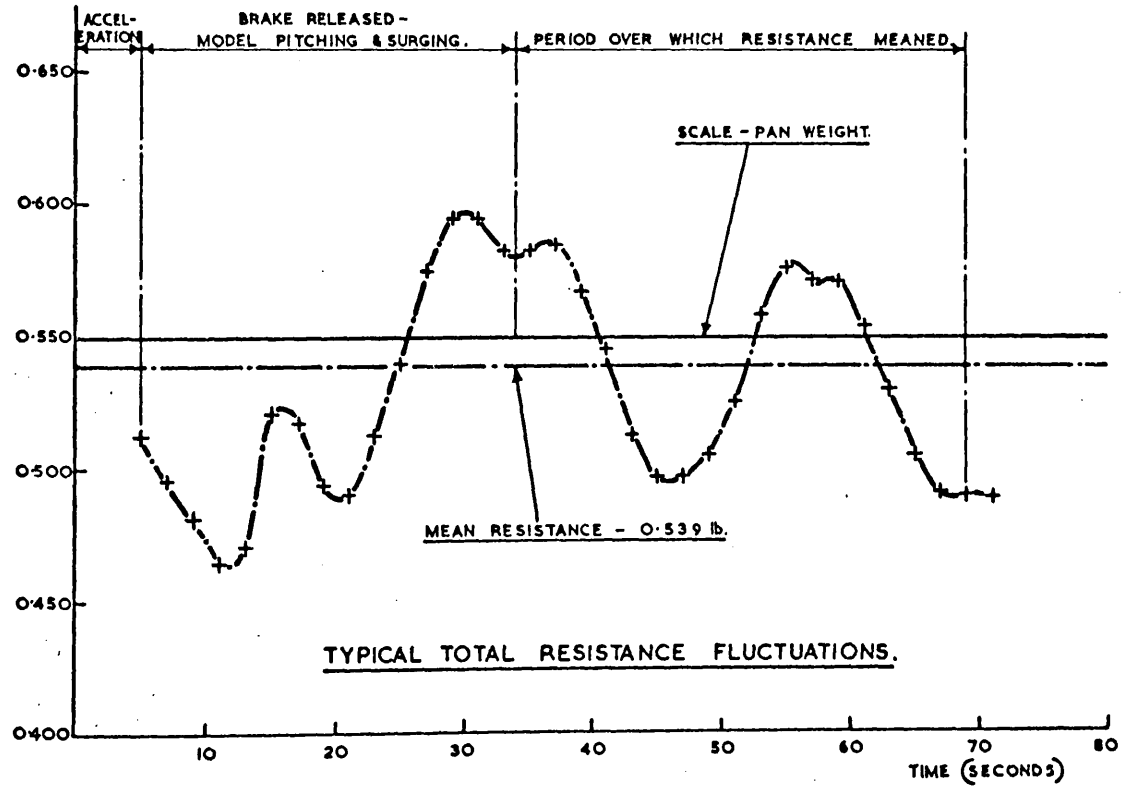

TYPICAL TOTAL RESISTANCE FLUCTUATIONS.

normal Law of Error. The Standard Error of the Mean, σ_s ($\sigma_s = \sigma/\sqrt{n}$ where n is the number of observations. see ref. 102, p62), was found to be :

Speed	Mean Total Resistance	σ_s
4.46 ft/sec	1.791 lbs	$\pm$ 0.004 lbs
5.75 ft/sec	4.075 lbs	$\pm$ 0.002 lbs

Table 6

Unfortunately, this analysis was limited to two speeds only, in the higher speed range, on favourable 'flat' parts of the resistance curve. Nevertheless, a mean value for total resistance error of $\pm$0.003 lb. was assumed, and taken to hold over the whole speed range ; this assumes that the out-of-balance force will always be of the same absolute order. It is of interest to note that Scott (103) obtained a value of $\pm$0.007 lb. for total resistance error from numerous results for a standard model.

Vertical Forces.

Vertical force measurements suffered from errors due to

i) Vibration of the system.

Carriage vibration was amplified and displayed on the ultra-violet recorder trace. This was of such a high frequency that mean lines were readily drawn and displacements measured.

ii) Rail height variation.

Lewison (44) investigated this thoroughly. The Glasgow Tank, being relatively new, had its rails recently aligned over a 270 ft. length to a tolerance of $\pm$0.004 inch. It was assumed that rail height variation would have a negligible effect on vertical force measurement. This was confirmed by taking zero readings at various positions along the tank, when no zero drift was observed.

iii) Cross-coupling

Cross-coupling of vertical forces and resistance is discussed in section 2.5.3. and appendix C.

An analysis from repeated vertical force and moment measurements gave the following values for errors assumed to hold for the whole speed range :

Error in Vertical Force $\delta Z = \pm 0.163$ lb.
Error in Trimming Moment $\delta M = \pm 0.625$ lb.ft.

Table 7

These error values take into account repeatability and cross-coupling.

Force measurements would also be affected by the initial acceleration of the carriage. This accelerates the wave system, a phenomenon which has been discussed theoretically by Wehausen (104). He found that an initial acceleration gives rise to a slowly-damped oscillatory term in the wave resistance which could still be measured after fourteen model lengths had been covered at steady speed. This represents a distance of about 120 ft. for the Glasgow Inuid. It seems probable that this effect can give rise to fluctuations both in resistance and vertical force measurements.

2.6.2. c. Attitude Measurement Errors.

Values of sinkage were taken from mean lines on the ultra-violet recorder traces as in fig. 26.

These traces always showed a regular fluctuation about a mean value, even when total resistance and applied towing force appeared well in balance for a particular run. Apart from initial acceleration effects, mentioned above, this was thought to be due to a combination of :

TYPICAL ULTRA VIOLET RECORDER TRACE.

MODEL: INUID S201

SPEED: 4·372 ft/sec.

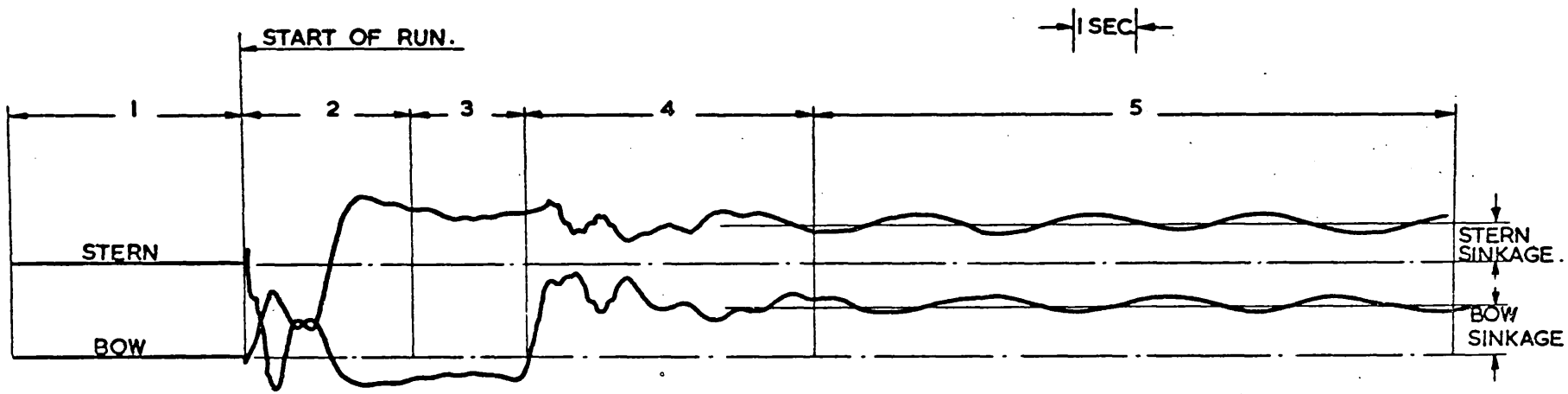

KEY:

1. AT REST (ZERO) POSITION.
2. ACCLERATION PERIOD OF CARRIAGE.
3. CARRIAGE ON STEADY SPEED.
4. BRAKE RELEASED – MODEL PITCHING.
5. STEADY SPEED.

FIG 26

i) Slight surging of the model due to the total resistance and applied towing force not being exactly in balance. (This effect is consequent upon carriage speed fluctuations and initial acceleration effects.) A check was made by linking a linear displacement transducer to the out-of-balance force recording pen, when the surging of this pen was found to be approximately in phase with the low-frequency fluctuations of the sinkage readings.

ii) Pitching due to the model being forcibly 'trimmed' while held by the brake during acceleration of the carriage. When the brake was released, the model pitched for a short period of time. This was checked by measuring the pitching period of the model which was found to be 0.86 seconds. This corresponded to the period of the high-frequency oscillations at the start of the steady speed portion of the run.

(Effects (i) and (ii) above also contributed towards fluctuations of the measured forces.)

Estimated bow and stern sinkage errors were :

Bow and stern sinkage error $\delta s^1 = \pm 0.001$ inches.

We note that the sources of error mentioned in this section cannot be considered as separate entities as all interact and the above demarcation is purely for convenience.

2.6.3. Model Errors.

A statistical estimate of the model error ε was made by measuring the model offsets and subtracting them from the offsets derived from those given by Sharma in ref. 53. Such an estimate allowed for errors arising from :

i) The model lines plan.

ii) Wax cutting and scraping errors in the manufacture of the mould.

iii) Shrinkage of the glass-fibre shell on curing.

iv) Uneven paint thickness.

v) Distortion of the model during and after manufacture.

Offsets were lifted from the model at 1181 positions, more being lifted from the forebody than the aft body. A clock gauge reading to $\pm$0.001 inch was used in conjunction with the cutting table equipment as shown in fig. 27.

Two major problems arose with offset error measurement and these were :

a) Model Shift

During the period when offsets were being lifted from the model, it was discovered that the model had settled bodily by approximately 0.050 inches. This occurred after all fore-body offsets had been lifted and prior to lifting the aft-body offsets. The effect of this on the measured offsets was determined by comparing midship section offsets measured before and after the settling. An approximate correction was made by adjusting each waterline offset in the aft-body by the discrepancy at that waterline at midships. This assumed the fore-body measured offsets to be correct.

b) Measurement problems near the keel

Reference to the body plan (figure 11) shows that near the keel the tangent to the body section approaches the horizontal. This resulted in the spherical end of the clock gauge touching the hull surface at a point different from that measured. (See fig. 27.)

This was partially overcome by replacing the spherical end with a pointed Tufnol cap. This tended to slip on the model surface due to any vertical movement of the clock-gauge shaft. Hence no reliable readings were obtained between the bottom of the keel and a waterline $\frac{1}{2}$ inch above it. Between this waterline and the 2 inch waterline all readings tended to be consistently low.

These readings were not discarded, however, for it was in this region that the model was expected to be least accurate. The flat tangent, coupled with an 'inside scrape' of the wax mould caused 'flats' which were only partially filled before the model was painted.

FIG. 27.

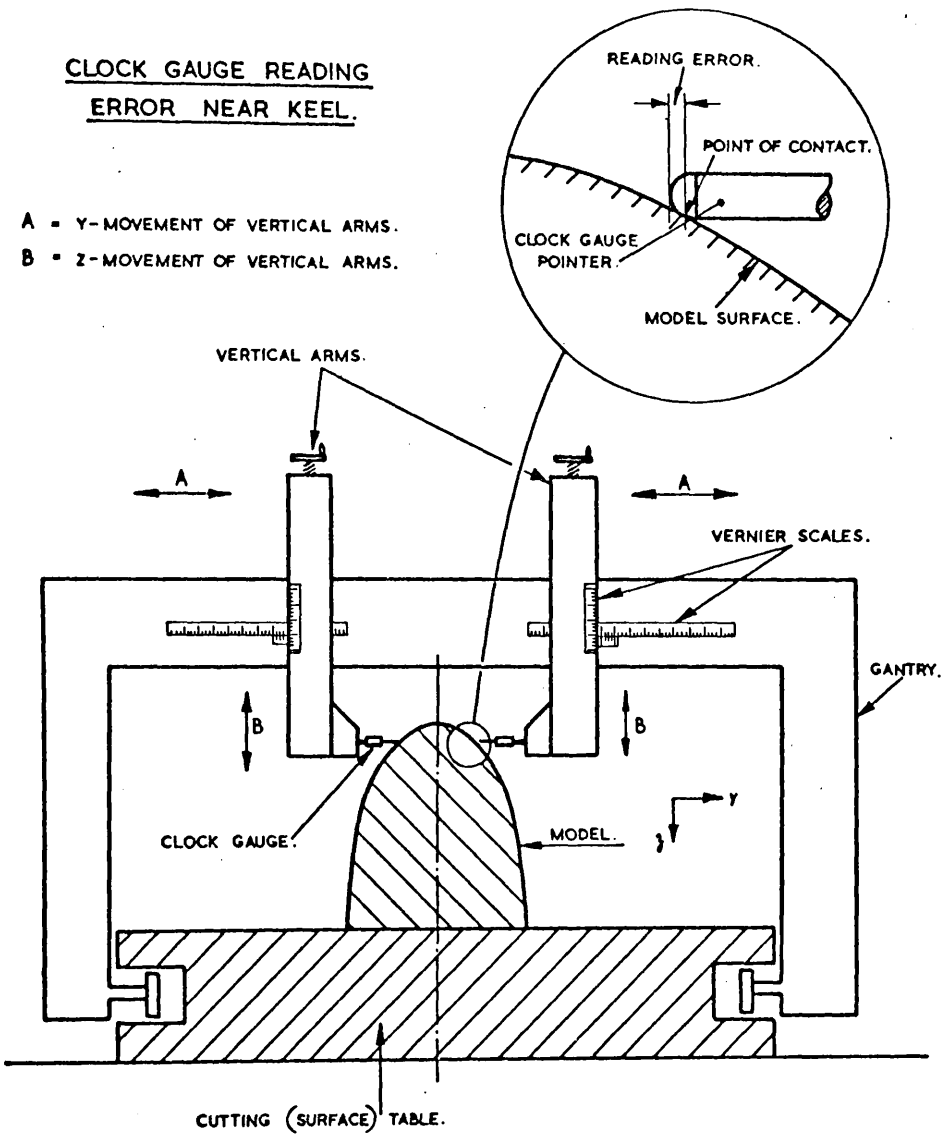

THE GANTRY IS FREE TO MOVE IN THE X-DIRECTION.

MEASUREMENT OF OFFSET ERRORS.

Offset errors were calculated and distributions plotted for four quarters of the underwater hull as shown in fig. 28. A mean error ($\bar{\epsilon}$) and a deviation of the mean (σ) were calculated for each quarter, each half, and for the total hull.

These results are given in table 8.

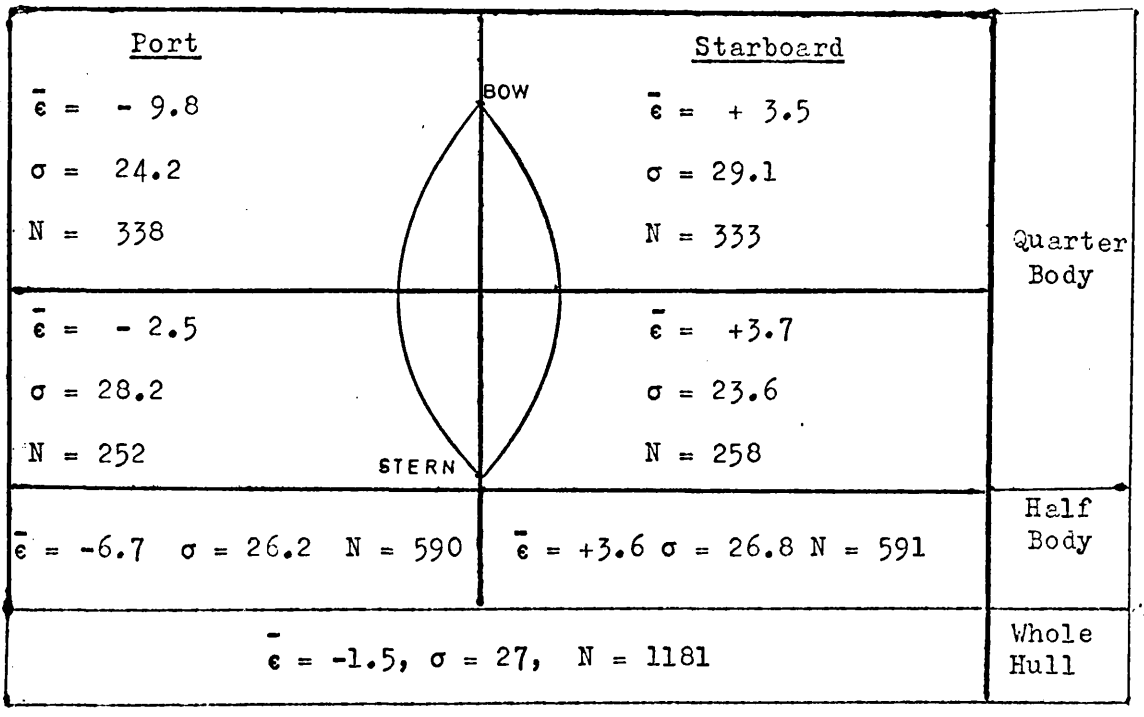

N.B. $\bar{\epsilon}$ and σ measured in thousandths of an inch.

N = Number of measured offsets

'+'= Model undersize, '-'= Model oversize

Table 8

A total error distribution is shown in figure 29. An attempt was made to fit a Normal Curve to this, but a χ^2 test (see ref. 104 p.249) indicated a very poor fit. It was therefore assumed that the Normal Error Law did not apply ; there is no reason why it should as the model offset errors are not random. Thus the overall offset errors were not compounded when errors in hull volumes and areas were computed (see below).

We see from table 8 that the final mean error was -0.0015 inch with a deviation of $\pm$0.027 inch. The mean of -0.0015 inch was probably due to

FIG. 28

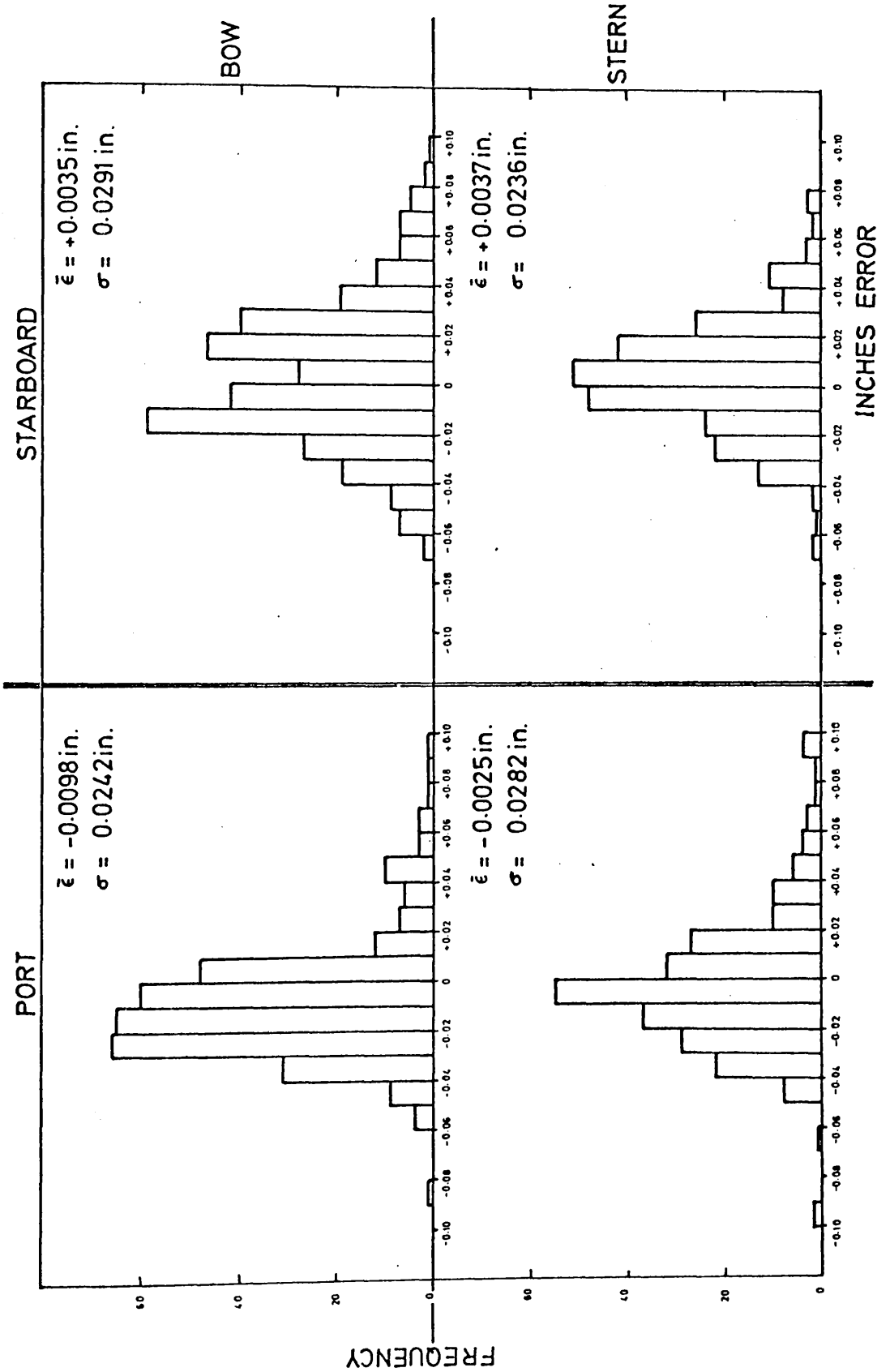
OFFSET ERROR FREQUENCY DISTRIBUTIONS
PORT
STARBOARD
BOW
STERN
$\bar{\epsilon}$ = -0.0098 in.
σ = 0.0242 in.
$\bar{\epsilon}$ = -0.0025 in.
σ = 0.0282 in.
$\bar{\epsilon}$ = +0.0035 in.
σ = 0.0291 in.
$\bar{\epsilon}$ = +0.0037 in.
σ = 0.0236 in.
FREQUENCY
INCHES ERROR

FIG. 29

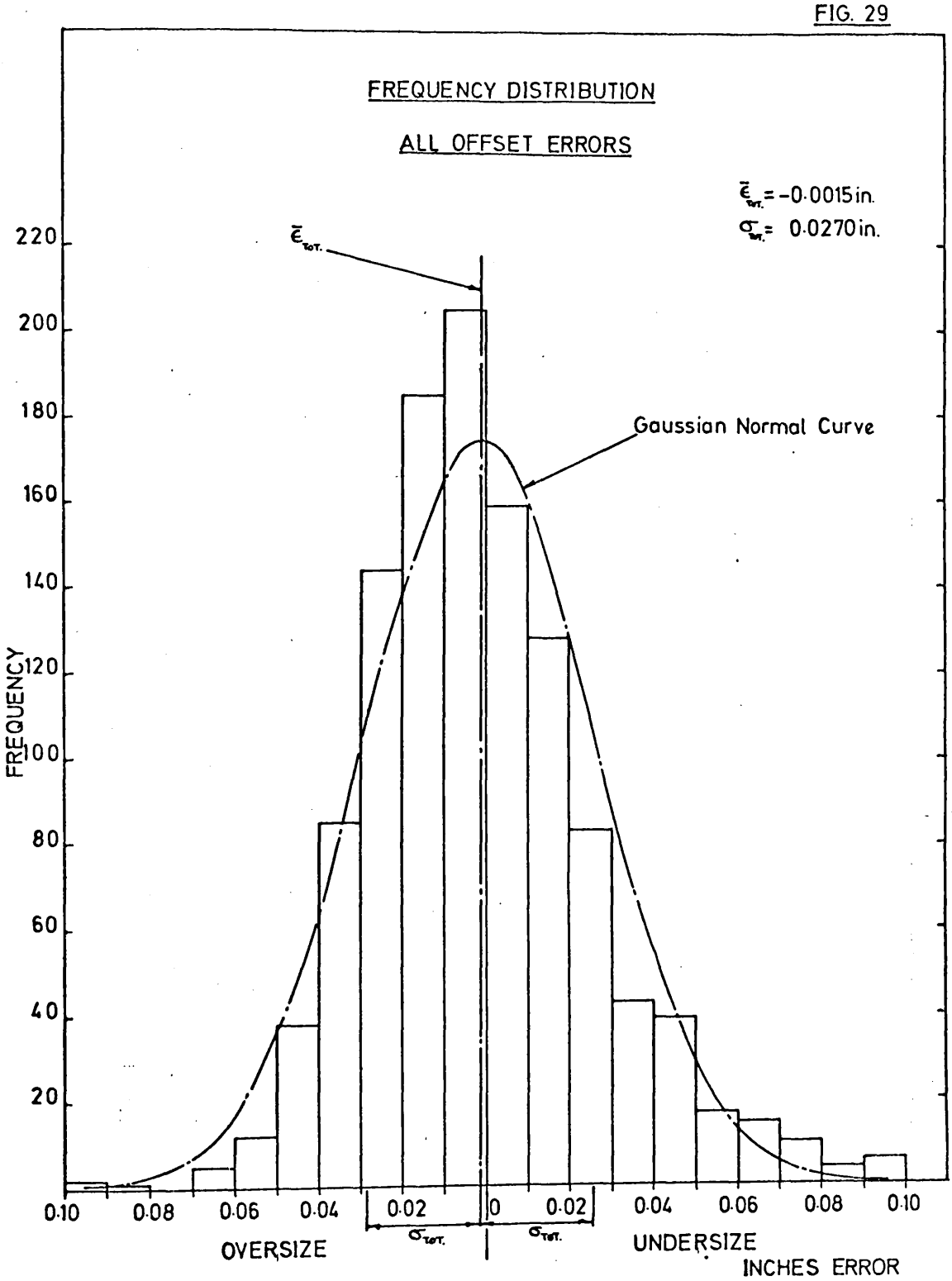
FREQUENCY DISTRIBUTION
ALL OFFSET ERRORS
$\bar{\epsilon}_{TOT.}$ = -0.0015 in.
$\sigma_{TOT.}$ = 0.0270 in.
$\bar{\epsilon}_{TOT.}$
Gaussian Normal Curve
FREQUENCY
220
200
180
160
140
120
100
80
60
40
20
0.10
0.08
0.06
0.04
0.02
0
0.02
0.04
0.06
0.08
0.10
$\sigma_{TOT.}$
$\sigma_{TOT.}$
OVERSIZE
UNDERSIZE
INCHES ERROR

i) Mis-alignment of the model on the surface table

ii) Asymmetry of the model.

This was neglected and an offset error of $\pm$ 0.027 inch assumed. Errors in the longitudinal and vertical directions were taken as $\pm$0.005 inch this being the accuracy of the Vernier scales on the cutting table equipment.

Thus errors in the three mutually perpendicular directions were taken to be :

$\delta x = \pm 0.005$ inch, $\delta y = \pm 0.027$ inch, $\delta z = \pm 0.005$ inch.

These errors were then used to compute errors in various hull volumes and areas as follows:

Error in Volume of Displacement, ∇

$$\nabla = 2\int_{-\ell(x)}^{\ell(x)} \int_{0}^{d(x)} y \, dx \, dz \qquad \ldots\ldots (2.6.1)$$

and

$$\delta\nabla = \frac{\partial\nabla}{\partial x}.\delta x + \frac{\partial\nabla}{\partial y}.\delta y + \frac{\partial\nabla}{\partial z}.\delta z \qquad \ldots\ldots (2.6.2)$$

(This value of $\delta\nabla$ is taken as the errors are not being compounded.)

Now

$$\frac{\partial\nabla}{\partial x} = 2\int_{0}^{d(x_i)} y \, dz = \text{BODY SECTION AREA AT } x = x_i$$

$$\frac{\partial\nabla}{\partial y} = 2\int_{-\ell(x_i)}^{\ell(x_i)} \int_{0}^{d(x_i)} dx \, dz = (\text{PROFILE AREA TO } x = x_i \text{ AT } y = y_i)\times 2 \qquad \ldots\ldots (2.6.3)$$

$$\frac{\partial\nabla}{\partial z} = 2\int_{-\ell(x_i)}^{\ell(x_i)} y \, dx = \text{WATERPLANE AREA TO } x = x_i \text{ AT } z = z_i$$

As $\partial\nabla/\partial x$, $\partial\nabla/\partial y$ and $\partial\nabla/\partial z$ are variable throughout the hull, we take their maximum values when computing the value of $\delta\nabla$, i.e., we

take the profile area at $y = o$ instead of $y = y_i$ and the waterplane area at $z = o$ instead of $z = z_i$. This gives an upper bound to $\delta\nabla$. Values of $\delta\nabla$ as a percentage of the total displacement volume ∇ are shown in figure 30.

It is seen from this figure that the maximum volume error is 0.755% of the total volume. (This represents ±89 tons in a 400 ft., 11,791 tons ship with the same hull form and is equivalent to a change in draft of the model of ±0.025 inches.)

Error in wetted surface, S.

This could be derived from the hull surface equation $y = \eta(x,z)$ and the relation

$$S = 2\int_{-\ell}^{\ell}\int_{o}^{d}\left[1+(\partial\eta/\partial x)^2 + (\partial\eta/\partial z)^2\right]^{\frac{1}{2}} dx\,dz \qquad \ldots\ldots (2.6.4)$$

The resulting expressions become complicated and do not lend themselves to physical interpretation as in equations (2.6.3). A simpler approach is to assume the wetted surface to be represented by :

$$S = K\nabla^{\frac{2}{3}} \qquad \ldots\ldots (2.6.5)$$

then

$$\log S = \log K + \tfrac{2}{3}\log\nabla$$

and, therefore,

$$\frac{\delta S}{S} = \frac{2}{3}\frac{\delta\nabla}{\nabla} \qquad \ldots\ldots (2.6.6)$$

Local values of $\delta S/S$ are shown in figure 30, the maximum value being 0.503%.

FIG. 30

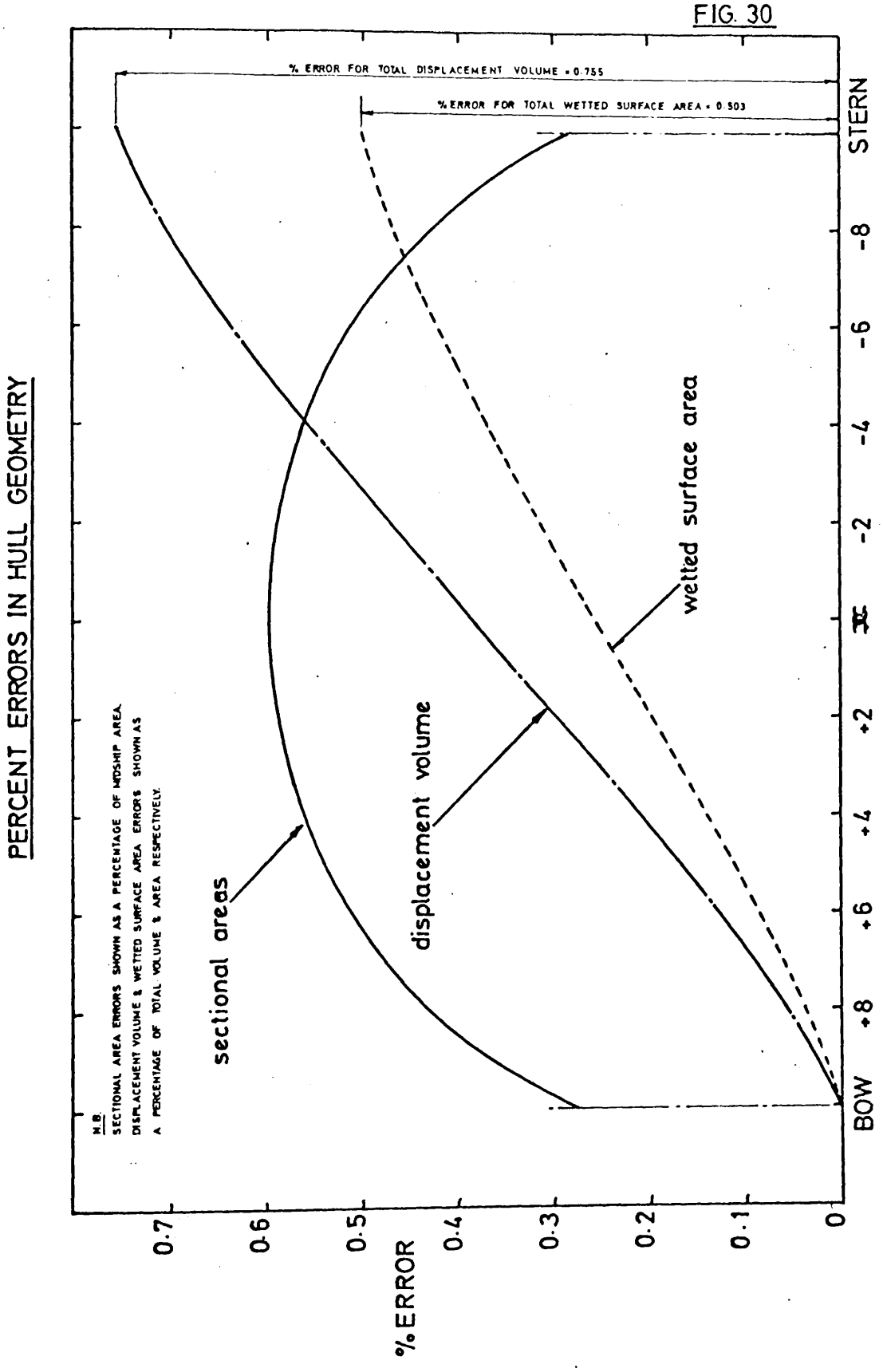
PERCENT ERRORS IN HULL GEOMETRY
% ERROR FOR TOTAL DISPLACEMENT VOLUME = 0.755
% ERROR FOR TOTAL WETTED SURFACE AREA = 0.503
N.B.
SECTIONAL AREA ERRORS SHOWN AS A PERCENTAGE OF MIDSHIP AREA.
DISPLACEMENT VOLUME & WETTED SURFACE AREA ERRORS SHOWN AS
A PERCENTAGE OF TOTAL VOLUME & AREA RESPECTIVELY.
sectional areas
displacement volume
wetted surface area
% ERROR
0.7
0.6
0.5
0.4
0.3
0.2
0.1
0
BOW
+8
+6
+4
+2
-2
-4
-6
-8
STERN

Error in Sectional Areas, $A(x_i)$

Now

$$A(x_i) = 2\int_0^{d(x_i)} y\,dx. \quad \text{For each } z_i \quad \ldots\ldots (2.6.7)$$

and so

$$\delta A = \frac{\partial A}{\partial z}.\delta z + \frac{\partial A}{\partial y}.\delta y$$

where $\frac{\partial A}{\partial y} = 2\int_0^{d(x_i)} dz$ = Twice the draft at (x_i, z_i)

$$\frac{\partial A}{\partial z} = 2y(x_i, z_i) \quad \ldots\ldots (2.6.8)$$

= The local beam at (x_i, z_i)

Maximum values of $\partial A/\partial y$ (twice the draft at $y = o$) and $\partial A/\partial z$ (the design waterline beam at $z = o$) gave an upper bound to δA. Again the errors are not compounded.

Values of δA as a percentage of the midship section area are shown in fig. 30. They range from 0.274% at the bow and stern to 0.597% amidships.

2.6.4. Force Coefficient Errors.

The effect of the above errors on the forces measured on the model must be assessed before measured values can be compared with theoretical values. Forces were calculated theoretically from the offsets given by Sharma and an allowance for the model errors discussed in section 2.6.3. is now made.

We make the arbitrary assumption that the calculated forces and moments are negligibly affected by random numerical errors such as rounding errors. We then compound errors to give 'error rectangles' on the various plots of results : errors for the ordinate and abscissa are estimated for the plots and are drawn as rectangles around representative experimental spots indicating that the spot could lie anywhere within the rectangle.

This involves an estimate of the error bounds for the general non-dimensional force coefficients. These coefficients involve the wetted surface S of the model in the denominator. By introducing the error in S calculated in section 2.6.3., we partially allow for the model error. The variations in wave pattern, boundary layer, and streamline flow are not accounted for and would be seen as a shift of the experimental curves over the speed range. The error bounds are generous, however, and it is assumed that they will envelop these other more obscure sources of error.

Error in Ct values

We have, by definition, that the total resistance coefficient, C_t, is :

$$C_t = R_T / \tfrac{1}{2} \rho S V^2$$

and, on taking logarithms this gives :

$$\text{Log}\, C_t = \text{Log}\, R_T - \text{Log}\, \tfrac{1}{2} - \text{Log}\, \rho - \text{Log}\, S - 2 \text{Log}\, V$$

Differentiation then gives :

$$\frac{\delta C_t}{C_t} = \frac{\delta R_T}{R_T} - \frac{\delta \rho}{\rho} - \frac{\delta S}{S} - 2\frac{\delta V}{V} \qquad \ldots\ldots (2.6.9)$$

Compounding the errors gives :

$$\frac{\delta C_t}{C_t} = \sqrt{\left(\frac{\delta R_T}{R_T}\right)^2 + \left(\frac{\delta \rho}{\rho}\right)^2 + \left(\frac{\delta S}{S}\right)^2 + \left(2\frac{\delta V}{V}\right)^2} \qquad \ldots\ldots (2.6.10)$$

Equation (2.6.10) was used for the error estimation of C_t.

Equation (2.6.9) shows the importance of accurate speed measurement. It is seen that for a 1% error in C_t we must have at least $\frac{1}{2}$% error in speed (assuming all other quantities have negligible error).

The only unknown component of error in equation (2.6.10) is that of water density ρ. It was found that this could be represented with sufficient accuracy by

$$\rho = a_0 + a_1 T + a_2 T^2 \qquad \ldots\ldots (2.6.11)$$

where $a_0 = 1.93582$

$a_1 = 2.47750.\ 10^{-4}$

$a_2 = 3.45022.10^{-6}$

T = Temperature in Fahrenheit degrees

Differentiation of equation (2.6.11) gives

$$\frac{\delta\rho}{\rho} = \frac{(a_1 + 2a_2 T)}{(a_0/T + a_1 + a_2 T)} \cdot \frac{\delta T}{T} = K(T).\frac{\delta T}{T} \qquad \ldots\ldots (2.6.12)$$

Values of K(T) for a range of temperatures were found to be :

Temperature (^{o}F):	50	55	60	65	70
K(T) x 10^{3}:	-2.51	-3.74	-5.15	-6.74	-8.51

The small numerical value of K(T) produces a very small error in ρ for a given error in T. For example, if $\delta T = 0.10^{o}$F at 60^{o}F, $\delta T/T = 0.17\%$ and $\delta\rho/\rho = 5.15.10^{-3}.\ 0.17 = -0.0008\%$.

The error in density due to inaccurate water temperature readings was therefore neglected.

Representative values of total resistance coefficient errors are given in table 9 from values for δR_T, $\delta S/S$ and δV found above.

Errors in Vertical Force and Trimming Moment Coefficients.

Expressions similar to equation (2.6.10) may be derived for the errors in C_Z and C_M:

$$\frac{\delta C_z}{C_z} = \sqrt{\left(\frac{\delta Z}{Z}\right)^2 + \left(\frac{\delta\rho}{\rho}\right)^2 + \left(\frac{\delta S}{S}\right)^2 + \left(2\frac{\delta V}{V}\right)^2} \qquad \ldots\ldots (2.6.13)$$

$$\frac{\delta C_m}{C_m} = \sqrt{\left(\frac{\delta M}{M}\right)^2 + \left(\frac{\delta\rho}{\rho}\right)^2 + \left(\frac{\delta S}{S}\right)^2 + \left(\frac{\delta L}{L}\right)^2 + \left(2\frac{\delta V}{V}\right)^2} \qquad \ldots\ldots (2.6.14)$$

Measurements of the model length indicated that the term $\delta L/L$ was 0.003% and could thus safely be neglected.

Using values of δZ and δM found in section 2.5.2 b, errors in C_Z and C_M were deduced and are shown in table 10.

2.6.5. Speed Function Errors.

a) Froude Number, $\mathcal{F}$.

$$\mathcal{F} = V/\sqrt{gL}$$

$$\left(\frac{\delta\mathcal{F}}{\mathcal{F}}\right)^2 = \left(\frac{\delta V}{V}\right)^2 + \left(\frac{1}{2}\frac{\delta L}{L}\right)^2 + \left(\frac{1}{2}\frac{\delta g}{g}\right)^2$$

$$\therefore \frac{\delta\mathcal{F}}{\mathcal{F}} \simeq \frac{\delta V}{V} \qquad \ldots\ldots (2.6.15)$$

b) Reynold's Number, R_n.

$$R_n = VL/\nu$$

$$\left(\frac{\delta R_n}{R_n}\right)^2 = \left(\frac{\delta V}{V}\right)^2 + \left(\frac{\delta L}{L}\right)^2 + \left(\frac{\delta \nu}{\nu}\right)^2$$

$$\therefore \frac{\delta R_n}{R_n} \simeq \frac{\delta V}{V} \qquad \ldots\ldots (2.6.16)$$

c) $(\log_{10} R_n - 2)^{-2}, \Lambda$.

$$\Lambda^{-\frac{1}{2}} = \log_{10} R_n - 2$$

$$\therefore -\tfrac{1}{2}\log\Lambda = \log(\log_{10} R_n - 2)$$

$$\therefore \frac{\delta\Lambda}{\Lambda} \simeq -\frac{2\,\delta(\log_{10} R_n)}{\log_{10} R_n}$$

We find that

$$\frac{\delta(\text{Log}_{10}R_n)}{\text{Log}_{10}R_n} \simeq \frac{\delta(\text{Log}_{10}V)}{\text{Log}_{10}V}$$

with the result that

$$\frac{\delta\Lambda}{\Lambda} \simeq \frac{2\,\delta(\text{Log}_{10}V)}{\text{Log}_{10}V} \qquad \ldots\ldots (2.6.17)$$

Representative values of $\delta\Lambda$ and $\delta\mathcal{F}$ are given in tables 9 and 10.

2.6.6. Errors in non-dimensional sinkage and trim values.

Mean sinkage s and trim τ were expressed in non-dimensional form.

$$C_s = \frac{s}{L}.10^2 \quad , \quad C_\tau = \frac{\tau}{L}.10^2$$

$$\therefore \frac{\delta C_s}{C_s} \simeq \frac{\delta s}{s} \quad , \quad \frac{\delta C_\tau}{C_\tau} \simeq \frac{\delta\tau}{\tau} \qquad \ldots\ldots (2.6.18)$$

Now, s and τ are defined by :

$$s = \frac{s_B + s_S}{2} \quad , \quad \tau = s_S - s_B \qquad \ldots\ldots (2.6.19)$$

where s_B = Bow sinkage

s_S = stern sinkage

$$\therefore \frac{\delta s}{s} = \frac{\sqrt{\delta s_B^2 + \delta s_S^2}}{s_B + s_S} \quad , \quad \frac{\delta\tau}{\tau} = \frac{\sqrt{\delta s_B^2 + \delta s_S^2}}{s_S - s_B}$$

But $\delta s_S = \delta s_B = \delta s^1$ from Section 2.5.2.c.

$$\frac{\delta s}{s} = \frac{\sqrt{2}.\delta s'}{(s_S + s_B)} \quad , \quad \frac{\delta\tau}{\tau} = \frac{\sqrt{2}.\delta s'}{(s_S - s_B)} \qquad \ldots\ldots (2.6.20)$$

Equation (2.6.20) is substituted into equation (2.6.18). Typical values of δC_s and δC_τ are shown in table 10.

2.6.7. Conclusions

A summary of the equipment and model errors, and the relevant expressions to deduce errors in the non-dimensional force, moment and speed coefficients are given in table 11.

'Error rectangles' are shown on all non-dimensional plottings of experimental results. Instead of drawing fair curves through experimental spots it is suggested that it is more appropriate to draw a narrow band, enveloping the error rectangles, the experimental results lying within this band. This is illustrated in figure 31.

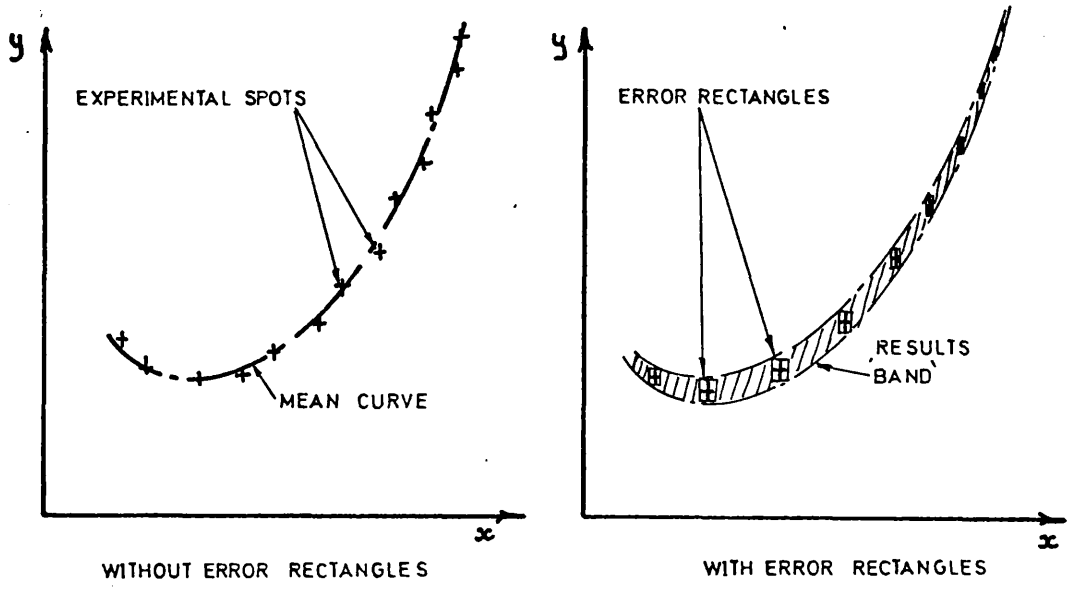

RESULTS PLOTTING SHOWING ERRORS

FIG. 31

The error rectangles shown in figures 14, 24 and 32 indicate that much of the scatter of the spots in the low-speed range is covered by the error rectangles. This corroborates Scott's conclusions in reference 103. Approximate values of scatter obtained from the results given in table 21 are compared with the out-to-out percentage C_t values ($200\ \delta C_t/C_t$) for a range of speeds in table 12.

V ft/sec.	$C_t.10^3$	$\delta C_t.10^3$	$\Lambda 10^2$	$\delta\Lambda 10^2$
2.107	4.627	±0.047	5.745	±0.007
2.674	4.557	±0.034	5.475	±0.003
2.996	4.644	±0.031	5.346	±0.003
3.928	4.240	±0.024	5.066	±0.002
6.480	7.161	±0.036	4.604	±0.001

Table 9

$\mathcal{F}$	$\delta\mathcal{F}$	$C_Z.10^2$	$\delta C_Z 10^2$	$C_M.10^3$	$\delta C_M 10^3$	C_s	δC_s	C_τ	δC_τ
0.2004	±0.0006	-2.449	±0.097	+3.247	±0.430	-0.124	±0.008	+0.004	±0.008
0.3063	±0.0006	-2.920	±0.068	+1.847	±0.184	-0.380	±0.008	+0.005	±0.008
0.4088	±0.0006	-3.858	±0.030	-1.281	±0.104	-0.842	±0.008	+1.301	±0.008
0.4983	±0.0006	-3.579	±0.025	-4.995	±0.074	-1.084	±0.008	+4.325	±0.008
0.6019	±0.0006	-2.432	±0.016	-4.807	±0.053	-0.928	+0.008	+5.537	±0.008

Table 10

Estimated Errors		Calculated Errors	
Quantity	Error	Quantity	Compounded Error
Speed, V	± 0.001 ft/sec	$C_t = R_T/\frac{1}{2}\rho S V^2$	$\left[\left(\frac{\delta R_T}{R_T}\right)^2 + \left(\frac{\delta S}{S}\right)^2 + \left(2\frac{\delta V}{V}\right)^2\right]^{\frac{1}{2}}$
Total resistance, R_T	± 0.003 lb	$C_Z = Z/\frac{1}{2}\rho S V^2$	$\left[\left(\frac{\delta Z}{Z}\right)^2 + \left(\frac{\delta S}{S}\right)^2 + \left(2\frac{\delta V}{V}\right)^2\right]^{\frac{1}{2}}$
Vertical Force, Z	± 0.163 lb.	$C_M = M/\frac{1}{2}\rho S L V^2$	$\left[\left(\frac{\delta M}{M}\right)^2 + \left(\frac{\delta S}{S}\right)^2 + \left(2\frac{\delta V}{V}\right)^2\right]^{\frac{1}{2}}$
Triming Moment, M	± 0.625 lb.ft.	$\mathcal{F} = V/\sqrt{gL}$	$\delta V/V$
Bow and Stern Sinkage, s^1	± 0.001 inches	$R_n = VL/\nu$	$\delta V/V$
Model offsets x,y,z	±0.005 in. ±0.027 in. ±0.005	$\Lambda = (\log_{10} R_n - 2)^{-2}$	$2\delta(\log_{10} V)/\log_{10} V$
Model disp. Volume, ∇	±0.031 $ft.^3$ max.	$C_s = S/L^2 \times 100$	$\sqrt{2}\,\delta s'/(S_s + S_s)$
Model wetted Surface, S	±0.078 ft^2 Max.	$C_\tau = \tau/L^2 \times 100$	$\sqrt{2}\,\delta s'/(s_s - S_s)$
Cross section area	±0.004 ft^2 (midships)		

Table 11

V ft/sec.	R_n 10^{-6}	Compounded 200 $\delta C_t/C_t$	Scatter 200 $\delta C_t/C_t$
2.107	1.47	2.0	2.1
2.674	1.87	1.5	2.0
2.996	2.10	1.3	1.5
3.928	2.76	1.1	1.1
6.480	4.55	1.0	0.4

Table 12

It was concluded that the sources of error listed in section 2.6.1 were responsible for most of the experimental scatter. After correction for blockage, temperature and tide, equipment errors were responsible for most of the remaining scatter.

It was found that comparatively large model offset errors had small effects on volumes and areas. It was not possible to allow for the effect of this model error on wave pattern, boundary layers and streamlines. This is important when attempting to compare experiment with theory, but it appeared that the deficiencies in the theory are such that a closer investigation of this point was unnecessary.

A comparison of figures 32, 41 and 42 shows that total resistance was measured more accurately than the vertical force Z and considerably more accurately than the trimming moment M. This is almost certainly due to the fact that the measurements of Z and M were made with the model rigidly attached to the towing carriage, a circumstance which was unavoidable. Carriage vibration was transmitted to the ultra violet records and their subsequent analysis was subject to inaccuracies. The trimming moment M, being a function of the difference of two large quantities (viz. the bow and stern vertical forces) was thus less accurate than Z.

2.7. DISCUSSION OF RESULTS

2.7.1. Geosim Series

Results for total resistance, mean sinkage and trim for the Glasgow model have been compared with the results of Inui and Sharma.

For the comparison of total resistance results, two different geosim plottings were used, one the well-known Telfer diagram and one due to Taniguchi (105).

2.7.1.a. Telfer Diagram (fig. 32)

Total resistance coefficients are given in table 13 and are shown in fig. 32 where they are plotted on a base of $(\log_{10}Rn-2)^{-2}$. This linearises certain basic friction lines. Also shown are the results obtained by Sharma and Inui. All the results shown have been corrected for blockage and temperature in the same manner.

Lines joining C_t values at equal Froude Numbers (iso-Froude lines) are shown in figure 14 and it was apparent that the Glasgow results were consistently low at all speeds.

This led to the adoption of plate studs described in section 2.5.2.a. These increased the total resistance coefficients slightly and these coefficients have been re-plotted in figure 32.

A basic friction line, due to Hughes (106) was used by Inui in conjunction with a constant from factor, r, to give a viscous resistance line of equation

$$C_v = (1+r)(1.328\,R_n^{-0.5} + 0.04\,R_n^{-0.114}) \qquad \ldots\ (2.7.1)$$

Sharma, in reference 53, gave a value of r as 0.18 ± 0.15. A viscous line given by equation (2.7.1) with $r = 0.18$ is shown in figure 32 and is apparently confirmed by the low-speed results of all three models.

Throughout the speed range $0.10 \leq \nabla \leq 0.35$ the iso-Froude lines are approximately parallel to this viscous line. A poor correlation between the iso-Froude lines and the viscous resistance line occurs in the speed range $0.35 \leq \nabla \leq 0.65$ and this may be due to the following causes :

i) Experimental errors.

Error rectangles show that some discrepancies will

$\mathcal{F}$	$\Lambda \times 10^2$	$C_t \times 10^3$	$\mathcal{F}$	$\Lambda \times 10^2$	$C_t \times 10^3$
0.311	4.810	7.97	0.372	4.648	8.07
0.126	5.757	4.07	0.368	4.658	7.80
0.153	5.528	4.45	0.385	4.619	8.62
0.184	5.328	4.52	0.380	4.632	8.30
0.215	5.164	4.57	0.396	4.595	9.19
0.251	5.013	5.95	0.407	4.572	10.40
0.198	5.249	4.54	0.401	4.585	9.72
0.232	5.090	5.52	0.413	4.561	10.94
0.263	4.966	5.89	0.425	4.536	12.16
0.255	4.997	6.05	0.420	4.545	11.80
0.143	5.609	4.53	0.441	4.504	13.70
0.257	4.989	5.98	0.434	4.518	13.12
0.278	4.913	5.97	0.454	4.480	14.65
0.272	4.933	5.74	0.455	4.479	14.75
0.289	4.879	6.42	0.450	4.487	14.59
0.299	4.847	7.25	0.427	4.531	12.59
0.317	4.792	8.36	0.340	4.728	8.20
0.332	4.751	8.42	0.295	4.858	6.98
0.325	4.769	8.59	0.266	4.954	5.84
0.340	4.730	8.26	0.204	5.220	4.83
0.331	4.752	8.61	0.196	5.264	4.73
0.354	4.693	7.81	0.168	5.428	4.53
0.347	4.711	7.99	0.138	5.651	4.51
0.361	4.675	7.84	0.143	5.609	4.52
0.115	5.864	4.48	0.224	5.124	5.13

L = 8.6 ft., S = 15.714 ft.^{2}

$\mathcal{F} = V/\sqrt{gL}$, $\Lambda = (\log_{10} R_n - 2)^{-2}$ $C_t = R_T/\frac{1}{2}\rho SV^2$,

ALL RESULTS CORRECTED FOR BLOCKAGE, TEMPERATURE AND TIDE EFFECTS.

NON-DIMENSIONAL RESISTANCE RESULTS TABLE 13

- NAKED HULL - PLATE STUD STIMULATION

FIG. 32

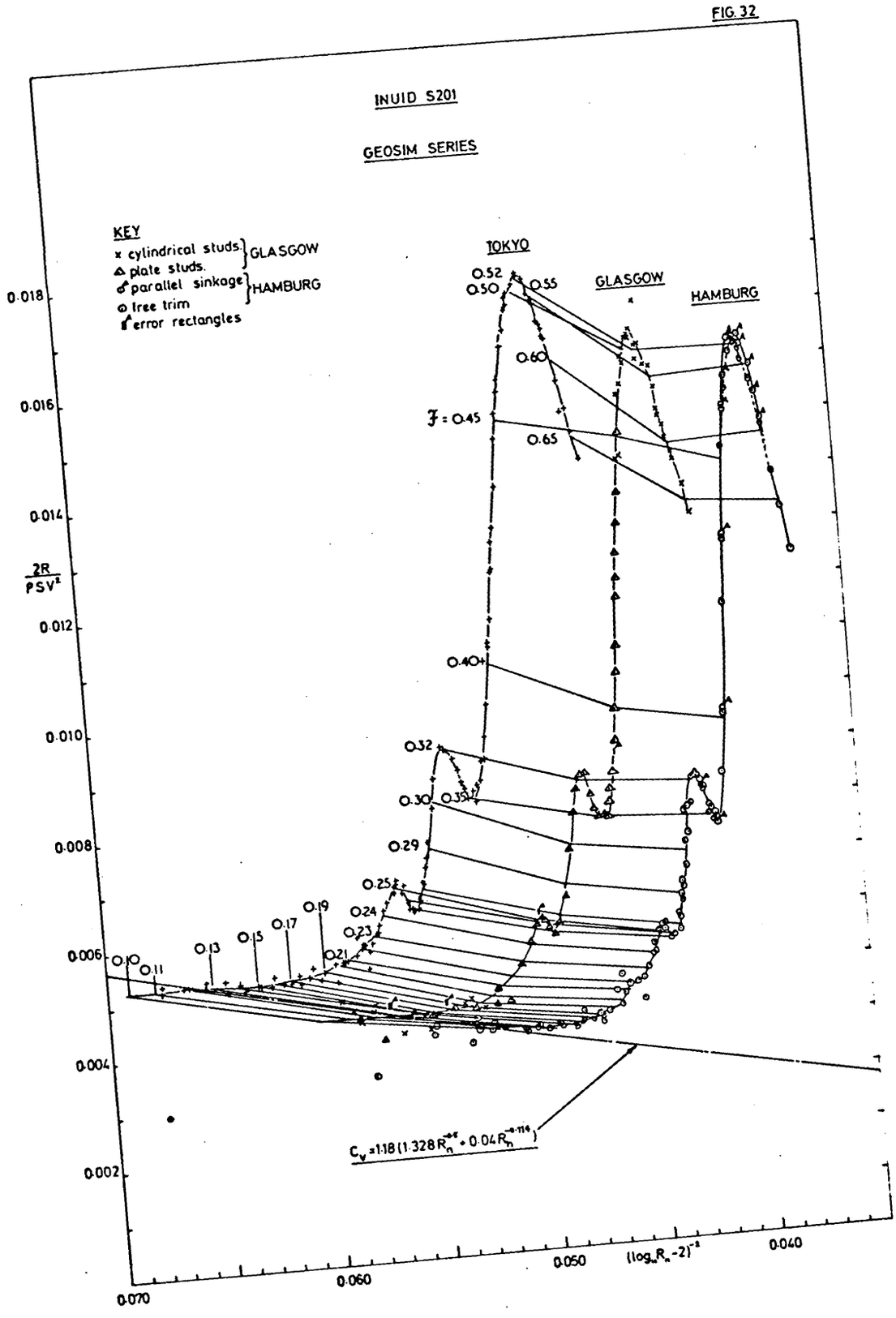
INUID S201
GEOSIM SERIES
KEY
× cylindrical studs } GLASGOW
△ plate studs.
♂ parallel sinkage } HAMBURG
⊙ free trim
error rectangles
TOKYO
GLASGOW
HAMBURG
0.52
0.50
0.55
0.60
F = 0.45
0.65
0.40
0.32
0.30
0.35
0.29
0.25
0.24
0.23
0.21
0.19
0.17
0.15
0.13
0.11
0.10
0.018
0.016
0.014
2R/ρSV²
0.012
0.010
0.008
0.006
0.004
0.002
0.070
0.060
0.050
(log₁₀R_n - 2)⁻²
0.040
C_v = 1.18 (1.328 R_n^-0.5 + 0.04 R_n^-0.114)

occur in the C_t values at a given Froude Number. Slight differences between the models due to manufacture were almost certain to exist and these would give rise to further errors. This is discussed further in section 2.7.1.c.

ii) Model size.

Inui's model was 5.74 ft. in length and accurate experimental results on such a small model are difficult to obtain. Webster has shown (107) that models less than 5 ft. in length are affected by surface tension effects.

iii) Parallel sinkage and free trim.

Inui's model was allowed only to sink and not to trim. Sharma presented results obtained with and without 'parallel sinkage' (Inui's term) whereas the Glasgow results were obtained without parallel sinkage, the model being allowed to take up its natural running trim. Both Sharma's 'free trim' and 'parallel sinkage' results are shown in figure 32 where it is obvious that at $\mathcal{F} > 0.45$ the geosim curve relevant to Inui's model is dissimilar to the others. It is also possible that at lower Froude numbers this parallel sinkage caused small discrepancies in C_t values.

iv) Variation of Form Resistance with Froude Number.

It is seen from equation (2.7.1) that 'form factors', r and r_{ff} may be defined as

$$r = (C_v/C_{f_o}) - 1 = (R_v/R_{f_o}) - 1 \qquad \ldots\ (2.7.2)$$

$$\text{cf. } r_{ff} = R_{ff}/R_{f_o}$$

where r is a measure of form resistance and r_{ff} a measure of friction form resistance.

Sharma obtained values for r from a comparison of his own and Inui's results (ref. 53 p.410) and found some variation of r with Froude Number. As r is some function of the slope of the iso-Froude lines any variation of r with Froude Number will appear as a change of slope of the iso-Froude lines in figure 32.

(Iso-Froude lines in figures 14 and 32 are shown as straight lines joining results for each model. This is not meant to imply that the lines are in fact straight - a deduction which could not be made without a larger geosim series - but is meant to give a general indication of their slope. To draw an arbitrary curve through three points at any Froude number, thus presupposing the shape of the iso-Froude lines, was considered unjustifiable.)

2.7.1.b. Taniguchi Diagram (figure 33)

Following Froude's assumptions, it is postulated that

$$C_t = C_v + C_w \qquad \ldots\ (2.7.3)$$

A further assumption, implied by equation (2.7.1) is that

$$C_v = (1+r)C_{fo}$$

Insertion of this relation in equation (2.7.3) gives

$$C_t = (1+r)C_{fo} + C_w \qquad \ldots\ (2.7.3a)$$

We may interpret equation (2.7.3.a) at any Froude number as the equation to a straight iso-Froude line; the gradient is (1+r), C_t is the dependent variable, C_{fo} the independent variable, and C_w a constant. A plotting of C_t as ordinate with C_{fo} as abscissa for a geosim series will thus yield the form factors r at any Froude Number from the slopes of the iso-Froude lines and values of C_w by extrapolation to the line $C_{fo} = o$. This method was used by Taniguchi

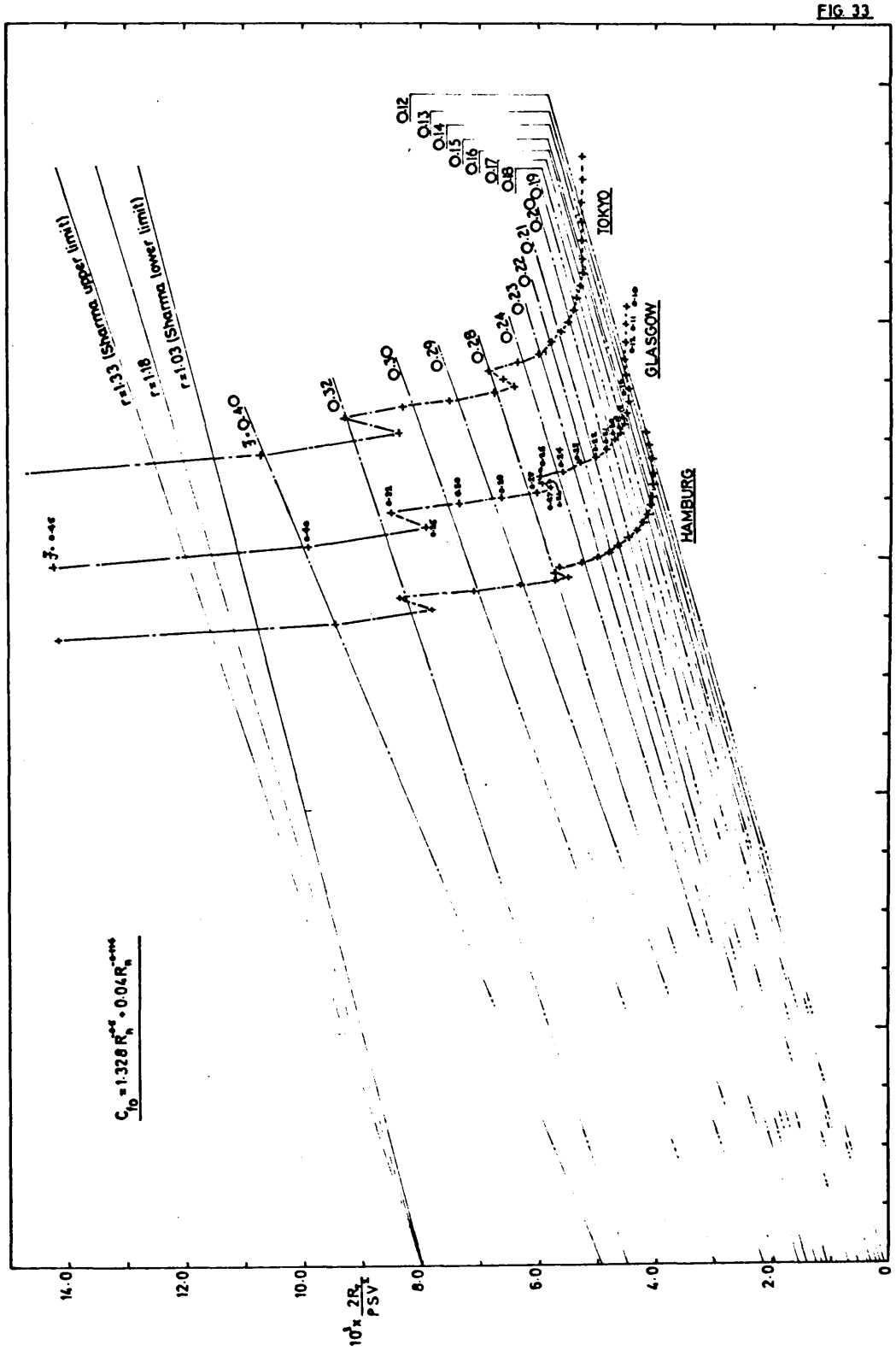
INJID S201 - GEOSIM SERIES
FIG. 33
$C_{10} = 1.328\,R_n^{-0.5} + 0.04\,R_n^{-0.5}$
r=1.33 (Sharma upper limit)
r=1.18
r=1.03 (Sharma lower limit)
TOKYO
GLASGOW
HAMBURG
$10^3 \times \frac{2R_n}{PSV^2}$
$C_{10} \times 10^3$

in reference 105 and by Conn and Ferguson in reference 59.

Also shown on figure 33 are the upper and lower bounds for r given by Sharma.

It is immediately apparent that the Glasgow C_t values are lower than would have been expected, in spite of the addition of plate studs. The Taniguchi plotting makes great demands on experimental accuracy and it shows up deficiencies in the results of the three Inuids. Iso-Froude lines were drawn using Sharma's and Inui's results in conjunction with the Glasgow results wherever possible.

2.7.1.c. Sinkage and trim results.

Values of C_s and C_τ for the Glasgow model are given in table 14 and are plotted with the results of Inui and Sharma in figures 34 and 35.

Mean sinkage.

Mean sinkage results for the three models are compared in figure 34. Both Sharma's and Inui's results for 'parallel sinkage' are given and these are seen to diverge from the free trim results above a Froude Number of 0.43. This corresponds to a slight increase of resistance in this speed range, shown in figure 22, which suggests that free trim has an effect on mean sinkage and total resistance.

From the arguments advanced in section 2.4, an increase in mean sinkage would be expected to correspond to an increase in form resistance which in turn would lead to an increase in total resistance. However, it is probable that boundary layer and wave pattern modification due to the presence or absence of free trim cause the apparently anomalous resistance results in this speed range.

It is apparent from figure 34 that Sharma's model has a correspondingly greater mean sinkage at low speeds than either the Glasgow or Tokyo models. This may be due to a scale effect on mean sinkage but a contributory factor may be that there is a slight discrepancy in the displacement volume of Sharma's model. The

FIG. 34

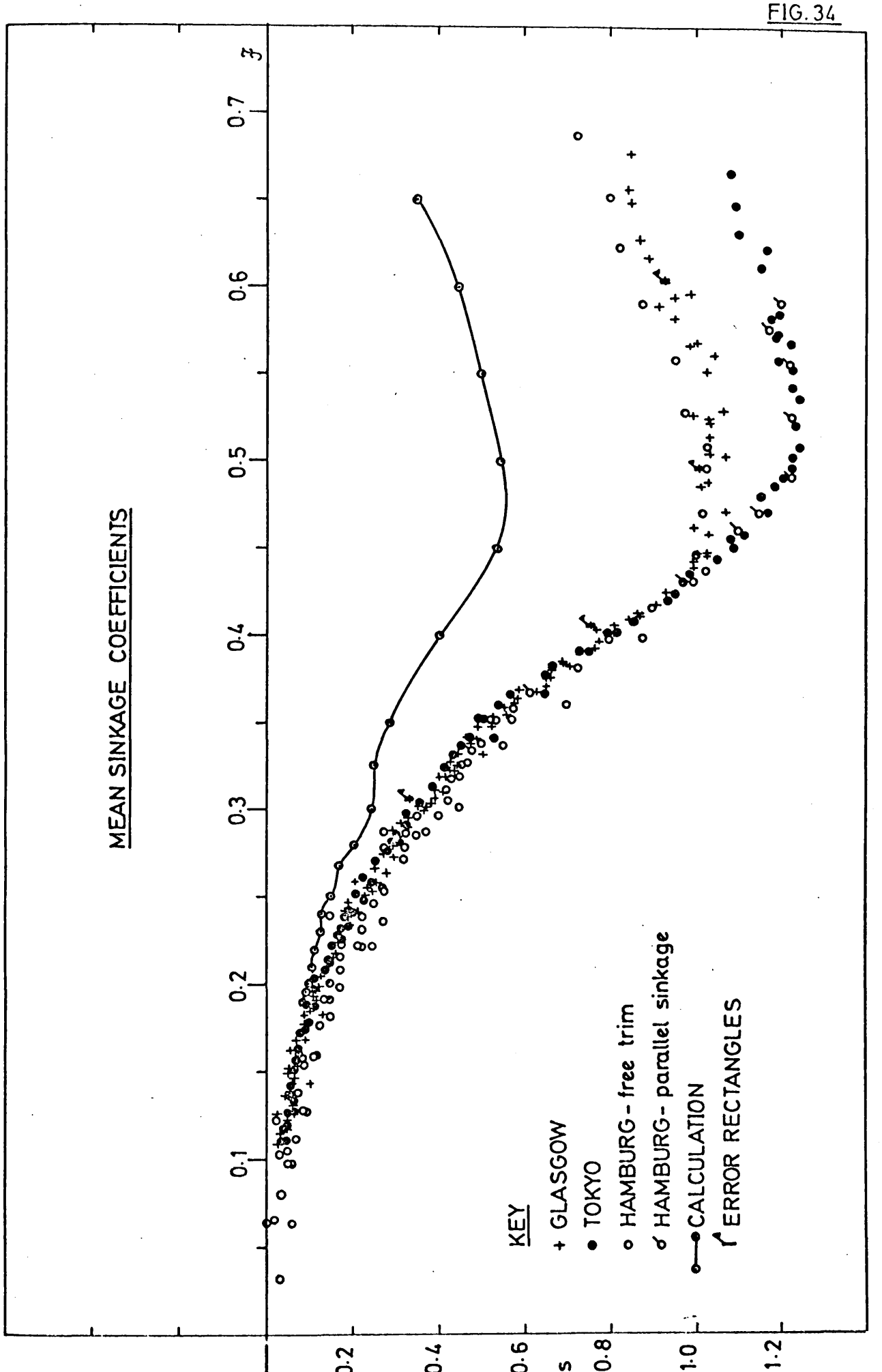
MEAN SINKAGE COEFFICIENTS
KEY
+ GLASGOW
• TOKYO
○ HAMBURG - free trim
σ HAMBURG - parallel sinkage
CALCULATION
ERROR RECTANGLES
C_s
$\frac{x}{}$
0.1
0.2
0.3
0.4
0.5
0.6
0.7
-0.2
-0.4
-0.6
-0.8
-1.0
-1.2

FIG. 35

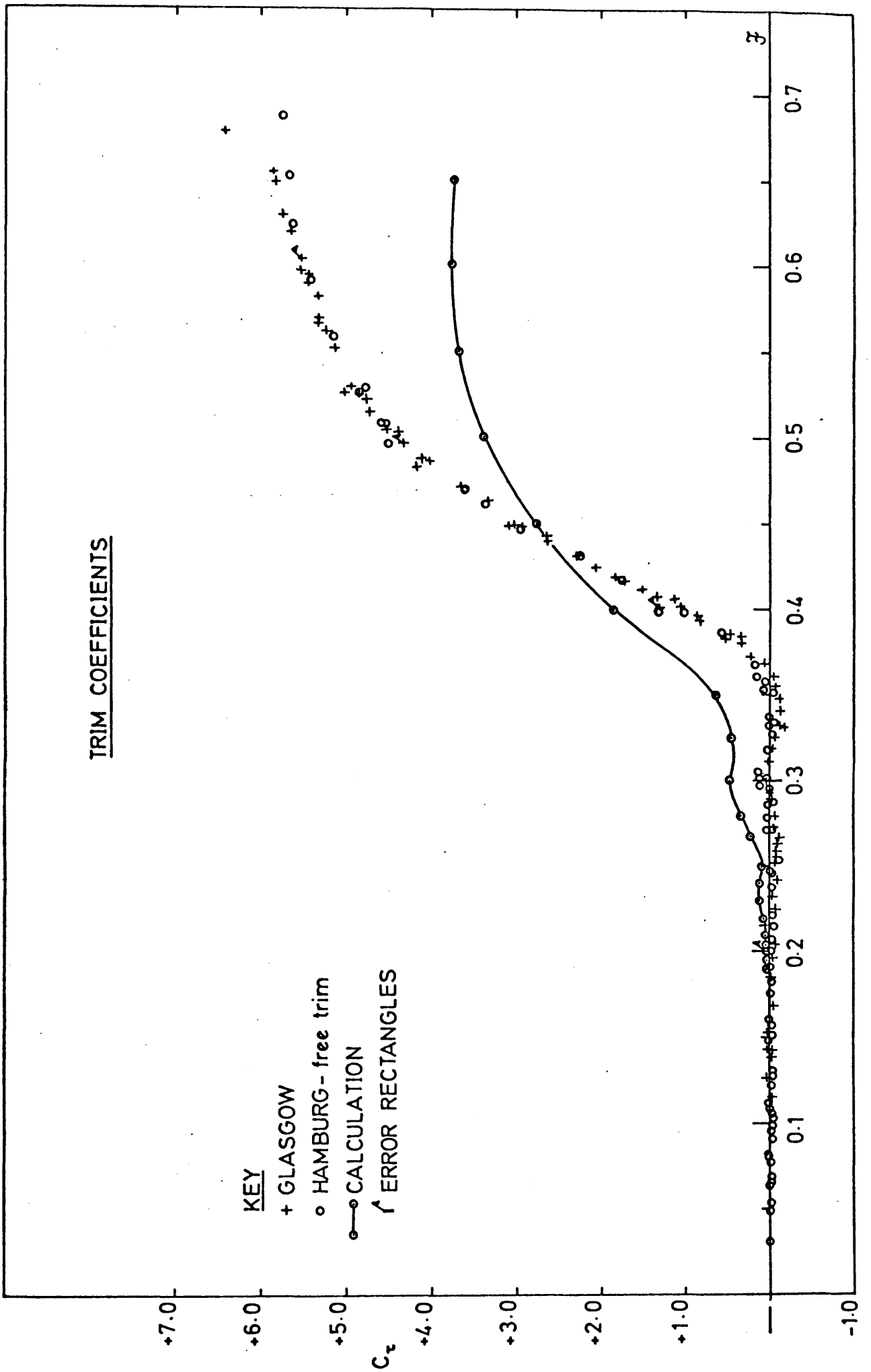
TRIM COEFFICIENTS
KEY
+ GLASGOW
o HAMBURG - free trim
CALCULATION
ERROR RECTANGLES
C_z
+7.0
+6.0
+5.0
+4.0
+3.0
+2.0
+1.0
-1.0
0.1
0.2
0.3
0.4
0.5
0.6
0.7
$\frac{x}{L}$

$\mathcal{F}$	C_s	C_t	$\mathcal{F}$	C_s	C_t
0.311	-0.415	+0.005	0.401	-0.810	+1.065
0.126	-0.026	+0.027	0.413	-0.865	+1.530
0.153	-0.071	+0.003	0.340	-0.462	-0.214
0.184	-0.105	-0.003	0.295	-0.331	-0.058
0.215	-0.159	+0.057	0.266	-0.259	-0.107
0.251	-0.234	-0.070	0.204	-0.131	-0.076
0.198	-0.124	+0.004	0.196	-0.119	-0.058
0.232	-0.202	-0.044	0.168	-0.094	-0.053
0.263	-0.280	-0.100	0.138	-0.057	-0.024
0.255	-0.238	-0.079	0.143	-0.061	-0.017
0.143	-0.106	+0.003	0.115	-0.034	-0.009
0.257	-0.259	-0.081	0.224	-0.167	-0.095
0.278	-0.298	-0.072	0.241	-0.182	-0.100
0.272	-0.299	-0.054	0.411	-0.868	+1.516
0.289	-0.333	-0.023	0.425	-0.934	+2.059
0.299	-0.366	-0.005	0.417	-0.906	+1.727
0.317	-0.416	-0.019	0.418	-0.906	+1.812
0.332	-0.446	-0.119	0.431	-0.972	+2.299
0.325	-0.444	-0.053	0.439	-0.998	+2.631
0.340	-0.490	-0.122	0.449	-1.056	+3.006
0.331	-0.511	-0.172	0.448	-1.002	+2.904
0.354	-0.560	-0.070	0.406	-0.809	+1.149
0.347	-0.525	-0.123	0.459	-1.028	+3.099
0.361	-0.579	-0.040	0.483	-1.155	+4.175
0.372	-0.649	+0.212	0.443	-0.991	+2.659
0.368	-0.588	+0.051	0.463	-0.996	+3.321
0.385	-0.690	+0.476	0.486	-1.018	+4.007
0.380	-0.666	+0.333	0.486	-1.034	+4.109
0.396	-0.786	+0.860	0.515	-1.035	+4.704
0.407	-0.842	+1.301	0.497	-1.084	+4.325

$\mathcal{F} = V/\sqrt{gL}$, $C_s = \frac{1}{2}(s_B + s_s) \times 100/L$, $C_t = (s_s - s_B) \times 100/L$, L = 8.6 ft.

NON-DIMENSIONAL MEAN SINKAGE AND TRIM RESULTS - NAKED HULL

Table 14

$\mathcal{J}$	C_s	C_τ	$\mathcal{J}$	C_s	C_τ
0.503	-1.073	+4.396	0.471	-1.068	+3.664
0.524	-1.025	+4.846	0.505	-1.036	+4.519
0.526	-0.997	+5.011	0.604	-0.928	+5.537
0.529	-1.062	+4.955	0.618	-0.891	+5.660
0.550	-1.028	+5.156	0.628	-0.868	+5.766
0.561	-1.044	+5.233	0.566	-0.986	+5.350
0.568	-1.000	+5.321	0.589	-0.912	+5.459
0.582	-0.950	+5.324	0.595	-0.987	+5.539
0.594	-0.954	+5.461	0.650	-0.851	+5.826
0.403	-0.766	+1.241	0.678	-0.852	+6.443

ALL RESULTS CORRECTED FOR BLOCKAGE AND TIDE EFFECTS

Table 14 Contd.

scale factor for Sharma's model in relation to Inui's model is 2.28571 which gives a scale displacement volume of 0.4137 m^3 for Sharma's model. Sharma quotes a displacement volume of 0.4102 m^3 a discrepancy of 0.0035 m^3.

The effect of this discrepancy on mean sinkage may be demonstrated by the use of Horn's analysis (equation 2.4.3.) and a result due to Havelock (12, p.610). Using Horn's equation (2.4.3), Havelock deduced the following approximate relation for the velocity increment over a semi-submerged prolate spheroid at low speeds :

$$\frac{\delta V}{V} = K_1 \qquad \ldots\ldots (2.7.4)$$

where K_1 is the virtual inertia coefficient of the spheroid for axial motion. Assuming that the shape of the Inuid S201 is sufficiently close to that of a spheroid for equation (2.7.4) to hold, equation (2.4.3) shows that there is some relation between mean sinkage, s, and K_1 thus

$$K_1 = f_m(V, s) \qquad \ldots\ldots (2.7.5)$$

Using a method due to Taylor, cited by Havelock (12, p.501) and Robertson (88, p.207), K_1 may be calculated approximately from the moment in the x-direction of the body source distribution M_s and the volume of displacement :

$$K_1 = \frac{4\pi M_s}{V\nabla} - 1 \qquad \ldots\ldots (2.7.6)$$

where

$$M_s = \int_s \sigma x \, dS \qquad \ldots\ldots (2.7.7)$$

If the models are all exactly geometrically similar K_1 will have the same value for each. Any slight model error, particularly in displacement volume, will have an effect on K_1. One might expect this to be reflected in the mean sinkage at low speeds if relation (2.7.5) hold

Inaccuracies in low-speed mean sinkage measurement for the Hamburg model could also account for the apparent scale effect but the close agreement between the results of the Tokyo and Glasgow models indicates

the existence of the greater systematic error discussed above.

Trim

Trim is seen to be slightly by the head in the speed range $0 \leq \nabla \leq 0.36$ and then changes sign to a trim by the stern accompanied by a decrease in mean sinkage as speed increases.

Scale effect on trim is not apparent except perhaps in the speed range $0.25 \leq \nabla \leq 0.37$ where trim is changing sign as the second wave crest moves aft with increase of speed. (See figure 36). In this speed range interaction between the model wave system and its boundary layer will affect, and be affected by, small changes of trim : as speed increases the increased bow wave height and length causes the bow to rise causing a trim by the stern. This is associated with a changed boundary layer and a changed total resistance. The total resistance will produce a moment opposing the trimming moment which will attempt to reduce the trim by the stern. This has been discussed in section 2.3 and by Bessho (84) who refers to it as a 'feed-back' effect. In this Froude number range the effect of flow conditions on trim is seen to be important. Any dissimilarity between the geosims would be expected to become apparent at these speeds.

2.7.2. Wave Resistance.

Values of wave resistance, deduced both from experiment and calculation, were compared.

2.7.2.a. Empirically deduced wave resistance

Wave resistance coefficients, $C_W = R_W/\frac{1}{2}\rho SV^2$, are shown in figure 37 for the three models. The coefficients have been deduced from equations (2.7.1) and (2.7.3) and also from figure 33 using the method described in section 2.7.1.b. Moderately good agreement between the two methods was obtained over most of the range $0.12 \leq \nabla \leq 0.40$ with good agreement in the lower speed range. The poor agreement at higher speeds is probably due to inaccuracies arising from total resistance results plotted in figure 33. Once again the difficulty of obtaining reliable measurements of wave resistance is emphasised.

FIG. 36

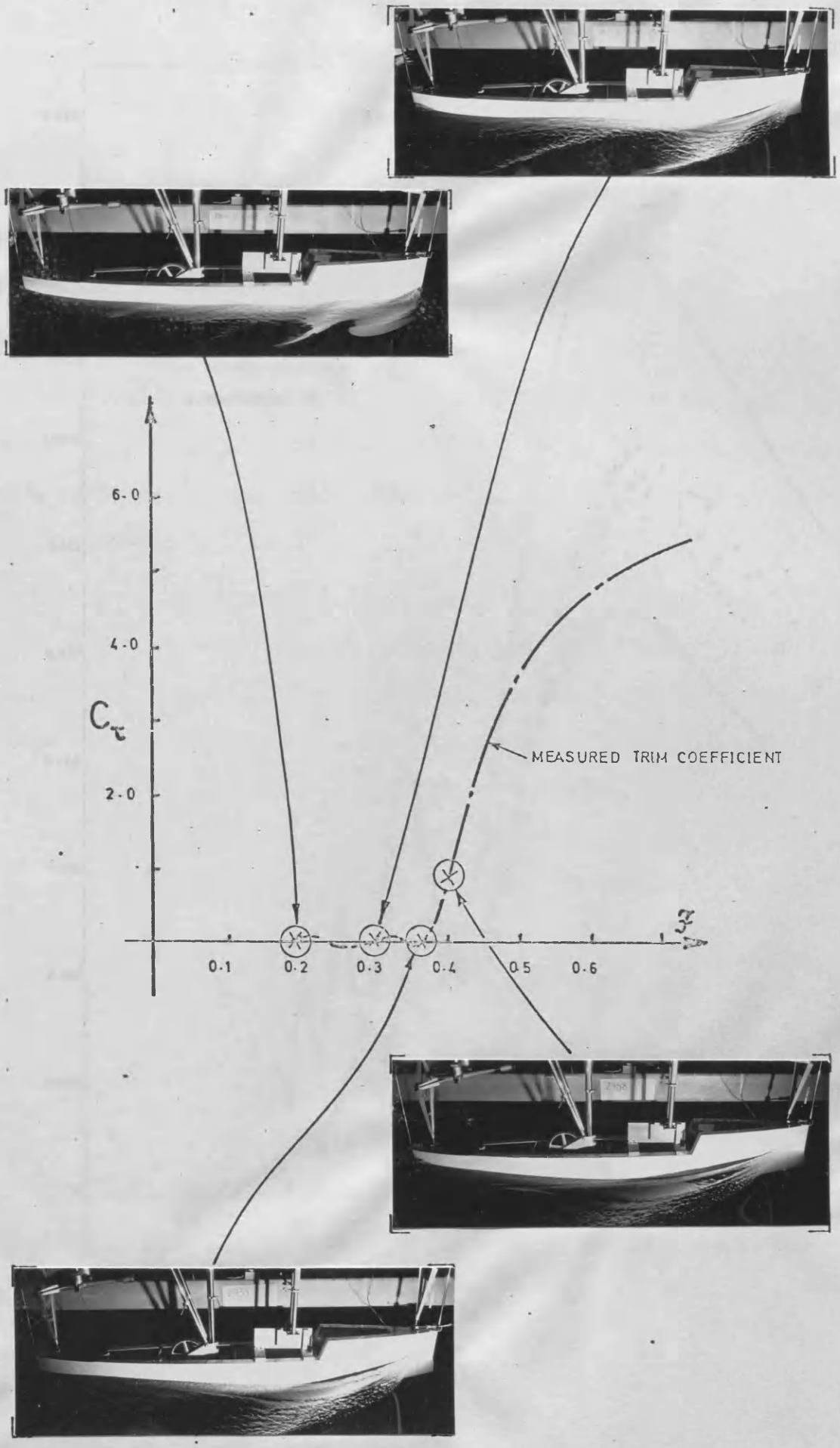

TRIM AND WAVE PROFILES

FIG. 37

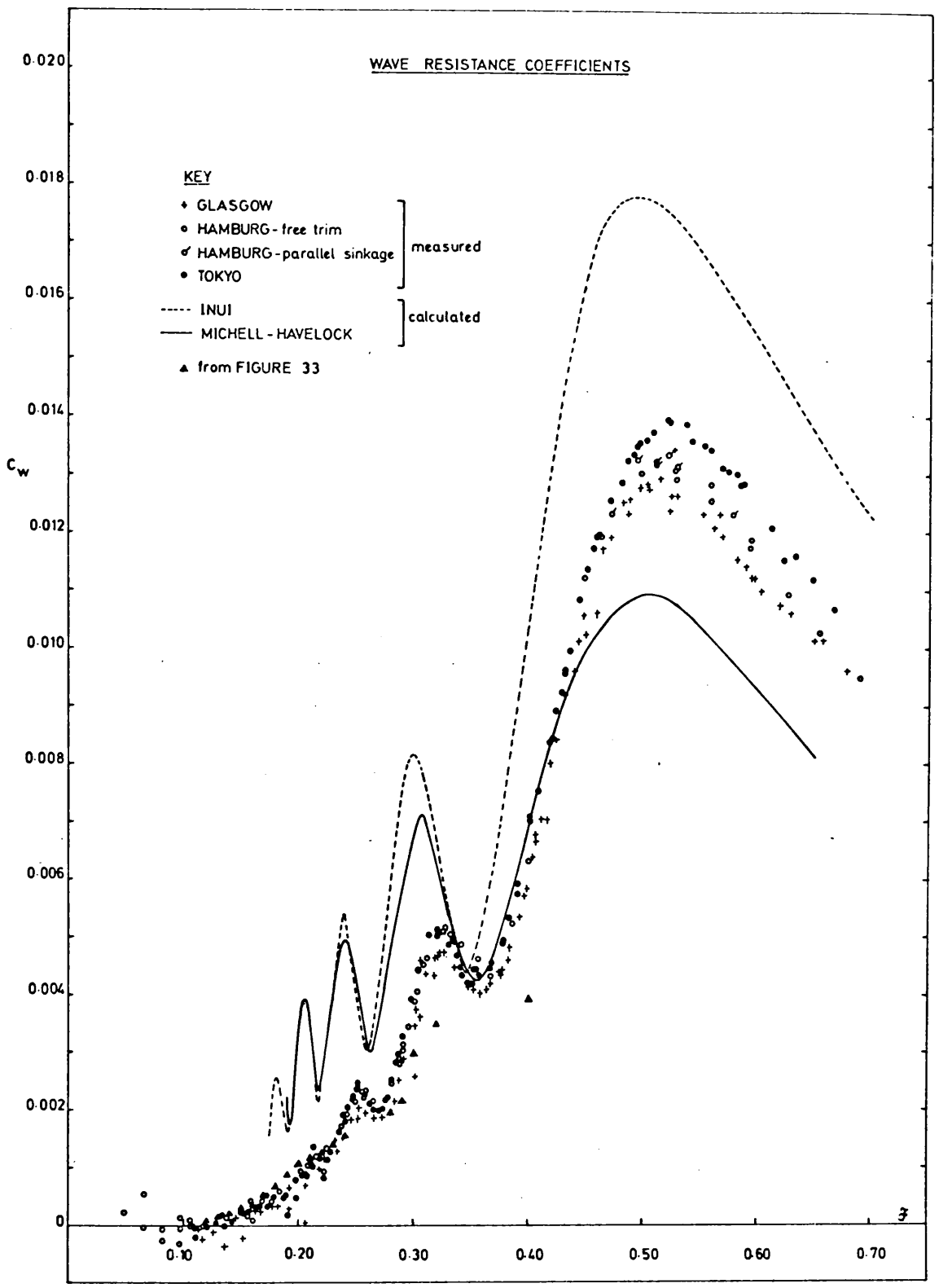
WAVE RESISTANCE COEFFICIENTS
KEY
GLASGOW
HAMBURG - free trim
HAMBURG - parallel sinkage
TOKYO
measured
INUI
MICHELL - HAVELOCK
calculated
from FIGURE 33
C_w
0·020
0·018
0·016
0·014
0·012
0·010
0·008
0·006
0·004
0·002
0
0·10
0·20
0·30
0·40
0·50
0·60
0·70
$\mathcal{F}$

Nevertheless a unique empirical curve of wave resistance appears reasonably well defined with the Glasgow results a little lower than those of Sharma and Inui, for reasons which have been discussed elsewhere. At high speeds the effects of 'parallel sinkage' and 'free trim' are apparent, the results of Inui being markedly higher than Sharma's 'parallel sinkage' values.

It appeared from observation that flow separation was occurring at high Froude Numbers. This would probably give rise to complex interaction between viscous and wave resistances which would invalidate equation (2.7.3.). Empirical wave resistance values at high speeds are therefore of doubtful value and their comparison with theory must be tentative.

2.7.2.b. Calculated Wave Resistance

Shown in figure 37 and table 15 are wave resistance coefficients calculated using both Inui's theory (section 2.2.2.) in conjunction with his asymptotic wave resistance functions (25 p.202) and the Michell-Havelock theory given in sections 2.1.2. a, 2.3 and appendix B.

It is at once apparent that for $\nabla > 0.25$ there is a wide discrepancy between C_W values calculated using the above theories. Inui's theory without correction factors gives values which overestimate C_W in the range $0.25 \leq \nabla \leq 0.65$ whereas the Michell theory gives good agreement in the range $0.33 \leq \nabla \leq 0.45$ thereafter tending to underestimate the values of C_W. But comparison between theory and experiment for $\nabla > 0.45$ is of doubtful value for reasons stated above.

At Froude Numbers less than 0.33 both theories exhibit exaggerated oscillations in C_W values which are slightly out-of-phase with the corresponding oscillations in the empirically determined curve. These are unfortunately common features of the calculated wave resistance at low speeds and their occurrence is generally ascribed to both the linearisations adopted within the theory and the total neglect of viscous effects. It is probable that boundary layer growth near the stern would damp out the oscillations to a certain extent and this has been demonstrated by Havelock (12, p.528). The effect of non-linearities is to a certain extent unknown, but it appears from figure 37 that complete fulfilment of the body surface boundary condition, equation (2.1.8 b), obtained by Inui's method gives slightly

∇	$C_W 10^3$ - Michell-Havelock
0.190	2.218
0.195	2.280
0.200	3.229
0.205	3.932
0.210	3.683
0.220	2.641
0.230	3.792
0.240	4.962
0.250	4.359
0.267	3.361
0.280	4.743
0.300	6.823
0.325	5.791
0.350	4.351
0.400	6.911
0.450	10.050
0.500	10.950
0.550	10.350
0.600	9.259
0.650	8.136

∇	$C_W 10^3$ - Inui
0.100	0.300
0.110	0.325
0.120	0.488
0.125	0.539
0.130	0.532
0.135	0.929
0.140	0.889
0.150	1.332
0.160	1.173
0.183	2.566
0.192	1.698
0.200	3.148
0.218	2.203
0.236	5.054
0.250	3.968
0.267	3.555
0.277	5.353
0.301	8.119
0.316	7.043
0.333	5.260
0.354	4.800
0.400	10.510
0.450	16.420
0.500	17.790
0.550	16.875
0.600	15.360
0.650	13.700

WAVE RESISTANCE VALUES CALCULATED BY MICHELL-HAVELOCK AND INUI'S (UNCORRECTED) THEORY-NAKED HULL

Table 15

FIG. 38

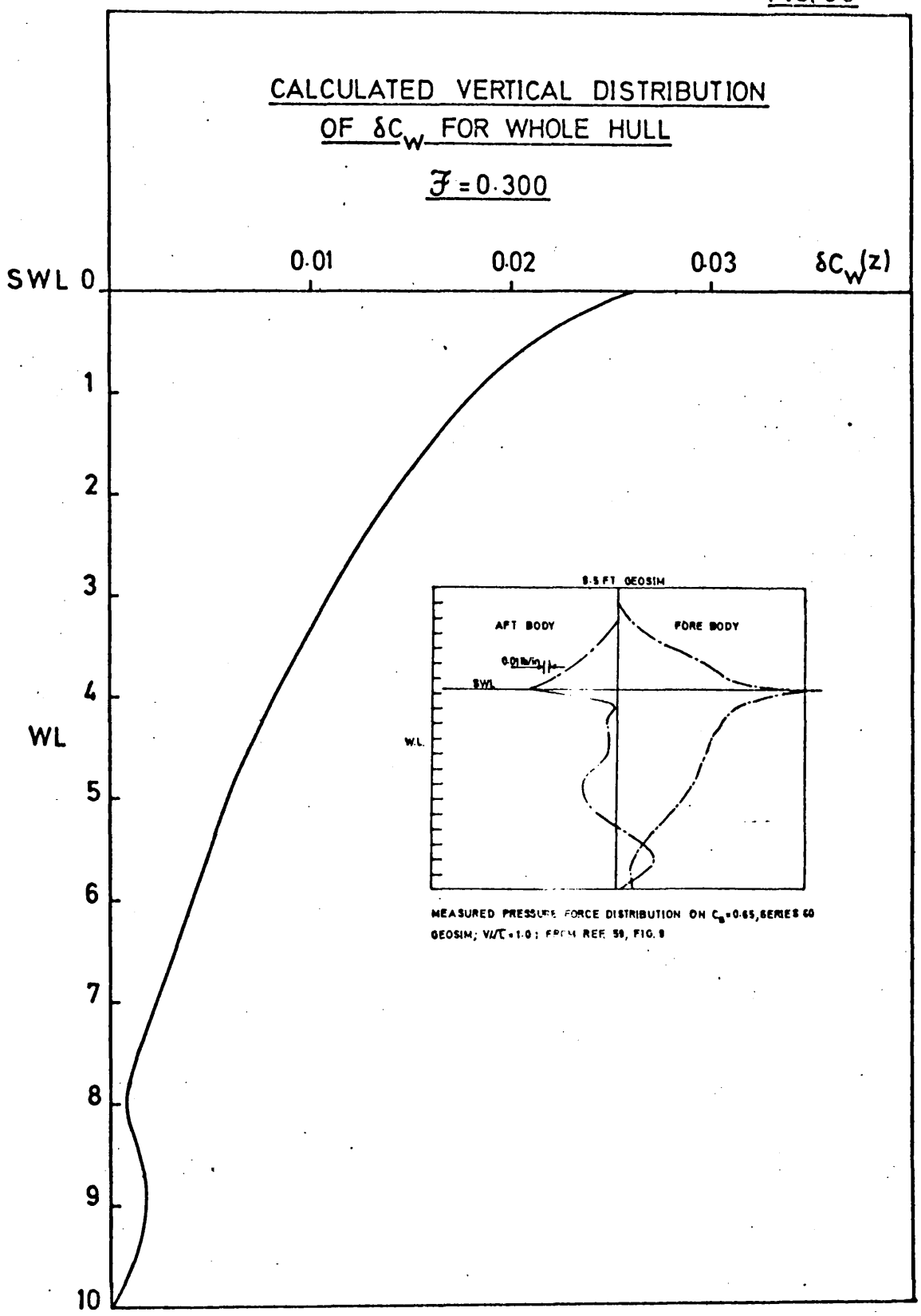
CALCULATED VERTICAL DISTRIBUTION
OF δC_w FOR WHOLE HULL
$\mathcal{F} = 0.300$
SWL 0
0.01
0.02
0.03
$\delta C_w(z)$
1
2
3
4
WL
5
6
7
8
9
10
8.5 FT GEOSIM
AFT BODY
FORE BODY
SWL
W.L.
MEASURED PRESSURE FORCE DISTRIBUTION ON C_B=0.65, SERIES 60
GEOSIM; V/√L = 1.0 ; FROM REF. 59, FIG. 8

worse agreement between theory and experiment at low speeds than the fully linear theory. At high speeds the linear theory gives appreciably better agreement between calculation and measurement.

The author concludes that the completely linear Michell-Havelock theory is better than the partially non-linear theory of Inui without empirical correction factors.

But agreement between theory and experiment still leaves much to be desired, particularly at low speeds. This may be because free surface non-linearities have been entirely neglected in the calculations. The contribution to resistance from the normal pressures in the wave system above the plane z=o has been illustrated in, for example, references 22, 59, 64 and 65. Shown in figure 38 is the calculated vertical distribution of the wave resistance at a Froude Number of 0.300. Comparison of this diagram with its counterparts in the above references reveals that an appreciable part of the wave resistance force distribution has been neglected by assuming a linear free surface.

A further difficulty encountered in the application of the Michell-Havelock theory to Inuid S201 was due to its curved keel line. It is seen from figures B3, B4, B8 and B9 that pressures relative to the waterlines in the vicinity of the curved keel were calculated as if each waterline was independent of its neighbours ; only the depth of the waterline, its local length and the speed of advance of the model were taken into account. It is unlikely that the actual pressure distribution will appear as such and the stagnation pressures observed in figures B3, B4 and B8 on the curved keel may not occur there in practice. The flow over the curved bottom will be far more complex with the probability of strong downward flow components. This is illustrated in figure 39 where it is suggested that rotational flow could occur thus contravening one of the basic assumptions of the theory. It appears that for the Inuid hull shape the mathematical model adopted to represent the flow was inadequate.

Values of d' defined by equation (2.3.7) were calculated for the speed range $0.10 \leq \nabla \leq 0.65$ and are shown in figure 40. Interesting

MATHEMATICAL MODEL

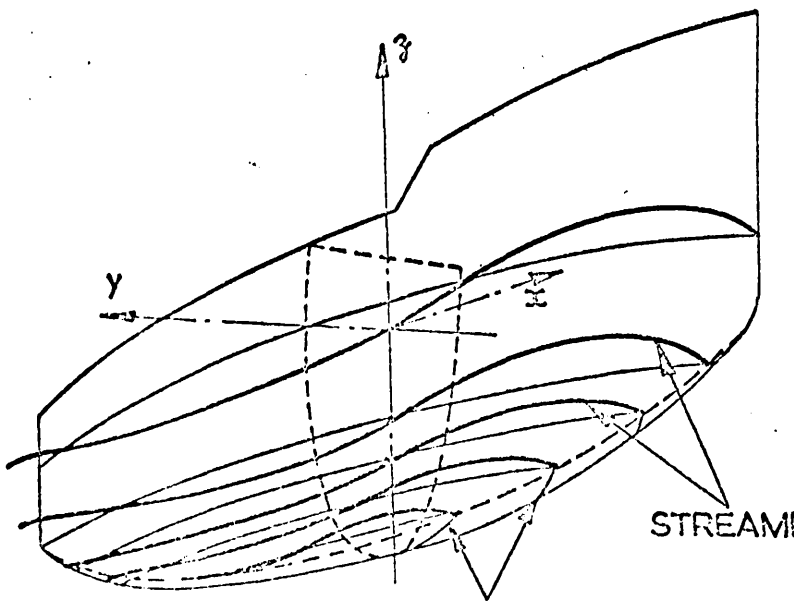

POSSIBLE PHYSICAL SYSTEM

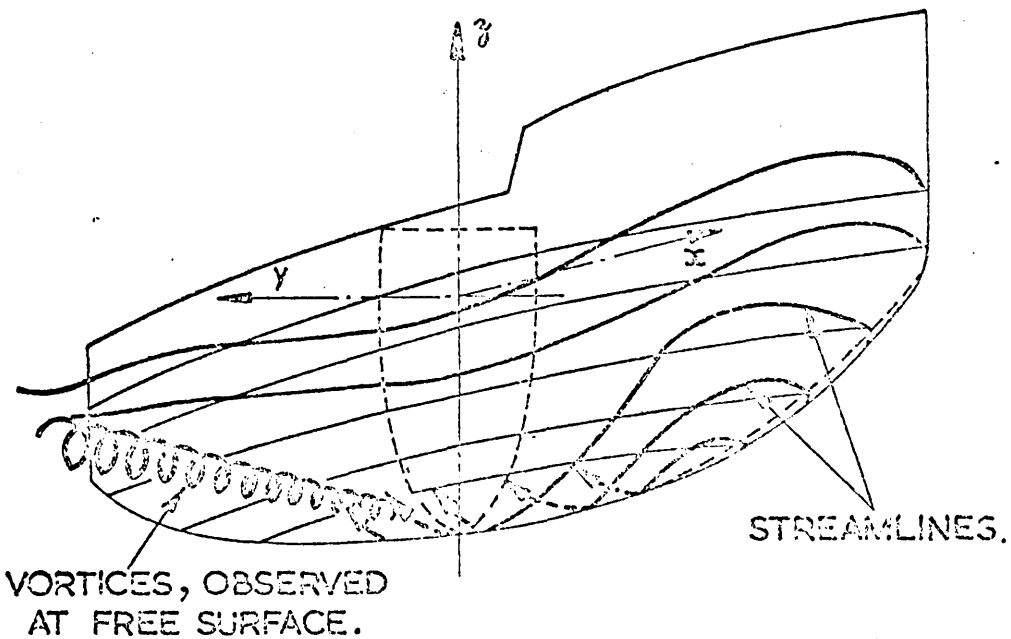

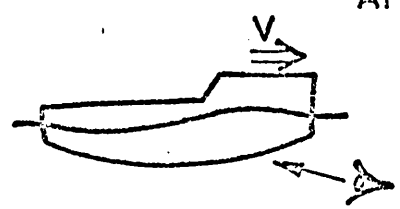

VIEWPOINT

COMPARISON OF ASSUMED AND POSSIBLE FLOW SYSTEMS UNDER INUID S 201.

FIG 33

FIG. 40

POINT OF APPLICATION OF R_W.

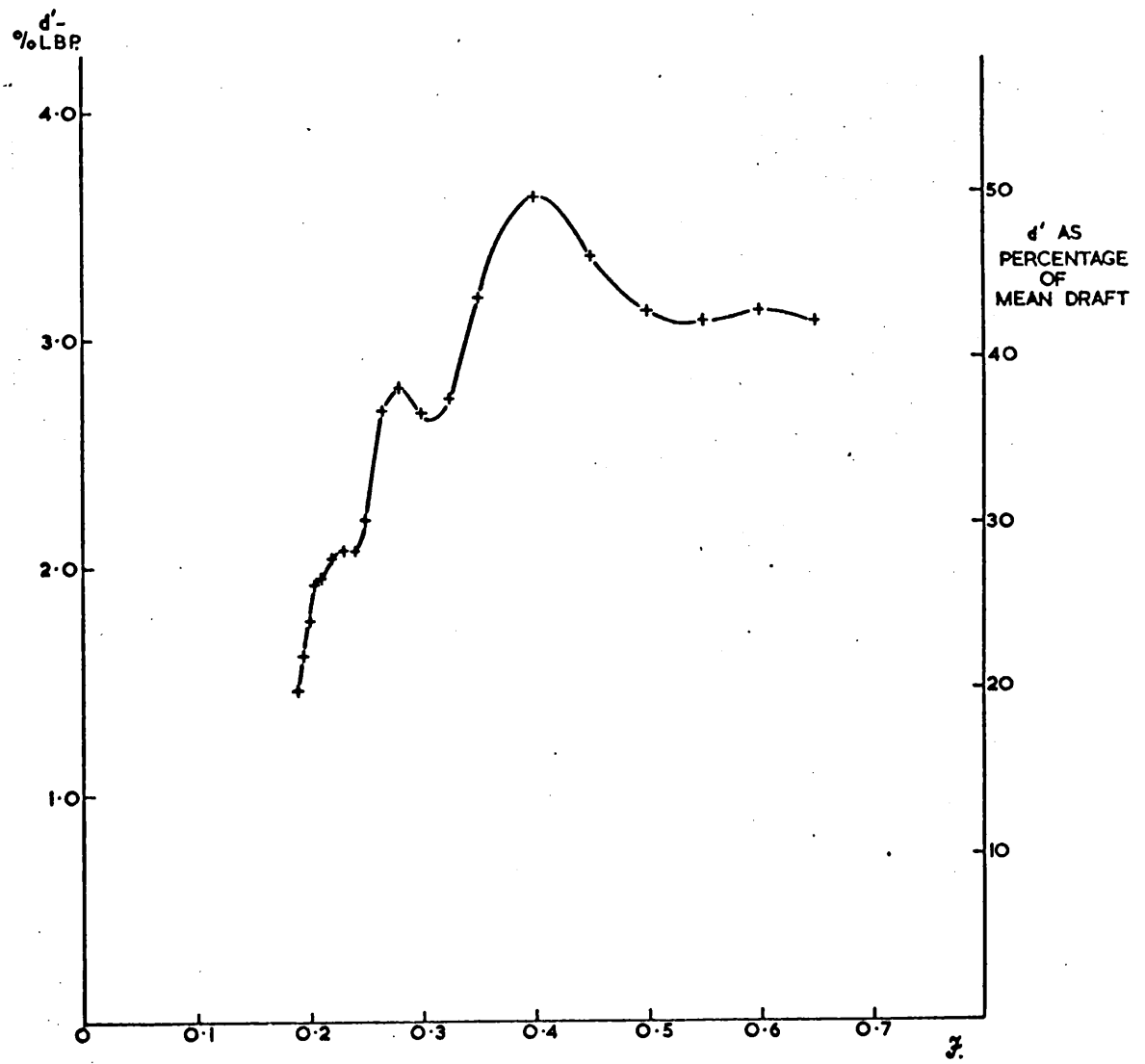

features of this plotting are both the oscillatory nature of the curve, the undulations approximately corresponding with those in the wave resistance curve, and the fact that d' rises to a maximum at ∇ = 0.40 and then sinks to an approximately constant value.

2.7.3. Vertical Forces and Trimming Moment

Measured vertical force and moment coefficients are given in table 16 and figures 41 and 42. Given in table 17 are calculated values of C_s, C_τ, C_Z and C_M which are also shown in figures 34, 35, 41 and 42.

2.7.3.a. Measured Vertical Forces and Trimming Moment

Figure 41 indicates that the measured sinkage force coefficient shows the same general characteristics as the measured mean sinkage coefficient shown in figure 34. At low speeds it appears to approach a constant value as indicated by the theory given in section 2.1.5. There is a phase shift between minimum measured C_s and minimum measured C_Z, the former occurring at ∇ = 0.52 and the latter at ∇ = 0.45. This is probably due to the changes in flow over the hull when restrained from sinking and trimming, necessary for the measurement of C_Z.

Measured trimming moment shows much scatter in the range $0.1 \leq \nabla \leq 0.3$. This may be due to oscillations in the curve not sufficiently well defined by the experimental spots, or inaccurate measurement of bow and stern forces ; trimming moment M is the difference of two nearly equal moments at low speeds and any errors in measurement will be magnified when M is plotted in a non-dimensional form.

2.7.3.b. Calculated Vertical Force and Trimming Moment

Vertical Force Coefficient C_Z and Mean Sinkage Coefficient C_s

Results given in figure 34 indicate that for $\nabla < 0.2$, close agreement between measured and calculated mean sinkage is obtained. At higher speeds the calculated and measured curves, while showing similar features, diverge, the calculated values being approximately

$\mathcal{F}$	$C_Z.10^2$	$C_M.10^3$	$\mathcal{F}$	$C_Z.10^2$	$C_M.10^3$
0.250	-2.735	-3.266	0.088	-0.727	-0.267
0.247	-2.685	-3.810	0.098	-1.505	-4.545
0.305	-2.836	-2.846	0.102	-1.876	-4.126
0.118	-2.158	-3.338	0.111	-2.007	-3.153
0.130	-2.128	-3.014	0.120	-1.890	-2.306
0.156	-2.475	-4.046	0.470	-3.856	+4.445
0.141	-2.466	-3.473	0.278	-2.714	-2.481
0.169	-2.455	-3.071	0.281	-2.947	-2.740
0.424	-3.848	+1.725	0.193	-2.390	-3.789
0.187	-2.200	-3.129	0.360	-3.252	-1.924
0.200	-2.449	-3.247	0.373	-3.317	-1.198
0.216	-2.562	-3.882	0.387	-3.591	-0.176
0.234	-2.476	-3.702	0.400	-3.788	+0.784
0.261	-2.748	-2.852	0.396	-3.816	+0.369
0.216	-2.478	-2.812	0.280	-3.051	-3.263
0.273	-2.905	-3.545	0.432	-3.996	+2.866
0.289	-2.958	-2.495	0.354	-3.144	-2.680
0.320	-3.016	-2.333	0.415	-4.001	+1.733
0.330	-3.111	-2.501	0.409	-3.858	+1.281
0.343	-3.073	-2.203	0.314	-3.027	-2.704
0.306	-2.920	-1.847	0.445	-4.051	+3.771
0.270	-2.841	-2.696	0.464	-3.860	+4.276
0.295	-2.978	-2.509	0.477	-3.799	+4.609
0.265	-3.631	-2.587	0.483	-3.816	+4.899
0.281	-2.888	-2.624	0.637	-2.136	+4.280
0.299	-2.972	-2.438	0.528	-3.293	+4.826

$\mathcal{F} = V/\sqrt{gL}$, $C_Z = Z/\frac{1}{2}\rho SV^2$, $C_M = M/\frac{1}{2}\rho SLV^2$, L = 8.6 ft., S = 15.714 sq.ft.

All results corrected for blockage and tide effects.

NON-DIMENSIONAL VERTICAL FORCE AND TRIMMING MOMENT

- NAKED HULL

Table 16

$\mathcal{J}$	$C_Z.10^2$	$C_M.10^3$	$\mathcal{J}$	$C_Z.10^2$	$C_M.10^3$
0.498	-3.579	+4.995	0.602	-2.432	+4.807
0.450	-3.943	+3.513	0.618	-2.291	+4.487
0.479	-3.803	+4.568	0.652	-2.110	+4.258
0.516	-3.379	+5.017	0.644	-2.139	+4.266
0.556	-2.942	+5.152	0.670	-1.965	+3.896
0.253	-2.841	-4.003	0.626	-2.238	+4.397
0.535	-3.188	+5.252	0.255	-2.856	-4.272
0.553	-2.951	+5.109	0.484	-3.699	+4.677
0.577	-2.721	+4.860	0.469	-3.853	+4.263
0.594	-2.516	+4.717			

Table 16 Cont.

FIG. 41

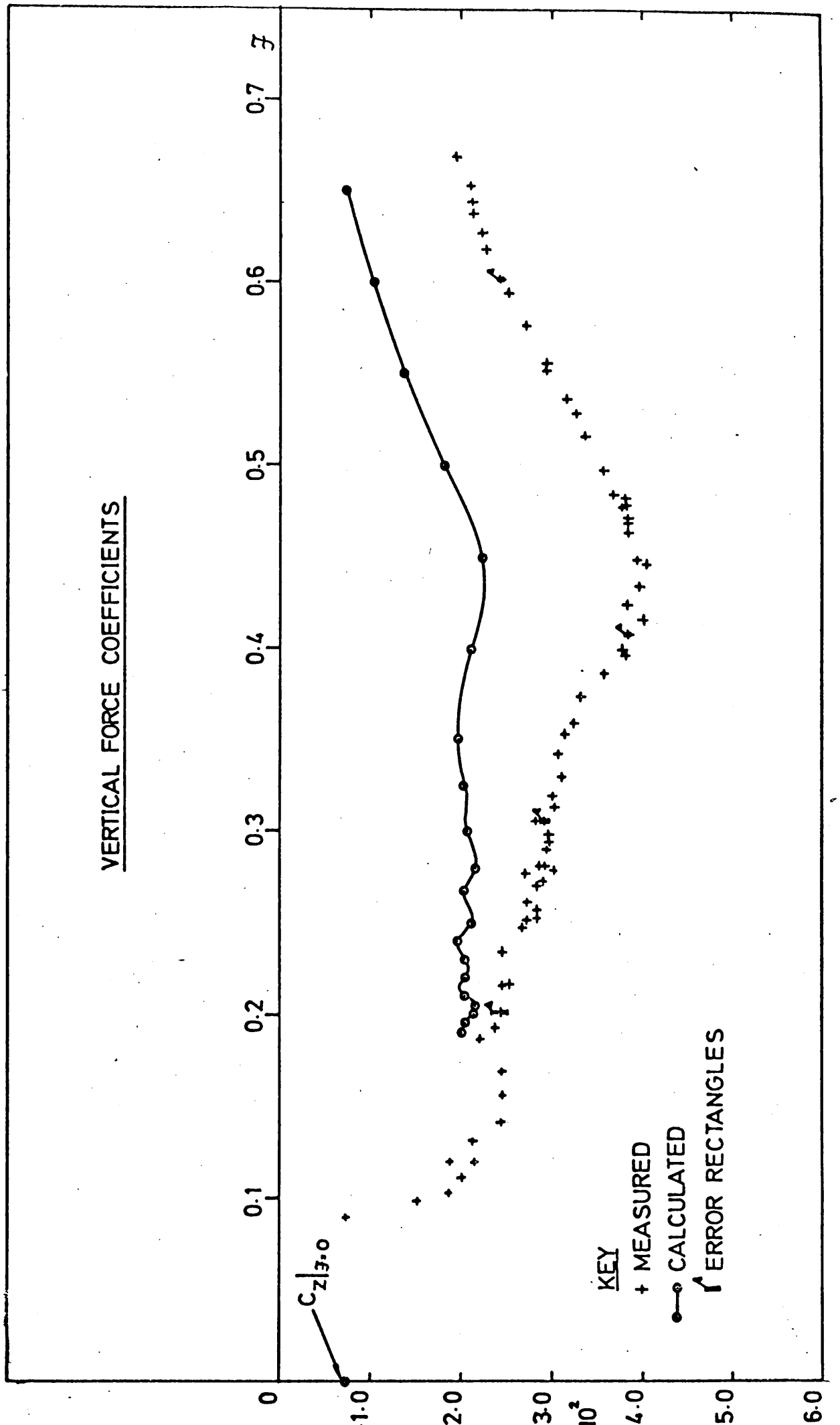
VERTICAL FORCE COEFFICIENTS
$C_{z|3\cdot0}$
KEY
+ MEASURED
CALCULATED
ERROR RECTANGLES
$C_z 10^2$
0
-1·0
-2·0
-3·0
-4·0
-5·0
-6·0
0·1
0·2
0·3
0·4
0·5
0·6
0·7
$\mathcal{Z}$

FIG.42

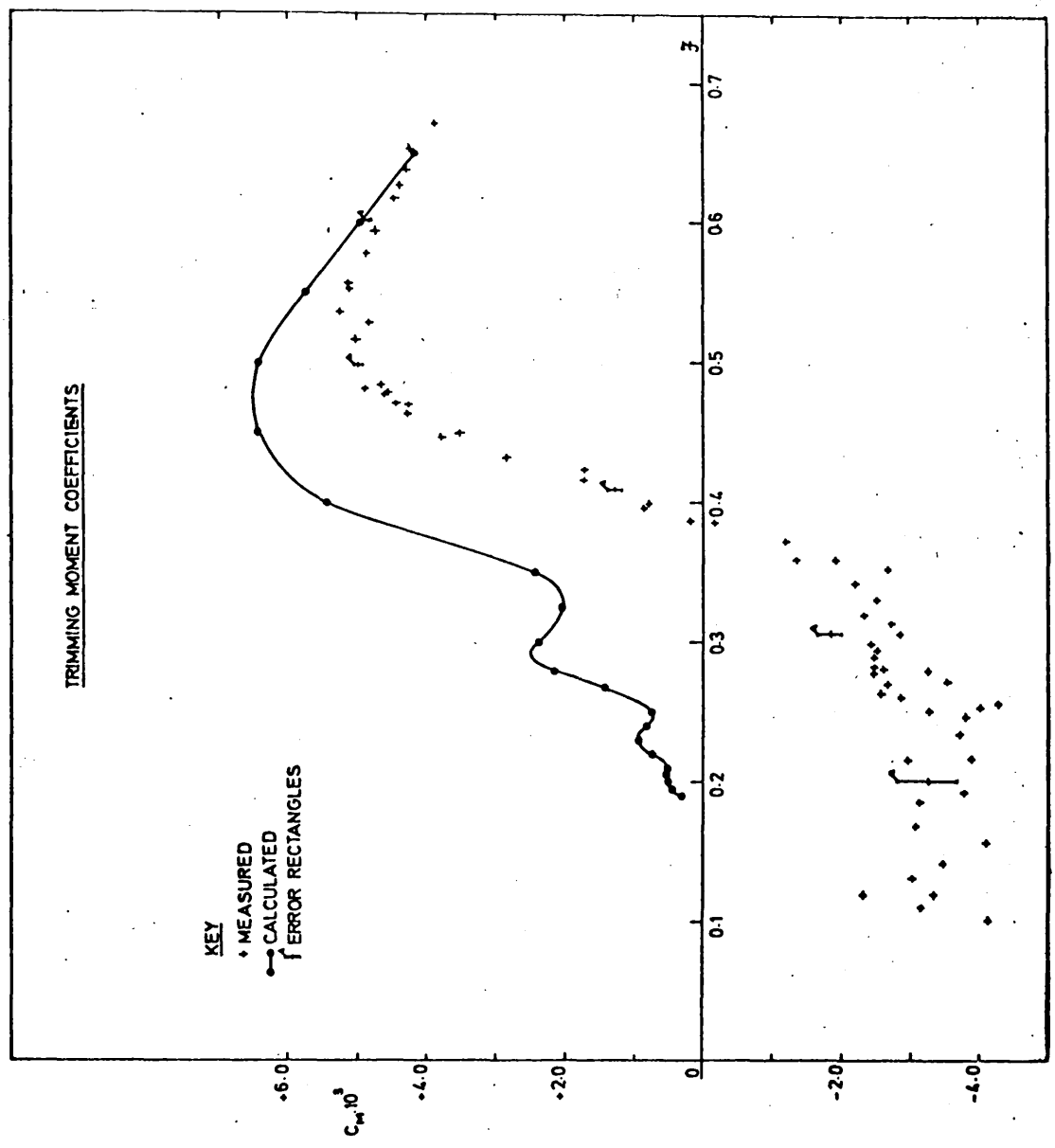
TRIMMING MOMENT COEFFICIENTS
KEY
MEASURED
CALCULATED
ERROR RECTANGLES
$C_m.10^3$
+6.0
+4.0
+2.0
0
-2.0
-4.0
0.1
0.2
0.3
+0.4
0.5
0.6
0.7
$\bar{x}$

∇	$C_Z \cdot 10^2$	$C_M \cdot 10^3$	C_s	C_τ
0.190	-2.033	+0.307	-0.087	+0.024
0.195	-2.055	+0.455	-0.093	+0.037
0.200	-2.114	+0.526	-0.100	+0.045
0.205	-2.194	+0.534	-0.110	+0.048
0.210	-2.065	+0.529	-0.108	+0.049
0.220	-2.066	+0.740	-0.119	+0.076
0.230	-2.063	+0.943	-0.130	+0.106
0.240	-1.996	+0.824	-0.137	+0.101
0.250	-2.116	+0.742	-0.157	+0.098
0.267	-2.059	+1.431	-0.174	+0.216
0.280	-2.182	+2.158	-0.203	+0.359
0.300	-2.077	+2.396	-0.222	+0.457
0.325	-2.016	+2.036	-0.253	+0.456
0.350	-1.983	+2.468	-0.289	+0.641
0.400	-2.113	+5.469	-0.402	+1.855
0.450	-2.242	+6.438	-0.539	+2.763
0.500	-1.837	+6.413	-0.546	+3.398
0.550	-1.399	+5.737	-0.503	+3.678
0.600	-1.043	+4.921	-0.446	+3.755
0.650	-0.751	+4.170	-0.377	+3.734

CALCULATED VERTICAL FORCE, TRIMMING MOMENT

MEAN SINKAGE AND TRIM COEFFICIENTS

- NAKED HULL

Table 17

half the measured values. This is probably due to deficiencies in the theory and the fact that the calculated values correspond to the model when restrained from sinking and trimming whereas the measured values do not. Moreover, the calculated C_s, equation (2.3.8), will become inaccurate at high speeds where the value for lbs/0.1 inch immersion, obtained from the Inuid hydrostatic particulars, will be unrealistic.

It is apparent in figure 37 that better agreement between theory and experiment is obtained when the model is free to trim.

Figure 41, relating to C_Z, once again indicates good agreement between theory and experiment for $\nabla < 0.20$. Oscillations in the calculated curve are well reproduced by the measured curve both in phase and relative amplitude, but the calculated values of C_Z at higher speeds are about half their measured counterparts. It is of interest to speculate on the reasons for this disagreement:

K.S.M. Davidson, in his discussion of reference 80 suggested that the vertical force Z was very little affected by viscosity. If this is so any disagreement between theory and experiment shown in figure 41 must be due to other deficiencies in the theory of which the largest is the neglect of non-linearities. At low speeds flow disturbances are small and a linear theory might be expected to give reasonable results. This is apparently the case with vertical forces but not so with wave resistance where at low speeds, calculated values greatly exceed measured values. This point is discussed further in part 4.

Figure 43 shows the calculated distribution in depth of vertical force for a Froude Number of 0.300. It is apparent that most of the vertical force is concentrated near the lower waterlines where $\partial r/\partial z$ values are of appreciable magnitude. Inaccuracies in estimation of both C_{PTOT} and $\partial r/\partial z$ in this region will have a profound effect on the calculated values of C_Z and will account for part of the discrepancy between calculation and observation apparent in figure 41.

FIG. 43

CALCULATED VERTICAL DISTRIBUTION OF δC_z FOR WHOLE HULL.

$\mathcal{F} = 0.300$

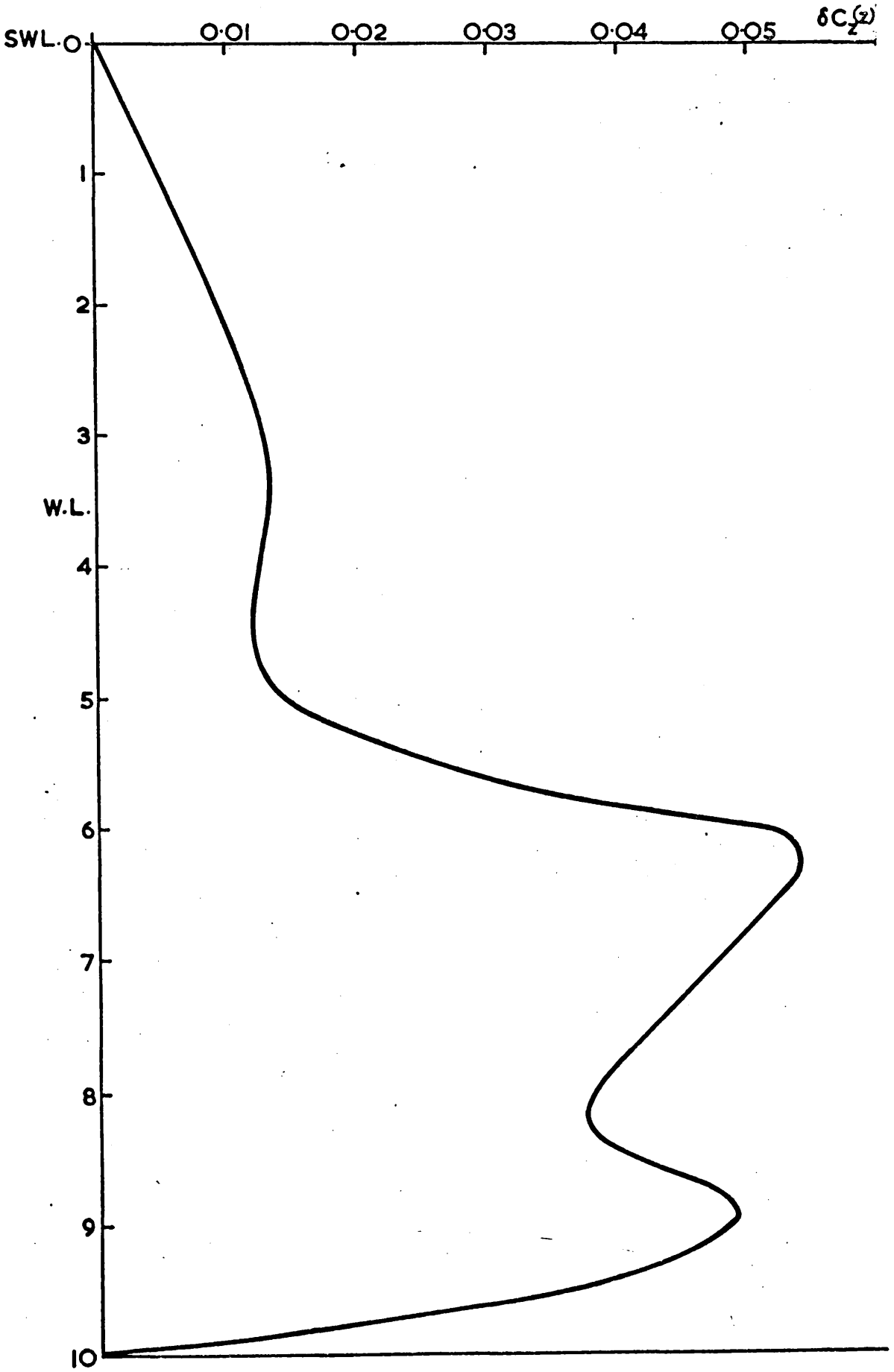

FIG. 44.

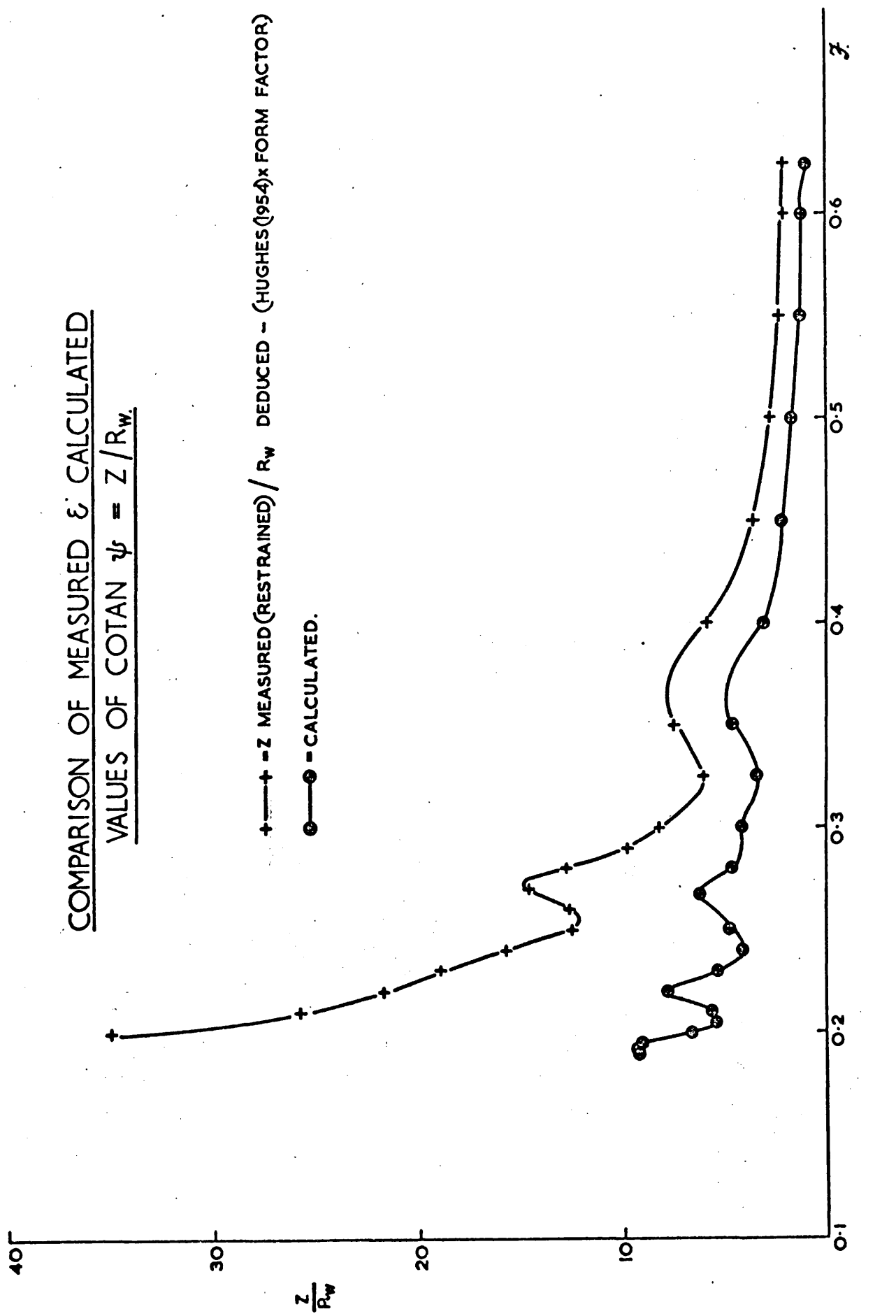
COMPARISON OF MEASURED & CALCULATED
VALUES OF COTAN ψ = Z/Rw.
+—+ = Z MEASURED (RESTRAINED) / Rw DEDUCED - (HUGHES (1954) x FORM FACTOR)
●—● = CALCULATED.
Z/Rw
40
30
20
10
0·1
0·2
0·3
0·4
0·5
0·6
ψ

Figure 44 shows a comparison of measured and calculated values of the ratio Z/R_W = cotan ψ where ψ is defined in figure 2. Agreement is poor over the whole speed range, but it appears that at high speeds the measured and calculated curves might coalesce. Once again disagreement is worse in the low speed range, due to over-estimation of R_W by the linear theory here. Moreover, it appears that the relationship between vertical force and wave resistance is complex and not well reproduced theoretically. This is unfortunate. Had there been better agreement between theory and experiment a simple and accurate method of deducing R_W from measured values of Z would have resulted from the application of the equation

$$R_{W(MEASURED)} = \left(\frac{R_W}{Z}\right)_{(CALCULATED)} . Z_{(MEASURED)} \qquad \ldots\ (2.7.8)$$

In the light of results obtained from this investigation, such a method seems unpromising.

Trimming Moment Coefficient C_M and Trim Coefficient C_τ

Figure 35 indicates poor agreement between calculated and measured values of C_τ over the whole speed range $0.2 \leq \nabla \leq 0.65$. Poor agreement occurs again in figure 42 where calculated and measured values of C_M are compared. In both figures the sign of the calculated trimming moment differs from the observed value in the range $0.2 \leq \nabla \leq 0.37$.

Oscillations in the calculated C_M may be reproduced in the measured values but scatter of the spots makes this uncertain.

The causes of these discrepancies are not obvious but are probably due as much to neglect of viscous effects as to neglect of non-linearities. The effect of the boundary layer over the aft-body is to reduce the wave-making properties of the stern (12, p.573). Incorrect wave heights are therefore calculated in the aft-body, in particular close to the stern and thus there is lack of agreement between calculated and measured trimming moments. The viscous component of M has been discussed theoretically by Bessho in reference 84, and is referred to again in Part 3.

Free surface non-linearities are shown in appendix A to be important near bow and stern. As $\partial\eta/\partial z = 0$ at the free surface for this model there can be no contribution to M from free-surface pressures. But if the indications shown in Appendix A apply to the remainder of the pressure distribution over the hull, the neglect of non-linearities at bow and stern will undoubtedly affect the calculated trimming moment M.

As mentioned in the discussion on calculated vertical force, accurate determination of $\partial\eta/\partial z$ near the keel is important. Incorrect values of $\partial\eta/\partial z$ in these regions could have large effects on the calculated value of M.

Fluid inertia forces acting on the fore-body, vortex formation over the aft-body and surface tension all have an unknown effect on measured trim and trimming moment ; this uncertainty will remain until a more sophisticated theory is evolved or until the present theory is extended to higher orders.

Nevertheless the conclusion emerges that calculated values of Z agree moderately well with measurement whereas calculated values of M and R_W do not. This is probably because Z is little affected by viscous forces and any discrepancy between measured and calculated values of Z is probably due to the neglect of non-linearities in the basic theory. Trimming moment M and running trim may affect, and be affected by, viscous forces to a marked extent. It remains to be seen whether Z is in fact affected by a change in viscosity and this is discussed in more detail in parts 3 and 4.

2.7.4. Form Resistance

One of the aims of this investigation was to compare form factors deduced by the methods of sections 2.4. and 2.7.1 b.

Values of r, defined by equation (2.7.2.) and deduced from

figure 33 are shown in figure 45 and table 18. They are compared with values given by Sharma (53, p.410, table 3.8) and values deduced from equations (2.4.5) and (2.4.15). Figure 46 compares equations (2.4.3) and (2.4.12) using both measured and calculated values of C_Z and C_W. From these diagrams it is apparent that

i) The form factor r is not constant over the range of speeds considered.

ii) Friction form resistance r_{ff} also varies over the speed range.

iii) There is in general an increase in r as speed increases. This is apparent both from Sharma's results and from deductions made from figure 33.

iv) Friction form resistance is a small fraction of total form resistance. Therefore, for the model in question, R_{VP} constitutes the predominant part of the form resistance.

Figure 46 shows that a discrepancy between measured and calculated values of r_{ff} exists, with agreement better at low speeds than at high speeds. This is because r_{ff} is strongly dependent on C_Z for which theory and experiment agree well at low speeds. Also, due to C_Z being approximately ten times C_W for $\mathcal{F} < 0.40$, interaction between friction form resistance and wave resistance is small in this speed range. The calculated curve shows no tendency for r_{ff} to increase as speed increases. This may be due to inaccuracies arising from mean sinkage measurement or it may be due to a viscous effect on mean sinkage : the growth of the boundary layer affects mean sinkage at higher speeds causing r_{ff} to increase.

It would seem however that viscous pressure forces predominate in form resistance. It has been inferred above (section 2.7.3.b) that trim τ affects and is affected by boundary layer growth. As R_{VP} is dependent on boundary layer shape, this suggests that there must be some functional relationship between R_{VP} and τ. Moreover, boundary layer growth will be affected by the normal pressure

FIG. 45

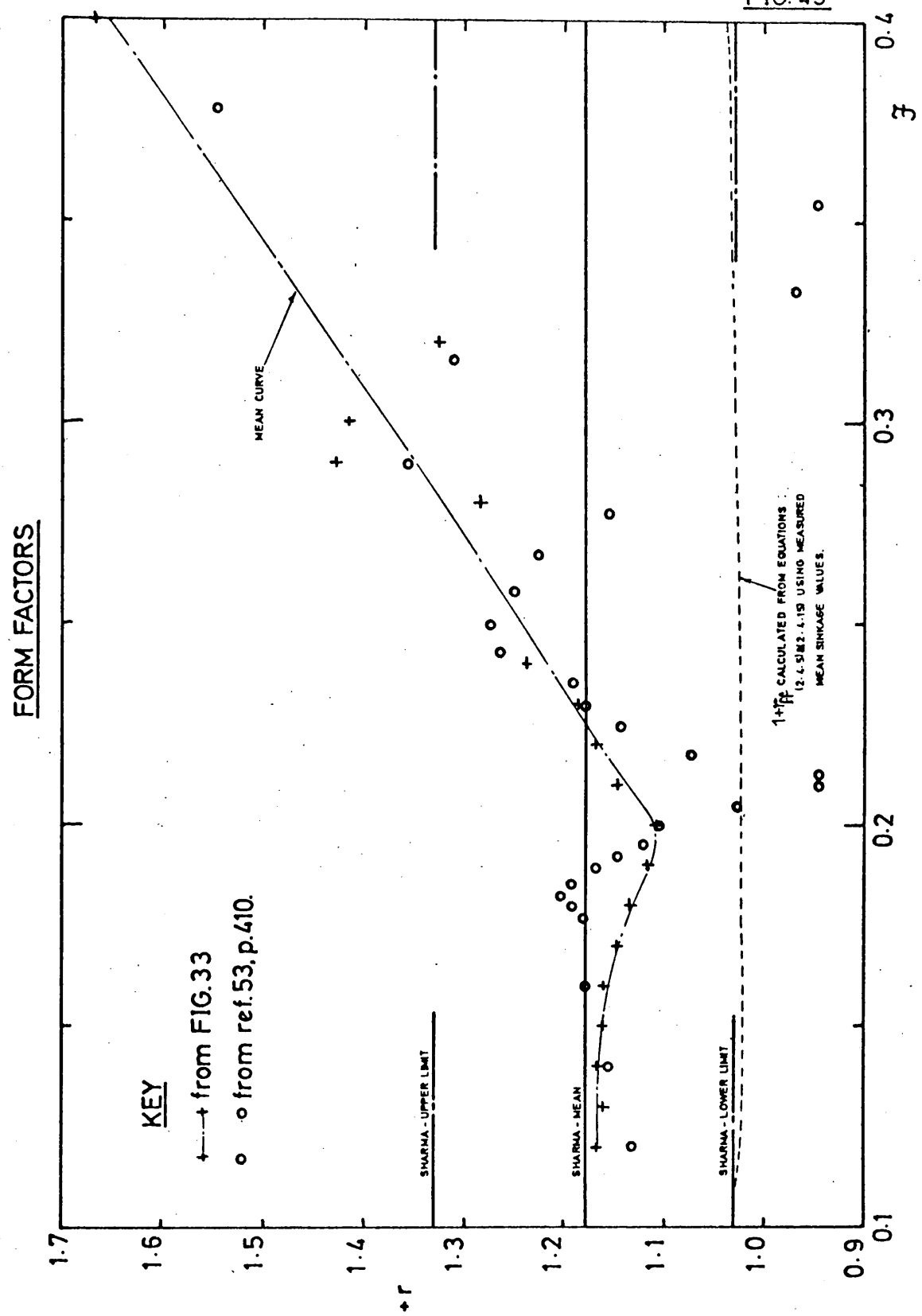
FORM FACTORS
KEY
from FIG.33
from ref.53, p.410.
MEAN CURVE
SHARMA - UPPER LIMIT
SHARMA - MEAN
SHARMA - LOWER LIMIT
1+r CALCULATED FROM EQUATIONS 12.4-5 & 12.4-19 USING MEASURED MEAN SINKAGE VALUES.
1+r
f
1·7
1·6
1·5
1·4
1·3
1·2
1·1
1·0
0·9
0·1
0·2
0·3
0·4

∇	r from Fig. 33	r_{ff} from equation (2.4.3)	r_{ff} from equation (2.4.12)	∇	r_{ff} calculated
0.11	-	0.066	0.028	0.190	0.019
0.12	0.168	0.058	0.024	0.195	0.019
0.13	0.160	0.054	0.023	0.200	0.020
0.14	0.167	0.048	0.021	0.205	0.020
0.15	0.162	0.049	0.021	0.210	0.019
0.16	0.160	0.049	0.021	0.220	0.019
0.17	0.148	0.050	0.021	0.230	0.019
0.18	0.136	0.052	0.022	0.240	0.019
0.19	0.118	0.053	0.022	0.250	0.020
0.20	0.107	0.056	0.024	0.267	0.019
0.21	0.148	0.058	0.024	0.280	0.020
0.22	0.169	0.058	0.025	0.300	0.020
0.23	0.190	0.059	0.025	0.325	0.019
0.24	0.230	0.061	0.026	0.350	0.019
0.25	-	0.061	0.026	0.400	0.020
0.26	-	0.062	0.027	0.450	0.023
0.27	-	0.065	0.028	0.500	0.020
0.28	0.285	0.067	0.029	0.550	0.016
0.29	0.423	0.069	0.030	0.600	0.013
0.30	0.400	0.071	0.030	0.650	0.010
0.32	0.326	0.074	0.032		
0.35	-	0.078	0.033		
0.375	-	0.082	0.035		
0.400	0.611	0.090	0.039		

NOTE: FORM FACTOR, $r = \delta R/R_{fo}$ WHERE $R_{fo} = \frac{1}{2}\rho SV^2(1.328\ R_n^{-0.5} + 0.04 R_n^{-0.114}$

FORM FACTORS - NAKED HULL

Table 18

FIG.46

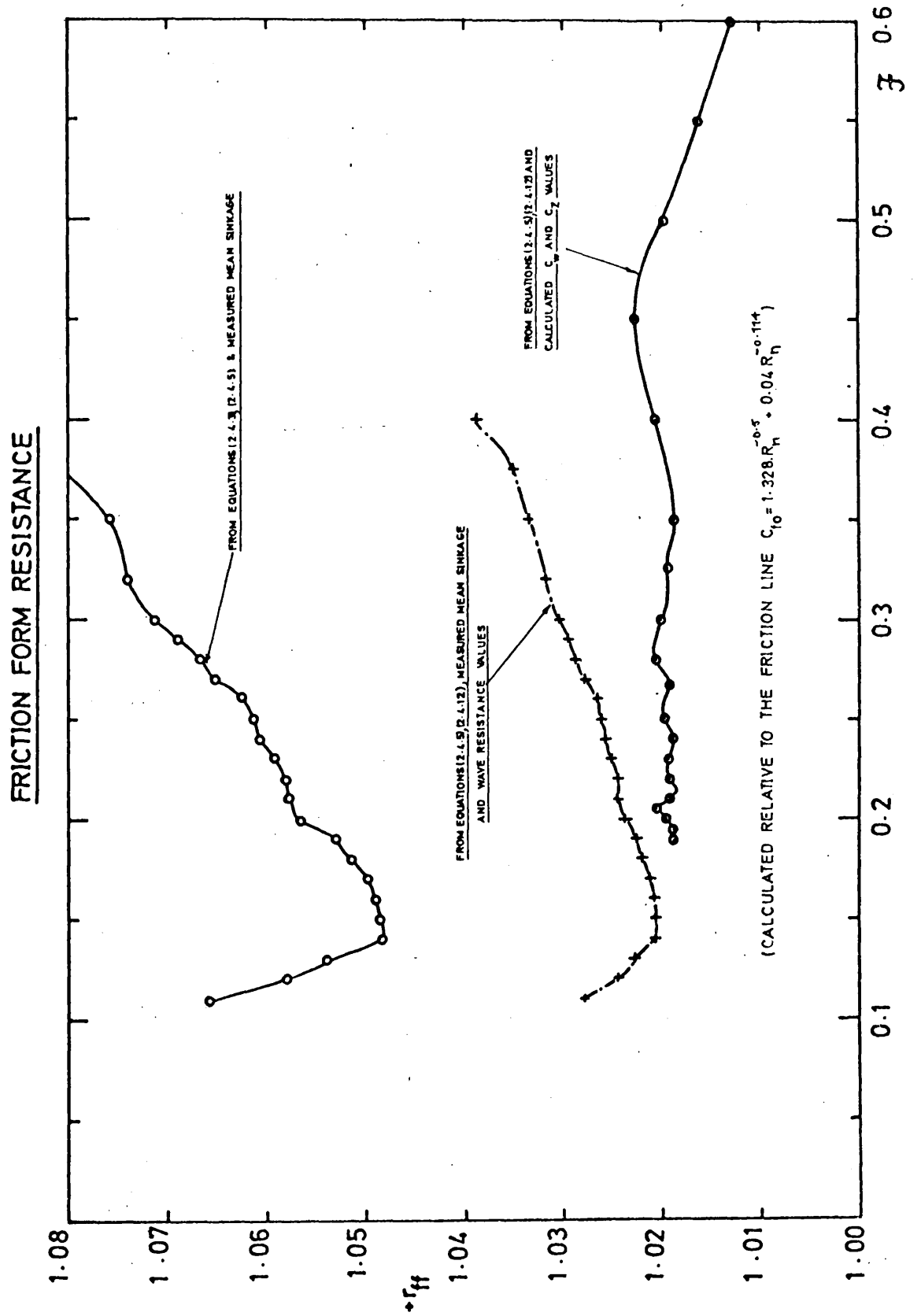
FRICTION FORM RESISTANCE
1+r_ff
1.08
1.07
1.06
1.05
1.04
1.03
1.02
1.01
1.00
0.1
0.2
0.3
0.4
0.5
0.6
F
FROM EQUATIONS (2.4.3) (2.4.5) & MEASURED MEAN SINKAGE
FROM EQUATIONS (2.4.5), (2.4.12), MEASURED MEAN SINKAGE AND WAVE RESISTANCE VALUES
FROM EQUATIONS (2.4.5)(2.4.12) AND CALCULATED C_w AND C_z VALUES
(CALCULATED RELATIVE TO THE FRICTION LINE C_f0 = 1.328.R_n^-0.5 + 0.04 R_n^-0.114)

distribution over the hull and the surface waves. This suggests that

$$R_{vp} = f(\tau, R_w, R_{f_o}) \qquad \ldots\ (2.7.9)$$

in a similar manner to the conclusion

$$R_{ff} = f(s, R_w, R_{f_o})$$

reached in section 2.4.

Unfortunately no simple analysis similar to that given in section 2.4. seems likely to define the relation in equation (2.7.9). Guilloton suggested (68) that, using the Froude Circular Constant notation,

$$\copyright_{pv} = m.\tau.\copyright_{f_o} \qquad \ldots\ (2.7.10)$$

He found that a value of m = 6 gave good agreement with measured values for the particular model under consideration. This rather arbitrary relationship between R_{VP} and τ seems to be excessively simple : trim τ and trimming moment M are strongly related to the potential flow and the model wave system as has been shown in 2.7.3.b, so that a relation such as equation (2.7.9.) seems more appropriate. It would appear that a comprehensive analysis such as that of Tanaka (96) would yield useful results if applied to floating bodies. The analysis would be greatly complicated by the introduction of a free surface with its boundary condition, equation (2.1.13).

Hence an empirical investigation of some relationship between τ and R_{VP} might prove useful. Before such an investigation can be considered, it is necessary to investigate if in fact a change in R_{VP} is obtained as a result of a change in trim, thus implying a relation between R_{VP} and τ . This was one of the aims of the bulbous bow investigation described in part 3 below.

2.8. CONCLUSIONS AND DEDUCTIONS

As a result of the theoretical and experimental investigation described above, the following main conclusions and deductions emerge :

(Conclusions marked * apply only to the Inuid S201 in this particular investigation : they may not be valid in general.)

* 1) Wave resistance calculated using the Michell-Havelock wholly linearised theory gives better agreement with empirically deduced wave resistance than that calculated using Inui's method without correction factors ; agreement is good at high speeds.

2) Inui's method, which assumes no prior knowledge of the hull shape but only of the source distribution, is inadequate for the calculation of Z and M, unless Lagally's Theorem is used.

* 3) The Michell-Havelock linearised theory gives moderately good agreement between calculated and measured vertical force coefficient values C_Z. Agreement is best at low Froude Numbers, and the phases of oscillations in the C_Z curves are correctly predicted by calculation.

Mean sinkage measured with the model free to trim agrees better with calculation than that measured with the model restrained from trimming but not sinking.

4) Measured and calculated values of C_Z tend to a constant value at zero and infinite Froude Numbers, the constant representing a downward vertical force at $\mathcal{F} = 0$ and an upward vertical force at $\mathcal{F} = +\infty$.

*5) Poor agreement between measured trim coefficients and those calculated by the Michell-Havelock theory is obtained over the range $0.2 \leq \mathcal{F} \leq 0.65$. The sign of the calculated C_M is wrong at low speeds and fluctuations in the curve are out-of-phase with measurement.

6) Vertical force Z is little affected by viscosity whereas trimming moment M is probably strongly affected by viscosity.

*7) The ratio $Z/R_W = \text{cotan}\,\psi$ shows poor agreement between measurement and calculation over the range $0.2 \leq \mathcal{F} \leq 0.65$. Agreement improves as speed increases.

*8) The form factor r is not constant but increases with Froude Number.

*9) Friction form resistance R_{ff} is a small part of the total form resistance ; viscous pressure resistance R_{VP} predominates.

10) Friction form resistance, vertical force, wave resistance and flat plate friction resistance are connected ; a simple analysis of their relationship is given in section 2.4.

11) Viscous pressure resistance, running trim and wave resistance are probably connected. There is a viscous component in the trimming moment.

Conclusions (9), (10) and (11) suggest that a modification to vertical force and trimming moment would produce a modification in form resistance.

3. BULBOUS BOW INVESTIGATION

3.1. The Action of a Bulbous Bow.

Bulbous bows are intended to reduce resistance at a certain speed. The mechanism by which they do this is by no means clear, but it seems probable that they can cause cancellation of some parts of the free wave system. Wave resistance theory is useful in analysing the action of a bulbous bow as a wave cancelling device. We state briefly the approaches adopted by three principal investigators in this field and then contrast their findings with some apparently anomalous results.

3.1.1. Wigley's Approach

Wigley (23) assumed that it was possible to superimpose the wave forms of the hull, ζ_H, and the bulb, ζ_B, to give the wave-form of the hull/bulb combination :

$$\zeta_C = \zeta_H + \zeta_B \qquad \ldots\ldots\ldots (3.1.1)$$

This implied that the bulb had no appreciable influence on the wave system of the hull alone and Wigley stated this would be the case provided that the area of the hull's side covered by the bulb was well below the water surface.

An expression for wave resistance, due to Havelock (12, p.389) is

$$R_w = \frac{\pi \rho V^2}{4} \int_0^{\frac{\pi}{2}} (F_1^2 + F_2^2) \cos^3\theta \, d\theta \qquad \ldots\ldots (3.1.2)$$

corresponding to a free wave pattern given by

$$\zeta = \int_0^{\frac{\pi}{2}} [F_1 \sin(K_0 x \sec\theta) + F_2 \cos(K_0 x \sec\theta)] \cos(K_0 y \sin\theta \sec^2\theta) \, d\theta \qquad \ldots\ldots (3.1.3)$$

where F_1 and F_2 are amplitude functions derived from the hull shape.

Wigley studied spherical bulbs (represented by a point doublet) and spheroidal bulbs (represented by a line source). From known expressions for the free wave forms of these bulbs ζ_B and using equation (3.1.1) he was able to deduce F_1 and F_2 for a mathematical hull/bulb combination in terms of the amplitude functions $A(\theta)$, $B(\theta)$

for the hull and bulb respectively. Inserting these values of F_1 and F_2 into equation (3.1.2) showed that the wave resistance of the hull/bulb combination comprised the wave resistances of the hull R_H, bulb R_B and an interference resistance R_I:

$$R_{H+B} = R_H + R_B + R_I \qquad \ldots\ldots\ldots (3.1.4)$$

where R_I was found to be

$$R_I = \frac{\pi\rho V^2}{2}\int_0^{\frac{\pi}{2}} A(\theta).B(\theta)\cos[(d_1 - L/2)K_0\sec\theta]\cos^3\theta\, d\theta \qquad \ldots\ldots\ldots (3.1.5)$$

where d_1 = distance of centre of bulb from the bow and the origin has been shifted to the bow.

By a suitable choice of d_1 and at a suitable speed V, R_I could be negative and thus would reduce R_{H+B} in equation (3.1.4).

Wigley investigated the optimum vertical and fore and aft position of a simple spherical bulb on a mathematical hull and found :

i) when $d_1 = 0$, R_I was predominantly negative.

ii) the upper surface of the bulb should not approach nearer the surface than a distance equal to its own total thickness.

iii) the maximum thickness of the bulb should be kept as low as possible.

3.1.2 Inui's Approach

Assuming equation (3.1.1) to be true Inui (24) derived an equation for the wave resistance of the hull/bulb configuration :

$$R_{H+B} = \frac{\pi\rho V^2}{2}\int_{-\frac{\pi}{2}}^{\frac{\pi}{2}} [A(\theta) - B(\theta)]^2\cos^3\theta\, d\theta \qquad \ldots\ldots\ldots (3.1.6)$$

which may be written

$$R_{H+B} = \frac{\pi\rho V^2}{2}\left\{\int_{-\frac{\pi}{2}}^{\frac{\pi}{2}} A(\theta)^2\cos^3\theta\, d\theta + \int_{-\frac{\pi}{2}}^{\frac{\pi}{2}} B(\theta)^2\cos^3\theta\, d\theta - 2\int_{-\frac{\pi}{2}}^{\frac{\pi}{2}} A(\theta).B(\theta)\cos^3\theta\, d\theta\right.$$

$$= R_H + R_B + R_I \qquad \ldots\ldots\ldots (3.1.7)$$

as in equation (3.1.4). (Note that the origin is at midships in equation (3.1.7).)

Inui, working from equation (3.1.6) instead of (3.1.7) sought a bulb with amplitude function B (θ) to minimise the wave resistance of the hull/bulb configuration. Using point doublets in conjunction with certain Inuid shapes, he was able to obtain large reductions in total resistance. Tank tests were run for comparison concurrently with the theoretical predictions and were used to obtain optimum bulbs having a large diameter with their centres forward of the fore perpendicular.

3.1.3. Pien's Approach

Pien (27) extended the work of Inui to generate low resistance hull forms which did not rely on large bulbs for wave cancellation. A polynomial source distribution of the general form :

$$\sigma(\xi,\zeta) = \sum_i \sum_j a_{ij} \xi^i \zeta^j \qquad \ldots\ldots\ldots (3.1.8)$$

was distributed on a surface $\eta = \pm f(\xi,\zeta)$. The wave resistance integral given by equation (3.1.2) was expressed in terms of the coefficients a_{ij} and minimised by setting $\partial R_w / \partial a_{ij} = 0$. The source distribution coefficients thus obtained were then used to derive a hull form by streamline tracing techniques using the 'Inverse Method' described in section 2.2.2.

Pien extended his investigations by adding line doublets to cancel free sine waves and line sources to cancel free cosine waves and thus differed from Inui who used point doublets exclusively. Pien further stated in the discussion to ref. 24 that it is not possible to design a bulb from a point doublet alone - the fairing used to blend the spherical bulb into the main hull being equivalent to the introduction of an additional source.

Despite using the 'Inverse Method' for relating hull forms to their source distribution, the approaches of both Inui and Pien have much to recommend them. Hull forms of low resistance can be generated on a high-speed digital computer. These hull forms give large resistance reductions when compared to conventional hull shapes(28

3.1.4 Ram Bow and Viscous Resistance

A ram bow is a bulbous bow with a high value of ram area ratio A_R in comparison to the bulb area ratio A_B. The ratios A_R and A_B have standard definitions due to the National Physical Laboratory and these are shown in figure 47.

Anomalous full-scale resistance results have occurred when ships with ram bows were run in the ballast condition with the ram just below the free surface. Model predictions were not fulfilled. Unusually large resistance reductions occurred which, in some cases, indicate that the viscous resistance was being reduced as well as the wave resistance.

Such phenomena (108) have defied explanation and have cast doubt on the validity of Froude's Law of Comparison for such hull shapes.

Initially these effects on resistance of the ram bulb at low immersion were thought to be confined to ships of fuller form, and a partial explanation in terms of wave cancellation was advanced for ships with small length-beam ratios (109). This still left unanswered several questions regarding the effect of the bulb on viscous resistance in the ballast condition, but it suggested that flow conditions around the bow were strongly influenced by the bulb immersion and the trim.

A study by Couch and Moss (110) reinforced the view that trim in the ballast condition was important and suggested that extrapolation from model results to full size could be seriously in error for the ballast condition. This was thought to be due to the modification of viscous flow by the bulb. This investigation also showed that large bulbs protruding forward as far as possible are best and the distribution of volume longitudinally may be more critical than size alone.

FIG. 47

N.P.L. STANDARD DEFINITIONS FOR BULBOUS BOWS

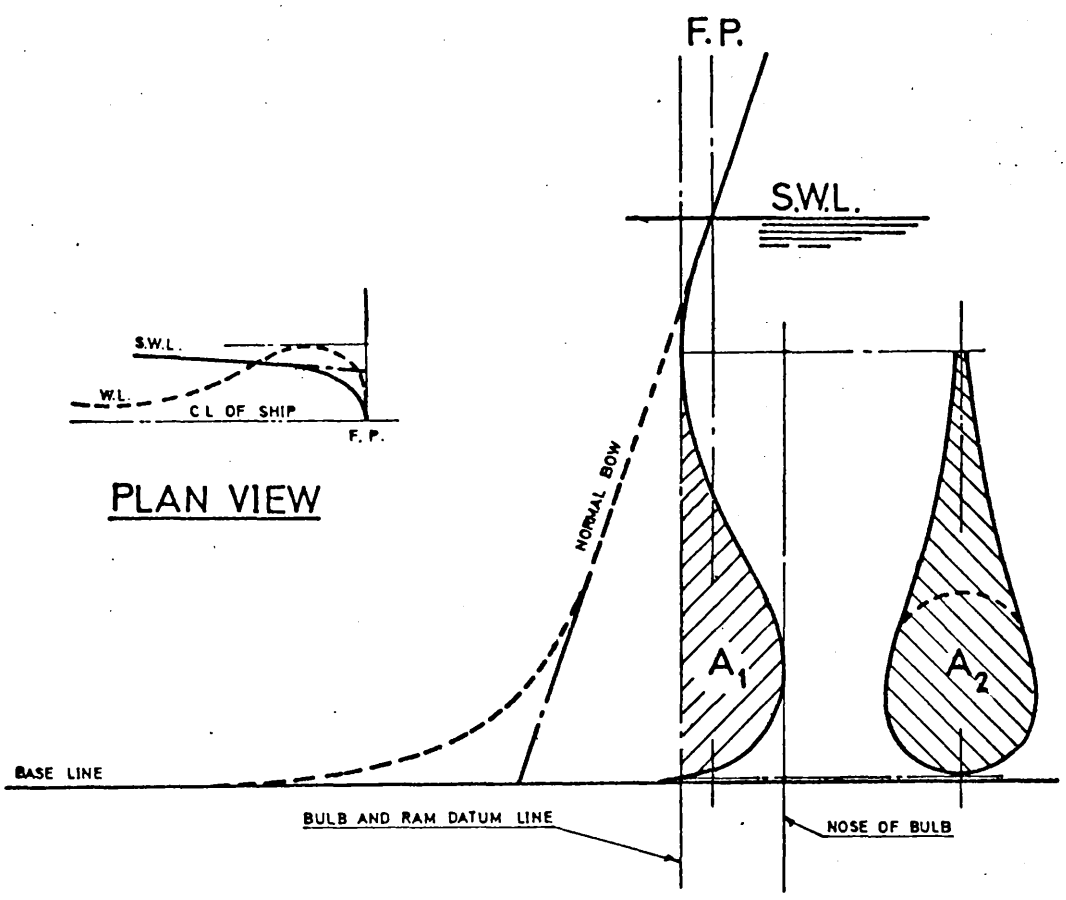

A_1 = AREA OF RAM.

A_2 = AREA OF BULB.

$\frac{A_1 \times 100}{A_M/2}$ = RAM AREA RATIO, A_R.

$\frac{A_2 \times 100}{A_M}$ = BULB AREA RATIO, A_B

A_M = MAXIMUM SECTION AREA OF SHIP TO S.W.L.

Studies by Clements (111) of resistance results for models with ram bows of various types fitted to tankers and bulk carriers emphasised once again the importance of bulb immersion. It was suggested that the draft forward should be as kept to a minimum, provided the point of maximum extension of the ram bow is immersed.

A survey of experimental results for finer hull forms fitted with ram bows (112) indicated once again that large resistance reductions were obtained both in the load and ballast conditions.

The principal conclusions arising from these surveys are :

i) Ram bows appear to affect viscous as well as wave resistance.

ii) Ram immersion is important. Greater resistance reductions are obtained with a reduced immersion for full forms and, to a certain extent, for fine forms.

iii) The ram must be kept immersed at all drafts.

iv) Trim in the ballast condition is important for stable flow conditions round the bow.

v) Extrapolation from model to full-scale is liable to serious errors.

vi) Bulbs which protrude well ahead of the forward perpendicular give the greatest resistance decreases.

It should be noted that conclusions i), ii), and vi) above directly oppose some of Wigley's and Inui's postulates obtained from linearised wave resistance theory.

3.2. THE DESIGN OF A BULBOUS BOW FOR INUID S201

3.2.1. Design criteria.

The following principal conclusions were reached as a result of the investigation described in part 2 :

i) The vertical hydrodynamic force Z is connected in some way with part of the form resistance. This small component of resistance is the frictional form resistance, R_{ff}. A dependence of R_{ff} on Z is approximately demonstrated by the analysis of section 2.4.3.

ii) Running trim has an effect on viscous resistance. It is probable that trim has an effect on boundary layer growth and is thus in some way related to viscous pressure resistance, R_{VP}.

iii) At low speeds where surface wavemaking is unimportant, calculated and measured values of Z agree well.

It was deduced that a change in Z should be accompanied by a modification in friction form resistance, a reduction in Z giving rise to a reduction in R_{ff}. It also seemed probable that a modification to running trim would have a marked effect on viscous resistance.

It therefore became apparent that a bulb designed to alter Z and M might show changes in viscous resistance. No attempt was made to design the bulb to cancel waves and thus reduce wave resistance.

3.2.2. Wigley's Work on Submerged Bodies in Motion

Wigley (80) and others have investigated hydrodynamic forces on various submerged bodies. (See Section 1.4.2.).

Wigley's results for submerged spheroids are reproduced in figure 48. The following conclusions may be drawn from his results :

i) The vertical forces for a submerged spheroid in the presence of a free surface are opposite in sign to those for a floating body over the whole speed range.

ii) As the immersion ratio f/l_s decreases, i.e., the closer the axis of the spheroid approaches the free surface, the magnitudes of both the wave resistance coefficient and vertical force coefficient increase considerably.

FIG. 48

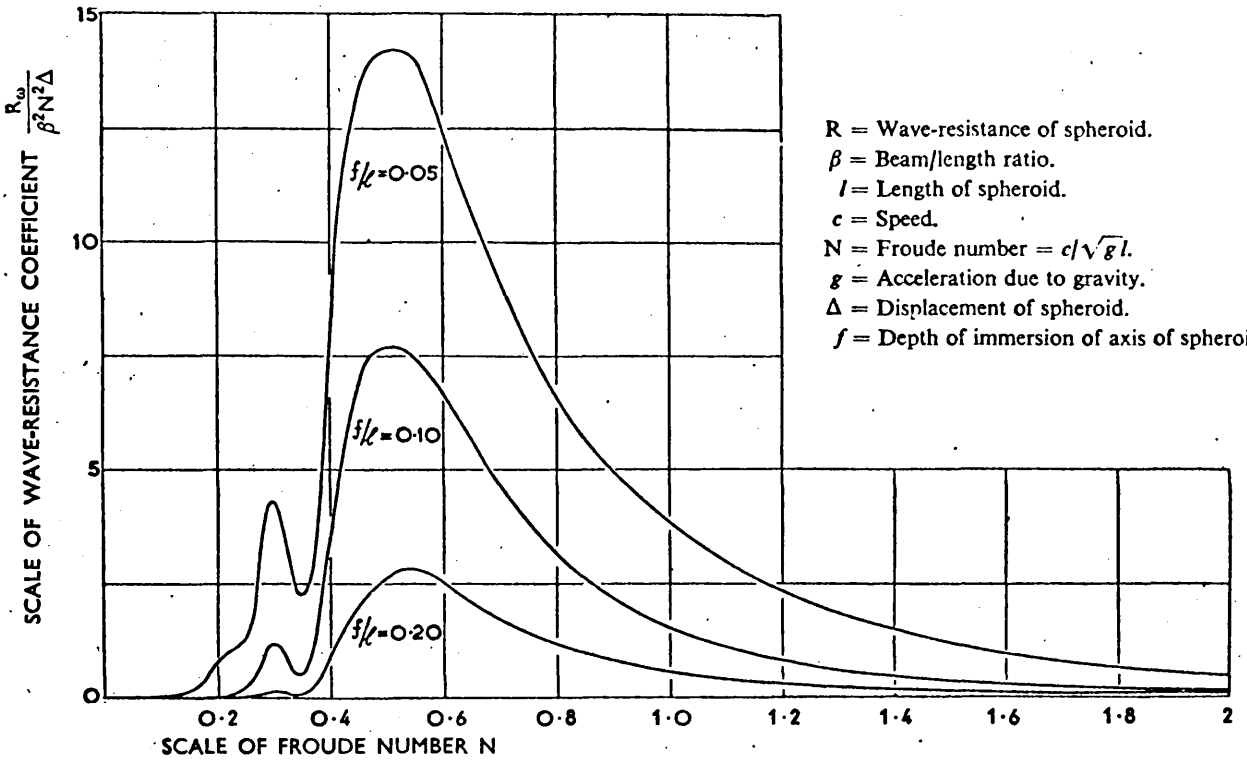

FIG. 1.—THE COEFFICIENT OF WAVE-RESISTANCE OF A SUBMERGED SPHEROID.

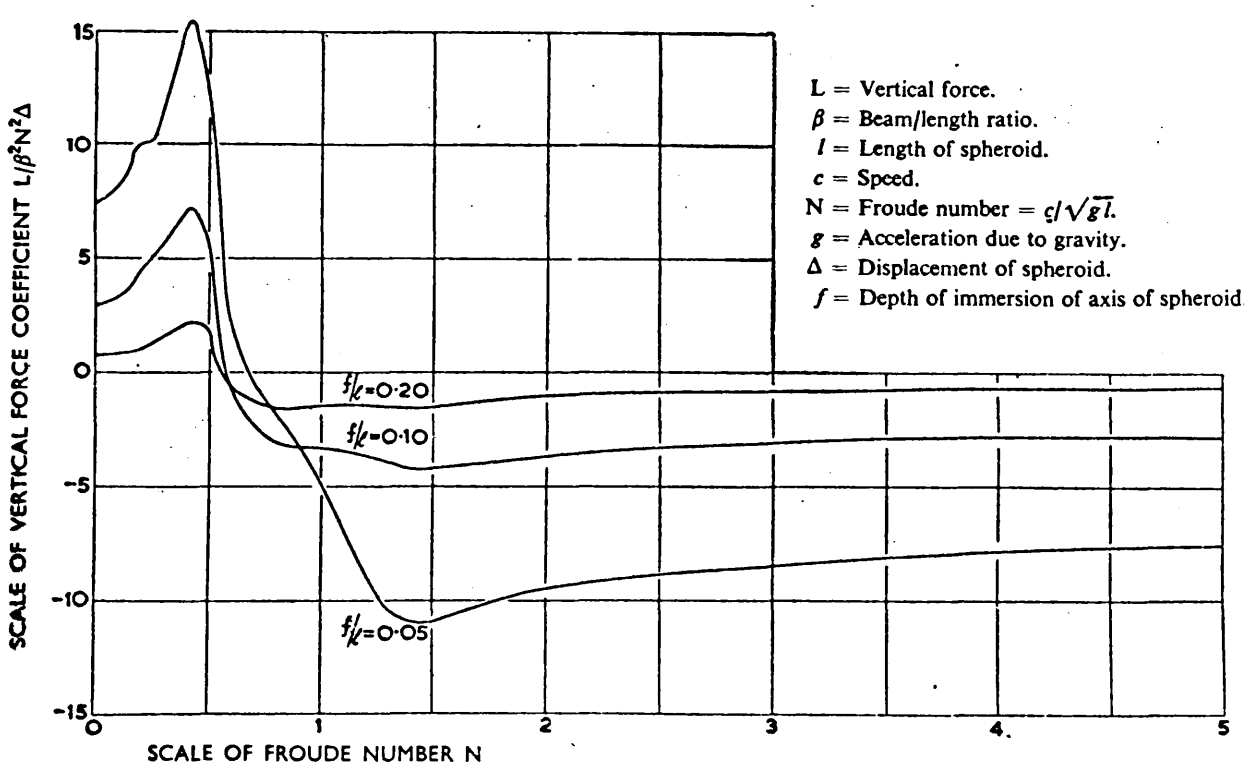

FIG. 2.—THE COEFFICIENT OF VERTICAL FORCE FOR A SUBMERGED SPHEROID

REPRODUCED FROM TRANS. R.I.N.A. VOL.95,1953, p.270,271.

iii) For low Froude Numbers, large positive (upwards) forces arise if the spheroid is close to the free surface.

iv) The factor by which forces and moments, calculated on the assumption of a fine body, must be multiplied, increases with increase of beam/length ratio δ, i.e., a fat spheroid might be expected to have a larger vertical force coefficient than a fine one.

A spheroidal bulb protruding ahead of the bow might exhibit characteristics similar to those mentioned above for a submerged body. In particular, at low values of N(where $N = V/\sqrt{gl_s}$, l_s being the length of the spheroid), the bulb would exert an upward force on the hull which would both reduce mean sinkage and alter the trim. If the bulb immersion is kept low, the magnitude of the force it exerts on the hull will be increased as shown in figure 48.

The vertical force due to the presence of the free surface will be modified by lift forces arising from circulation if the running trim is altered. These lift forces were neglected in the design of the bulb as it was intended to compare calculation and measurement with the model restrained from sinking and trimming.

3.2.3. The Choice of Bulb Shape Parameters.

In order that a sufficiently large force would be exerted by the bulb on the model, the value of N had to be small. Assuming for the moment the bulb to be a complete spheroid of length l_s attached to the model of length L in some way, we have the following relation for N :

$$N = \sqrt[3]{\frac{L}{l_s}} \qquad \ldots\ldots\ldots (3.2.1)$$

From equation (3.2.1) it is seen that, for N to be sufficiently small, l_s must be large. This indicates that the bulb must protrude well ahead of the bow.

Two design criteria are now established :

i) The bulb should protrude well ahead of the bow.

ii) The upper surface of the bulb should be close to the

l_s, Length of equivalent spheroid	2.00 ft.
b_s, Breadth " " "	4.80 in.
β, b_s/l_s	0.20
f/l_s	0.125
f, depth of immersion of C.L. of spheroid	3.00 in.
∇, equivalent spheroid	0.1675 ft^3
∇, bulb	0.1132 ft^3
surface area of bulb	1.762 ft^2
ram area ratio	177.64%
bulb area ratio	17.764%
γ, ∇ bulb/∇ eq. spheroid	0.676
surface area of hull and bulb	17.076 ft^2

Bulb Particulars Table 19

N	$\mathcal{F}$	$Z_B = \gamma Z_s$ (lb)	Z(Meas.) (lb)	Z % Change	M_B (lb.ft)	M(Meas) (lb.ft)	M % Change
0.2	0.096	0.04	-0.6	+7	+0.18	-1.5	+12
0.3	0.145	0.12	-2.2	+6	+0.55	-2.8	+20
0.4	0.193	0.25	-3.7	+7	+1.09	-4.2	+26
0.5	0.241	0.33	-6.2	+5	+1.46	-8.1	+18
0.6	0.289	-0.09	-10.2	-1	-0.41	-7.75	-5
0.8	0.386	-0.58	-22.3	-3	-2.56	-1.10	-85

+ Force Upwards ; + % Change - reduction in sinkage force and trim by head ;

Trim by head - negative

Estimated Force and Moment Changes due to Spheroidal Bulb Table 20

free surface. It should not pierce the free surface or the bulb will cease to act as a submerged body.

These two criteria are in accord with conclusions ii), iii) and vi) reached from the empirical study of ram bows described in section 3.1.4.

It was further assumed that the resultant vertical force acting on the hull and bulb combination was equal to the sum of the vertical forces due to the bulb and hull acting separately. (See figure 49.)

In order to obtain an idea of the size of the bulb, values of the vertical force due to the bulb Z_B were calculated from Wigley's results. Quantitative agreement between calculation and observation was not expected due to the approximate nature of the theory used to calculate the forces on the spheroid. The theoretical results were used in the design of the bulb in the absence of any suitable experimental results; theoretical and measured values of vertical forces were later compared.

The bulb was not, however, a complete spheroid due to its being faired into the hull. The vertical force due to the bulb Z_B differed from the vertical force acting on the equivalent spheroid Z_s. A reduction factor γ where

$$\gamma = \frac{Z_B}{Z_s} \qquad \ldots\ldots\ldots (3.2.2)$$

was introduced. For the initial design, a value of 0.60 was assumed for γ ; this enabled l_s, f/l_s and f to be estimated. A more rational estimation for γ could then be made from the relation :

$$\gamma = \frac{\nabla_{BULB}}{\nabla_{EQUIVALENT\ SPHEROID}} \qquad \ldots\ldots\ldots (3.2.3)$$

the calculated forces being adjusted accordingly.

Justification for equation (3.2.3) was obtained from Wigley's calculations; a value of Z_s is given by

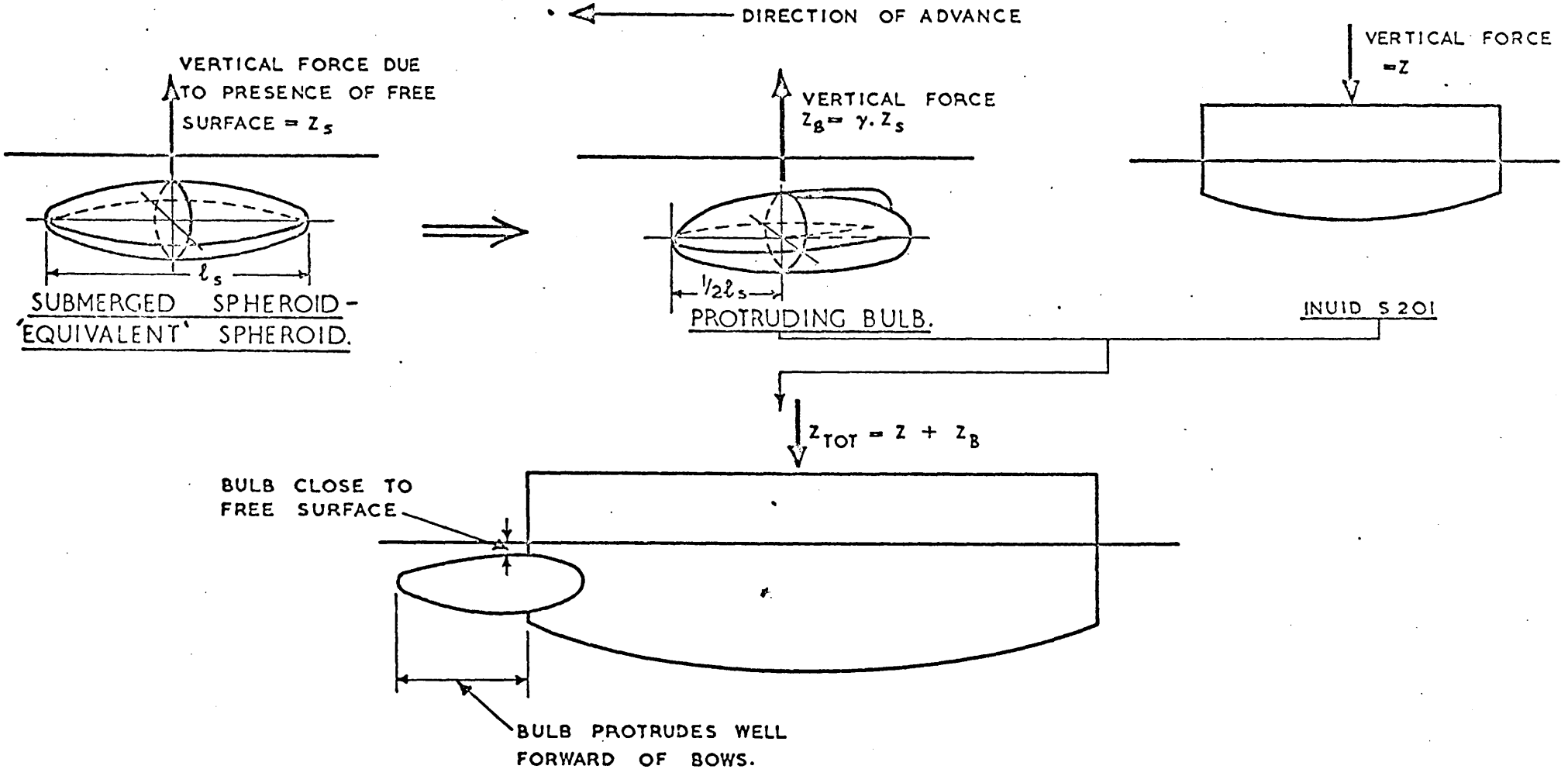

SPHEROIDAL BULB - DESIGN CONCEPT.

FIG 49

$$Z_s = C_{Z_s} \cdot \beta^2 \cdot N^2 \cdot \Delta_{SPHEROID} \qquad \ldots\ldots\ldots (3.2.4)$$

Thus for a constant $\beta, f/l_s$ and N, Z_s is proportional to the volume of displacement. Other factors, such as changes in the shape of the bulb from that of a spheroid, invalidate equation (3.2.3) to some extent but this relation for ν was considered sufficiently accurate for estimation purposes.

3.2.4. The Bulb.

A bulb was designed using the concepts outlined in section 3.2.3 and its geometrical properties are shown in figure 50 and table 19. No arbitrary fairing was attempted in order to blend the bulb into the hull as it was considered that this might give rise to forces other than those due to the bulb alone thereby making final conclusions less certain.

It is seen that the bulb is spheroidal ahead of the bow and cylindrical aft of the bow until it intersects the hull. This was in order to minimise flow separation in this region.

A wooden bulb was made and its surface made smooth. It was then painted with four coats of polyurethane yacht enamel which was burnished and wax-polished to achieve the same surface finish as that of the Inuid.

The bulb was fixed to the model as shown in plate 5. Plate turbulence stimulation studs were fitted 0.05 l_s from the nose of the bulb at a spacing of 10 mm. ; these are also shown in plate 5.

The changes in vertical force and trimming moment estimated for this bulb are shown in Table 20 and Figure 51. Values of Z_B and M_B, the vertical force and moment due to the bulb, were calculated from reference 80. (Measured values of Z and M were used in preference to calculated values due to the poor agreement between theory and experiment shown in part 2.)

It is seen that whereas the probable changes of sinkage force are small, large changes in trimming moment might occur.

FIG 50

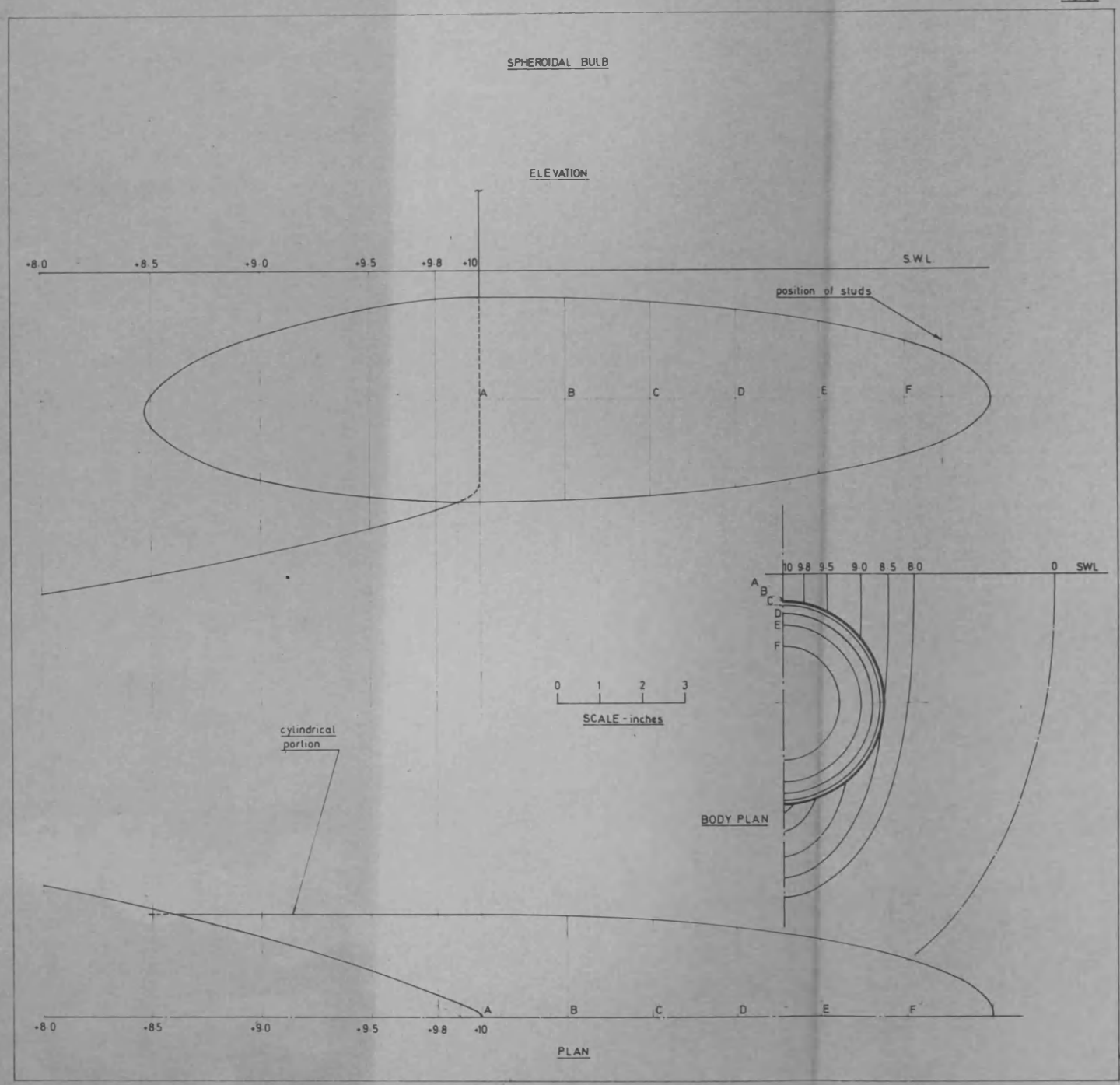
SPHEROIDAL BULB
ELEVATION
+8.0
+8.5
+9.0
+9.5
+9.8
+10
S.W.L
position of studs
A
B
C
D
E
F
10 9.8 9.5 9.0 8.5 8.0 0 SWL
0 1 2 3
SCALE - inches
cylindrical portion
BODY PLAN
PLAN

FIG. 51

VERTICAL FORCE FROM SPHEROID.

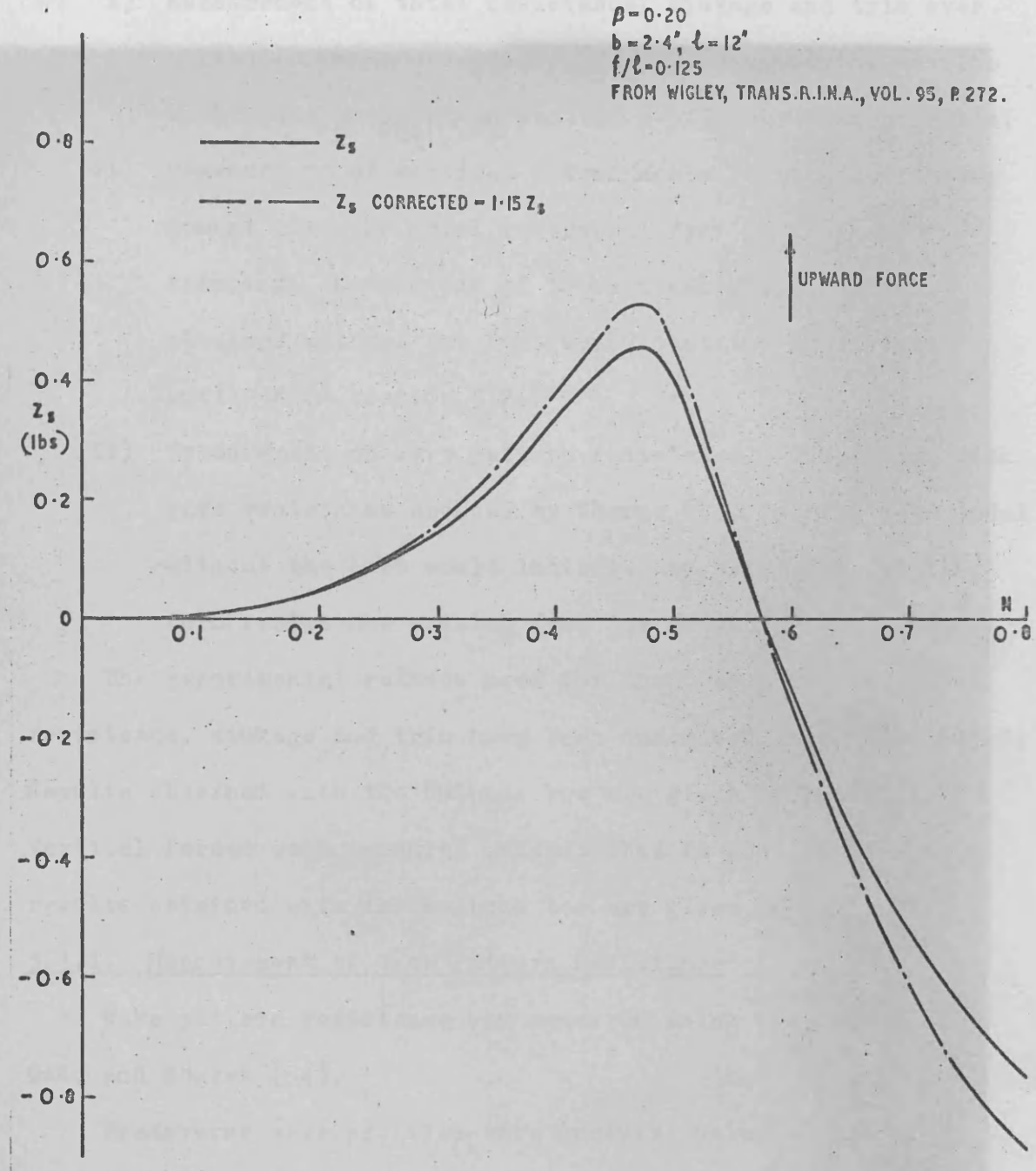

3.3. MODEL EXPERIMENTS

Model tests were performed on the Inuid S201 with spheroidal bulb. The experiments had the following aims:

i) Measurement of total resistance, sinkage and trim over a limited range of speeds. Comparison of these results with those obtained in section 2.5.2. was then possible.

ii) Measurement of vertical hydrodynamic force and trimming moment with the model restrained from sinking and trimming. Comparison of these results with those obtained without the bulb would test the hypotheses outlined in section 3.2.

iii) Measurement of wave pattern resistance. Comparison with wave resistance deduced by Sharma (53) for the same model without the bulb would indicate any alteration of the form resistance arising from the action of the bulb.

The experimental methods used for the measurement of total resistance, sinkage and trim have been described in section 2.5.2. Results obtained with the bulbous bow are given in table 21. Vertical forces were measured as described in section 2.5.3.; results obtained with the bulbous bow are given in table 22.

3.3.1. Measurement of Wave Pattern Resistance

Wave pattern resistance was measured using the method of Gadd and Hogben (54).

Transverse wave profiles were measured using a comb of 45 wave probes spaced 2 inches apart. The comb was mounted on a sub-carriage as shown in figure 52 and the pointers adjusted manually until they touched the water surface.

Two transverse wave 'cuts' were measured at each speed over a speed range of $0.15 \leq \mathcal{F} \leq 0.30$.

A cut spacing of $2\pi V^2/7g$ was used as recommended in reference 54 to avoid mathematical singularities in the subsequent analysis. The position of the cuts aft of the model X was approximately in accord with that used by Sharma (51 and 53); values of cut spacing and X are given in table 23.

Carriage Speed ft/sec	Tide ft/sec	Resistance lbs	Temp. °C	C_s Bow	C_s Stern
3.064	-0.007	0.725	16.00	-0.049	-0.074
3.023	+0.001	0.716	16.10	-0.078	-0.102
3.054	-0.030	0.719	16.12	-0.090	-0.113
2.107	0	0.342	16.16	-0.038	-0.068
4.004	-0.005	1.134	16.16	-0.227	-0.175
3.480	-0.013	0.875	16.18	-0.132	-0.140
2.518	-0.012	0.484	16.19	-0.049	-0.088
4.480	-0.032	1.400	16.20	-0.280	-0.172
3.267	-0.020	0.808	16.12	-0.144	-0.178
2.674	-0.011	0.539	15.91	-0.072	-0.123
3.673	-0.021	0.973	15.81	-0.187	-0.164
4.202	-0.021	1.246	15.77	-0.284	-0.209
4.312	-0.020	1.302	15.85	-0.304	-0.206
3.807	+0.008	1.044	16.34	-0.212	-0.172
4.647	-0.015	1.567	16.53	-0.331	-0.243
4.757	0	1.725	16.78	-0.329	-0.253
4.965	-0.014	2.100	16.95	-0.359	-0.288
5.210	0	2.602	17.06	-0.401	-0.330
2.007	0	0.305	17.25	0	-0.034
1.910	-0.021	0.230	17.27	0	-0.011
2.255	-0.015	0.379	17.27	-0.008	-0.058
3.064	-0.013	0.721	17.25	-0.079	-0.116
2.720	-0.019	0.558	17.21	-0.008	-0.071
2.838	-0.020	0.610	17.15	-0.034	-0.073
5.450	0	2.963	17.10	-	-
5.391	-0.008	2.908	16.20	-0.451	-0.337
4.199	-0.013	1.247	16.15	-0.253	-0.171
2.372	-0.015	0.431	16.10	-0.041	-0.061
3.406	-0.010	0.859	16.10	-0.110	-0.113
2.882	-0.002	0.642	16.11	-0.052	-0.094

Plate Stud Turbulence Stimulation

Total Resistance, Sinkage and Trim Results - Model with Bulb

TABLE 21

Carriage Speed ft/sec	Tide ft./sec.	Resistance lb.	Temp. °C	C_s Bow	C_s Stern
3.196	-0.007	0.786	16.18	-0.112	-0.133
2.515	-0.011	0.474	16.24	-0.082	-0.097
1.995	-0.011	0.300	16.32	-0.043	-0.055
1.830	-0.010	0.259	16.35	-0.020	-0.030
5.081	-0.010	2.329	16.35	-0.358	-0.297
2.359	-0.015	0.416	15.97	-0.069	-0.097
1.762	-0.016	0.239	16.00	-0.037	-0.032
1.507	-0.016	0.183	16.02	-0.028	-0.036
3.430	-0.021	0.862	16.06	-0.138	-0.113
5.546	-0.019	3.077	16.10	-0.499	-0.368
5.561	-0.019	3.092	16.14	-0.484	-0.379
3.337	-0.005	0.855	16.30	-0.142	-0.135
3.003	-0.007	0.694	16.34	-0.067	-0.113
2.279	-0.007	0.389	16.37	-0.011	-0.048
2.286	-0.021	0.392	16.40	+0.011	-0.030
2.722	-0.001	0.563	16.43	-0.011	-0.062
2.550	-0.007	0.492	16.47	-0.030	-0.066
1.942	-0.005	0.279	16.50	-0.023	-0.039
1.876	-0.005	0.273	15.90	-0.045	-0.041
2.723	-0.005	0.537	15.90	-0.089	-0.122
3.544	-0.006	0.929	15.91	-0.179	-0.159
4.468	-0.009	1.400	15.93	-0.334	-0.238
4.124	-0.009	1.187	15.94	-0.246	-0.210
3.933	-0.005	1.091	16.04	-0.190	-0.141
1.999	-0.012	0.302	16.05	-0.013	-0.047
2.248	-0.009	0.365	16.08	-0.024	-0.048
4.452	-0.011	1.384	16.15	-0.296	-0.202
2.807	-0.008	0.585	16.21	-0.033	-0.069
5.866	-0.020	3.400	16.27	-0.557	-0.441
5.959	+0.026	3.565	16.22	-0.593	-0.525
5.708	-0.037	3.224	16.27	-0.544	-0.395

Table 21 Cont.

Carriage Speed ft/sec	Tide ft/sec	Resistance lbs	Temp. °C	C_s Bow	C_s Stern
6.169	+0.013	3.976	16.31	-0.559	-0.651
2.794	+0.018	0.588	16.41	-0.069	-0.097
6.479	+0.001	5.030	16.42	-0.436	-0.998
6.738	-0.037	6.225	16.49	-0.242	-1.252
6.606	+0.018	5.563	16.52	-0.354	-1.133
4.732	+0.001	1.684	16.61	-0.317	-0.246
4.656	-0.027	1.558	16.64	-0.313	-0.239
4.935	+0.001	2.059	16.70	-0.354	-0.287
2.366	-0.010	0.420	16.74	0	-0.044
1.998	0	0.307	16.76	0	-0.030
2.829	-0.010	0.609	16.79	-0.019	-0.069

TABLE 21 Contd.

$\mathcal{F}$	Z_{Bow} lbs.	Z_{Stern} lbs.	Z_{Total} lbs.	Trimming Moment, M lb.ft.
0.174	-1.572	-1.491	-3.062	-0.797
0.200	-2.317	-2.117	-4.433	-1.437
0.129	-0.681	-0.845	-1.526	+0.301
0.239	-3.425	-3.228	-6.653	-1.803
0.238	-3.379	-3.180	-6.559	-1.795
0.415	-10.856	-17.308	-28.164	+17.311
0.143	-0.909	-1.137	-2.046	+0.436
0.109	-0.504	-0.525	-1.029	-0.105
0.158	-1.046	-1.260	-2.306	+0.339
0.140	-0.778	-0.866	-1.644	+0.024
0.183	-1.674	-1.791	-3.465	-0.185
0.192	-1.978	-2.031	-4.009	-0.497
0.221	-2.919	-2.696	-5.615	-1.717
0.212	-2.412	-2.518	-4.930	-0.475
0.170	-1.325	-1.502	-2.827	+0.127
0.153	-1.049	-1.233	-2.283	+0.242
0.251	-4.040	-3.603	-7.643	-2.794
0.234	-3.287	-3.082	-6.370	-1.781
0.274	-4.708	-4.533	-9.240	-2.166
0.262	-4.404	-4.016	-8.419	-2.755
0.297	-5.609	-5.503	-11.112	-2.247
0.286	-5.246	-5.215	-10.461	-1.881
0.150	-1.000	-1.235	-2.236	+0.424
0.119	-0.597	-0.621	-1.218	-0.122
0.161	-1.340	-1.296	-2.637	-0.597
0.159	-1.096	-1.258	-2.353	+0.154
0.352	-8.452	-8.529	-16.982	-2.616
0.330	-7.152	-6.936	-14.088	-3.129
0.316	-6.494	-6.327	-12.822	-2.747
0.153	-1.032	-1.108	-2.140	-0.104

Froude Numbers corrected for blockage and tide effects

Measured Vertical Forces and Trimming Moment

- Hull and Bulb

Table 22

$\mathcal{F}$	Z_{Bow} lbs.	Z_{Stern} lbs.	Z_{Tot} lbs.	Trimming Moment, M lb.-ft.
0.342	-7.743	-7.447	-15.190	-3.589
0.312	-6.264	-6.159	-12.423	-2.467
0.364	-8.923	-9.319	-18.243	-1.738
0.109	-0.455	-0.527	-0.982	+0.082
0.211	-2.181	-2.656	-4.837	+0.804
0.394	-10.407	-13.615	-24.022	+6.910
0.380	-9.561	-11.198	-20.760	+2.085
0.266	-4.325	-4.046	-8.370	-2.374
0.148	-0.913	-1.062	-1.975	+0.178
0.149	-1.012	-1.057	-2.069	-0.194
0.182	-1.656	-1.691	-3.347	-0.447
0.180	-1.555	-1.721	-3.276	+0.010
0,234	-3.046	-2.994	-6.040	-1.201
0.293	-5.405	-5.310	-10.714	-2.142
0.199	-1.948	-2.085	-4.032	-0.215
0.123	-0.737	-0.741	-1.478	-0.240
0.360	-8.569	-8.781	-17.350	-2.219
0.224	-2.965	-2.744	-5.709	-1.724

Table 22 Cont.

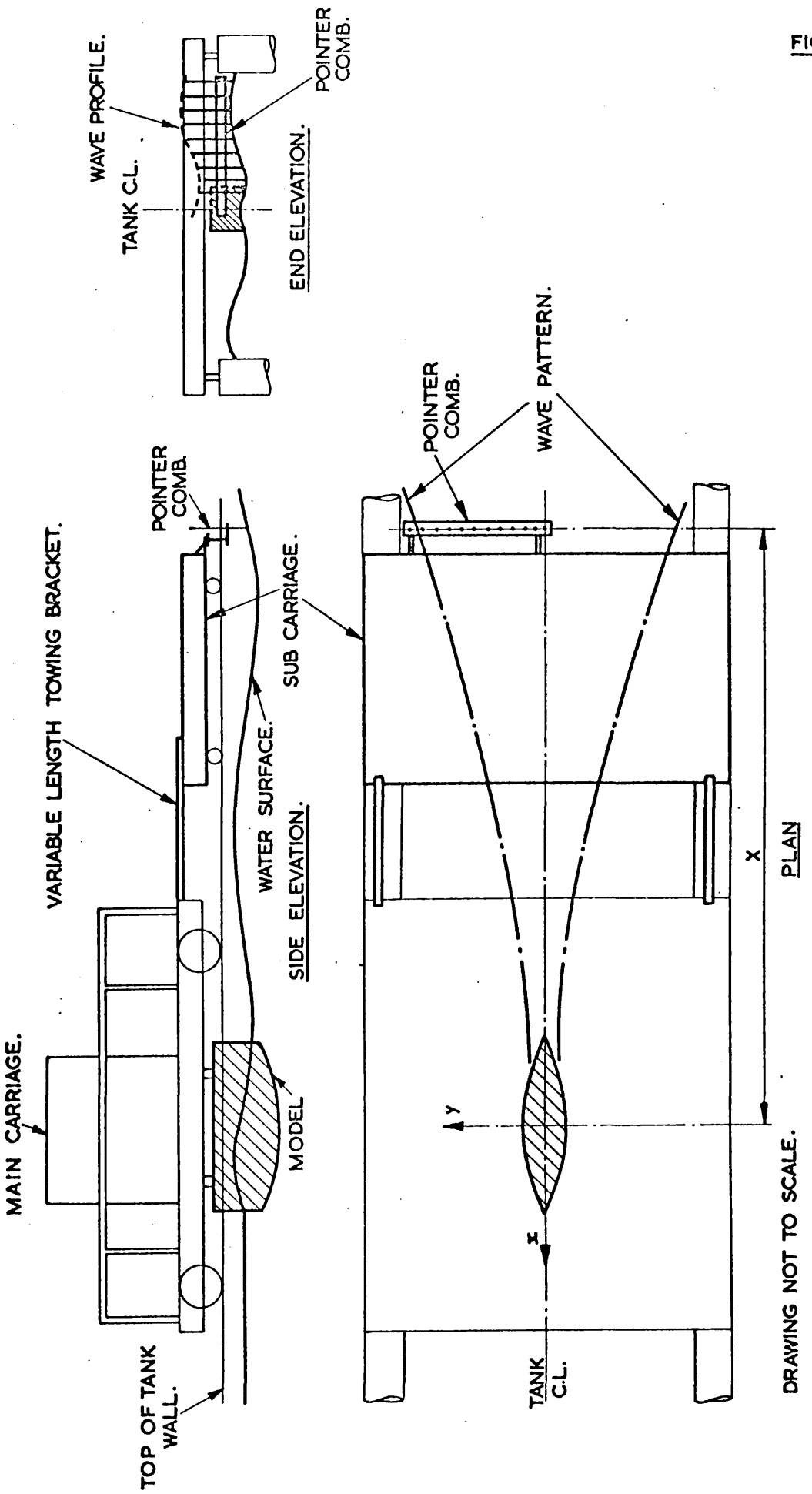

FIG. 52.

WAVE PATTERN MEASUREMENT - APPARATUS.

Run	Speed ft/sec	2Δ Cut spacing ft.	X ft.
a	3.993	0.446	12.856
b	4.193	0.492	12.879
c	4.526	0.572	12.919
d	4.742	0.626	12.946
e	4.892	0.669	12.967
f	5.041	0.705	12.985
g	4.243	0.505	12.885
h	4.126	0.475	12.870
i	4.443	0.553	12.909
h	4.126	0.475	12.870
i	4.443	0.553	12.909
j	3.561	0.352	12.809
k	3.195	0.284	12.775
l	2.729	0.209	12.737
m	3.012	0.209	12.737
n	2.463	0.171	12.718
o	2.862	0.228	12.747
p	3.710	0.383	12.824

N.B. Cuts at $x = -(X \pm 2\Delta)$

Wave Pattern Measurements -

Speeds and Cut Spacings

Table 23

A computer program, similar to that given in reference 54, accepted the wave profile ordinates for both cuts at each speed and computed a wave pattern resistance coefficient. Also computed were the analytical wave profiles and these were compared with the measured values. See figure 53 and table 24.

Accuracy of the measured wave profile ordinates varied from approximately ± 0.05 inches at low speeds to ± 0.10 inches at higher speeds where manual adjustment of the pointers was more difficult. The error analysis described in section 2.6. was assumed to be applicable to the bulbous bow experiments.

FIG.53

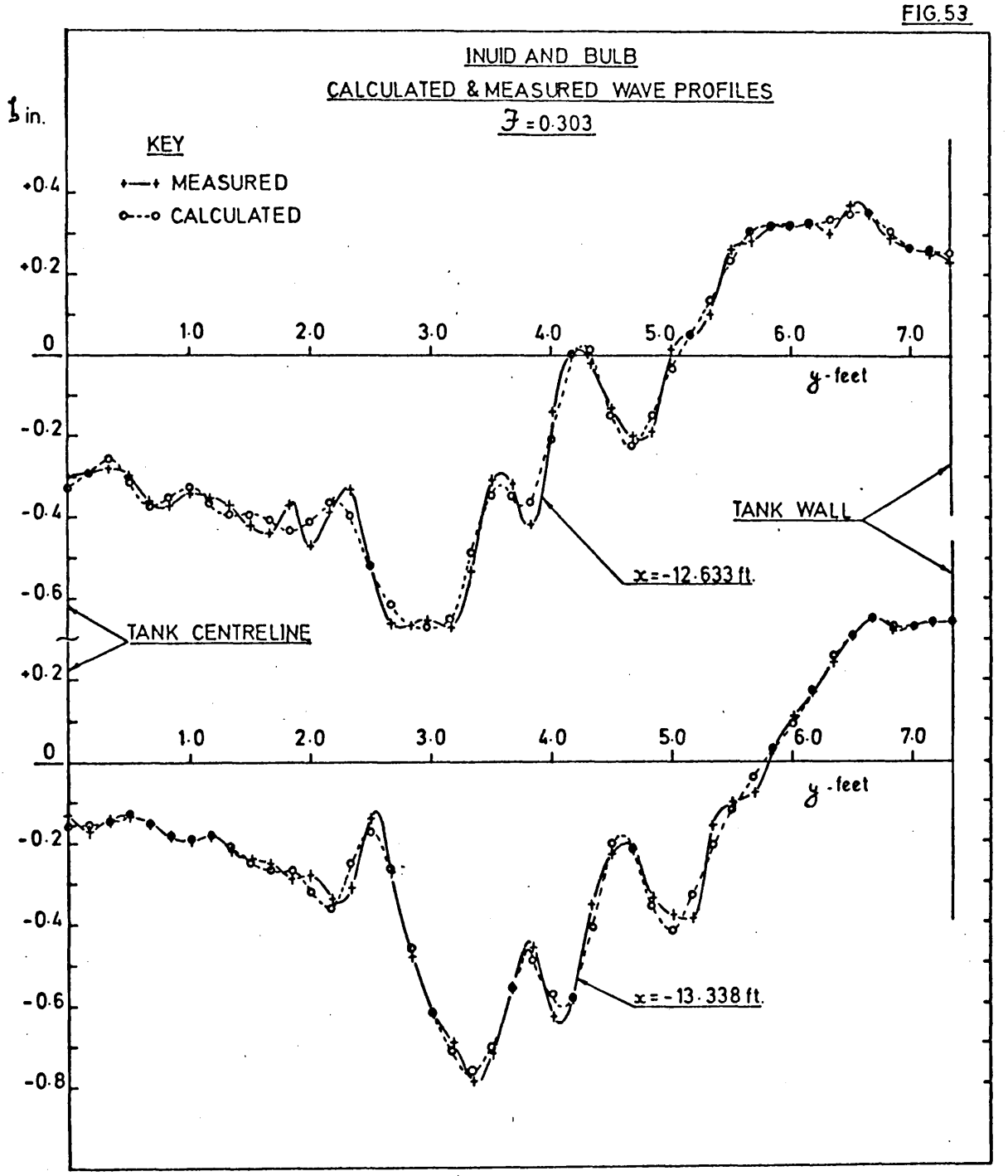
INUID AND BULB
CALCULATED & MEASURED WAVE PROFILES
F = 0.303
ζ in.
KEY
MEASURED
CALCULATED
+0.4
+0.2
0
-0.2
-0.4
-0.6
-0.8
1.0
2.0
3.0
4.0
5.0
6.0
7.0
y - feet
TANK WALL
x = -12.633 ft.
TANK CENTRELINE
x = -13.338 ft.

i	y ft.	x = -12.633 ft.			x = -13.338 ft.		
		ζ_i'' Meas.	ζ_i'' Calc.	Residual	ζ_i'' Meas.	ζ_i'' Calc.	Residual
0	0	-0.300	-0.323	+0.023	-0.130	-0.160	+0.030
1	0.167	-0.290	-0.286	-0.004	-0.170	-0.158	-0.012
2	0.333	-0.280	-0.257	-0.023	-0.140	-0.146	+0.006
3	0.500	-0.300	-0.313	+0.013	-0.130	-0.132	+0.002
4	0.667	-0.360	-0.372	+0.012	-0.150	-0.148	-0.002
5	0.833	-0.370	-0.356	-0.014	-0.180	-0.181	+0.001
6	1.000	-0.340	-0.332	-0.008	-0.190	-0.187	-0.003
7	1.167	-0.350	-0.362	+0.012	-0.180	-0.181	+0.001
8	1.333	-0.370	-0.395	+0.025	-0.220	-0.210	-0.010
9	1.500	-0.420	-0.392	-0.027	-0.240	-0.250	+0.010
10	1.667	-0.440	-0.406	-0.034	-0.250	-0.255	+0.005
11	1.833	-0.370	-0.434	+0.064	-0.290	-0.266	-0.023
12	2.000	-0.470	-0.409	-0.061	-0.280	-0.323	+0.043
13	2.167	-0.390	-0.361	-0.029	-0.340	-0.340	0
14	2.333	-0.330	-0.400	+0.070	-0.310	-0.251	-0.059
15	2.500	-0.520	-0.521	+0.001	-0.140	-0.177	+0.037
16	2.667	-0.660	-0.616	-0.044	-0.270	-0.265	-0.005
17	2.833	-0.660	-0.664	+0.004	-0.480	-0.461	-0.019
18	3.000	-0.650	-0.697	+0.047	-0.620	-0.619	-0.001
19	3.167	-0.670	-0.652	-0.018	-0.790	-0.713	+0.023
20	3.333	-0.530	-0.488	-0.042	-0.790	-0.763	-0.027
21	3.500	-0.310	-0.346	+0.036	-0.720	-0.710	-0.010
22	3.667	-0.320	-0.348	+0.028	-0.560	-0.562	+0.002
23	3.833	-0.420	-0.361	-0.059	-0.460	-0.491	+0.031
24	4.000	-0.140	-0.209	+0.069	-0.630	-0.566	-0.064
25	4.167	0	-0.004	+0.004	-0.590	-0.589	-0.001
26	4.333	-0.020	+0.011	-0.031	-0.350	-0.409	+0.059
27	4.500	-0.130	-0.142	+0.012	-0.230	-0.203	-0.027
28	4.667	-0.200	-0.227	+0.027	-0.220	-0.208	-0.012

Measured and calculated wave profiles - $\mathcal{F} = 0.303$

Table 24

i	y ft	x = -12.633 ft.			x = -13.338 ft.		
		ζ_i" Meas.	ζ_i" Calc.	Residual	ζ_i" Meas.	ζ_i" Calc.	Residual
29	4.833	-0.190	-0.154	-0.036	-0.340	-0.361	+0.021
30	5.000	0.010	-0.035	+0.045	-0.380	-0.421	+0.041
31	5.167	0.050	0.049	+0.001	-0.390	-0.331	-0.059
32	5.333	0.100	0.135	-0.035	-0.160	-0.210	+0.050
33	5.500	0.260	0.236	+0.024	-0.100	-0.121	+0.021
34	5.667	0.280	0.304	-0.024	-0.080	-0.042	-0.038
35	5.833	0.320	0.321	-0.001	0.030	0.033	-0.003
36	6.000	0.320	0.318	+0.002	0.110	0.095	+0.015
37	6.167	0.330	0.323	+0.007	0.170	0.166	+0.003
38	6.333	0.300	0.337	-0.037	0.240	0.253	-0.013
39	6.500	0.370	0.351	+0.019	0.310	0.313	-0.003
40	6.667	0.340	0.342	-0.002	0.350	0.328	+0.022
41	6.833	0.290	0.302	-0.012	0.320	0.327	-0.007
42	7.000	0.270	0.262	+0.008	0.330	0.333	-0.003
43	7.167	0.260	0.251	+0.009	0.340	0.338	+0.002
44	7.333	0.230	0.255	-0.025	0.340	0.338	+0.002

TABLE 24 Contd.

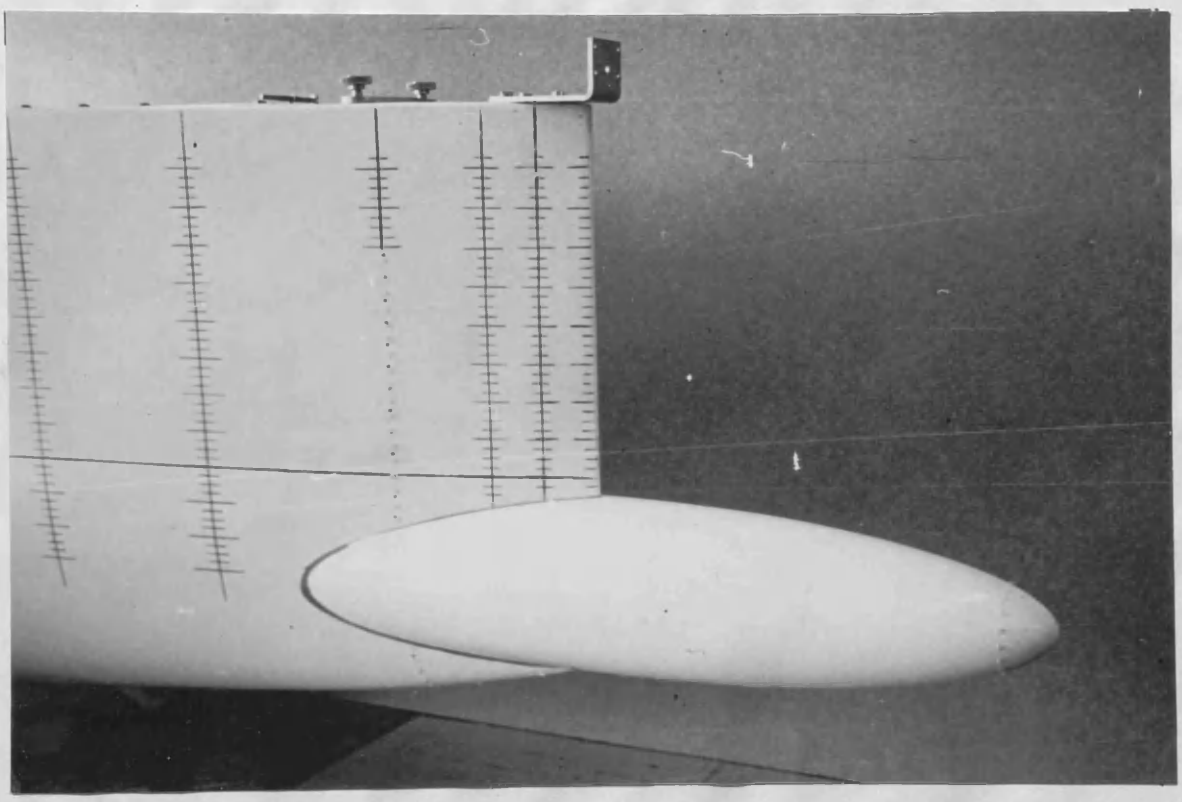

PLATE 5

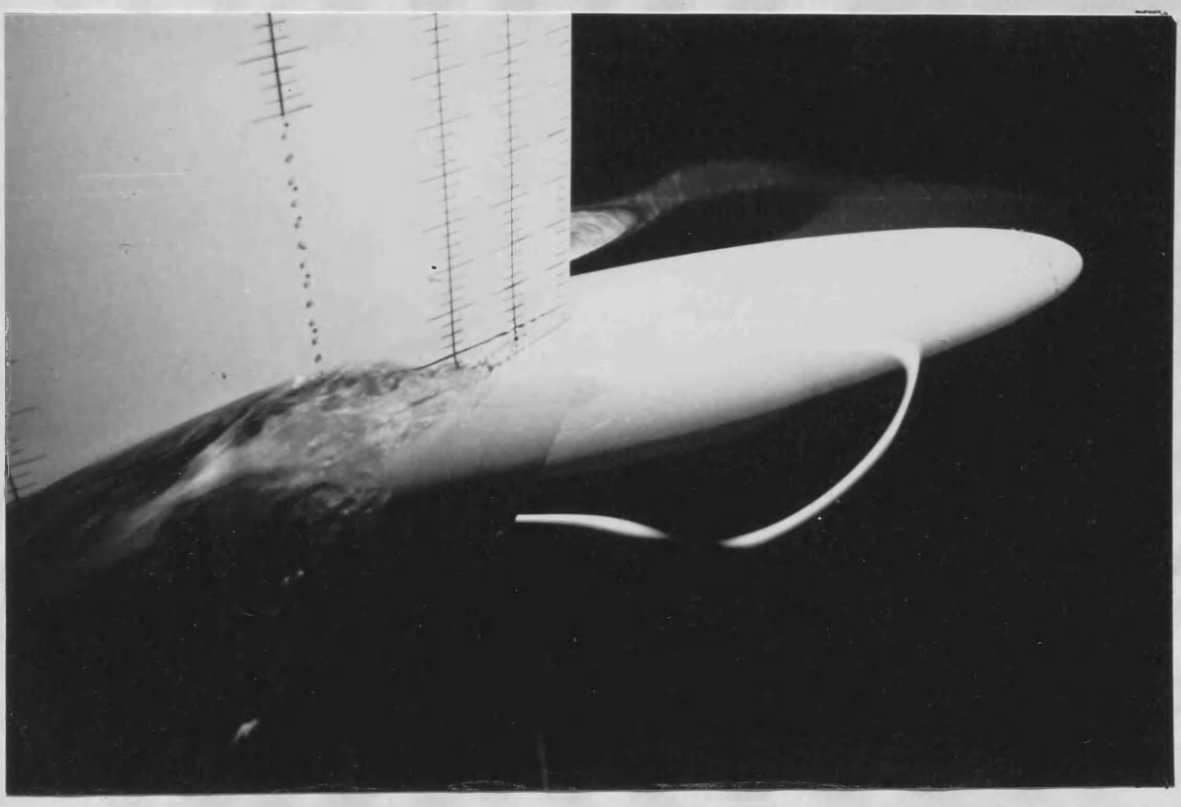

$\mathcal{F}$ = 0·170

PLATE 6

3.4. DISCUSSION OF RESULTS

3.4.1. Resistance, Sinkage and Trim - Model Free

Total Resistance

Results for total resistance coefficients are given in table 25 and compared with those for the naked hull in figure 54. All results have been corrected for temperature, blockage and tide effects.

A comparison of C_t values obtained with and without the bulb is shown in figure 55.

It is seen that in the speed range $0.2 \leq \nabla \leq 0.4$ large resistance reductions have been obtained with the use of a spheroidal bulb. Below a Froude Number of 0.20 there is a slight increase in resistance.

The Inuid S201 hull has no shoulders or other discontinuities. There is therefore little cancellation of waves by the hull itself due to its shape. The Inuid S201 is thus a resistful form and the addition of any appendage which interferes with the wave system may give rise to large resistance reductions. A total resistance estimation using Gertler's (113) method for a conventional ship having the same form parameters as Inuid S201 is shown in figure 54. In the speed range $0.17 \leq \nabla \leq 0.27$ the conventional hull shape has markedly lower resistance values, and no resistance 'hump' at a Froude Number of 0.25. These observations are of importance when comparing C_t values for the Inuid with and without a spheroidal bulb.

Mean Sinkage

Values of mean sinkage coefficient C_s, given in table 26, are compared with those for the naked hull in figure 56. The mean sinkage for the hull and bulb is seen to be less than that for the hull alone over the whole speed range.

In the speed range $0.10 \leq \nabla \leq 0.20$ the mean sinkage showed a curious behaviour. The curve exhibited large oscillations which were repeatable and were moderately well defined by the experimental

$\mathcal{F}$	$\Lambda \times 10^2$	$C_t \times 10^3$	$\mathcal{F}$	$\Lambda \times 10^2$	$C_t \times 10^3$	$\mathcal{F}$	$\Lambda \times 10^2$	$C_t \times 10^3$
0.185	5.324	4.652	0.330	4.756	5.906	0.113	5.890	4.673
0.183	5.336	4.697	0.326	4.768	6.006	0.164	5.452	4.359
0.183	5.336	4.717	0.253	5.004	4.268	0.214	5.172	4.448
0.127	5.745	4.627	0.142	5.613	4.657	0.270	4.943	4.218
0.242	5.049	4.254	0.205	5.214	4.468	0.249	5.020	4.201
0.210	5.192	4.369	0.174	5.388	4.644	0.237	5.066	4.240
0.151	5.542	4.628	0.193	5.279	4.638	0.120	5.816	4.592
0.269	4.945	4.244	0.151	5.544	4.541	0.135	5.673	4.372
0.196	5.260	4.598	0.120	5.817	4.582	0.269	4.947	4.208
0.161	5.475	4.557	0.110	5.924	4.702	0.169	5.420	4.484
0.221	5.139	4.370	0.307	4.822	5.426	0.354	4.694	5.953
0.253	5.005	4.268	0.142	5.619	4.542	0.362	4.673	5.953
0.260	4.980	4.233	0.106	5.976	4.706	0.343	4.721	5.999
0.231	5.095	4.307	0.090	6.182	4.942	0.374	4.645	6.223
0.280	4.907	4.385	0.206	5.210	4.449	0.170	5.414	4.470
0.288	4.882	4.580	0.334	4.744	6.025	0.392	4.604	7.161
0.299	4.844	5.146	0.335	4.741	6.023	0.406	4.575	8.283
0.315	4.797	5.754	0.201	5.233	4.623	0.401	4.585	7.579
0.121	5.803	4.575	0.181	5.346	4.644	0.286	4.886	4.514
0.114	5.878	3.904	0.137	5.656	4.531	0.280	4.907	4.368
0.135	5.672	4.562	0.137	5.659	4.594	0.299	4.847	5.072
0.184	5.326	4.671	0.164	5.451	4.571	0.142	5.613	4.557
0.163	5.459	4.614	0.154	5.526	4.575	0.121	5.809	4.634
0.170	5.412	4.632	0.117	5.847	4.476	0.170	5.412	4.614

$L = 8.6$ ft. $S = 17.076$ ft^2, $\mathcal{F} = V/\sqrt{gL}$, $\Lambda = (\log_{10} R_n - 2)^{-2}$

$R_n = VL/\nu$, $C_t = R_T/\frac{1}{2}\rho S V^2$.

All results corrected for blockage, temperature and tide effects.

Non-dimensional Resistance Results -

Hull and Bulb - Plate Stud Stimulation

Table 25

FIG.54

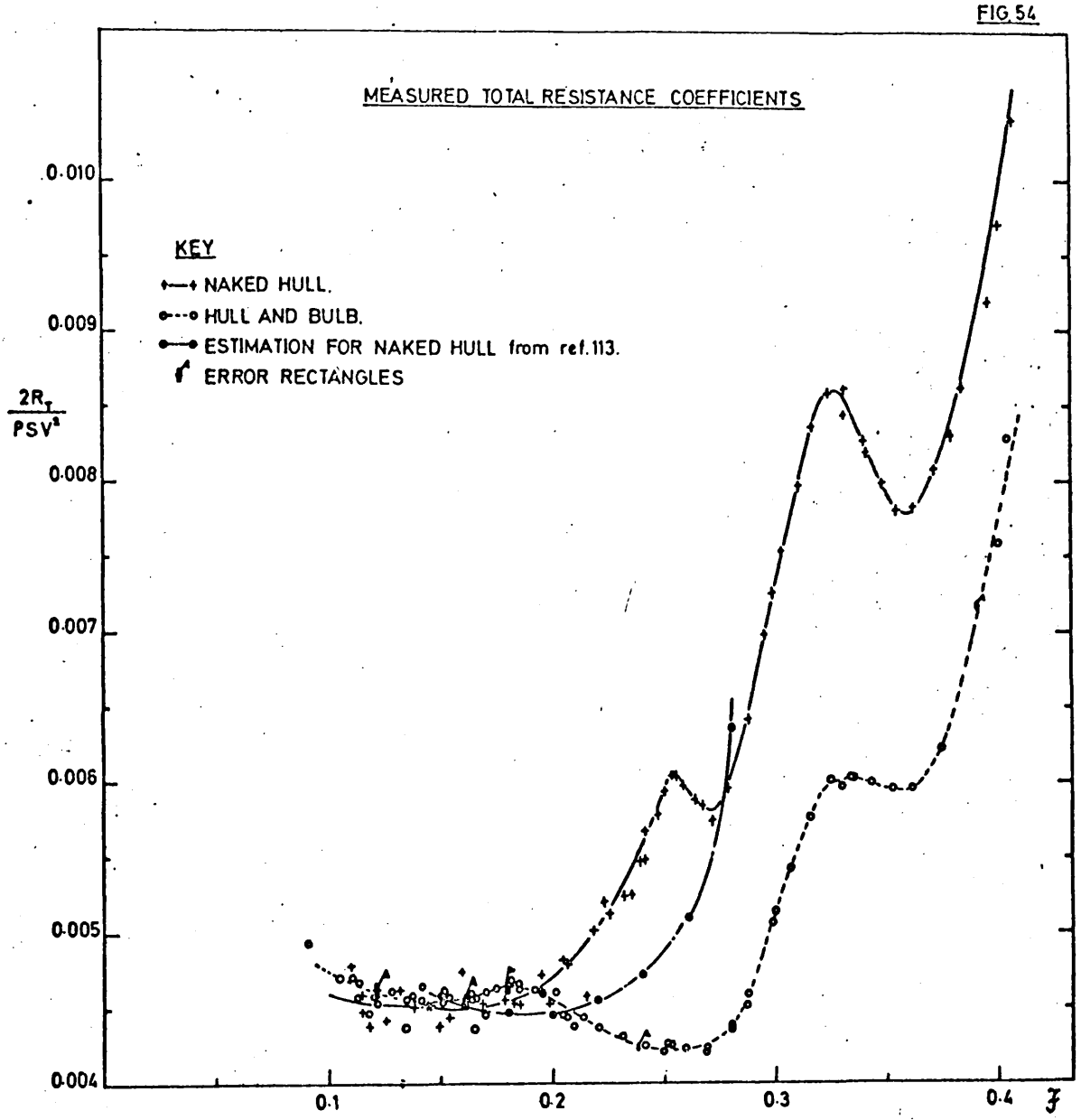
MEASURED TOTAL RESISTANCE COEFFICIENTS
KEY
NAKED HULL.
HULL AND BULB.
ESTIMATION FOR NAKED HULL from ref.113.
ERROR RECTANGLES
$\frac{2R_T}{\rho S V^2}$
0·010
0·009
0·008
0·007
0·006
0·005
0·004
0·1
0·2
0·3
0·4
$\mathcal{F}$

FIG.55

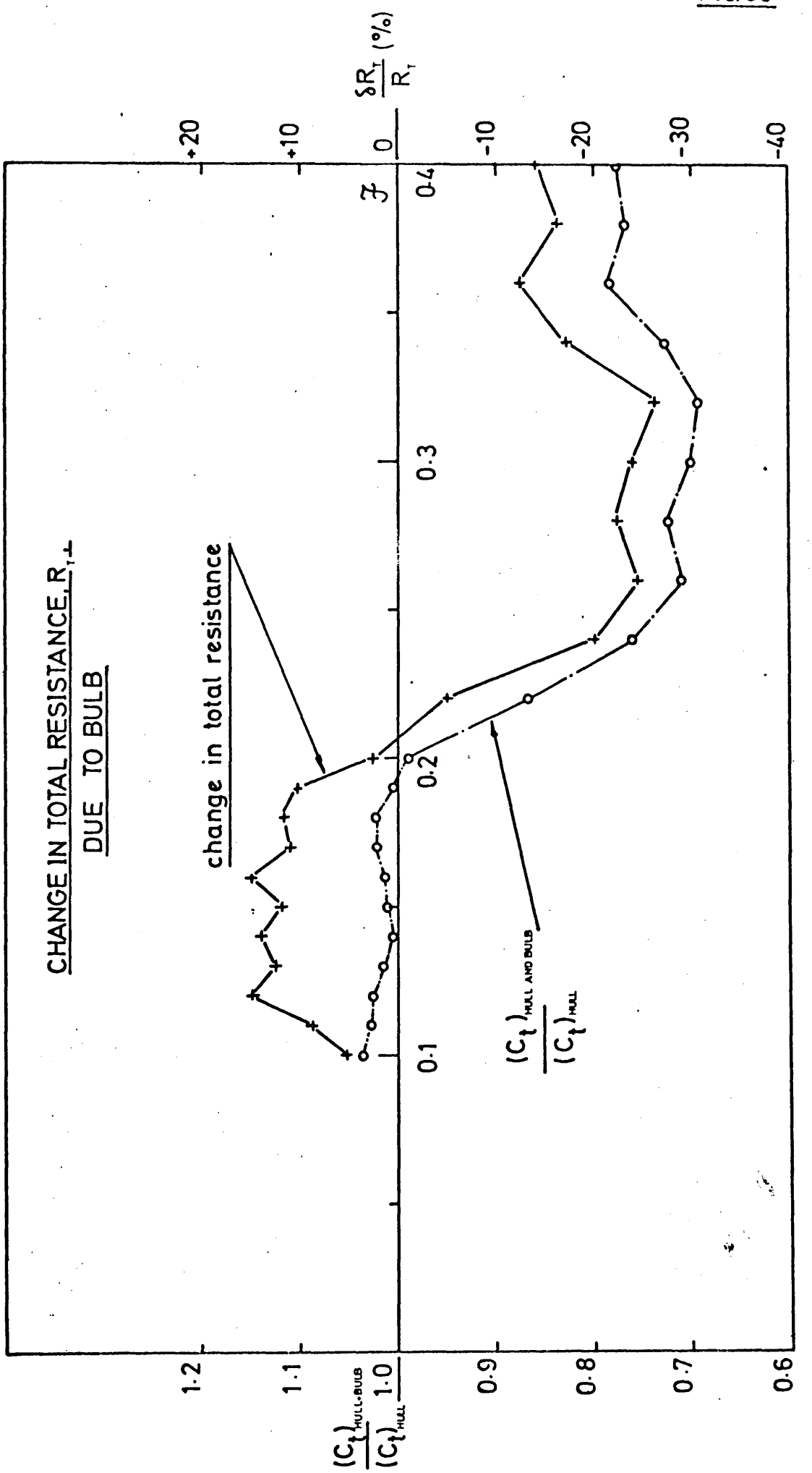
CHANGE IN TOTAL RESISTANCE, R_T, DUE TO BULB
change in total resistance
$\frac{(C_t)_{HULL+BULB}}{(C_t)_{HULL}}$
$\frac{(C_t)_{HULL\ AND\ BULB}}{(C_t)_{HULL}}$
$\frac{\delta R_T}{R_T}$ (%)
$\mathcal{F}$
1·2
1·1
1·0
0·9
0·8
0·7
0·6
+20
+10
0
-10
-20
-30
-40
0·1
0·2
0·3
0·4

$\mathcal{F}$	C_s	C_τ	$\mathcal{F}$	C_s	C_τ	$\mathcal{F}$	C_s	C_τ
0.185	-0.062	+0.025	0.326	-0.394	-0.114	0.164	-0.105	+0.032
0.183	-0.089	+0.024	0.253	-0.212	-0.082	0.214	-0.169	-0.020
0.183	-0.101	+0.023	0.142	-0.051	+0.020	0.270	-0.286	-0.096
0.127	-0.053	+0.030	0.205	-0.112	+0.003	0.249	-0.228	-0.036
0.242	-0.201	+0.052	0.174	-0.073	+0.042	0.237	-0.166	-0.049
0.210	-0.136	+0.007	0.193	-0.122	+0.021	0.120	-0.030	+0.034
0.151	-0.068	+0.038	0.151	-0.089	+0.015	0.135	-0.036	+0.024
0.269	-0.226	-0.107	0.120	-0.049	+0.012	0.269	-0.249	-0.094
0.196	-0.161	+0.034	0.110	-0.025	+0.010	0.169	-0.051	+0.036
0.161	-0.097	+0.051	0.307	-0.327	-0.061	0.354	-0.499	-0.116
0.221	-0.175	-0.023	0.142	-0.083	+0.028	0.362	-0.559	-0.067
0.253	-0.246	-0.075	0.106	-0.034	-0.006	0.343	-0.470	-0.149
0.260	-0.255	-0.096	0.090	-0.032	+0.006	0.374	-0.605	+0.092
0.231	-0.192	-0.039	0.206	-0.126	-0.025	0.170	-0.083	+0.028
0.280	-0.287	-0.088	0.334	-0.433	-0.132	0.392	-0.717	+0.562
0.288	-0.291	-0.076	0.335	-0.432	-0.106	0.406	-0.747	+1.010
0.299	-0.324	-0.071	0.201	-0.138	-0.006	0.401	-0.744	+0.779
0.315	-0.366	-0.071	0.181	-0.090	+0.046	0.286	-0.281	-0.071
0.121	-0.017	+0.034	0.137	-0.030	+0.037	0.280	-0.276	-0.074
0.114	-0.006	+0.011	0.137	-0.010	+0.042	0.299	-0.321	-0.067
0.135	-0.033	+0.050	0.164	-0.037	+0.051	0.142	-0.022	+0.044
0.184	-0.098	+0.036	0.154	-0.048	+0.036	0.121	-0.015	+0.030
0.163	-0.039	+0.063	0.117	-0.031	+0.016	0.170	-0.044	+0.050
0.170	-0.054	+0.039	0.113	-0.043	-0.003			

$\mathcal{F} = V/\sqrt{gL}$, $C_s = \frac{1}{2}(s_B + s_S) \times 100/L$, $C_\tau = (s_S - s_B) \times 100/L$, L = 8.6 ft.

All results corrected for blockage and tide effects

Non-dimensional Sinkage and Trim Results

- Hull and Bulb

Table 26

FIG. 56

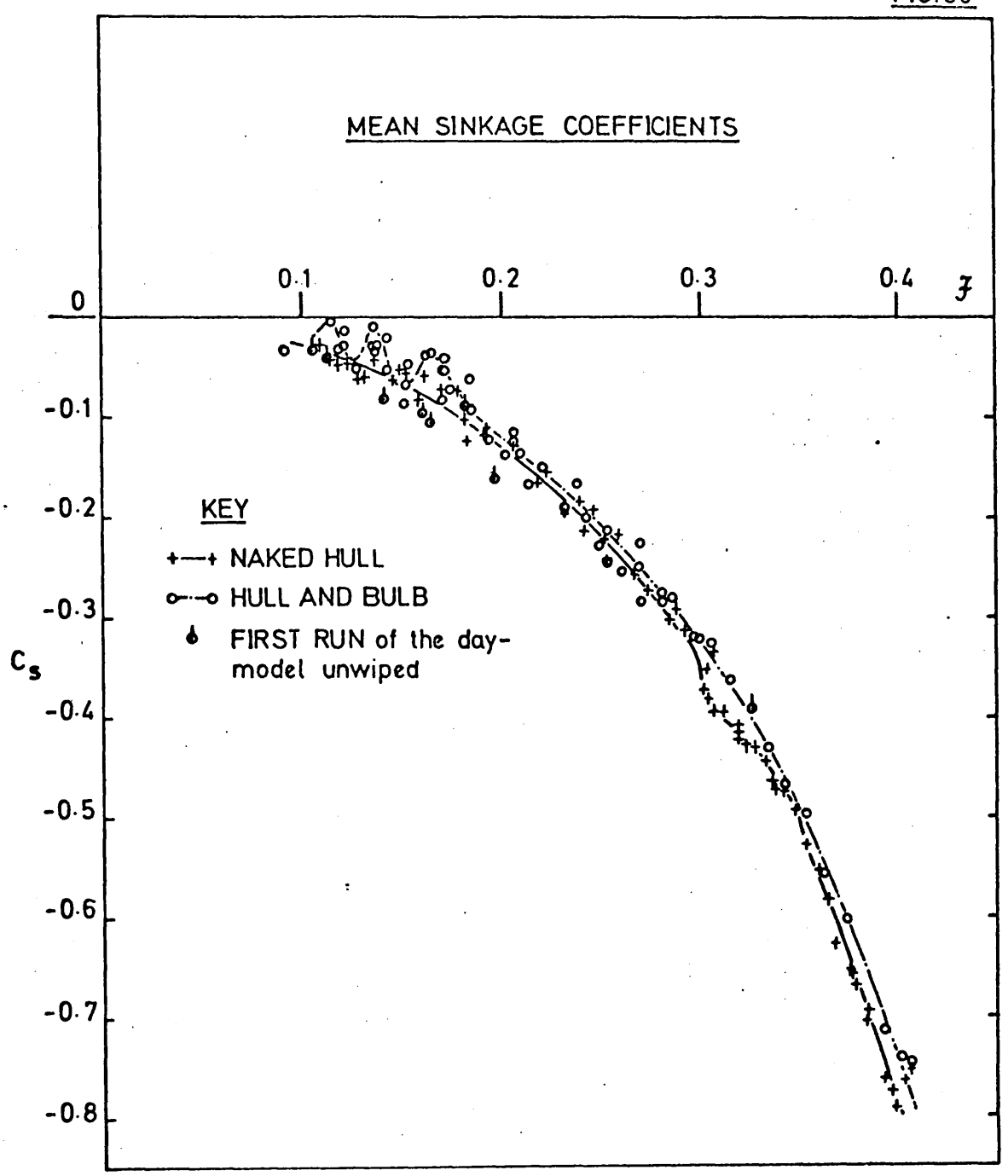
MEAN SINKAGE COEFFICIENTS
0
0·1
0·2
0·3
0·4
$\mathcal{F}$
-0·1
-0·2
-0·3
-0·4
-0·5
-0·6
-0·7
-0·8
C_s
KEY
NAKED HULL
HULL AND BULB
FIRST RUN of the day-
model unwiped

spots. It was in this speed range that reductions in mean sinkage due to the action of the bulb were anticipated (see table 20). It seems probable that the bulb was acting as a submerged body and producing an upward force at low speeds. This caused a reduction in trim by the head (see figure 58) bringing the bulb nearer to the free surface and increasing Z_B, in accord with Wigley's calculations.

These large reductions in mean sinkage were not reproduced on the first run of the day unless the model was wiped before the run. Mean sinkage values obtained without wiping the model were greater than those obtained at the same speed several runs later. These results are also shown in figure 56.

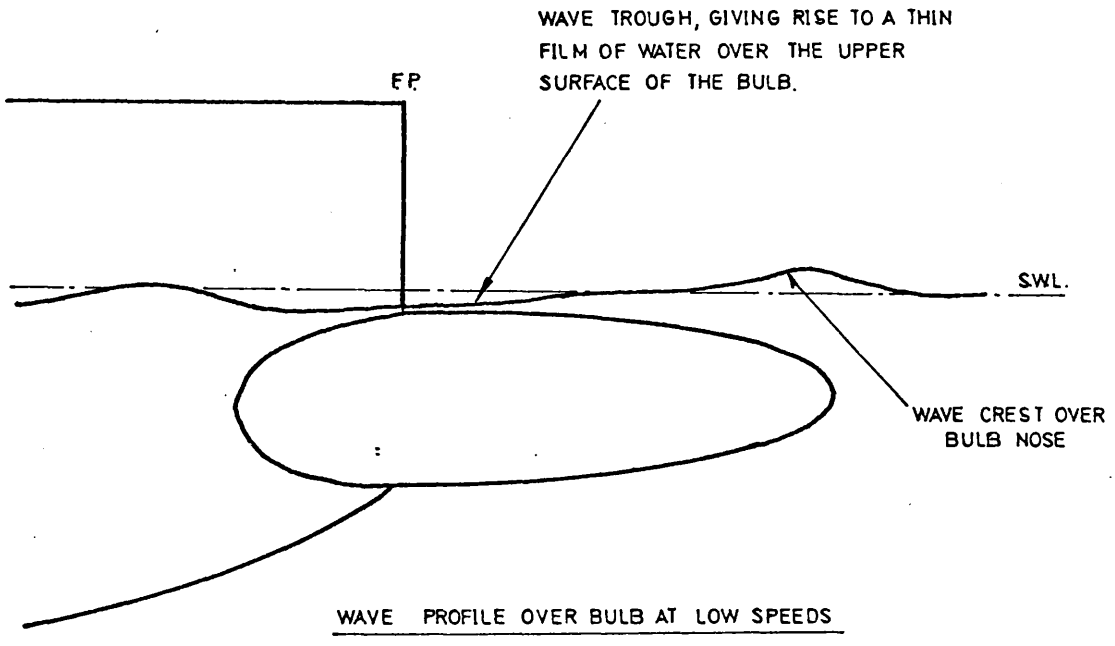

WAVE PROFILE OVER BULB AT LOW SPEEDS

FIG. 57

It was observed that the flow over the bulb at low speeds was characterised by a wave trough as shown in figure 57 and plate 6. At Froude Numbers corresponding to the peaks in the C_s curve, this wave trough gave rise to a very thin film of water over the bulb. Undoubtedly surface tension as well as viscosity was important to maintain stable flow conditions. In the absence of the correct flow conditions over the bulb at these speeds, the correct bulb forces would not be generated and the mean sinkage peaks would not be obtained. It is probable that during the

first run of the day correct flow conditions were not present over the bulb at low speeds so that anomalous results were obtained.

Trim

Values of the trim coefficient C_τ are given in table 26 and are compared with those obtained without the bulb in figure 58.

It is seen from figure 58 that for $0.10 \leq \nabla \leq 0.20$ the trim is by the stern for the hull with bulb. This contrasts with trim results obtained without the bulb where trim is seen to be by the head in this speed range. In the range $0.20 \leq \nabla \leq 0.26$ the addition of the bulb reduced trim by the head but for the range $0.26 \leq \nabla \leq 0.37$ the model with the bulb trims more by the head. Over the remainder of the speed range the model with the bulb exhibits less trim by the stern than the naked hull.

These trim results all indicate that the bulb is acting as a submerged body as suggested in section 3.2. An upward vertical force from the bulb at low speeds reduces trim by the head. As speed increases, the 'bulb Froude Number, N' increases and the vertical force from the bulb begins to act downward, thus reducing trim by the stern.

The generation of lift by the bulb probably accompanies the vertical force Z_B. Moreover, fluid inertia forces will also appear as the angle of attack of the bulb changes due to trim (80, p.273). The generation of lift would almost certainly be affected by the proximity of the free surface and is therefore difficult, if not impossible, to estimate accurately. It appears from the trim results at $\nabla > 0.36$ that the lift force, if it acts upwards for a positive angle of attack, is small compared to the hydrodynamic vertical force Z_B. Direct measurement of Z_B with the model restrained from sinking and trimming, i.e., with the bulb prevented from presenting an angle of attack to the flow, is discussed in section 3.4.2. below.

FIG. 58

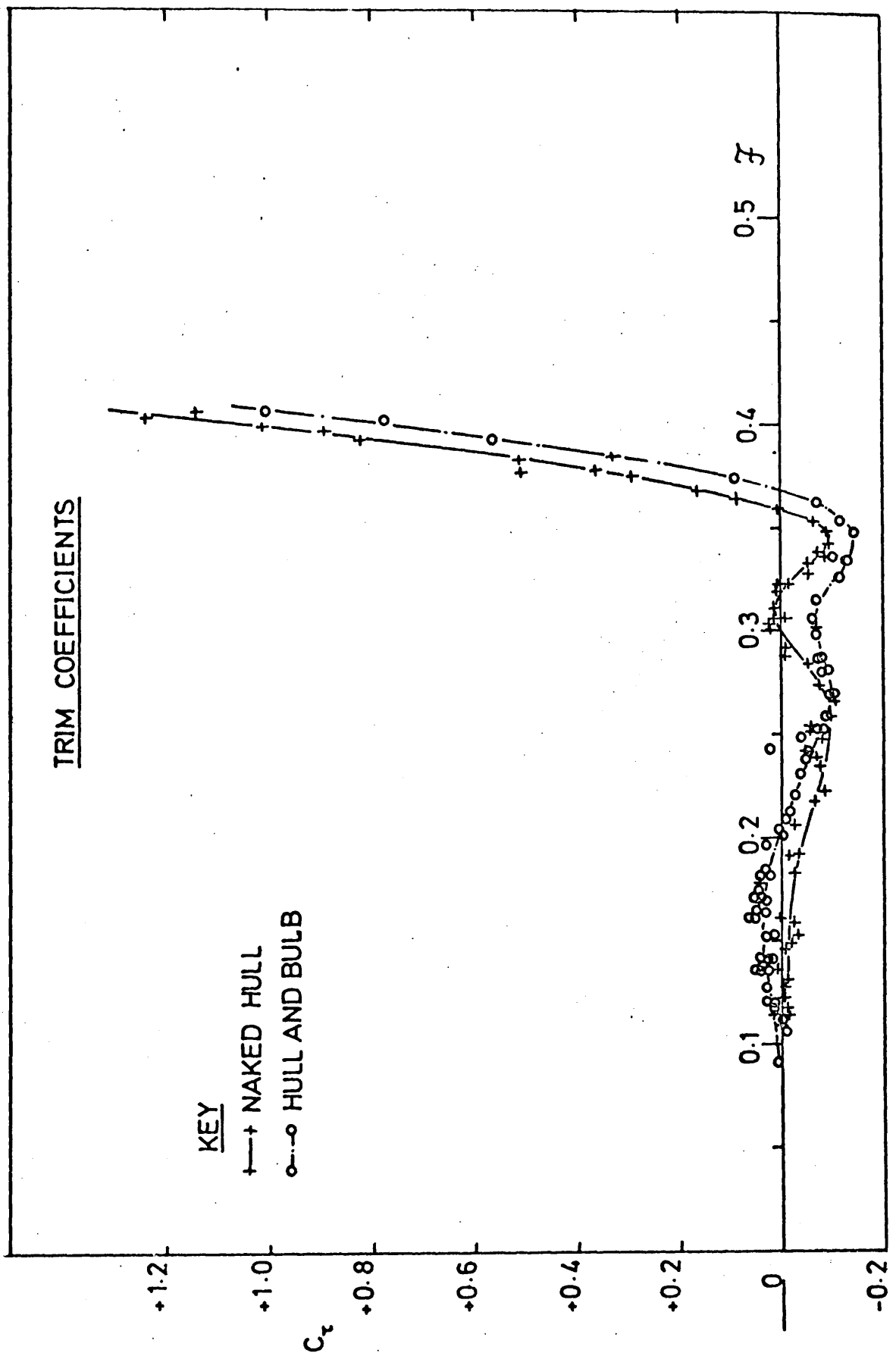
TRIM COEFFICIENTS
KEY
NAKED HULL
HULL AND BULB
C_τ
+1.2
+1.0
+0.8
+0.6
+0.4
+0.2
0
-0.2
0.1
0.2
0.3
0.4
0.5
$\mathcal{F}$

It is of interest to compare the trim changes due to the bulb (figure 58) with the resistance changes (figure 54). In the speed range $0.10 \leq \vartheta \leq 0.20$ a resistance increase is seen to correspond to a change from trim by the head to trim by the stern. It will be shown below that in this speed range the bulb produces an increase in viscous resistance (see section 3.4.4). It appears, therefore, that by altering the trim at low speeds, the bulb modifies the viscous flow over the hull. It is probable that the trim angle has a marked effect on boundary layer growth (see Robson (114 p.277)) and thus is related to the viscous pressure resistance, R_{VP}. (See section 2.7.4.)

If a correlation coefficient ρ_c is defined by

$$\rho_c(x,y) = \frac{\sum xy}{\sqrt{\sum x^2}.\sqrt{\sum y^2}}$$

it is found that the curves representing change in trim due to the bulb, δt, and change in total resistance due to the bulb, δR_T, are well correlated over the range $0.10 \leq \vartheta \leq 0.40$. The correlation coefficient is given by

$$\rho_c(\delta t, \delta R_T) = 0.672$$

This result is interesting but not necessarily illuminating as care is needed in relating cause to effect when considering the complex fluid flow around hull and bulb. It is not suggested therefore that a change in total resistance is caused in some way by change of trim : wave interference undoubtedly accounts for most of the resistance reduction. Change of trim is but one indication of a modification of both the viscous and potential flow over the hull due to the bulb, one consequence of which is a reduction in total resistance.

3.4.2. Wave Pattern Resistance and Wave Profiles

Wave Pattern Resistance

Wave pattern resistance coefficients C_{wp} are given in table 27

Run	$\mathcal{F}$	$C_{wp} \times 10^4$
a	0.240	1.854
b	0.252	1.294
c	0.272	1.622
d	0.285	3.886
e	0.294	5.540
f	0.303	9.084
g	0.255	1.481
h	0.248	1.359
i	0.267	1.455
j	0.214	2.172
k	0.192	2.212
l	0.164	0.701
m	0.181	1.551
n	0.148	0.513
o	0.172	4.525
p	0.223	2.375

$\mathcal{F} = V/\sqrt{gL}$, $\quad C_{wp} = R_{wp}/\frac{1}{2}\rho S V^2$

$S = 17.076$ ft^2 $\quad L = 8.6$ ft.

Non-dimensional Wave Pattern Resistance Results - Hull and Bulb

Table 27

FIG. 59

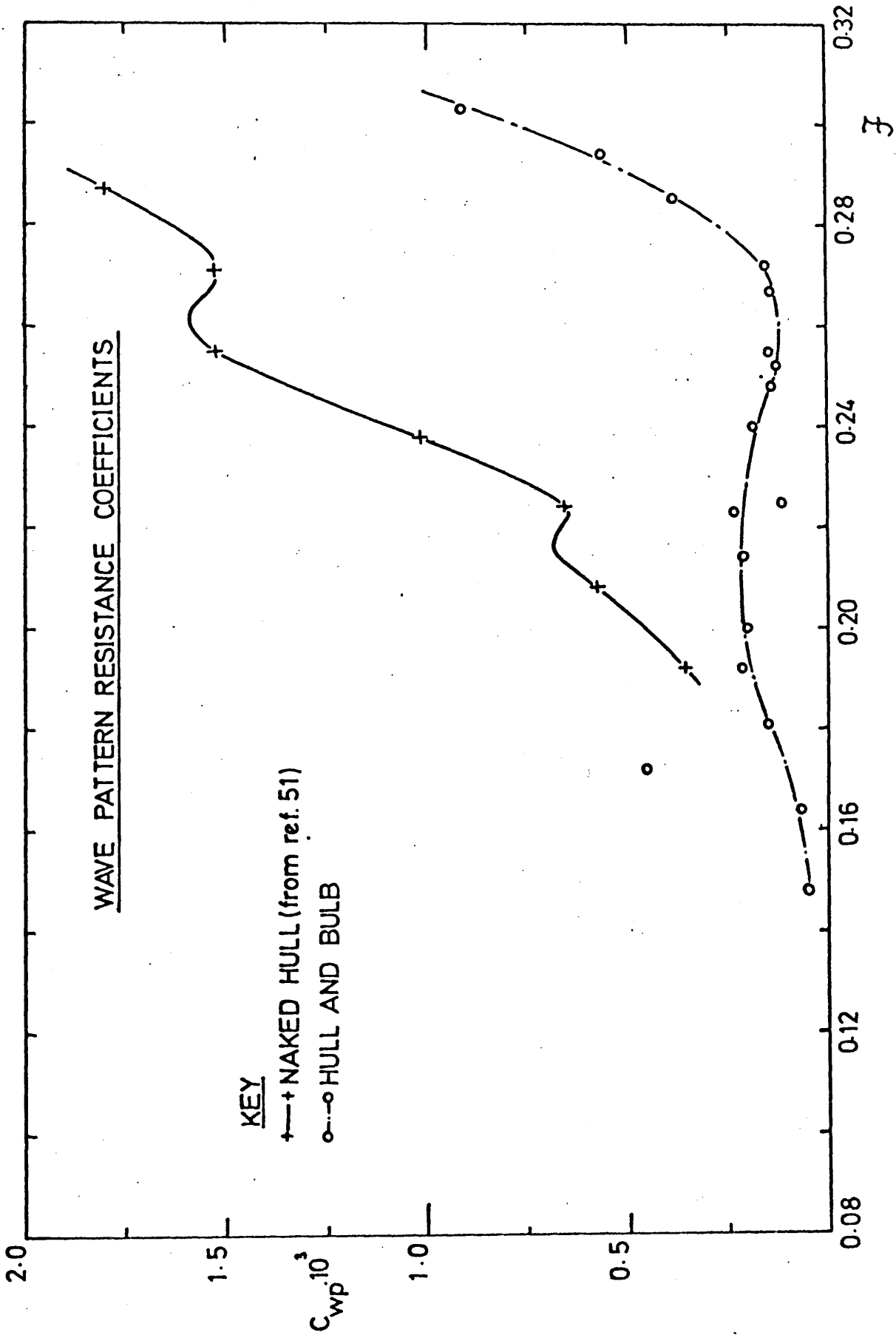
WAVE PATTERN RESISTANCE COEFFICIENTS
KEY
+—+ NAKED HULL (from ref. 51)
o-·-o HULL AND BULB
$C_{wp}.10^3$
2·0
1·5
1·0
0·5
0·08
0·12
0·16
0·20
0·24
0·28
0·32
$\mathcal{F}$

FIG. 60

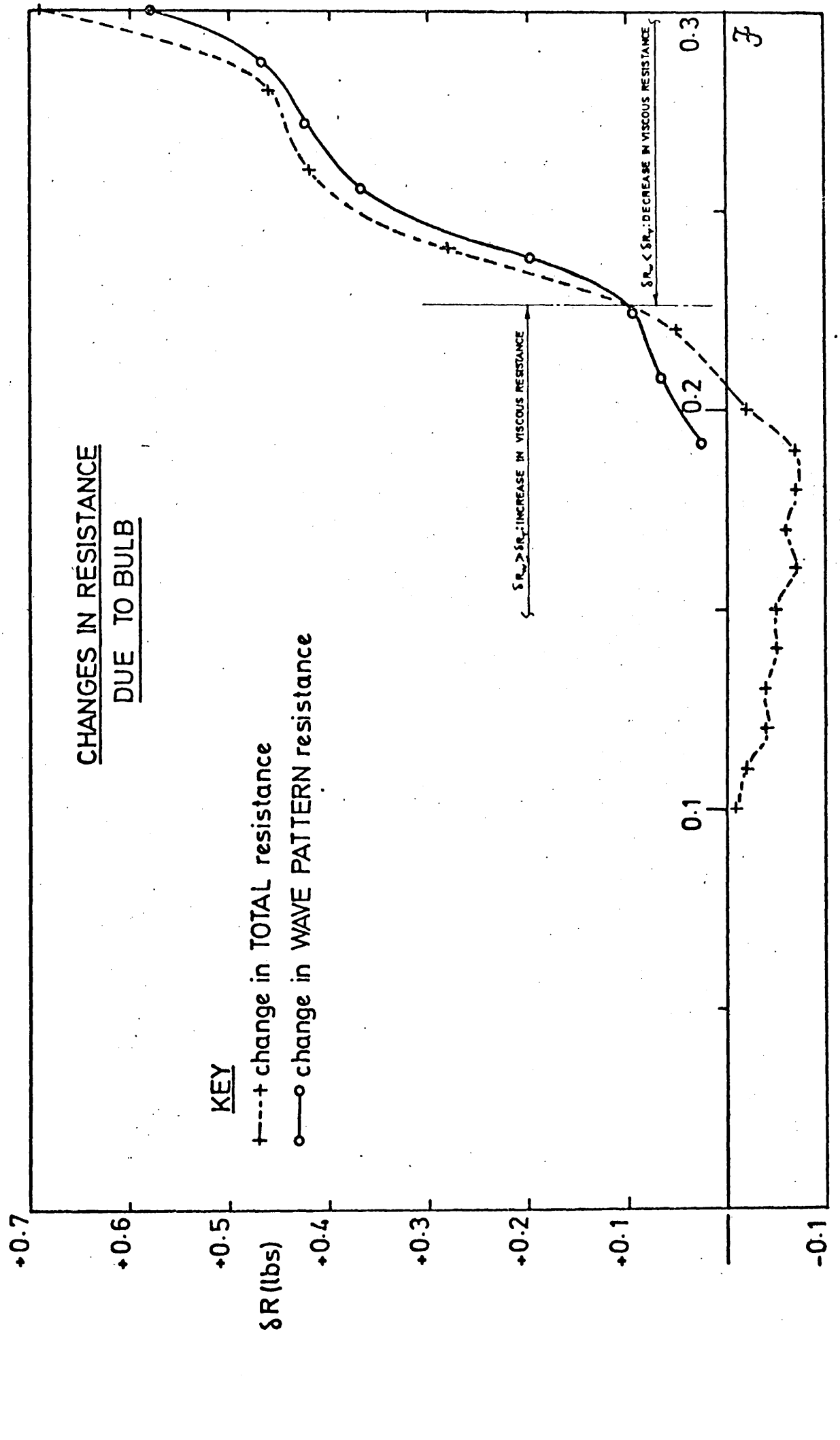
CHANGES IN RESISTANCE
DUE TO BULB
KEY
+---+ change in TOTAL resistance
o——o change in WAVE PATTERN resistance
δR (lbs)
+0.7
+0.6
+0.5
+0.4
+0.3
+0.2
+0.1
-0.1
0.1
0.2
0.3
J
δR_w > δR_t : INCREASE IN VISCOUS RESISTANCE
δR_w < δR_t : DECREASE IN VISCOUS RESISTANCE

and compared with values measured by Sharma for the naked hull in figures 59 and 60.

It should be remembered that such a comparison is only valid if

i) The values of C_{wp} measured by Sharma and the author are not subject to scale effect.

ii) The errors between Sharma's Inuid and the Glasgow Inuid have a small effect on C_{wp}.

iii) The differences in experimental methods of measuring C_{wp} at Hamburg and Glasgow have negligible effect on wave pattern resistance.

Of these conditions, (iii) is likely to be the most important. Sharma obtained several 'wave cuts' during each run and solved a redundant set of simultaneous equations to obtain amplitudes and phases. At Glasgow only one cut was obtained during each run at any speed. This speed had to be repeated for another run to obtain a second cut. From these two cuts amplitudes and phases were calculated using the method of reference 54. Inaccuracies in the method used at Glasgow have been discussed elsewhere (54), but it was assumed that they would not seriously affect the comparison of C_{wp} values due to the large changes in wave pattern resistance brought about by the bulb.

Large reductions in C_{wp} were obtained over the speed range $0.20 \leq \nabla \leq 0.30$ with complete cancellation of the resistance hump obtained with the naked hull at a Froude number of 0.27.

Wave Profiles

Wave profiles along the hull with and without the bulb are shown in plates 7,8,9 and 10 for Froude Numbers of 0.172 and 0.356. Wave profiles for the hull bulb configuration are shown in plates 11,12 and 13 for a range of Froude Numbers.

It is seen that at a Froude Number of 0.172 the bulb shifts the bow wave crest aft. It was observed that the upper surface of the bulb and the free surface appeared to act as a venturi, accelerating the flow and causing a large perturbation velocity

NAKED HULL $\mathcal{F} = 0.172$ PLATE 7

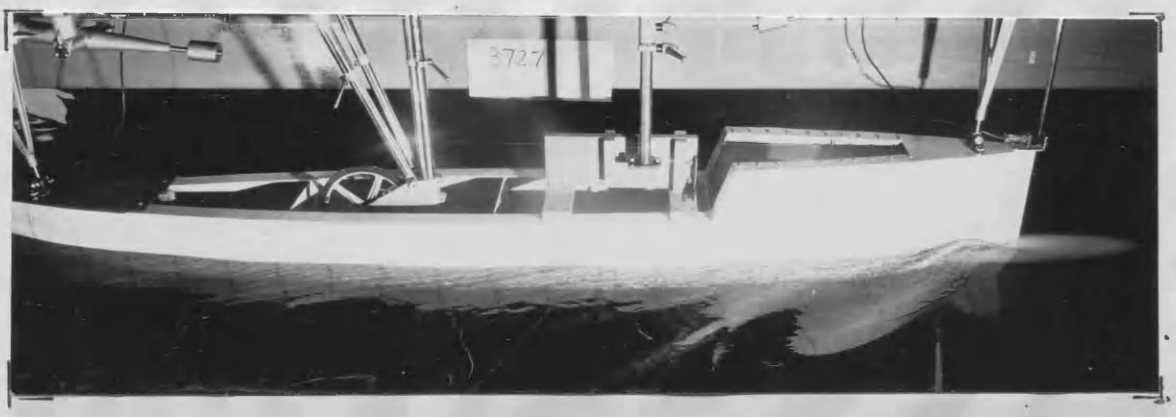

HULL AND BULB $\mathcal{F} = 0.172$ PLATE 8

NAKED HULL $\mathcal{F} = 0.356$ PLATE 9

HULL AND BULB $\mathcal{F} = 0.356$ PLATE 10

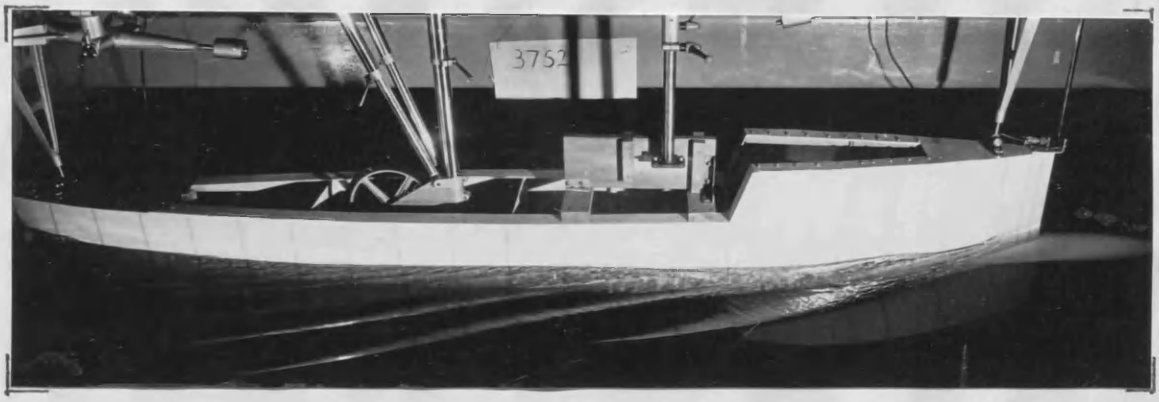

$\mathcal{F}$ = 0.120 PLATE 11

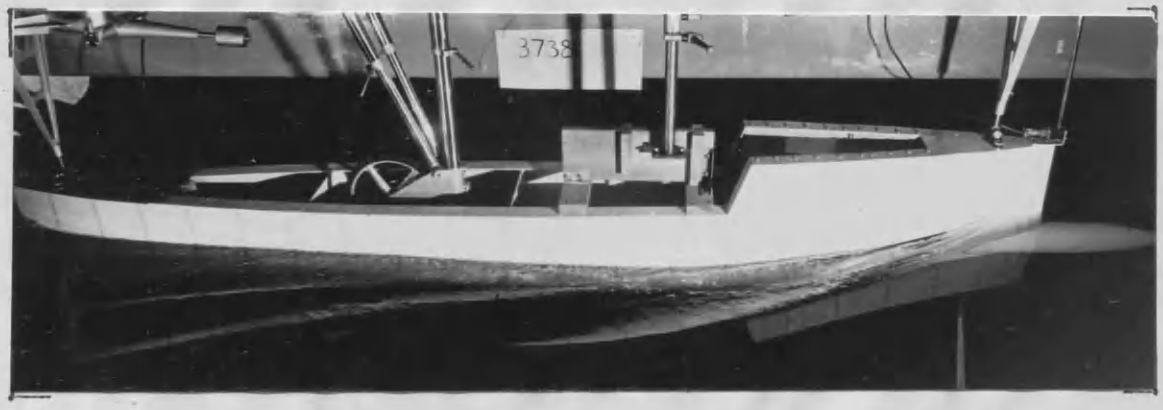

$\mathcal{F}$ = 0.334 PLATE 12

$\mathcal{F}$ = 0.404 PLATE 13

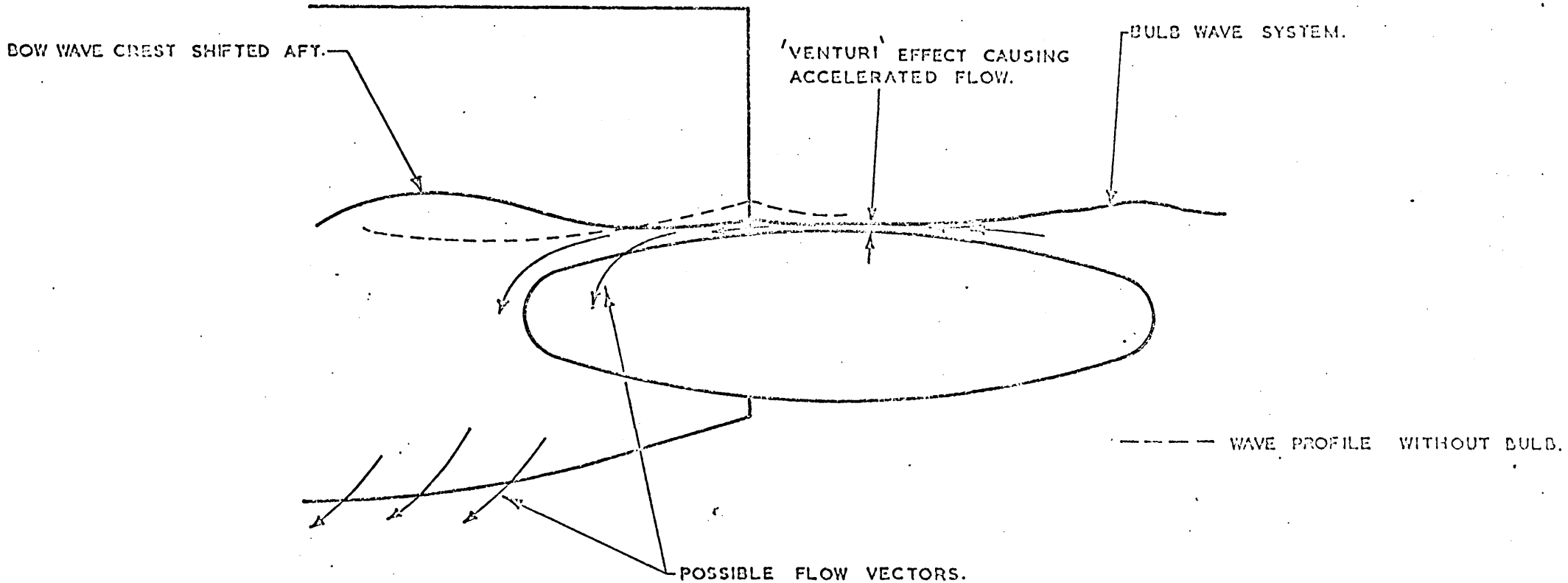

EFFECT OF BULB ON WAVE PROFILE.

FROUDE NUMBER ≏ 0·17

FIG 61

in the negative x-direction. This large horizontal component of flow appeared to delay formation of the bow wave crest until aft of station +9.5 at which point the flow was presumably downwards over the aft end of the bulb. (See figure 61.) At this speed it seemed probable that there was a slight reduction in wave pattern resistance (see figure 60). This can only be inferred, as no wave pattern results were available below a Froude Number of 0.192 for the model without the bulb.

At a Froude Number of 0.356, it appeared that the bulb was not acting in this way as there was no shift of the bow wave crest. It is probable that the reduction in wave pattern resistance at this speed was due to wave interference effects discussed in section 3.1.

The above discussion is based on observation and supposition and should be tested by detailed flow and pressure measurements. It is well-known that the form of the water-lines near the free surface have a greater effect on pressure resistance than those near the keel. Thus a bulb near the free surface which modified the flow over the upper waterlines would be expected to alter the pressure resistance markedly. Linear superposition of the hull wave system and bulb wave system to give the total wave system was assumed by Wigley and others as shown in section 3.1. It is doubtful if this approach is justified for a bulb close to the free surface and a fresh approach, such as consideration of the 'venturi' effect of the bulb and free surface, seems appropriate.

3.4.3. Vertical Forces and Moments - Model Restrained

Vertical forces, moments and non-dimensional coefficients, measured with the model restrained, are given in table 28. Forces and moments are compared with those obtained with the non-bulbous model in figures 62 and 63; vertical force and moment coefficients are compared with those obtained with the non-bulbous model in figures 65 and 66. All results have been corrected for blockage, temperature and tide effects.

$\mathcal{F}$	$C_Z \times 10^2$	$C_M \times 10^3$	$\mathcal{F}$	$C_Z \times 10^2$	$C_M \times 10^3$
0.174	-2.217	-0.671	0.161	-2.212	-0.582
0.200	-2.421	-0.912	0.159	-2.041	+0.156
0.129	-2.003	+0.460	0.352	-2.999	-0.537
0.239	-2.540	-0.800	0.330	-2.828	-0.730
0.238	-2.532	-0.806	0.316	-2.801	-0.698
0.415	-3.567	+2.549	0.153	-1.989	-0.112
0.143	-2.189	+0.542	0.342	-2.826	-0.776
0.109	-1.893	-0.224	0.312	-2.791	-0.644
0.158	-2.025	+0.346	0.364	-3.002	-0.332
0.140	-1.832	+0.031	0.109	-1.804	+0.175
0.183	-2.255	-0.140	0.211	-2.361	+0.456
0.192	-2.364	-0.349	0.394	-3.369	+1.127
0.221	-2.513	-0.894	0.380	-3.139	+0.367
0.212	-2.395	-0.283	0.266	-2.582	-0.852
0.170	-2.133	+0.112	0.148	-1.974	+0.207
0.153	-2.135	+0.263	0.149	-2.040	-0.222
0.251	-2.650	-1.128	0.182	-2.213	-0.344
0.234	-2.545	-0.254	0.180	-2.206	+0.008
0.274	-2.684	-0.732	0.234	-2.417	-0.559
0.262	-2.672	-1.017	0.293	-2.729	-0.634
0.297	-2.743	-0.645	0.199	-2.224	-0.138
0.286	-2.790	-0.583	0.123	-2.119	-0.400
0.150	-2.180	+0.480	0.360	-2.922	-0.434
0.119	-1.892	-0.220	0.224	-2.493	-0.875

$\mathcal{F} = V/\sqrt{gL}$, $C_Z = Z/\frac{1}{2}\rho SV^2$, $C_M = M/\frac{1}{2}\rho SLV^2$, L = 8.6 ft., S = 17.076 ft^2

All results corrected for blockage and tide effects.

Non-dimensional Vertical Force and Trimming Moment Coefficients

- Hull and Bulb

Table 28

FIG. 62

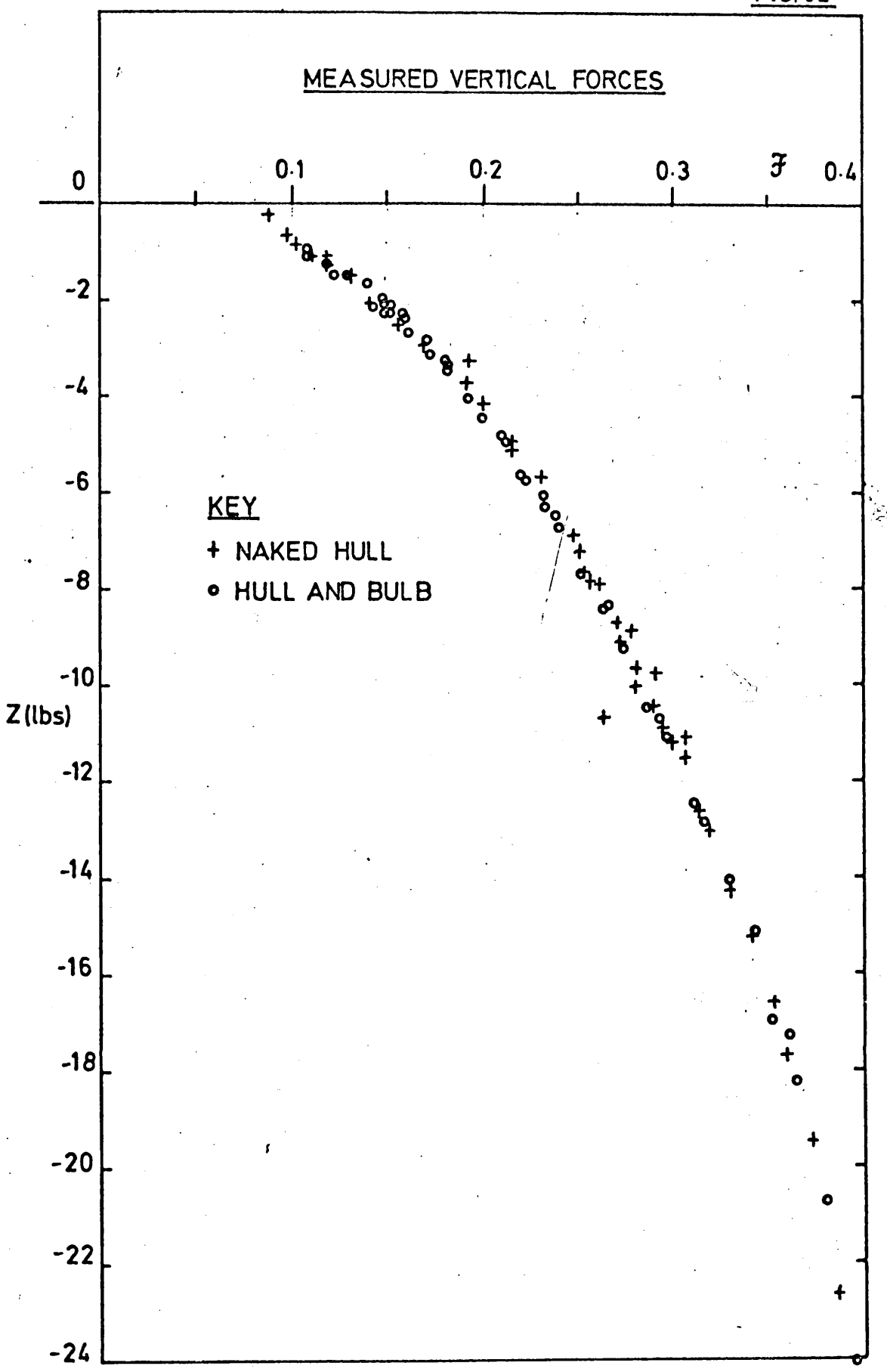
MEASURED VERTICAL FORCES
0
0·1
0·2
0·3
$\mathcal{F}$
0·4
-2
-4
-6
-8
-10
-12
-14
-16
-18
-20
-22
-24
Z(lbs)
KEY
+ NAKED HULL
o HULL AND BULB

FIG. 63

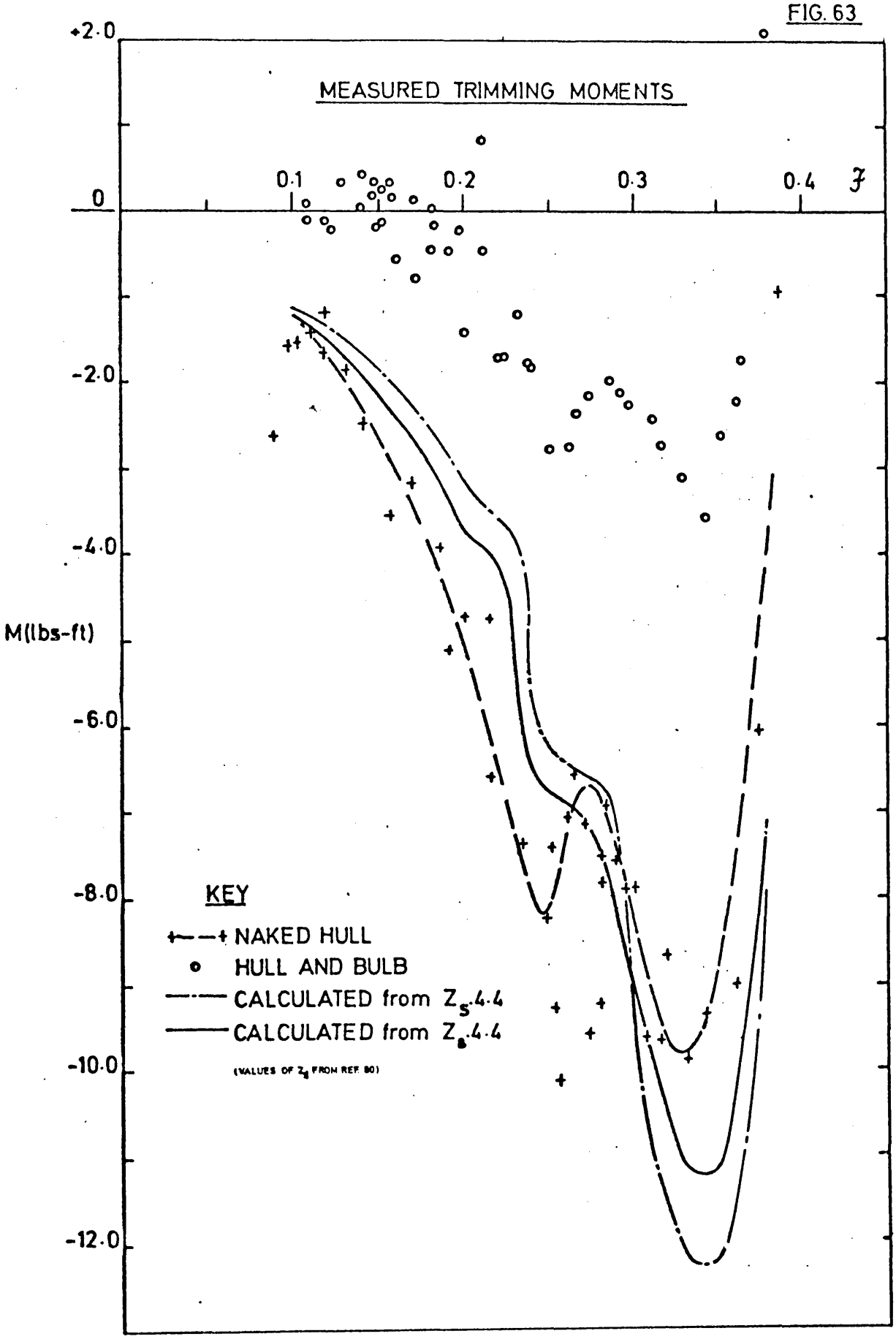
MEASURED TRIMMING MOMENTS
+2·0
0
-2·0
-4·0
-6·0
-8·0
-10·0
-12·0
M(lbs-ft)
0·1
0·2
0·3
0·4
ℱ
KEY
NAKED HULL
HULL AND BULB
CALCULATED from Z_S·4·4
CALCULATED from Z_B·4·4
(VALUES OF Z_B FROM REF. 80)

MEASURED VERTICAL FORCE COEFFICIENTS

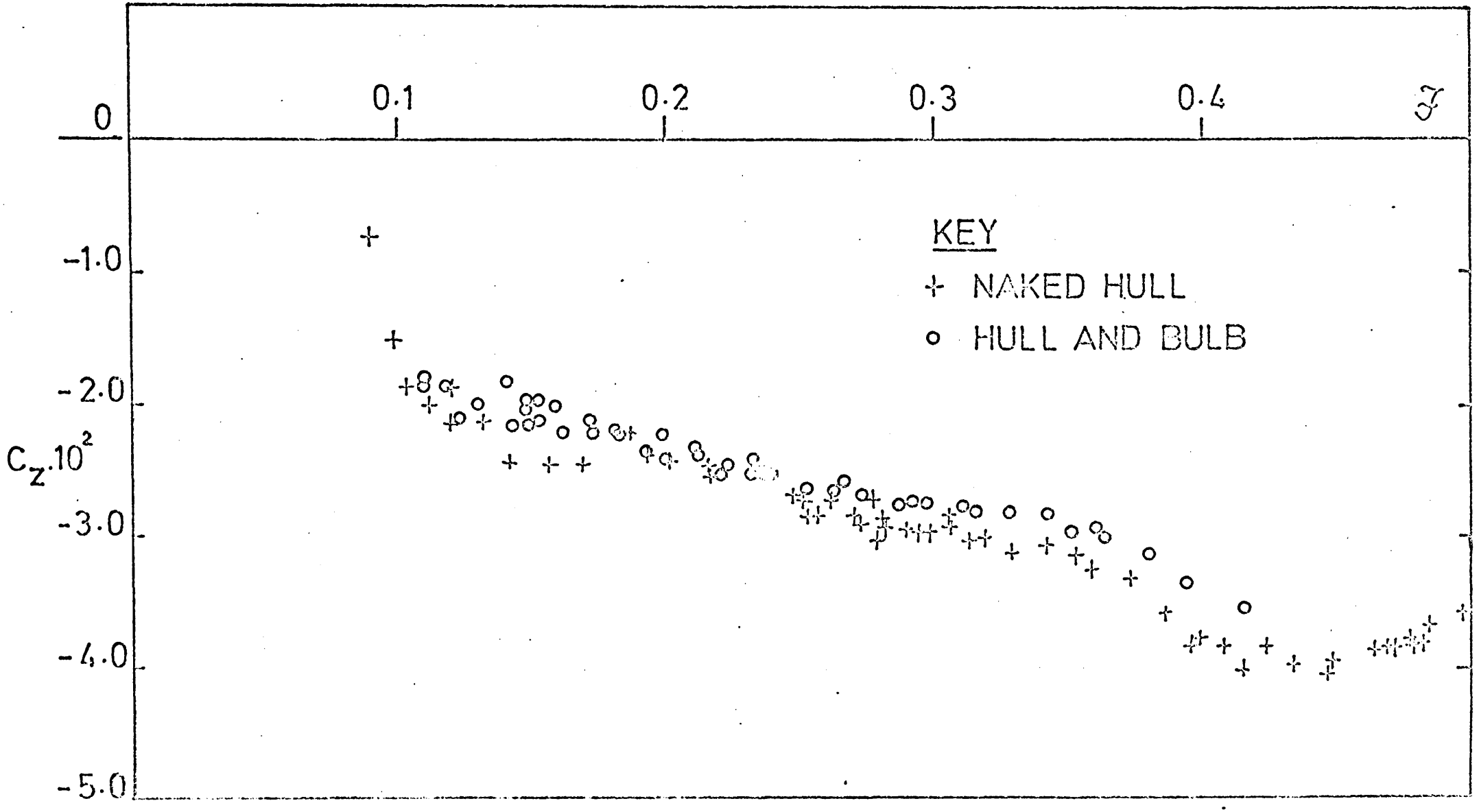

FIG. 64

FIG. 65

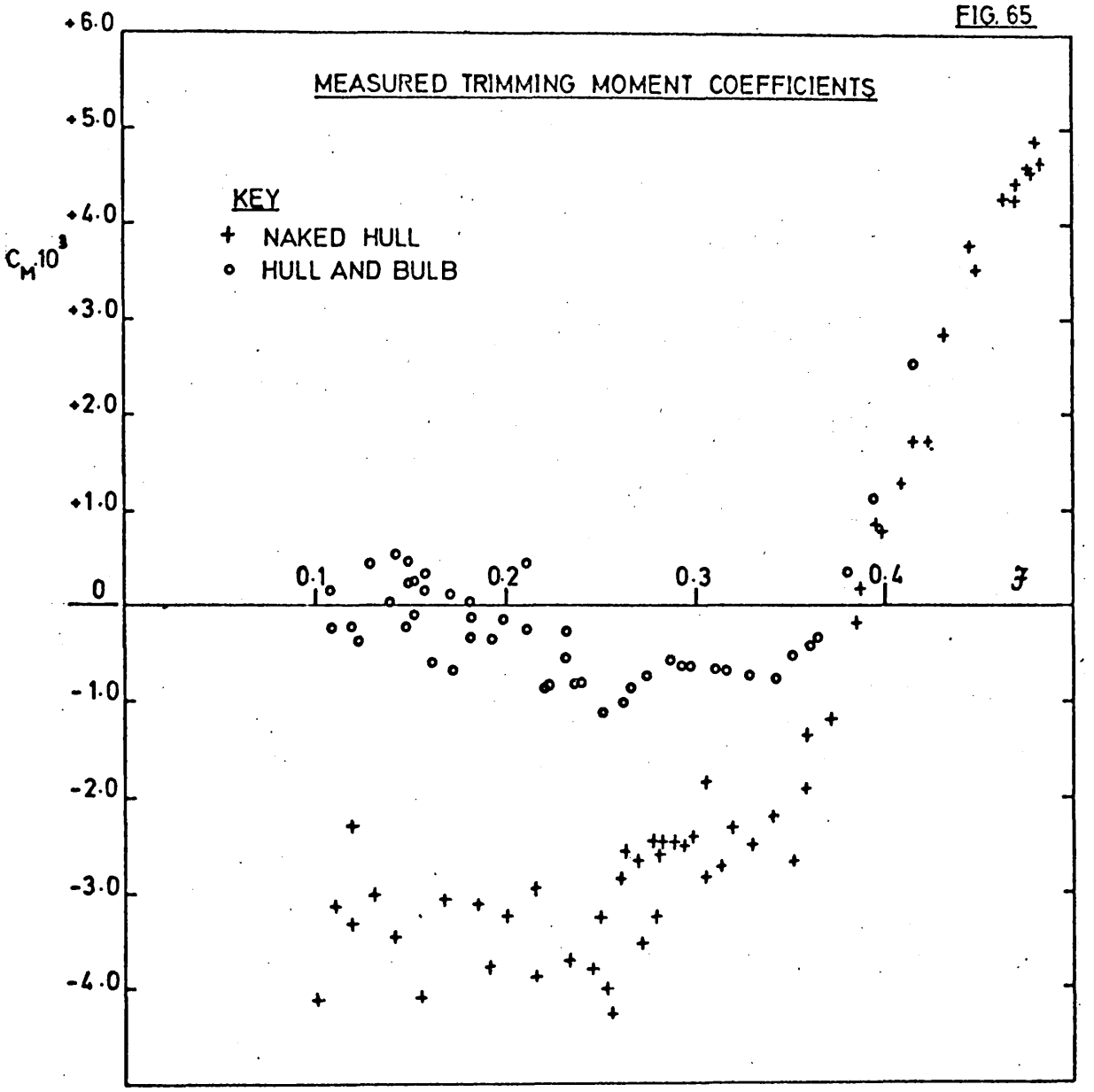
MEASURED TRIMMING MOMENT COEFFICIENTS
KEY
+ NAKED HULL
o HULL AND BULB
$C_M 10^3$
+6·0
+5·0
+4·0
+3·0
+2·0
+1·0
0
-1·0
-2·0
-3·0
-4·0
0·1
0·2
0·3
0·4
$\mathcal{F}$

Vertical Forces

It is seen from figure 62 that there is no apparent change in the magnitude of the total vertical force Z due to the action of the bulb. The slight reduction in C_Z observed in figure 64 is due entirely to the change in wetted surface S which appears in the denominator of the coefficient.

The negligible change in total vertical force is in accord with the predictions of section 3.2.4. summarised in table 20.

Trimming Moments.

Whereas no change in total vertical force could be measured, a marked change in measured trimming moment was observed over the range $0.10 \leq \mathcal{F} \leq 0.40$. Figure 63 shows that the addition of the bulb changed the sign of the trimming moment in the speed range $0.10 \leq \mathcal{F} \leq 0.20$ thereby making the model trim by the stern. This corroborates results obtained from the model when free to trim, discussed in section 3.4.1.

Also shown in figure 63 are the trimming moments estimated for the hull/bulb configuration using Wigley's values for Z_B and Z_s in conjunction with an assumed lever arm of 4.4 ft. from midships. It is at once apparent that the change in trim is greater than anticipated using calculated values of Z_B or Z_s. This may be due to a combination of the following causes :

i) The bulb wave system has been shown to be characterised by a pronounced wave trough at certain speeds. This brings the upper surface of the bulb into closer proximity to the free surface. Figure 66, derived from Wigley's calculations for the equivalent spheroid, shows that a reduction in immersion ratio from $f/l_s = 0.125$ to 0.100 at any value of N can have a marked effect on the vertical force coefficient. Figure 66 shows that at N = 0.40 such a reduction in immersion increases the value of C_Z for the equivalent spheroid from 4.9 at $f/l_s = 0.125$ to 6.9 at $f/l_s = 0.100$. At an immersion ratio of $f/l_s = 0.100$ the upper surface of the bulb is in the free surface at the

FIG. 66

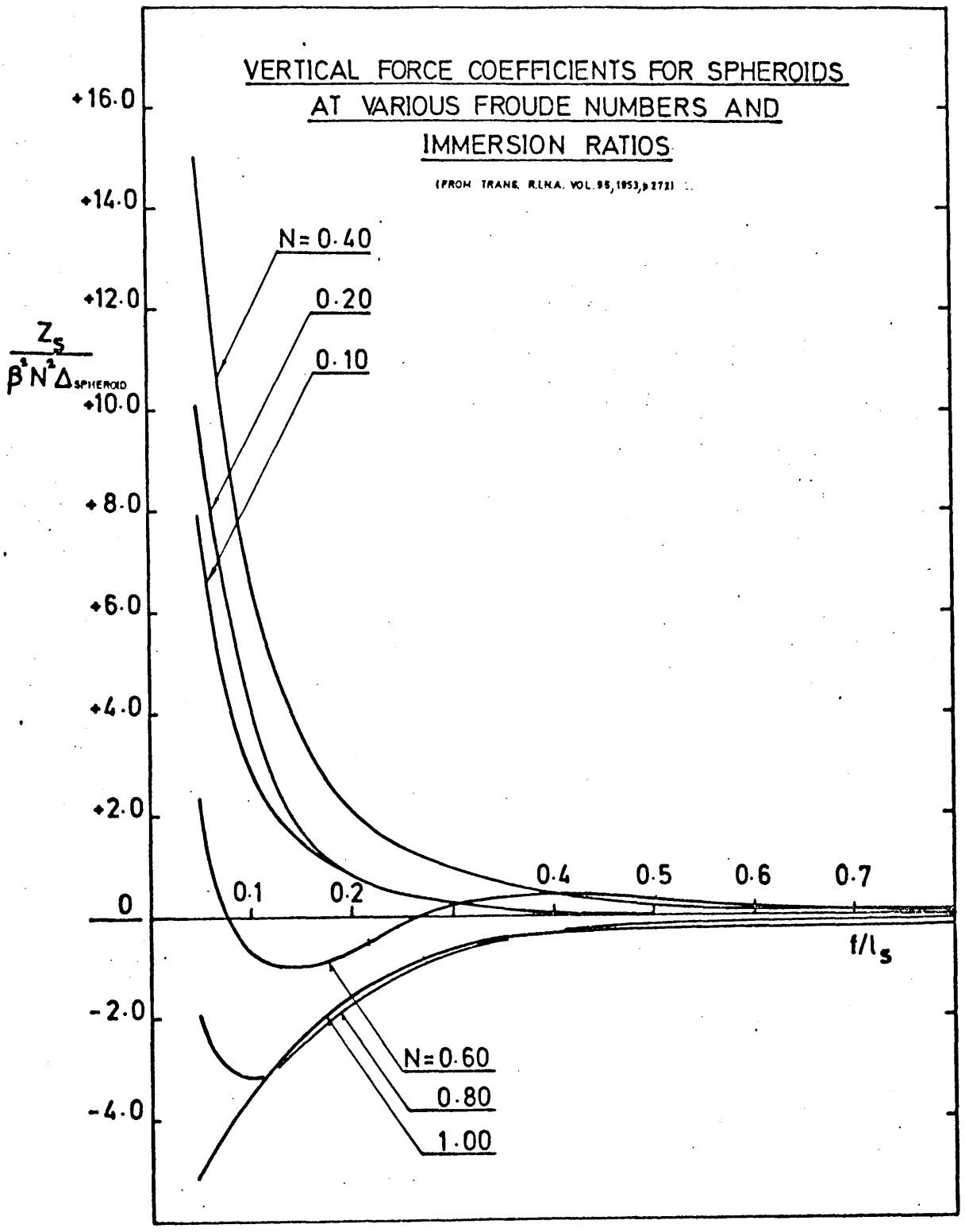
VERTICAL FORCE COEFFICIENTS FOR SPHEROIDS
AT VARIOUS FROUDE NUMBERS AND
IMMERSION RATIOS
(FROM TRANS. R.I.N.A. VOL. 95, 1953, p 272)
+16.0
+14.0
+12.0
+10.0
+8.0
+6.0
+4.0
+2.0
0
-2.0
-4.0
$\frac{Z_S}{\beta^2 N^2 \Delta_{SPHEROID}}$
N = 0.40
0.20
0.10
N = 0.60
0.80
1.00
0.1
0.2
0.4
0.5
0.6
0.7
f/l_s

bow ; it is possible that this might occur with certain bulb wave systems.

ii) The flow over the bulb probably differs considerably from that over the equivalent spheroid due to the presence of the hull. It is suggested in section 3.4.2. that there is a strong downward component of flow over the after part of the bulb. Furthermore, constriction of the flow between the upper surface of the bulb and the free surface will modify the flow and probably invalidate the concept of a 'bulb Froude Number', N, used in the calculation of Z_s.

iii) It may be seen from figures 62 and 63 that whereas the magnitude of the total vertical force was unchanged by the addition of the bulb, the longitudinal distribution of vertical forces was markedly altered, thereby resulting in large changes in trimming moment. In the range $0.10 \leq \mathcal{F} \leq 0.40$ there appears to be a greater concentration of forces acting in the positive z-direction on the forebody and a corresponding decrease on the aft body. This change of distribution is apparently inadequately represented by a simple superposition of hull and bulb vertical forces as indicated in figure 49. There is probably interference between hull and bulb forces of which no account was taken in the calculated values shown in figure 63. However, the longitudinal distribution of vertical forces is probably affected more by modifications to the wave system and the boundary layer discussed in iv) and v) below.

iv) Modification of the wave system is illustrated in plate 14.

MODEL RESTRAINED $\mathcal{F} = 0.210$ PLATE 14

As observed when the model was free to trim, the bulb shifted the bow wave aft. This indicates that the upward force of the bow wave now acts further aft in a region of the hull where the surface slopes $\partial\eta/\partial z$ are larger than those nearer the bow.

Equation (2.3.5c) indicates that a change in trimming moment would then result. Downward flow over the bulb and modified flow over the bottom of the hull, in conjunction with the modified wave system, will also alter the vertical force distribution.

Furthermore, streamlines approaching the curved keel probably do so at a different incidence angle due to the presence of the bulb. A possible flow system, illustrated in figure 67, would tend to lift the bow due to fluid inertia forces acting at the keel, thus reducing trim by the head.

v) It is shown in section 3.4.4. that a marked change in viscous resistance occurred over the speed range $0.21 \leq \mathcal{F} \leq 0.30$. This indicates that the presence of the bulb has an effect on the viscous flow around the hull and implies changes in the boundary layer structure. Moreover, it is shown in section 3.4.4 that the addition of the bulb causes a change in viscous pressure resistance R_{VP}, assuming that there is no change in flat plate resistance. As viscous pressure resistance results from the growth of the boundary layer over the hull the supposition that the bulb is affecting the growth of the boundary layer is confirmed.

From measurements of normal pressures over a series of geometrically similar hulls, it was suggested (59) that there is a component of the trimming moment arising from viscous sources, presumably from viscous pressure forces. Thus a modification to the boundary layer structure which modified the viscous pressure forces might be expected to affect the trimming moment.

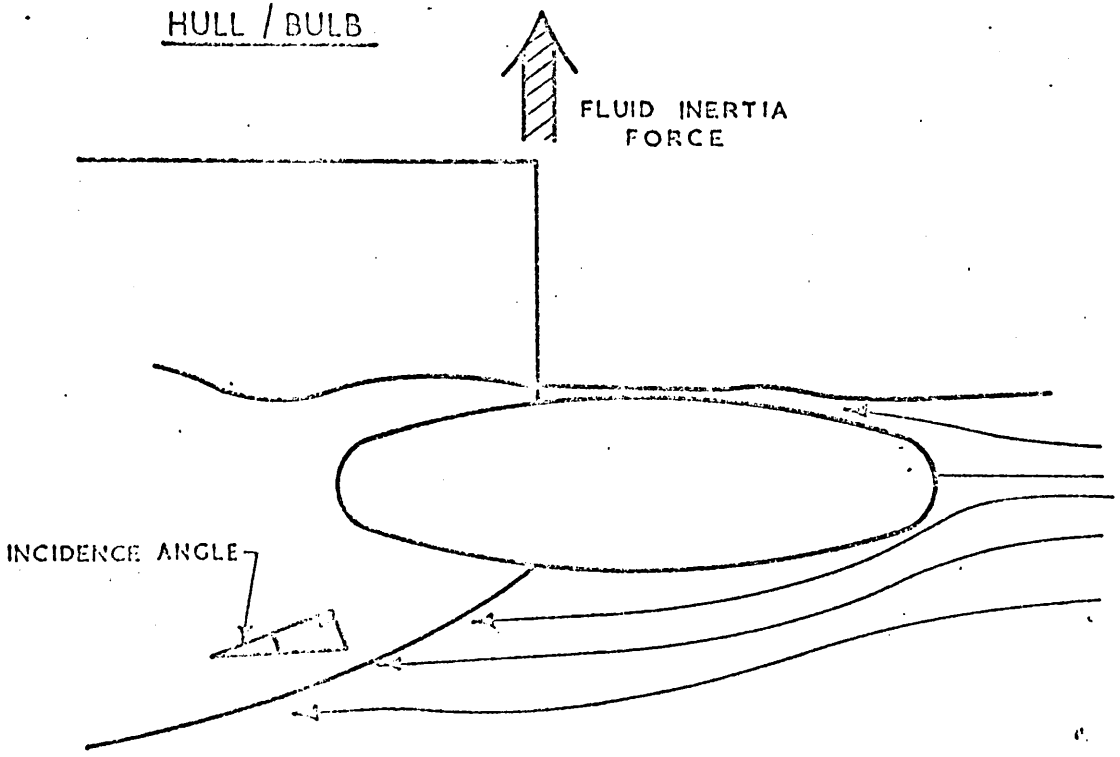

STREAMLINES AT LARGE ANGLE OF INCIDENCE TO KEEL - LARGE UPWARD FLUID INERTIA FORCES.

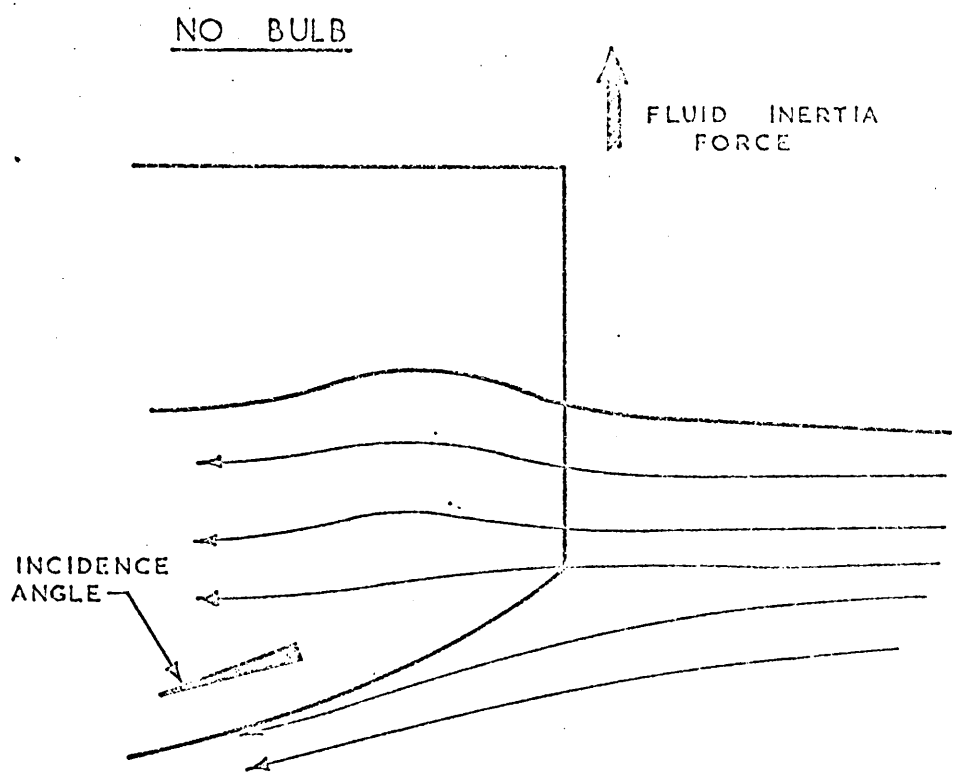

STREAMLINES AT SMALL ANGLE OF INCIDENCE TO KEEL - SMALL UPWARD FLUID INERTIA FORCES.

FIG. 82

POSSIBLE FLOW MODIFICATION DUE TO BULB.

It has been shown in section 2.7.1. that a change of turbulence stimulation studs can have a marked effect on total resistance. This is due to changes in the viscous flow around the hull, which must affect the trimming moment and hence suggests that the positioning and shape of stimulation studs is important when measuring trimming moments.

It is shown in ref. 115, p.405 - 409 that deeply submerged bodies of revolution at low incidence shed vortices within the boundary layer. These affect the distribution of side-force on such a body, this being indicated in figure IX.11 of the same reference. If it is assumed that the effect of the free surface is such that the viscous flow on the Inuid is similar to that over such a body; the addition of a bulb will undoubtedly modify this vortex formation with further modification to the distribution of vertical forces. Such a modification to boundary layer flow would also be of importance in the consideration of resistance reductions due to a bulb.

vi) Finally, the discrepancy between calculation and experiment must also arise from limitations in the theory. In part 2 it was shown that the linearised calculation under-estimates the magnitude of the vertical force acting on a floating body. The limitations of the theory have been discussed and it was apparent that the flow around the hull/bulb configuration was highly non-linear. Apart from neglect of viscous effects, neglect of free surface non-linearities is a serious omission in the theoretical treatment of vertical forces. The general indications given by the theory were that whereas a small change in total vertical force might be expected due to the action of the bulb, large changes in trimming moment might arise. Qualitatively the theory was correct, quantitatively it was not.

3.4.4. Form Resistance

Friction form resistance calculated using the method of section 2.4. is shown in figure 68.

Changes in R_{wp} due to the action of the bulb are compared

FIG 68

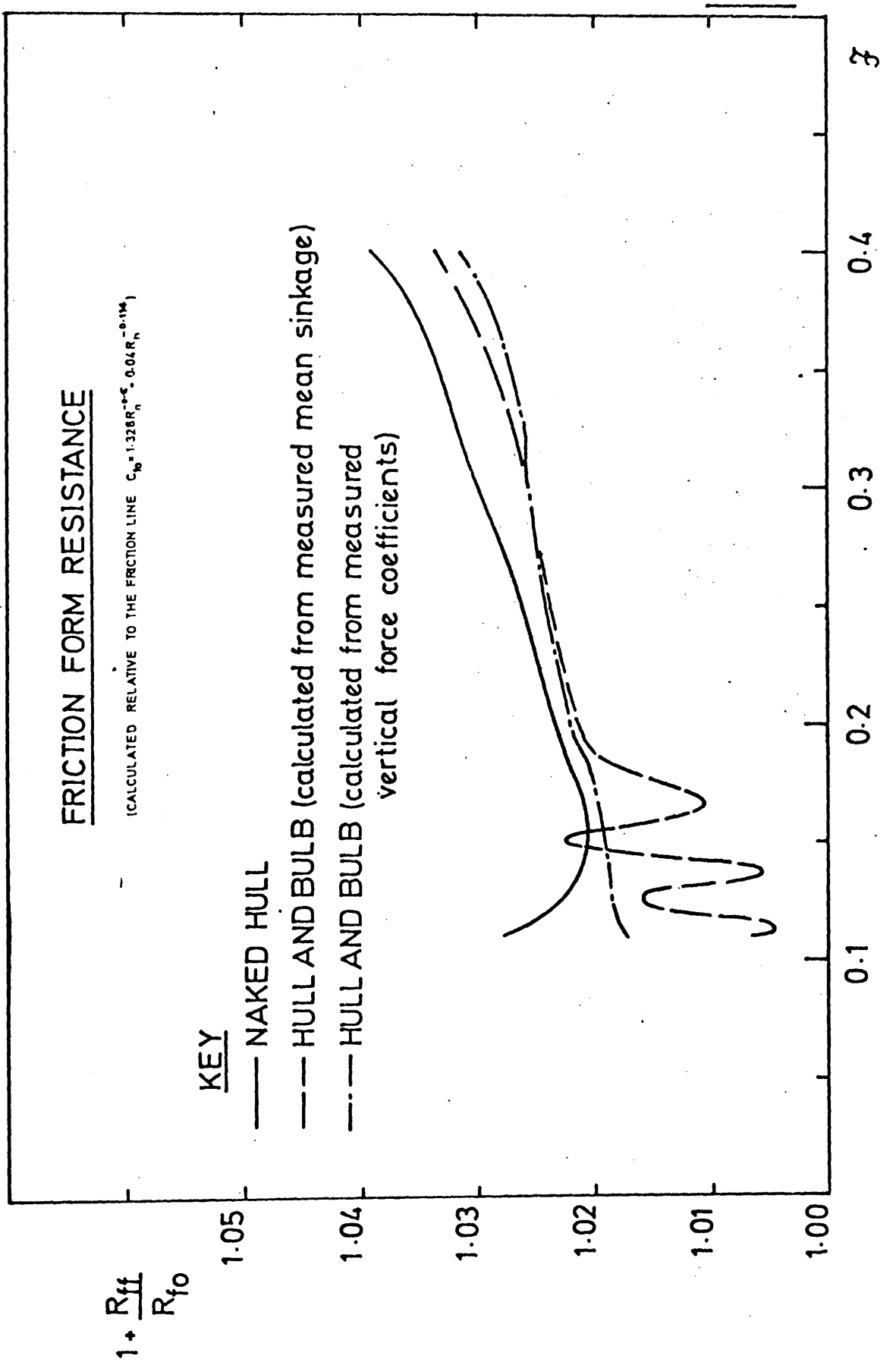
FRICTION FORM RESISTANCE
(CALCULATED RELATIVE TO THE FRICTION LINE $C_{fo} = 1.328R_n^{-0.5} - 0.04R_n^{-0.154}$)
KEY
NAKED HULL
HULL AND BULB (calculated from measured mean sinkage)
HULL AND BULB (calculated from measured vertical force coefficients)
$1 + \frac{R_{ff}}{R_{fo}}$
1.05
1.04
1.03
1.02
1.01
1.00
0.1
0.2
0.3
0.4
ζ

with changes in R_T in figure 60. The changes in total resistance are seen to be greater than the changes in wave pattern resistance over the speed range $0.225 \leq \nabla \leq 0.30$. This implies a change in viscous resistance.

The addition of the bulb increased the wetted surface and therefore may be expected to increase the flat plate resistance, R_{fo}. In order to remove the effect of this apparent friction resistance increase on any comparison of viscous resistance changes, a curve given by

$$\left(\frac{R_T}{R_{fo}}\Big|_{HULL} - \frac{R_T}{R_{fo}}\Big|_{HULL+BULB}\right) - \left(\frac{R_{WP}}{R_{fo}}\Big|_{H} - \frac{R_{WP}}{R_{fo}}\Big|_{H+B}\right) = \frac{\delta R_T}{R_{fo}} - \frac{\delta R_{WP}}{R_{fo}} = \frac{\delta R_V}{R_{fo}} \quad \ldots\ldots\ldots \quad (3.4.1)$$

is plotted in figure 69.

This curve is compared with the form factor r defined by equation (2.7.2) deduced both from figure 33 for the hull without the bulb and by Sharma in reference 53. It is at once apparent that the curve given by equation (3.4.1) is of the order of the form resistance for the naked hull implying that the bulb is in fact reducing part of the form resistance over the range $0.21 \leq \nabla \leq 0.30$.

Friction form resistance, calculated for the hull with and without the bulb by the method of section 2.4.3, is shown in figure 68. It is seen that this component of resistance is altered by the addition of the bulb. But, as friction form resistance is a small part of the total form resistance (see fig.45), it was concluded that a reduction in viscous pressure resistance by the action of the bulb accounted for most of the resistance change given by equation (3.4.1).

But the wider implications of viscous resistance modification by the bulb are many. The extrapolation of model results to the full scale in general uses the concept of a smooth viscous resistance curve which depends only on Reynold's Number in conjunction with a form factor r which applies both to model and ship. Moreover, r is assumed to be independent of both Froude Number and Reynold's Number. Recent investigations (59, 61, 62) have shown

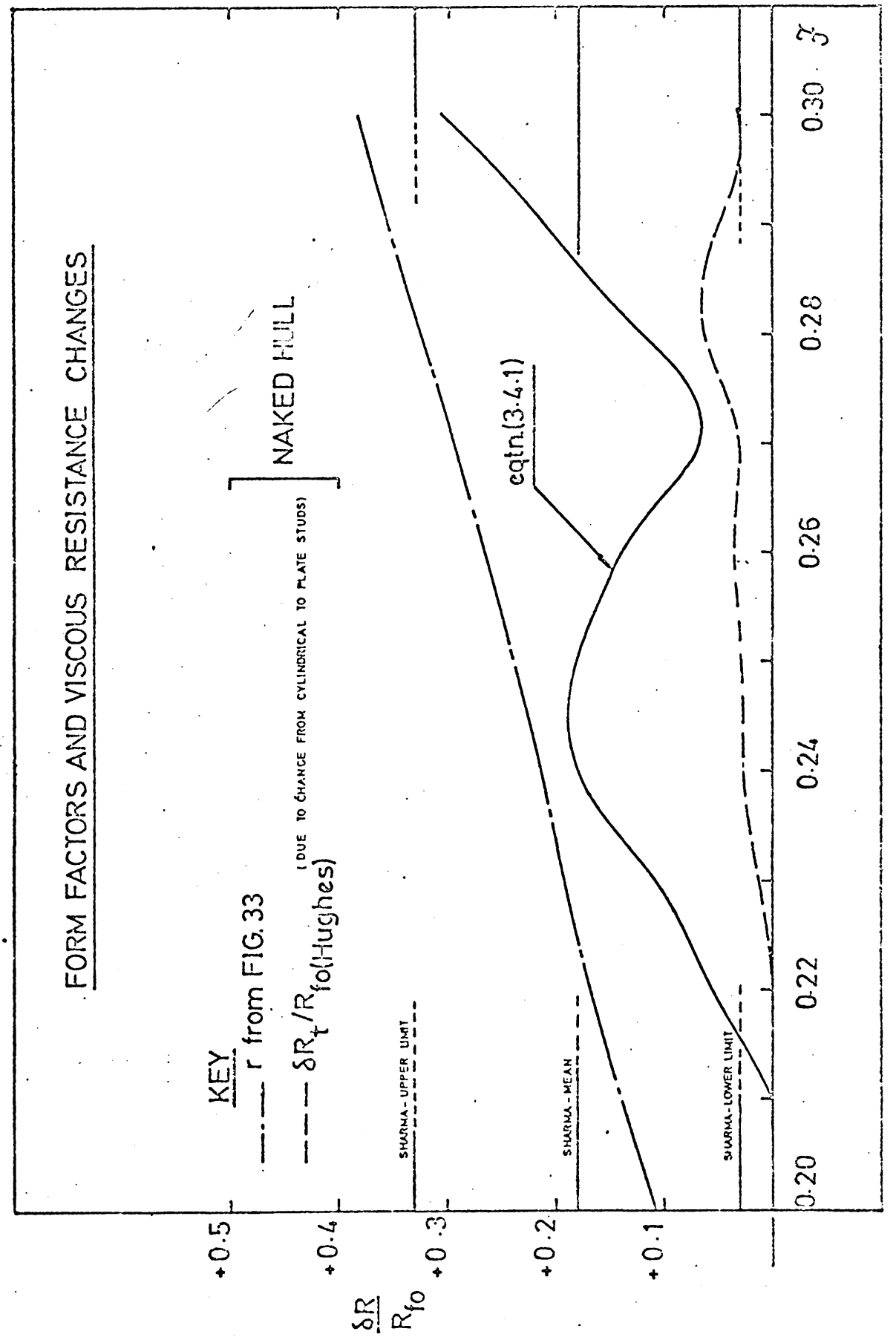
FORM FACTORS AND VISCOUS RESISTANCE CHANGES
KEY
r from FIG. 33
δR_t/R_fo(Hughes) (DUE TO CHANGE FROM CYLINDRICAL TO PLATE STUDS)
NAKED HULL
SHARMA - UPPER LIMIT
SHARMA - MEAN
SHARMA - LOWER LIMIT
eqtn.(3.4.1)
δR/R_fo
+0.5
+0.4
+0.3
+0.2
+0.1
0.20
0.22
0.24
0.26
0.28
0.30
x

FIG. 69

that viscous resistance depends on Froude Number and the present study has shown that r can be greatly modified by the addition of a bulb.

Moreover, due to the impossibility of running the model at the ship Froude and Reynold's Numbers simultaneously, artificial turbulence stimulation is employed over the model surface so that a suitable turbulent basic friction line may be used as an extrapolator. Also shown in figure 69 are the changes observed in R_T when cylindrical studs were changed for plate studs on the basic Inuid S201. Plotted as a curve of $\delta R_T/R_{fo}$ it is seen that the change in total resistance is an appreciable fraction of the deduced form resistance. This assumes that the change of studs did not affect the wave resistance, which seems a plausible assumption. Hence, in order to measure the true viscous resistance modification due to a bulb, the type and positioning of turbulence stimulation studs is of the utmost importance.

At speeds lower than $\nabla = 0.21$, an increase in form resistance is indicated by figure 61. This corresponds to a reversal of trim due to the bulb, the model trimming by the stern at these speeds. It is possible that fluid inertia forces acting on the curved keel tend to increase form resistance in this speed range or that a complex inter-action between viscous forces and normal pressure forces is giving rise to the resistance increase. It is important to note that a reduction in wave pattern resistance is apparent in the range $\nabla \leq 0.20$ whereas there was a total resistance increase.

Thus it is seen that the modification in viscous resistance due to the addition of a bulb is the result of a complicated inter-action of several forces and moments. Not only can viscous resistance be reduced. It can also be increased over certain speed ranges. Trim can be altered significantly ; mean sinkage can show instability at low speeds. Because form resistance can be modified, extrapolation from model to ship must be fraught with uncertainty, especially when high block coefficient forms with large form resistance are

considered. The model boundary layer structure is altered by large bulbs and this structure depends on the artificial turbulence stimulation used. It has been shown that different types of stimulation studs alter the total resistance by an amount which is appreciable in comparison with the form resistance. The size of the measured viscous resistance reduction must therefore depend on the type of stimulation used.

All these points indicate that it is probably fortunate that the writer of ref. 108 was able to report an unexpectedly large full-scale resistance reduction obtained by the addition of a ram bow to a tanker. Extrapolation from model to ship for such forms could be sufficiently uncertain for an unexpectedly large full-scale resistance increase to occur with subsequent economic penalties.

3.5. CONCLUSIONS and DEDUCTIONS

Results obtained in part 2 indicated mean sinkage and trim were related to viscous form resistance. A large bulb was designed for the Inuid S201 and tested with a view to modifying sinkage and trim and noting any change in viscous resistance. Wave pattern resistance was measured for the hull/bulb combination and compared with that measured elsewhere for the hull alone.

The principal conclusions obtained from this investigation were as follows :

1) The addition of the bulb caused changes in both mean sinkage and trim, the latter to a marked degree.

2) In the speed range $0.1 \leq \nabla \leq 0.40$ the bulb acted in the manner indicated by Wigley for submerged bodies, (ref. 80.) The design concept enunciated in section 3.2. seems vindicated although the magnitude of the vertical bulb forces were much greater than expected.

3) To obtain large vertical forces from the bulb, it should protrude well forward and its upper surface should be close to the free surface.

4) When the model was free to trim it was difficult both to obtain and maintain stable flow conditions over the bulb at low speeds due to surface tension and viscous flow effects.

5) A strong correlation between total resistance changes and trim changes due to the bulb was found in the speed range $0.1 \leq \nabla \leq 0.4$.

6) Large reductions of wave pattern resistance were obtained. The mechanism of wave cancellation was obscure and probably not due to a simple superposition of bulb and hull wave systems. The bow wave was modified by a strong x-component of flow due to a 'venturi' effect between the free surface and the upper surface of the bulb.

7) The distribution of vertical forces along the hull was altered by the addition of the bulb, their total magnitude remaining approximately the same. This was due to

i) Modification to the wave system

ii) Modification of the boundary layer.

8) Viscous pressure resistance was markedly modified by the bulb; friction form resistance was modified to a lesser extent. This was connected with marked changes in trim accompanied by small changes in mean sinkage. Thus the action of the bulb in modifying trim did more to reduce viscous resistance than the modification of mean sinkage.

9) The position and type of turbulence stimulation studs can affect the measured change in viscous resistance.

10) Extrapolation from model to ship for hull forms with ram-type bulbs is unreliable because the magnitude of the viscous resistance change produced by such bulbs is uncertain.

11) The bulb increased viscous resistance over certain speed ranges, reducing it over others.

The final conclusion reached was that any resistance change due to the action of a bulb is brought about by a complex interaction of viscous and normal pressure forces. Changes occur not only in total resistance, but also in vertical forces and trimming moment. Investigation of these forces and moments may throw light on changes in the more obscure components of resistance, such an investigation having the additional merit of giving an insight into the behaviour of the hydrodynamic force system as a whole.

4. GENERAL DISCUSSION

In conclusion it is of some interest to consider the above investigation in perspective against the general background of ship hydrodynamics. Some results which have been obtained are relevant both to the problem of extrapolation from model to ship and to hull design.

4.1. Extrapolation from Model to Ship

The problem of extrapolation from model to ship is complex. It may be likened to an initial value problem in three dimensional C_t-$\mathcal{F}$-R_n space (see figure 70). Model C_t values are known for a range of $\mathcal{F}$ and R_n values which lie in a straight line at an angle λ_m to the Froude Number axis where

$$\tan \lambda_m = \frac{\mathcal{F}}{R_n} = \frac{\nu}{g^{\frac{1}{2}} L_m^{\frac{3}{2}}} \qquad \ldots\ldots (4.1.1)$$

where L_m is the model length.

Ship results will lie on a line at angle λ_s where

$$\tan \lambda_s = \frac{\nu}{g^{\frac{1}{2}} L_s^{\frac{3}{2}}}$$

where L_s is the length of the ship.

Some function relating C_t, $\mathcal{F}$ and R_n is needed in order to extrapolate from model to ship. Dimensional analysis shows that such a relationship must in fact exist and, in principle, it could be derived from the fundamental equations of fluid flow - the Navier-Stokes equations. These equations, however, have proved impossible to solve analytically in all but the simplest cases.

The assumption of an inviscid irrotational fluid simplifies the Navier-Stokes equations to those described in section 2.1. These equations must be further simplified before they are tractable analytically and the consequence of these approximations has been a theory which apparently bears little relation to the physical processes involved.

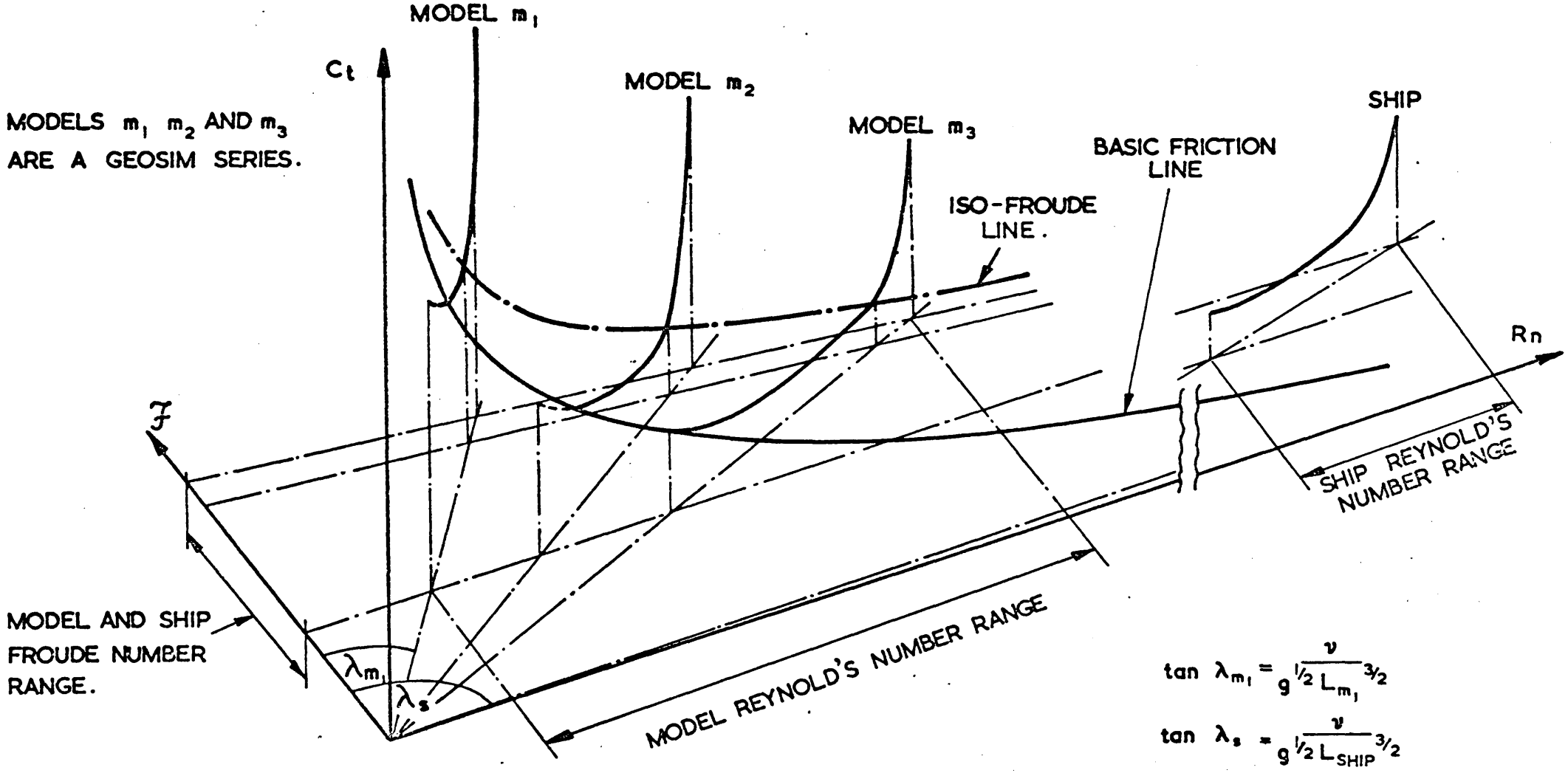

THE MODEL-SHIP EXTRAPOLATION PROBLEM.

FIG.70

The inadequacy of the theory has led to empirical determination of the unknown function $C_t(\mathcal{F}, R_n, r_1, r_2, r_3 \ldots\ldots)$ where r_1, r_2, r_3 ... are some parameters defining the shape of the body. Model tests using geosims and Froude's Method in conjunction with flat plate friction data have led to an acceptable, if approximate, method of extrapolating from model results to full scale.

However, Froude's basic hypotheses were conceived in the days when hull forms were not greatly removed in shape from the 'planks' used to deduce frictional resistance data ; block coefficients, prismatic coefficients, and ∇/L^3 were in general small, implying small form resistance. Interaction between wave resistance and viscous resistance was probably small and the assumption that the two major components could be treated separately was a good 'engineering approximation'.

But modern hull forms with high block and prismatic coefficients and large values of ∇/L^3 have high form resistances and large interactions between wave-making and viscous resistance. The above investigation has shown that form resistance is not constant with speed and is difficult to measure accurately. Extrapolation from model to ship for full forms is thus very difficult. Moreover, ship Reynold's Numbers are increasing as ship lengths tend to increase with the result that the gap in size between model and ship is widening. Supertanker models of 12 metres length have been tested in Japan to reduce the size gap and improve prediction, but economic and technical considerations must preclude the general use of such models and the requisite large tanks to accommodate them.

Two ways to resolve this problem present themselves

i) A closer study of form resistance and interaction of the various components of resistance to improve present methods of extrapolation from model to ship is necessary. Such a study is being widely pursued at present and the above investigation is intended to supplement the results obtained. The observation that viscous resistance behaves in a complex manner has already been made (61) and makes the extrapolation problem all the more perplexing.

The above investigation has shown that mean sinkage and running

trim may be related to the two components of form resistance : simple relationships between sinkage, trim, friction form resistance and viscous pressure resistance may hold which would facilitate their determination and dispense with long and costly experimental investigations of viscous flow over the hull.

ii) A more reliable mathematical model of the physical effects of water flow past a ship's hull is needed. In an experiment tank only a limited number of physical quantities can be measured directly. Examples are total resistance, wave profiles, sinkage, vertical forces and normal and tangential pressures. To relate these to components of resistance with a view to reliable model-to-ship extrapolation demands a sound theory. For example, wave resistance can only be deduced : it cannot be measured directly, with the result that it defies precise definition. With a theory which encompassed the total flow over the hull, definition of separate components of resistance would be unnecessary as total resistance could be calculated ab initio and compared with measurement.

Linearised wave resistance theory is deficient in two respects : it neglects viscosity and it neglects non-linearities. It was supposed that the neglect of viscosity was more serious than the neglect of non-linearities. Recent work (22) has shown that this is probably not entirely correct. The above investigation has shown that vertical force Z is not affected by changes in viscosity (figure 62) ; calculated values of Z agree well with measurement at low speeds where non-linearities might be expected to be negligible, the agreement becoming progressively worse as speed increases and non-linearities cease to be negligible. This, in conjunction with results derived in appendix A, suggests that the inclusion of non-linearities in the inviscid fluid theory might substantially improve agreement between calculation and observation.

To accomplish this analytically and obtain a wholly (not partial) non-linear theory is probably impossible at present. But considerable success in the approximate numerical solution of fluid flows has been obtained (77, 116). The advent of large digital computers which can handle tedious and lengthy numerical calculations suggests a new approach

to the problem of ship resistance determination : The role of the computer would be that of an experimental facility so that a reliable theory could be evolved with the help of both the test tank and the computer. Less empiricism might produce less uncertainty in ship resistance prediction and might well suggest better and more efficient hull forms ; an example of this is to be found in the use of linearised theory in the design of bulbous bows.

The problems of numerical calculation of fluid flows are by no means minor ; correct determination of the radiation conditions and fulfilment of the free surface conditions would pose major problems. But these problems are not insurmountable as the work described in reference 77 shows. It is probably better to direct energy toward solving these numerical problems than to persevere with an inadequate but elegant theory and an inadequate empirical extrapolation procedure. Tank predictions can be in error and the economic consequences of low power estimates could be unfortunate.

4.2. Hull Design

It was stated above that the present trend in hull design, particularly of bulk carriers and tankers, is toward larger block coefficients and larger ∇/L^3 values. This gives rise to hydrodynamicall inefficient hull shapes. To maintain efficiency, hull design modifications using, for example, bulbous bows are essential. These reduce the total hull resistance which will not only result in a reduced fuel bill, but also many fundamental design parameters will be affected : examples are the choice and size of propelling machinery, propeller design, cargo space made available by a possibly smaller engine, additional displacement due to a bulbous bow or stern and so on.

The bulbous bow investigation in part 3 has shown that substantial resistance reductions may be obtained with a bulb which contravenes some of the basic design postulates deduced from linearised wave resistance theory. The bulb was shown to have a marked effect on mean sinkage and running trim ; viscous resistance was reduced which indicates again that extrapolation from model to ship would be uncertain.

Furthermore, linearised theory indicated a mode of action of a bulb near to the free surface which would have been difficult to show empirically : measurements of the vertical force on a submerged spheroid at speed abound with experimental problems. Thus an inadequate and incomplete theory has been of use in suggesting an unexpected aspect of the physics of bulbous bows : a complete theory would be of still greater benefit.

It is appropriate to conclude this discussion with the words of Sir Thomas Havelock (12, p.261).

" . . . our chief aim will have been achieved if we have gained more insight into the nature of the problem ; for in this respect at least, the pursuit of theoretical investigations, even if apparently remote from practical requirements, is essential to a complete and scientific solution of the various problems of ship motion".

5. SUMMARY OF CONCLUSIONS

A mathematical model was tested in calm water and total resistance, trim and vertical forces were measured. Measurements were compared with calculations made using a linearised theory. A large bulb was added to the hull in order to modify the flow thereon and thus test some deductions made as a result of the vertical force investigation. Total resistance, wave pattern resistance, sinkage, trim and vertical forces were again measured after the addition of the bulb. The main conclusions emerging from this study are :

1) Wave resistance of Inuid S201 calculated by the Michell-Havelock theory gives better agreement with measurement than that calculated by Inui's theory without correction factors.

2) The Michell-Havelock theory gives moderately good agreement between calculation and measurement for the vertical force coefficient C_Z. Poor agreement between theory and experiment was observed in the case of trim and trimming moments.

3) The vertical force Z is little affected by viscosity whereas the trimming moment M is strongly affected by viscosity.

4) Neglect of non-linearities in the theory account for the poor agreement between calculated and measured Z values.

5) Friction form resistance, vertical force, wave resistance and flat plate friction resistance are connected.

6) Viscous pressure resistance, running trim, wave resistance and flat plate friction resistance are probably connected.

7) The addition of the bulb caused changes in both mean sinkage and trim.

8) To obtain large trim changes and hence large viscous pressure resistance changes, the bulb should protrude well forward of the bow and its upper surface should be close to the free surface.

9) Large reductions in wave pattern resistance due to the bulb were obtained. The mechanism of this resistance reduction is not clear.

10) The distribution of vertical forces along the hull was altered by the addition of the bulb, their total magnitude remaining approximately the same.

11) Viscous pressure resistance was markedly modified by the bulb ; friction form resistance was modified to a lesser extent.

12) The position and type of turbulence stimulation studs can affect the measured change in viscous resistance.

13) Extrapolation from model to ship is unreliable for hull-forms with ram-type bulbs.

14) A more realistic mathematical model of flow conditions over a ship's hull is urgently required.

ACKNOWLEDGMENTS

The work described above took place during the period September 1964 - September 1967 while the author was holder of the Royal Commissioners for the Exhibition of 1851 Post Graduate Scholarship in Naval Architecture.

The author is deeply grateful to his supervisor Professor J.F.C. Conn for his continued help and friendly encouragement throughout the investigation.

The author also thanks Mr. A.M. Ferguson, Superintendent of the Glasgow University Experiment Tank, not only for the use of the excellent experiment facilities of the Tank, but also for his advice and encouragement in many aspects of the work. Members of the Glasgow University Tank Staff towhom the author is particularly grateful are Messrs. R. Christison and J. Aitken for their help in making apparatus and Mr. D. Hogg who undertook the tedious job of lifting model offsets for the error analysis of section 2.6.

The computer programs were punched by Miss J. Taggart and were run on the EELM KDF9 digital computer of the University of Glasgow Computing Department. Thanks are due to all members of the Computing Department for their help.

The preliminary typing of this work was done by Miss R.P.Winter to whom the author is most grateful.

Finally to his parents, for their support and encouragement throughout this work, the author is especially indebted.

REFERENCES.

1. FROUDE, W.E.: ' On Experiments with H.M.S. Greyhound ' Trans.R.I.N.A Vol. 15, 1874, pp 36-73.

2. CRAGO, W.A.: 'The Predictions of Yacht Performance from Tank Tests Trans. R.I.N.A. Vol. 105, 1963, p 155.

3. EULER, LEONHARD: ' Principes Généraux du Mouvement des Fluides ' Hist. de l' Acad. de Berlin, 1755.

4. CAUCHY, A.: 'Mémoire sur la Théorie des Ondes ' Mém. de l'Academie Roy. des Sciences 1816.

5. THOMSON, W. (LORD KELVIN) : 'On the Waves Produced by a Single Impulse in Water of any Depth, or in a Dispersive Medium ' Proc. Roy. Soc. A 42, 1887.

6. RANKINE, W.J. MACQUORN : 'On Plane Waterlines in Two Dimensions' Phil. Trans. Royal Society, 1863.

7. RANKINE, W.J. MACQUORN : ' On Stream-line Surfaces' Trans. R.I.N.A. Vol. II, 1870.

8. TAYLOR, D.W. : ' On Ship-Shaped Stream Forms ' Trans. R.I.N.A. Vol. 35, 1894.

9. LAMB, H. : 'Hydrodynamics ' Cambridge University Press, Sixth Edition, 1932.

10. MICHELL, J.H. : ' The Wave Resistance of a Ship ' Phil. Mag. 1898, p.106.

11. GUILLOTON, R. : 'Examinen Critique des Méthodes d'Étude Theorique des Carènes de Surface ' Schiffstechnik Bd 9 - 1962 - Heft 45.

12. WIGLEY, W.C.S. (Editor) : ' The Collected Papers of Sir Thomas Havelock on Hydrodynamics ' Office of Naval Research, Department of Navy, ONR-ACR-103.

13. HAVELOCK, T.H. : Discussion of ' A Note on the Experimental Determination of Wave Resistance ' by R. Guilloton, Trans. R.I.N.A. Vol. 94, 1952, p.356.

14. LAMB, H.: ' Wave Resistance ' Proc. Roy. Soc. A 111 1926, pp.14-25.

15. LAMB, H.: ' On Wave Patterns due to a Travelling Disturbance ' Phil. Mag. xxxi 539 1916.

16. WIGLEY, W.C.S.: ' Ship Wave Resistance - An Examination and Comparison of the Speeds of Maximum and Minimum Resistance in Practice and Theory ' Trans. N.E.C.I.E.S. Vol. 47, p.153, 1931.

17. WIGLEY, W.C.S. : ' A Comparisdn of Experiment and Calculated Wave Profiles and Wave Resistance of a Form having Parabolic Waterlines ' Proc. Roy. Soc. Series A, Vol. 144, 1934.

18. WEINBLUM, G.: ' Schiffsform und Wellenwiderstand ' Jahrb. S.B.T.G. 33, S. 389.

19. HOGNER, E. : ' Eine Interpolationsformel für den Wellenwiderstand von Schiffen ' Jahr. S.T.G. Bd. 33, 1932.

20. HOGNER, E. : A Contribution to the Theory of Ship Waves ' Arhiv. fur Math. Astronomie och Fysik, Vol. 17, No. 12, 1922-23.

21. GUILLOTON, R. : ' Contribution à l'Étude des Carenes Minces' Doctoral Thesis, 1939.

22. EMERSON, A. : ' The Calculation of Ship Resistance : an Application of Guilloton's Method ' Trans. R.I.N.A. Vol. 109, p.241. 1967.

23. WIGLEY, W.C.S. : 'The Theory of the Bulbous Bow and its Practical Application ' Trans. N.E.C.I.E.S. Vol. 52, 1935.

24. INUI, T. : ' Wave-making Resistance of Ships ' Trans. A.S.N.A.M.E. Vol. 70, 1962.

25. INUI, T. : ' Study on Wave-making Resistance of Ships ' 60th Anniversary Series Vol. 2, Society of Naval Architects of Japan, 1960.

26. INUI, T. : ' A New Theory of Wave-making Resistance, based on the Exact Condition of the Surface of Ships ' Journal of the Zosen Kiokai Vol. 102.

27. PIEN, P., MOORE, W. : 'Theoretical and Experimental Study of Wave-making Resistance of Ships ' International Seminar on Theoretical Wave Resistance, Vol. 1, Ann Arbor, 1963.

28. PIEN, P. : ' Some Experimental Results of Hull Form Research ' D.T.M.B. Report No. 2144.

29. MARUO, H. : 'Problems Relating to the Ship Form of Minimum Wave Resistance ' Fifth Symposium on Naval Hydrodynamics, Bergen, 1964.

30. MARUO, H. : ' Experiments on Theoretical Ship Forms of Least Wave Resistance ' Int. Sem. on Theor. Wave Resistance Proceedings Vol. 3, Ann Arbor, 1963.

31. KARP, S., KOTIK, J., NURYE, J.: ' On the Problems of Minimum Wave Resistance for Struts and Strut-like Dipole Distributions. ' Third Symposium on Naval Hydrodynamics, Wageningen, 1960.

32. WEINBLUM, G., WUSTRAU, D., VOSSERS, G. : ' Schiffe Geringsten Widerstandes ' Jahrbuch S.T.G. 1957, p.175-214.

33. PETERS, A.S. STOKER, J.J. : ' The Motion of a Ship, as a Floating Rigid Body in a Seaway ' Institute of Mathematical Sciences, Report No. IMM-203, New York University,1954.

34. MARUO, H.: ' A Note on the Higher Order Theory of Thin Ships ' Bulletin of the Faculty of Engineering, Yokohama National University, Vol. 15, March, 1966.

35. SISOV, V.G. : ' On the Theory of the Wave Resistance of a Ship in Still Water ' Iswestijis Acad. Nauk. S.S.S.R., Otd. Tech. Nauk. Mech. i Maschinastrojenie, 1961, 1, pp.75 - 85.

36. EGGERS, K.W.H. : ' On Second Order Contributions to Ship Waves and Wave Resistance ' Sixth Naval Hydrodynamics Symposium, Washington, 1966.

37. WEHAUSEN, J.V. : ' An Approach to Thin Ship Theory ' Int. Sem. on Theor. Wave Resistance, Ann Arbor, 1963, p.821.

38. BESSHO, M. : ' On the Theory of Wave Resistance ' Journal of the Zosen Kiokai, Vol. 105, July, 1959.

39. BESSHO, M.: ' On the Theory of Wave Resistance - 2nd Report ' Journal of the Zosen Kiokai, Vol. 106, January, 1960.

40. BESSHO, M.: ' On the Boundary Value Problem in the Theory of Wave-making Resistance ' Memoirs of the Defense Academy of Japan, Vol. VI, No. 4, pp 457-468, 1967.

41. VOSSERS, G. : ' Some Applications of the Slender Body Theory in Ship Hydrodynamics ' Doctoral Dissertation, Delft. 1962.

42. TUCK, E.O. : ' The Steady Motion of a Slender Ship ' Ph.D. Thesis, Cambridge, 1963.

43. MARUO, H. : 'Calculation of the Wave Resistance of Ships, the Draught of which is as Small as the Beam ' Journal of the Zosen Kiokai, Vol. 112, 1962.

44. LEWISON, G.R.G. : ' Hydrodynamic Forces on a Partly Immersed Axisymmetric Body of Revolution ' Ph.D. dissertation, Cambridge University, 1964.

45. SMITH, A.M.O., HESS, J. : ' Calculation of Non-lifting Potential Flow about Arbitrary Three-Dimensional Bodies ' Douglas Aircraft Company Report No. ES 40622, March, 1962.

46. BRESLIN, J., KING ENG.: ' Calculation of the Wave Resistance of a Ship Represented by Sources Distributed over the Hull Surface ' Int. Seminar on Theor. Wave Res., Ann Arbor, 1963.

47. BESSHO, M. : ' On the Wave Resistance of a Submerged Body ' 60th Anniversary Series, Vol. II, pp. 135-172, Society of Naval Architects of Japan, 1960.

48. BESSHO, M. : ' Some Notes on the Theory of Wave Resistance in Two Dimensions ' Memoirs of the Defense Academy of Japan, Vol. VI, No. 4, pp. 443-456, 1967.

49. TUCK, E.O. : 'The Effect of Non-Linearity at the Free Surface on Flow Past a Submerged Cylinder ' Journal of Fluid Mechanics, Vol. 22, part 2, pp. 401-414, 1965.

50. WARD, L.W. : ' A Method for the Direct Experimental Determination of Ship Wave Resistance ' Doctoral Dissertation, Stevens Institute of Technology, Hoboken, N.J. 1962.

51. EGGERS, K.W.H., SHARMA, S.D. WARD, L.W. : ' An Assessment of Some Experimental Methods for Determining the Wave-making Characteristics of a Ship Form ' Trans. A.S.N.A.M.E., 1967.

52. EGGERS, K.W.H. : ' Uber die Ermittlung des Wellenwiderstandes eines Schiffsmodells durch Analyse seines Wellensystems Teil 1 and 2, Schiffstechnik, Vol. 9, 1962, Heft 46, pp. 79-84, 85 and Vol. 10, 1963, Heft 52, pp. 93-106.

53. SHARMA, S.D. : ' Untersuchungen uber den Zahigheits - und Wellenwiderstand mit besonderer Beruchsichtigung ihrer Wechselwirkung ' Institut fur Schiffbau der Universitat Hamburg, If. S-Bericht, Nr. 138.

54. HOGBEN, N., GADD, G.E. : 'The Determination of Wave Resistance from Measurements of the Wave Pattern ' National Physical Laboratory Ship Report 70, November, 1965.

55. KOBUS, H.E. : ' Examination of Eggers' Relationship between Transverse Wave Profiles and Wave Resistance ' Journal of Ship Research, December, 1967.

56. LAUTE, W. : ' Investigations of Pressure and Flow on a Ship Model ' Jahrbuch der S.T.G. Vol. 34, 1933, p.402.

57. HOGBEN, N. : ' Ship Hull Pressure Measurements ' Trans. R.I.N.A. 1957, Vol. 99, 1946.

58. TOWNSIN, R.H. : ' Frictional and Pressure Resistance of a Victory Model ' Trans. N.E.C. Inst. 1961-62, Vol. 78, p.445.

59. CONN, J.F.C., FERGUSON, A.M. : 'Results obtained with a series of Geometrically Similar Models ' Trans. R.I.N.A., 1968.

60. LANDWEBER, L., WU, T.Y. : ' A Formal Contribution on Resistance - The Variation of Viscous Drag with Froude Number ' 10th I.T.T.C., London, 1963.

61. TOWNSIN, R.L. : ' Viscous Drag from a Wake Survey. Measurements in the Wake of a 'Lucy Ashton Model '. Trans. R.I.N.A. 1968.

62. STEELE, B.N., PEARCE, G.B. : ' Experimental Determination of the Distribution of Skin Friction on a Model of a High-Speed Liner ' Trans. R.I.N.A., Vol. 110, 1968.

63. WIGLEY, W.C.S. : ' Effects of Viscosity on the Wave-making of Ships' Trans. Inst. Eng. and Shipbuilders in Scotland, Vol. 81, 1937-38.

64. SHEARER, J.R., CROSS, J.J. : ' The Experimental Determination of the Components of Ship Resistance ' Trans. R.I.N.A. Vol. 107, 1965.

65. LACKENBY, H. : ' An Investigation into the Nature and Interdependence of the Components of Ship Resistance ' Trans. R.I.N.A., Vol. 107, 1965.

66. HORN, F. : ' Einfluss der Form auf dem Reibungswiderstand ' Verandlungen der Tagung der Leiter der Schleppversuchsanstalten, Berlin, 1937.

67. WIGLEY, W.C.S. : ' Calculated and Measured Wave Resistance of a Series of Forms Defined Algebraically, the Prismatic Coefficient and Angle of Entrance being Varied Independently ' Trans. R.I.N.A. Vol. 84, 1942.

68. GUILLOTON, R. : ' A Note on the Experimental Determination of Wave Resistance ' Trans. R.I.N.A. Vol. 94, 1952.

69. EMERSON, A. : ' The Application of Wave Resistance Calculations to Ship Hull Design ' Trans. R.I.N.A. Vol. 96, 1954.

70. K.S. ENG., BRESLIN, P. : ' Theoretical-Experimental Study of the Effect of Viscosity on Wave Resistance ' Davidson Laboratory Report 1236, Oct., 1967.

71. GUILLOTON, R. : ' L'Étude Theorique du Bateau en Fluide Parfait ' A.T.M.A. Vol. 64, 1964.

72. SRETENSKY, L.N. : ' On the Resistance due to Waves in a Viscous Fluid Proc. Symposium of Behaviour of Ships in a Seaway, p. 729 Vol. II Wageningen, Sept., 1957.

73. WU, T.Y., MESSICK, R.E. : 'Viscous Effect on Surface Waves Generated by Steady Disturbances ' California Institute of Technology Report No. 85-8, February, 1958.

74. CUMBERBATCH, E. : ' Effects of Viscosity on Ship Waves ' Journal of Fluid Mechanics, Vol. 23, Part 3, pp. 471-479, 1965.

75. WIGLEY, W.C.S. : ' Effects of Viscosity on Wave Resistance ' Proc. Int. Sem. on Theoretical Wave Resistance, Ann Arbor, 1963, p.1295.

76. WU, T.Y. : ' Interaction between Ship Waves and Boundary Layer ' Proc. Int. Sem. on Theoretical Wave Resistance, Ann Arbor, 1963, p.1263.

77. HARLOW, F., WELCH, J., SHANNON, J., DALY, B. : ' The Mac Method - A Computing Technique for Solving Viscous, Incompressible, Transient Fluid-Flow Problems involving Free Surfaces ' Las Alamos Scientific Laboratory Report No. LA-3425, March, 1966.

78. HORN, F. : ' Hydromechanische Problems des Schiffsantriebs ' Hamburg p.94, 1932.

79. SAUNDERS, H.E. : ' The Running Attitude of the Ship and its Effect upon Performance ' ' Hydrodynamics in Ship Design ' Vol. I, Chapter 29, p.418.

80. WIGLEY, W. C. S. ' Water Forces on Submerged Bodies in Motion ' Trans. R.I.N.A. Vol. 95, 1953.

81. POND, H.A. : ' The Moment Acting on a Rankine Ovoid Moving under a Free Surface ' D.T.M.B. Report No. 795, 1951.

82. HARLOW, F.H., FROMM, J.E.: 'Dynamics and Heat Transfer in the von Karman Wake of a Rectangular Cylinder' Physics of Fluids, Vol. 7, 1147, 1964.

83. KINOSHITA, M., ABE, A., OKADA, S.: 'Two Examples of the Theory of Wave Resistance ' Journal of the Zosen Kiokai, Vol. 77, Nov. 1946.

84. BESSHO, M. : ' On the Formula of Wave-making Force Acting on a Ship ' Journal of the Zosen Kiokai, Vol. 110, December, 1961.

85. LAGALLY, M. : ' Berechnung der Kräfte und Momente, die stromende Flussikeiten auf ihre Begrenzung ausüben 'Zeit. fur Angewandte Math und Phys. Bd. 2. Heft 6, December, 1922.

86. STOKER, J.J. : ' Water Waves ' - ' The Motion of a Ship in a Seaway ' Interscience, 1957.

87. TUCK, E.O. : ' Sinkage and Trim in Shallow Water of Finite Width ' Schiffstechnik, Bd. 14, Heft 73, 1967.

88. ROBERTSON, J.M.: ' Hydrodynamics in Theory and Application ' Prentice Hall International Series in Theoretical and Applied Mechanics, 1965.

89. LUNDE, J.K. : ' On the Linearised Theory of Wave Resistance for Displacement Ships in Steady and Accelerated Motion ' Trans. A.S.N.A.M.E. Vol. 1952.

90. SNEDDON, I.N.: ' Fourier Transforms ' McGraw-Hill International Series in Pure and Applied Mathematics, 1951.

91. WATSON, G.N.: ' A Treatise on the Theory of Bessel Functions ' Cambridge University Press, 1966.

92. KELLOG, O.D.: ' Foundations of Potential Theory ' Berlin Springer, 1929

93. LUNDE, J.K.: ' Wave Resistance Calculations at High Speeds ' Trans. R.I.N.A., Vol. 91, 1949, pp. 182-196.

94. KAJITANI, H.: ' The Second-Order Treatment of Ship Surface Condition in the Theory of Wave-making Resistance of Ships ' Journal of Zosen Kiokai, Vol. 118.

95. COOKE, J.C.: ' Three Dimensional Turbulent Boundary Layers ' Aeronautical Research Council C.P. 635.

96. TANAKA, T.: ' Form Effects on Viscous Resistance of Ships ; Parts I and II Journal of the Zosen Kiokai, Vols. 113 and 114.

97. FERGUSON, A.M.: ' An Optical Method of Measuring Ground Speed ' University of Glasgow Experiment Tank, Report No. TR-6.

98. FERGUSON, A.M.: ' An Investigation into the Effects of Temperature Difference on Water Movement ' Trans. R.I.N.A. Vol. 108, 1966.

99. CONN, J.F.C.: Discussion on 'Ship Model Size and Tank Boundary Correction ' by A. Emerson, Trans. N.E.C. Inst., 1959-60, Vol. 76, p.D2.

100. TAGORI, T.: ' On the Effect of Various Shaped Turbulence Stimulators and Resistance of these Stimulators Own ' Journal of the Zosen Kiokai, Vol. 110, December, 1961, pp.167-183.

101. DAND, I.W. : ' The Effect of Towing Point Height on Resistance, Sinkage and Trim Measurements for a Model in Steady Motion ' Glasgow University Tank Report No. TR-7.

102. TOPPING, J.: ' Errors of Observation and their Treatment ' The Institute of Physics and the Physical Society Monographs for Students, 1965.

103. SCOTT, J.R. : ' On Ship Model Resistance Measurement Errors ' Trans. R.I.N.A. Vol. 106, p.449, 1964.

104. MORONEY, M.J.: ' Facts from Figures ' Pelican Books, 1962.

105. TANIGUCHI, K.: ' Study on Scale Effect of Propulsive Performance by Use of Geosims of a Tanker ' Journal of the Zosen Kiokai, Vol. 120, December, 1966.

106. HUGHES, G.: ' Friction and Form Resistance in Turbulent Flow, and a Proposed Formulation for use in Model and Ship Correlation ' Trans. R.I.N.A. Vol. 96, 1954.

107. WEBSTER, W.C.: ' The Effect of Surface Tension on Ship Wave Resistance ' University of California, College of Engineering, Report No. N.A.-66-6, 1966.

108. FERGUSON, W.: ' The Trident-Lithgow Ram Bow- Comparative Sea Trial Results ' Shipping World and Shipbuilder, December, 1966.

109. SATO, S., OKADA, S., SUDO, S., TAKAGI, M.: ' Effect of a Bulbous Bow upon the Resistance of Ships with Small Length-Beam Ratio and Large Block Coefficient' Journal of the Zosen Kiokai, Vol. 118, December, 1965.

110. COUCH, R.B., MOSS, J.L.: ' Application of Large Protruding Bulbs to Ships of High Block Coefficient ' Trans. A.S.N.A.M.E. Vol. 19.

111. CLEMENTS, R.E.: 'Ram Bows for Tankers and Bulk Carriers - A Preliminary Assessment ' N.P.L. Ship Division T.M.142, July, 1966.

112. WHITE, G.F.: ' Ram Bows on High Speed **Cargo** Liner Forms - A Preliminary Survey ' N.P.L. Ship Division T.M. 140, June, 1966.

113. GERTLER, M.: ' A Re-Analysis of the Original Test Data for the Taylor Standard Series ' D.T.M.B. Report No. 806, March, 1954.

114. ROBSON, W.: Discussion on ' The Frictional and Pressure Resistance of Two Lucy Ashton Geosims ' Trans. R.I.N.A. Vol. 109, 1967.

115. THWAITES, B. ' Incompressible Aerodynamics ' Oxford-Clarendon Press, 1960.

116. LORGERE, H.: ' The Mekong Delta Model ' Science Journal, Vol. 4, No. 7, July, 1968:

117. ABRAMOWITZ,M., STEGUN, I.A.: ' Handbook of Mathematical Functions ' National Bureau of Standards, 1964.

118. KAPLAN, E.L.: ' Numerical Integration near a Singularity ' Journal of Mathematics and Physics, Vol. 31, 1952, pp.1-28.

119. LUNDE, J.K.: ' On the Theory of Wave Resistance and Wave Profile ' Shipmodelltankens Meddelelse, No. 10, April, 1952.

120. NIELSEN, N.: ' Theorie des Integrallogarithmus ' B.G. Teubner, Leipzig, Germany, 1906.

121. Admiralty Research Laboratory, Teddington, Middlesex. Publication A.R.L.-T.9- Maths 2.7, November, 1956.

122. NOBLE, B.: ' Numerical Methods : 2 ' University Mathematical Tests, Oliver and Boyd, 1964, pp.241-242.

123. TAKAHEI, T.: ' An Analysis of Wave Profile Alongside the Ship ' Proceedings of Int. Sem. on Theor. Wave Resistance, Ann Arbor, 1963, Vol. II, p.471.

APPENDIX A.

FREE SURFACE PERTURBATION VELOCITIES - THEIR DERIVATION FROM THE WAVE PROFILE

From Bernoulli's Theorem,

$$p + \frac{1}{2}\rho q^2 + \rho g \zeta = \text{CONSTANT} \qquad \ldots\ldots\ldots \text{(A 1)}$$

subject to the following assumptions :

i) The fluid is inviscid.

ii) The fluid is incompressible and uniform.

iii) The motion is steady.

Along a streamline, equation (A1) becomes

$$p_1 + \frac{1}{2}\rho q_1^2 + \rho g \zeta_1 = p_2 + \frac{1}{2}\rho q_2^2 + \rho g \zeta_2 \qquad \ldots\ldots\ldots \text{(A2)}$$

Consider now a model advancing into still water creating a wave system. On the free surface, taking atmospheric pressure as a datum, equation (A2) may be re-written :

$$\frac{1}{2}\rho q_1^2 + \rho g \zeta_1 = \frac{1}{2}\rho q_2^2 \qquad \ldots\ldots\ldots \text{(A3)}$$

where subscript 1 refers to conditions at the model, subscript 2 refers to conditions in still water ahead of the model. i.e. $q_2 = V$ the speed of advance.

But from equation (2.1.2.)

$$q_1^2 = (V+u)^2 + v^2 + w^2 \qquad \ldots\ldots\ldots \text{(A4)}$$

where u,v and w are the perturbation velocities in the directions of the axes of co-ordinates.

Equations (A3) and (A4) above enable u,v and w to be calculated on the free surface from the measured wave profile. The hull is assumed to have a surface equation $y = \pm F(x,z)$ and the free surface to have an equation $\zeta = \zeta(x,y)$.

The free-stream velocity q may be resolved into its component

FIG. A1.

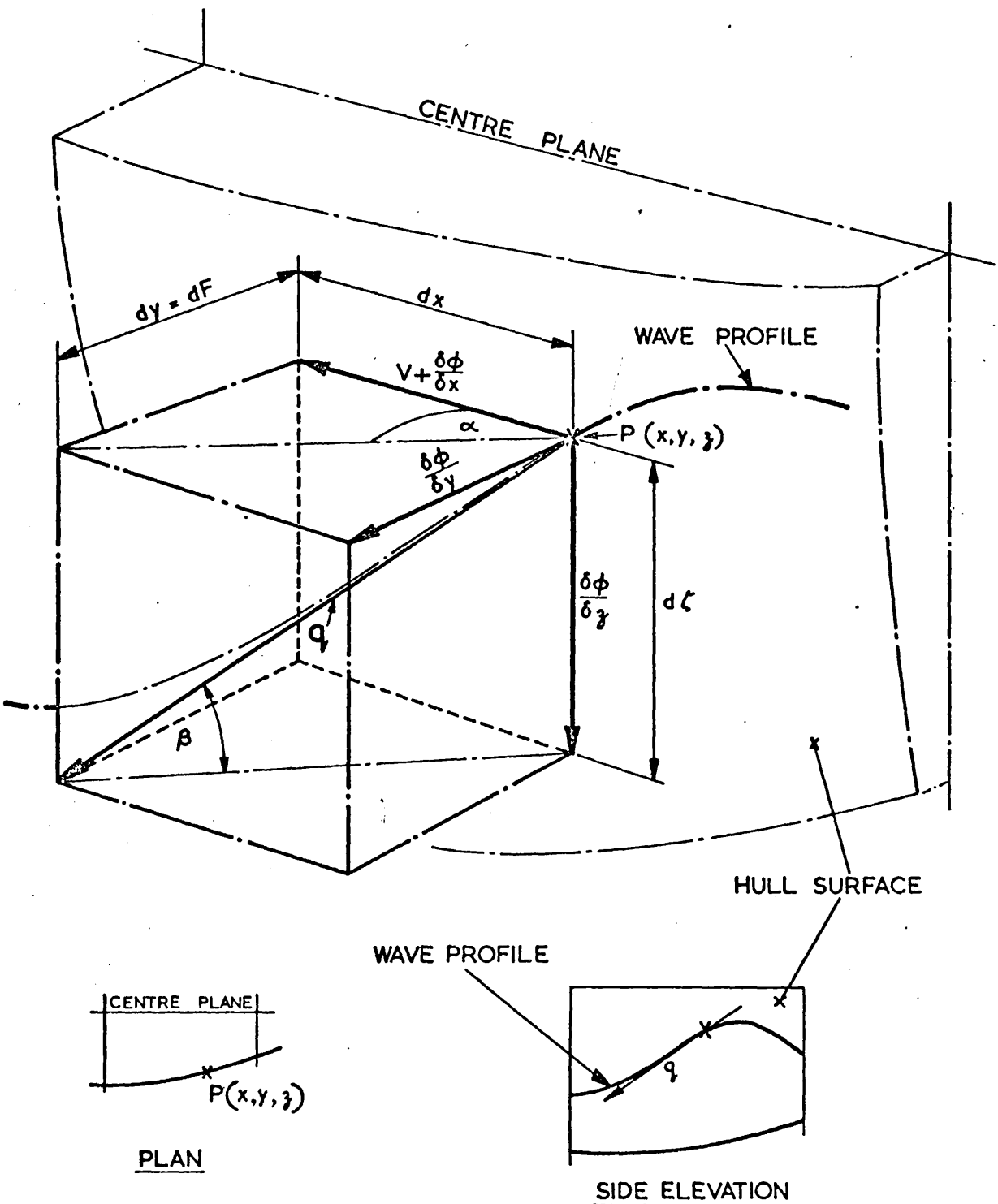

RESOLUTION OF FREE STREAM VELOCITY, q, INTO PERTURBATION VELOCITIES.

parts as in figure A1.

From this figure we have :

$$\tan\alpha = \frac{\partial F}{\partial x}$$

$$\cos\alpha = \frac{1}{\left(1 + \left(\frac{\partial F}{\partial x}\right)^2\right)^{\frac{1}{2}}}$$

$$\sin\alpha = \frac{\frac{\partial F}{\partial x}}{\left(1 + \left(\frac{\partial F}{\partial x}\right)^2\right)^{\frac{1}{2}}}$$

$$\cos\beta = \frac{\left(1 + \left(\frac{\partial F}{\partial x}\right)^2\right)^{\frac{1}{2}}}{\left(1 + \left(\frac{\partial F}{\partial x}\right)^2 + \left(\frac{\partial \zeta}{\partial x}\right)^2\right)^{\frac{1}{2}}} \qquad \ldots\ldots\ldots \text{(A5)}$$

$$\sin\beta = \frac{\left(\frac{\partial \zeta}{\partial x}\right)}{\left(1 + \left(\frac{\partial F}{\partial x}\right)^2 + \left(\frac{\partial \zeta}{\partial x}\right)^2\right)^{\frac{1}{2}}}$$

Hence, the various components of q_1 may be written :

$$(V+u) = q_1 \cos\alpha\cos\beta = \frac{q_1}{\left(1 + \left(\frac{\partial F}{\partial x}\right)^2 + \left(\frac{\partial \zeta}{\partial x}\right)^2\right)^{\frac{1}{2}}}$$

$\ldots\ldots\ldots$ (A6)

$$v = q_1 \sin\alpha\cos\beta = \frac{q_1 \frac{\partial F}{\partial x}}{\left(1 + \left(\frac{\partial F}{\partial x}\right)^2 + \left(\frac{\partial \zeta}{\partial x}\right)^2\right)^{\frac{1}{2}}}$$

$\ldots\ldots\ldots$ (A7)

$$w = q_1 \sin\beta = \frac{q_1 \frac{\partial \zeta}{\partial x}}{\left(1 + \left(\frac{\partial F}{\partial x}\right)^2 + \left(\frac{\partial \zeta}{\partial x}\right)^2\right)^{\frac{1}{2}}}$$

$\ldots\ldots\ldots$ (A8)

Values of u, v and w have been calculated in this way for the Inuid S201 at a Froude Number of 0.300. Results are given in table A1 and figure A2.

Stn.	ζ in.	q ft/sec	u ft/sec	v ft/sec	w ft/sec	$\frac{A_1}{B}$ %	$\frac{A_2}{B}$ %	$\frac{A_3}{B}$ %	$\frac{A}{B}$ %
F.P.	3.31	2.676	-2.606	1.105	-0.499	26.05	4.60	0.96	31.61
9½	3.75	2.190	-2.932	0.733	-0.128	29.30	1.87	0.05	31.22
9	3.52	2.456	-2.683	0.651	0.526	26.82	1.49	1.04	29.35
8	1.55	4.074	-1.199	0.747	1.286	12.08	4.58	13.75	30.41
6	-1.05	5.528	0.439	0.652	0.798	4.55	9.09	14.77	28.41
4	-1.30	5.647	0.636	0.399	-0.242	6.30	2.36	0.94	9.60
2	-0.60	5.305	0.293	0.180	-0.428	3.39	1.02	6.27	10.68
0	0.15	4.911	-0.085	0	-0.216	0.59	0	5.29	5.88
-2	0.21	4.878	-0.120	-0.166	0.180	1.25	2.08	2.50	5.83
-4	-0.55	5.279	0.284	-0.375	0.375	2.81	4.91	4.91	12.63
-6	-0.78	5.395	0.364	-0.643	-0.027	3.56	11.37	0.03	14.96
-8	-0.45	5.228	0.125	-1.008	-0.353	1.20	81.20	10.00	92.40
A.P.	0.68	4.612	-0.821	-1.931	-0.384	8.54	45.61	1.71	55.92

NOTE : $A = A_1 + A_2 + A_3$; $A_1 = u^2/2g$; $A_2 = v^2/2g$; $A_3 = w^2/2g$;

$B = |Vu/g|$, $V = 4.992$ ft/sec., $\mathcal{F} = 0.300$

Table A1

It has been shown in section 2.1.2. that the wave elevation $\zeta(x,y,z)$ is given by

$$\zeta(x,y,z) = -\frac{V}{g}u - \frac{1}{2g}(u^2 + v^2 + w^2)\Big|_{z=\zeta}$$

This becomes, after linearisation,

$$\zeta(x, y, z) = -\frac{V}{g} u \Big|_{z=\zeta}$$

or

$$\zeta(x, y, o) = -\frac{V}{g} u \Big|_{z=0}$$

Writing

$$\zeta(x, y, z) = -(A + B)$$

where

$$A = A_1 + A_2 + A_3$$

and $A_1 = u^2/2g$, $A_2 = v^2/2g$, $A_3 = w^2/2g$, $B = Vu/g$

the consequences of linearisation may be examined. Values of A, A_1, A_2, A_3 are also shown in figure A2 at each station at the free surface where they are expressed as a percentage of B. Linearisation is only valid at the free surface if A is sufficiently small compared to B.

Figure A2 shows that A is never less than 5% of B and is greater than 30% of B at bow and stern. The neglected term A is seen to be 92% of the local value of B at station - 8. This is due to a combination of a low value of u with a large value of v at this point. It is possible that such large values could occur at other parts of the wave profile not included in the analysis above.

It is therefore concluded that free surface non-linearities are important and should not be neglected. It is possible that the use of the linearised Free Surface Condition is as great a contributory factor to the poor agreement between theory and experiment as the neglect of viscosity.

FIG. A2

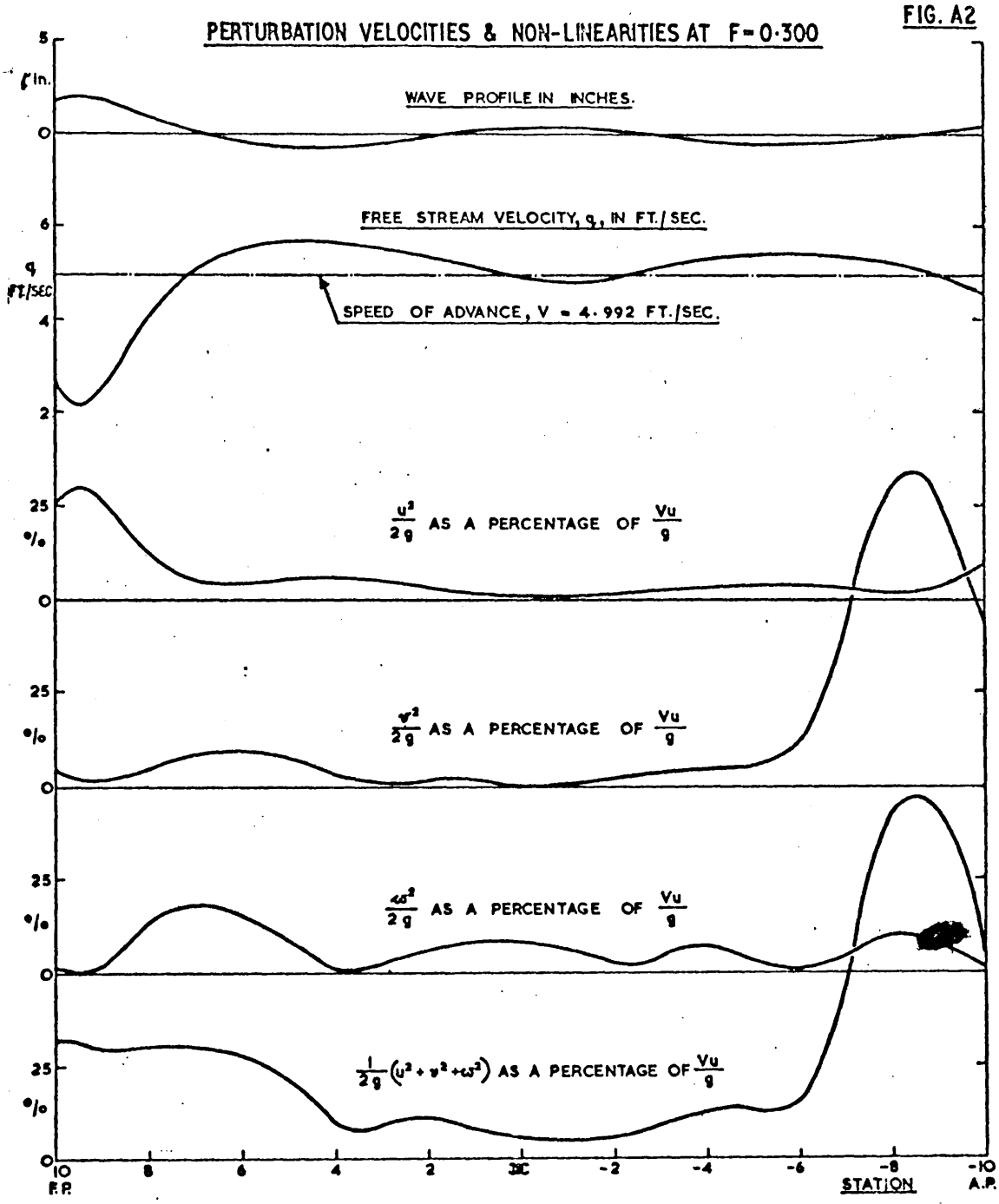
PERTURBATION VELOCITIES & NON-LINEARITIES AT F = 0·300
5
ζ in.
0
WAVE PROFILE IN INCHES.
6
q FT/SEC
4
2
FREE STREAM VELOCITY, q, IN FT./SEC.
SPEED OF ADVANCE, V = 4·992 FT./SEC.
25
%
0
u²/2g AS A PERCENTAGE OF Vu/g
25
%
0
v²/2g AS A PERCENTAGE OF Vu/g
25
%
0
ω²/2g AS A PERCENTAGE OF Vu/g
25
%
0
1/2g (u² + v² + ω²) AS A PERCENTAGE OF Vu/g
10 F.P.
8
6
4
2
0 AC
-2
-4
-6
-8 STATION
-10 A.P.

APPENDIX B

THE REDUCTION AND NUMERICAL EVALUATION OF SOME INTEGRALS USED IN THE ANALYSIS

In section 2.3. the following results were derived

$$C_{P_0}(x,0,z) = \frac{1}{2\pi}\int_{-\ell(z)}^{\ell(z)} d\lambda \int_0^{d(x)} \frac{\partial \eta}{\partial \lambda} \frac{(x-\lambda)\, d\zeta}{[(x-\lambda)^2+(z+\zeta)^2]^{\frac{3}{2}}} - \frac{1}{2\pi}\int_{-\ell(z)}^{\ell(z)} d\lambda \int_0^{d(x)} \frac{\partial \eta}{\partial \lambda} \frac{(x-\lambda)}{[(x-\lambda)^2+(z-\zeta)^2]^{\frac{3}{2}}}\, d\zeta$$

$$C_{P_L}(x,0,z) = -\frac{4\kappa_0}{\pi^2}\int_{-\ell(z)}^{\ell(z)} \frac{\partial \eta}{\partial \lambda}\, d\lambda \int_0^{d(x)} d\zeta \int_0^{\frac{\pi}{2}} \sec\theta\, d\theta \int_0^{\infty} \frac{e^{-m|x-\lambda|\cos\theta}\,[\kappa_0 \sec^2\theta \sin m(\zeta-z) - m\cos m(\zeta-z)]\, m\, dm}{\kappa_0^2 \sec^4\theta + m^2}$$

$$C_{P_W}(x,0,z) = \frac{4\kappa_0^2}{\pi}\int_{-\ell(z)}^{\ell(z)} \frac{\partial \eta}{\partial \lambda}\, d\lambda \int_0^{d(x)} d\zeta \int_0^{\frac{\pi}{2}} e^{-\kappa_0(\zeta-z)\sec^2\theta} \cos[\kappa_0(x-\lambda)\sec\theta] \sec^3\theta\, d\theta$$

..... (B1)

Before numerical values for these pressure coefficients could be obtained, the geometry of the hull surface had to be specified numerically.

B.1. DEFINITION OF THE HULL SURFACE

B.1.1. Calculation of $\partial\eta/\partial x$ and $\partial\eta/\partial z$ values

The fore and aft symmetry of the hull enabled all derivatives to be calculated from a quarter of its surface as shown in figure B1.

Initially the underwater hull was divided vertically into ten equally spaced sections bounded by the water-planes 0 to 10. Waterplane 0 corresponded to the at-rest waterplane and waterplane 10 to that at maximum draft, d_{max}. This lowest waterplane was given by the point $(0, 0, -d_{max})$ and was associated with an infinite value of $\partial\eta/\partial z$ due to the shape of the body sections near the keel. The contributions of the elementary pressures to C_Z and C_M would therefore be indeterminate at this point. As the elementary pressure coefficients given by equation (B1) vanish on a waterplane of zero

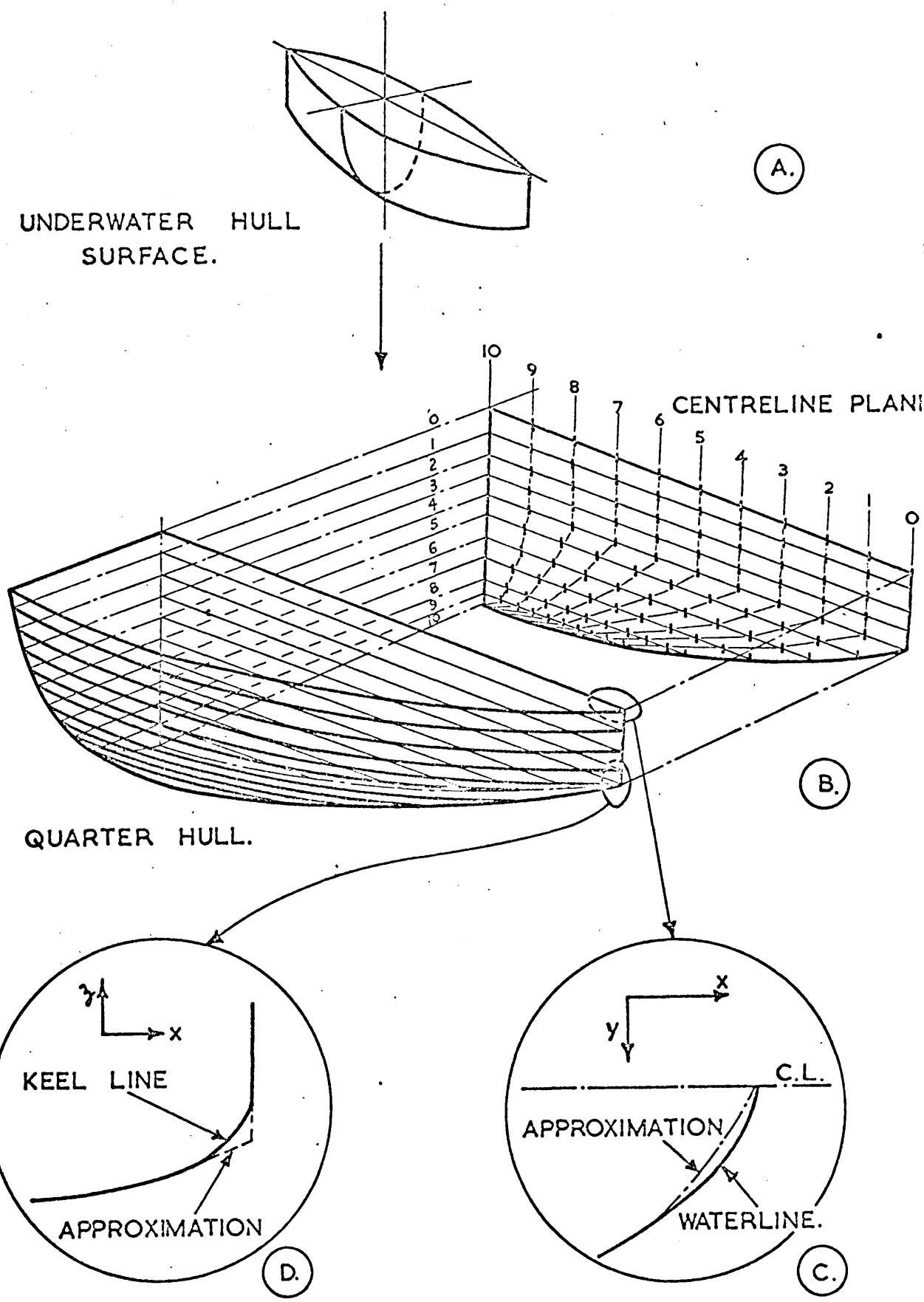

DEFINITION OF HULL SURFACE.

length, physical considerations suggest that there are no contributions to C_Z and C_M from pressures at this point. It was therefore assumed that C_{PO}, $C_{P\ell}$ and C_{PW} all tended to zero more rapidly than $\partial\eta/\partial z$ tended to infinity at the point $(0, 0, -d_{max})$.

Each waterplane was divided into ten equal parts as shown in figure B1B. Values of $\partial\eta/\partial x$ and $\partial\eta/\partial z$ were then calculated from the hull offsets at stations 0 to 10 for each waterplane using the Lagrange Five Point numerical differentiation formula:

$$\left.\frac{\partial \eta}{\partial x}\right|_{x=x_j} = \frac{1}{4!\,h} \sum_{i=0}^{4} A_i\, \eta(x_i) \qquad \ldots\ldots\ldots \text{(B2)}$$

where the coefficients A_i for values of j from 0 to 4 were obtained from ref. 117 p.914. In equation (B2) $h = \ell/10$ where ℓ is the local length of the waterplane shown in figure B1B. For example, waterplane 0 had a local length of 4.300 ft., whereas waterplane 9 had a local length of 2.046 ft. due to the curved keel line.

In the subsequent analysis it was necessary to interpolate intermediate values of $\partial\eta/\partial x$. This was accomplished on the computer by fitting a polynomial surface to discrete numerical values of $\partial\eta/\partial x$ calculated for the various waterplanes, thus obtaining a 'machine table' of polynomial coefficients.

This was accurate to ± 0.0005 at any point (x, y, z) except for an approximation introduced to avoid infinite values of $\partial\eta/\partial z$ at the point $(\pm\ell, o, z)$. (See figure B1C.)

Intermediate values of the derivative at any point on the hull surface were readily obtained by evaluation of the two-dimensional polynomial.

Intermediate values of $\partial\eta/\partial z$ were not required and so an array of discrete values was stored in the computer.

B.1.2. Representation of plane $y = 0$

All integrations in the analysis were performed over the plane $y = o$. Due to the curved keel, the draft was not uniform over the length. The draft was therefore represented as an eighth order polynomial in x which was accurate to ± 0.0005 ft. at any point (x, o, z) except for an approximation at bow and stern shown in

figure B1D.

To facilitate the computation the x- and h-origins were shifted to the bow. All subsequent analysis uses this origin.

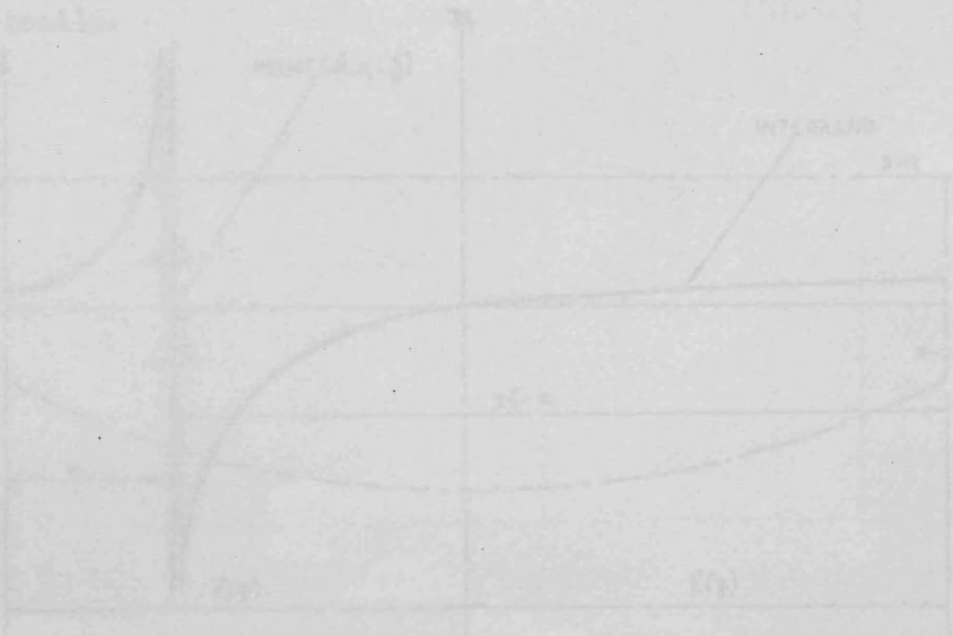

FIG B2

B.2. CALCULATION OF $C_{PO}(x,o,z)$ VALUES. COMPUTER PROGRAM NO

From equation (B1),

$$C_{Po}(x,0,z) = \frac{1}{2\pi}\int_0^{2\ell(z)} d\ell \int_0^{d(x)} \frac{\partial \mu}{\partial \alpha}\left\{\frac{(x-\ell)}{[(x-\ell)^2+(z+\beta)^2]^{\frac{3}{2}}} - \frac{(x-\ell)}{[(x-\ell)^2+(z-\beta)^2]^{\frac{3}{2}}}\right\} d\beta$$

which reduces to

$$C_{Po}(x,0,z) = \frac{1}{2\pi}\int_0^{2\ell(z)} \frac{\partial \mu}{\partial \ell}\frac{1}{(x-\ell)}\left[\frac{(d(x)-z)}{[(x-\ell)^2+(d(x)-z)^2]^{\frac{1}{2}}} - \frac{(d(x)+z)}{[(x-\ell)^2+(d(x)+z)^2]^{\frac{1}{2}}} + \frac{2z}{[(x-\ell)^2+z^2]^{\frac{1}{2}}}\right] d\ell$$

..... (B3)

Equation (B3) shows that C_{PO} vanishes at z = o indicating that at infinite speed the free surface pressure coefficient vanishes in the vicinity of the hull.

Using a result obtained in section 2.1.4. b, equation (2.1.33b) gives a value for C_{PO} at zero speed of

$$C_{Po}(x,0,z)\Big|_{V=0} = -\frac{1}{2\pi}\int_0^{2\ell(z)} \frac{\partial \mu}{\partial \ell}\, d\ell \int_{-d(x)}^{d(x)} \frac{(x-\ell)}{[(x-\ell)^2+(z-\beta)^2]^{\frac{3}{2}}}\, d\beta$$

..... (B4)

which reduces to

$$C_{Po}(x,0,z)\Big|_{V=0} = -\frac{1}{2\pi}\int_0^{2\ell(z)} \frac{\partial \mu}{\partial \ell}\left[\frac{(d(x)+z)}{[(x-\ell)^2+(d(x)+z)^2]^{\frac{1}{2}}} + \frac{(d(x)-z)}{[(x-\ell)^2+(d(x)-z)^2]^{\frac{1}{2}}}\right]\frac{d\ell}{(x-\ell)}$$

..... (B5)

The integrals in equations (B3) and (B5) were evaluated numerically.

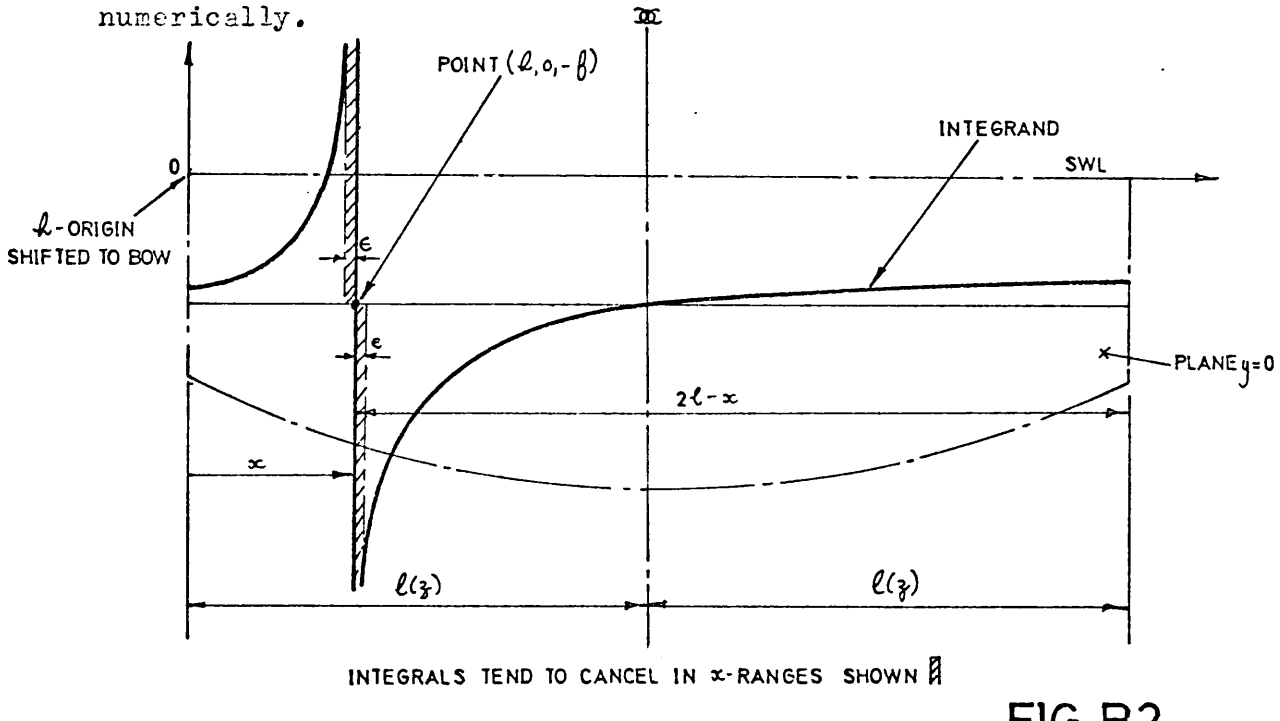

FIG. B2

The integrand of equation (B3) consists of three parts, each of which is singular at h = x and decreases monotonically at points remote from the singularity, (see figure B2). These parts were treated separately and then summed to give values of C_{PO} and $C_{PO}|_{V = o}$ at any point (h,o, -f).

The integrands were well-behaved and tended to infinity like $(x-h)^{-1}$ at (x-h) = o. The principal value of each integral was taken, numerical integration extending to a point $(x-h) = \pm\epsilon$ on either side of the singularity. The contributions to the integral from the regions near $(x-h) = \pm\epsilon$ effectively cancelled each other, thus minimising errors due to the integration technique used.

Integration near to the singularity was performed using Kaplan's method (118) which approximates the functions $A(\xi)$ in the singular integrand $\xi^n A(\xi)$ with a polynomial function.

Constant intervals in ξ are used and very accurate results may be obtained. The method may be extended for integration up to certain singularities.

Simpson's second rule was used to evaluate the integral over the remainder of the range. The ordinate spacings used are shown in table B1.

x^1	ordinate spacing	No. of intervals	Integration Rule
0.100/81 - 0.100/27	0.100/81	2	Kaplan
0.100/27 - 0.100/9	0.100/27	2	Kaplan
0.100/9 - 0.100/3	0.100/9	2	Kaplan
0.100/3 - 0.100	0.100/3	2	Kaplan
0.100 - 0.05ξ	0.0125ξ	4	Simpson
0.05ξ - 0.10ξ	0.025ξ	2	Simpson
0.10ξ - ξ	0.045ξ	20	Simpson

$x^1 = |x-h|$, ξ= x-0.100 or $(2\ell-x)$ - 0.100

ℓ = local waterline length

Table B1

Computer program WO calculated values of C_{PO} and $C_{PO}|_{V=o}$ over the plane y=o; these are shown in figure B3 and B4. Large values of C_{PO} occur at the fore and aft stagnation points and it was suspected that these values were subject to numerical inaccuracies ; values of the integral near $(x-h) = \pm\epsilon$ would not be cancelled at these points. The derivative vanishes at $(\pm\ell, o, z)$ for waterlines 0 to 5 so there is no contribution to C_{PO} from these points, but large contributions to C_{PO} and $C_{PO}|_{V=o}$ arise from the points (ℓ, o, z) for waterlines 6 to 9 inclusive. This indicates that much of the sinkage force Z arises from the lower waterlines, the contributions from the region of the bow and stern being important.

This conclusion could not have been reached using Inui's theory (section 2.3). The source distribution for Inuid S201 is uniform in the negative z-direction and could not have given the correct vertical force distribution unless values of $\partial\eta/\partial z$ were known in advance.

FIG. B3.

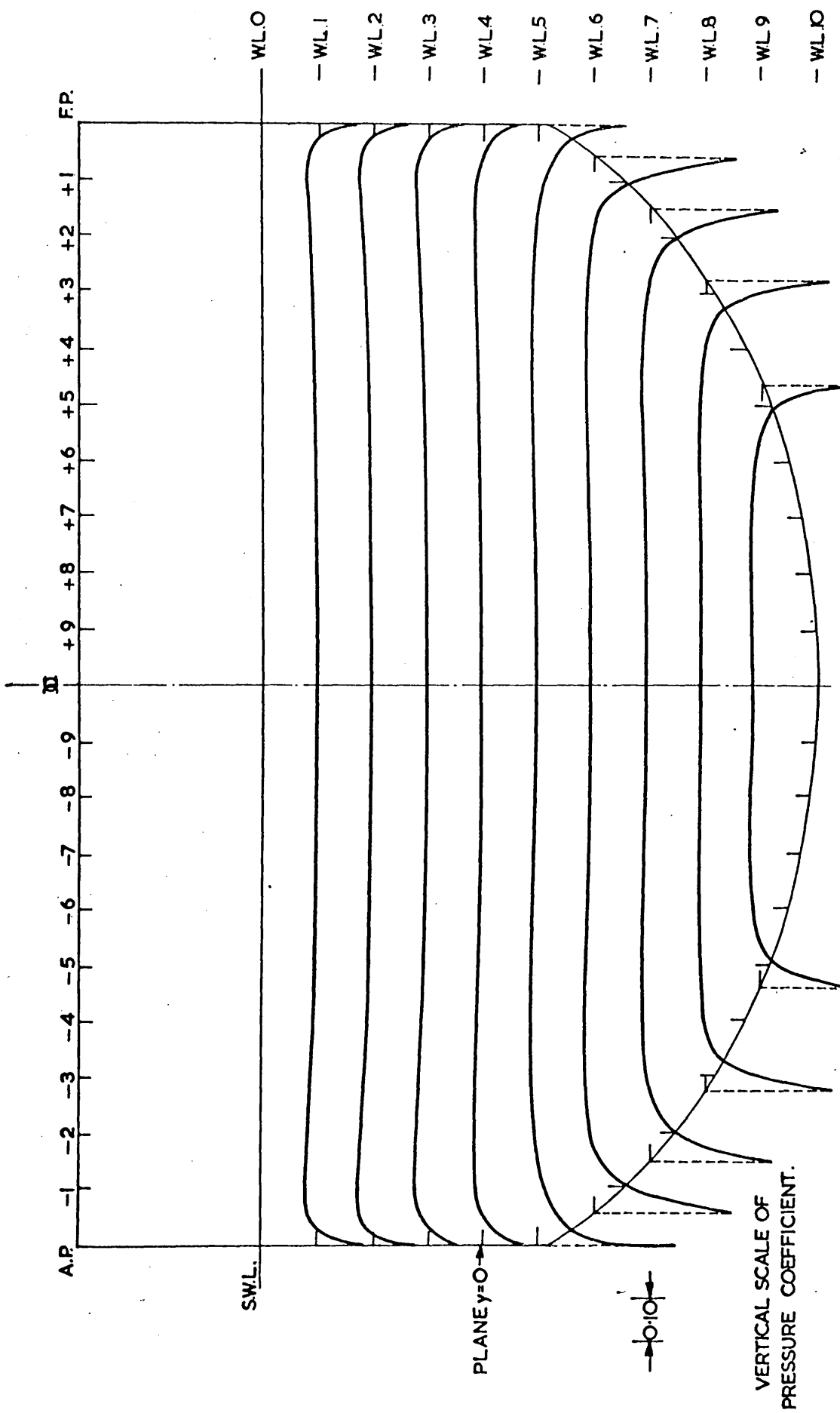

CALCULATED DISTRIBUTION OF C_{PO} OVER CENTREPLANE ($\mathcal{F}=+\infty$)

FIG. B4

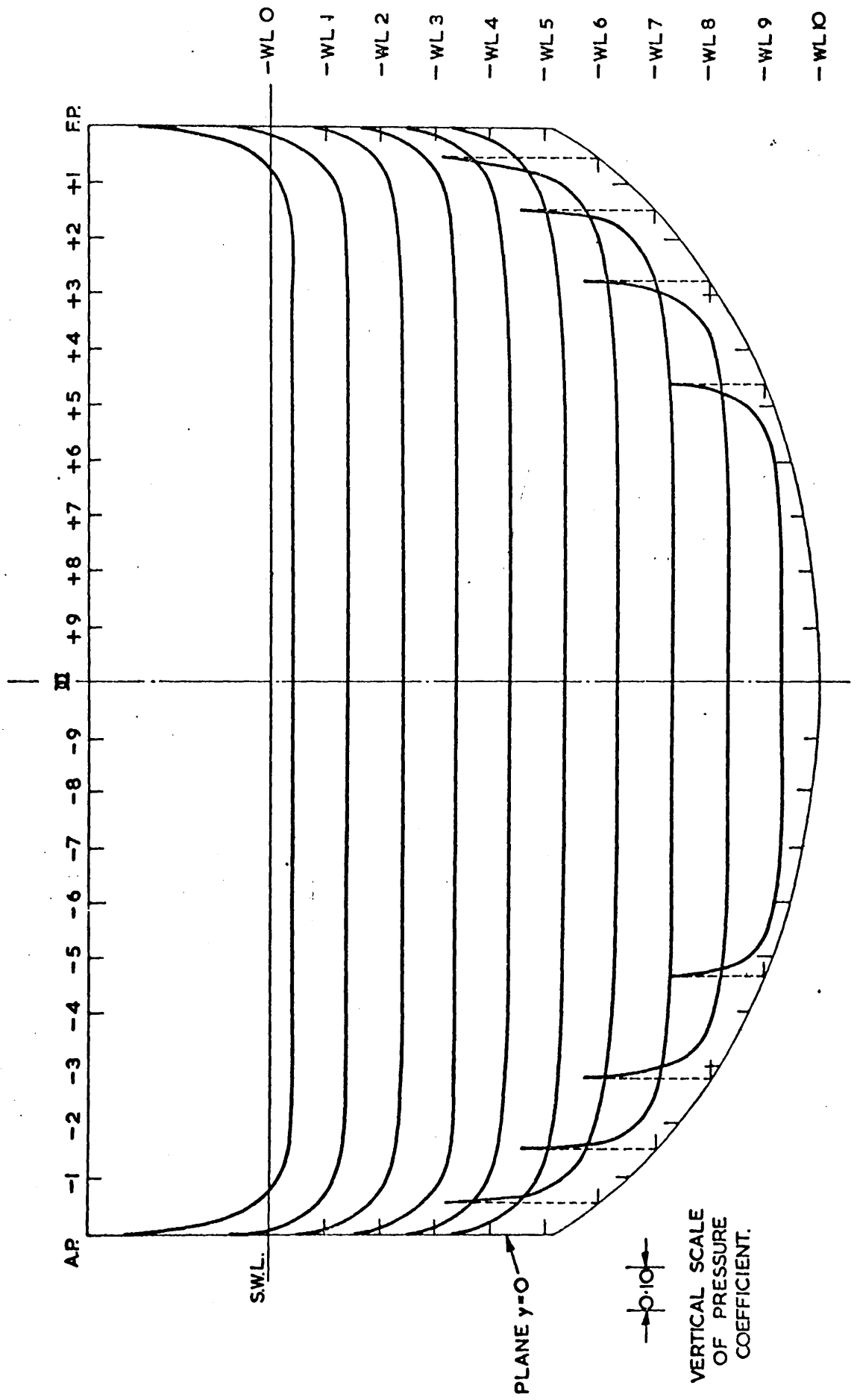

CALCULATED DISTRIBUTION OF $C_{PO}/_{V=0}$ OVER CENTRE PLANE ($\mathcal{F}=0$)

B.3. CALCULATION OF $C_{pl}(x,o,z)$ VALUES, COMPUTER PROGRAM L3

From equation (B1), putting z = -z in equations (2.3.5) for convenience,

$$C_{pl}(x,0,z) = -\frac{4K_0}{\pi^2}\int_0^{2l(z)} \frac{\partial y}{\partial l}\,dl \int_0^{d(x)} df \int_0^{\frac{\pi}{2}} \sec\theta\, d\theta \int_0^{\infty} \frac{e^{-m|x-l|\cos\theta}\,[K_0\sec^2\theta \sin m(f+z) - m\cos m(f+z)]\,m\,dm}{K_0^2\sec^4\theta + m^2}$$

B.3.1. Calculation in the range $0 \le K_0.x \le 10$, $0 \le K_0.z \le 5$

Using the result

$$\int_0^d [A\sin m(f+z) - B\cos m(f+z)]\,df = \frac{A\cos mz}{m} + \frac{B\sin mz}{m} - \left[\frac{A\cos m(d+z)}{m} + \frac{B\sin m(d+z)}{m}\right]$$

where $A = K_0\sec^2\theta$, $B = m$ we have

$$C_{pl}(x,0,z) = -\frac{4K_0}{\pi^2}\int_0^{2l(z)} \frac{\partial y}{\partial l}\left\{J[K_0(x-l), K_0 z] - J[K_0(x-l), K_0(d(x)+z)]\right\} dl \qquad \ldots\ldots\ldots \text{(B6)}$$

where

$$J(K_0x, K_0z) = \int_0^{\frac{\pi}{2}} \sec\theta\, d\theta \int_0^{\infty} \frac{[K_0\sec^2\theta\cos mz + m\sin mz]\,e^{-mx\cos\theta}}{K_0^2\sec^4\theta + m^2}\,dm \qquad \ldots\ldots\ldots \text{(B7)}$$

Values of the function J(Ko.x, Ko.z) were calculated over the range $0 \le K_0.x \le 10$, $0 \le K_0.z \le 5$ using the substitutions $\rho = K_0.z\sec^2\theta$, $u = mz$ in equation (B7) which gives

$$J(K_0x, K_0z) = \int_0^{\frac{\pi}{2}} \sec\theta\, d\theta \int_0^{\infty} \frac{\rho\cos u + u\sin u}{\rho^2 + u^2}\, e^{-\frac{\alpha}{\sqrt{\beta\rho}}\cdot u}\,du = \int_0^{\frac{\pi}{2}} J'(\alpha,\beta,\theta)\sec\theta\, d\theta \qquad \ldots\ldots\ldots \text{(B8)}$$

where $\alpha = K_0.x$, $\beta = K_0.z$

When Ko.x = 0, equation (B8) reduces to

$$J(0, K_0.z) = \pi\int_0^{\frac{\pi}{2}} e^{-\rho}\sec\theta\, d\theta = \frac{\pi}{2}e^{-\frac{1}{2}K_0z}K_0\left(\tfrac{1}{2}K_0z\right) \qquad \ldots\ldots\ldots \text{(B8a)}$$

where $K_0(x)$ is the modified Bessel Function of zero order and we have made use of the results given by Lunde (119) and the known result (120 p.24):

$$\int_0^{\infty} \frac{\rho\cos u + u\sin u}{\rho^2 + u^2}\,du = \pi e^{-\rho},$$

$$(\rho = K_0.z\sec^2\theta)$$

Values of $J'(\alpha,\beta,\theta)$ sec θ were calculated over the range $0 \leq \theta \leq \frac{\pi}{2}$ for any α,β and integrated numerically. The function $J'(\alpha,\beta,\theta)$ was calculated using a method similar to that used by Havelock (12, p.293):

We consider the integral $\int_0^\infty \frac{e^{-iu}\, e^{-au}}{u+i\rho}\, du$ and see that

$$J' = -\mathrm{Im}\int_0^\infty \frac{e^{-iu}\, e^{-au}}{u+i\rho}\, du = -\mathrm{Im}\int_0^\infty \frac{(u-i\rho)(\cos u - i\sin u)e^{-au}}{\rho^2+u^2}\, du \qquad \ldots\ldots\ldots \text{(B9)}$$

Using the known result (117, p.230) that

$$\int_0^\infty \frac{e^{-ty}}{t+x}\, dt = e^{-xy}\, li(e^{-xy}) \qquad \ldots\ldots\ldots \text{(B10)}$$

where $li(x) = \int_0^x \frac{dt}{\ln(t)}$ is the logarithmic integral

equation (B9) reduces to

$$J' = \mathrm{Im}\; e^{i\rho(i+a)}\, li\,(e^{-i\rho(i+a)})$$

$$= \mathrm{Im}\; e^{-\rho}.e^{i\rho a}(Ei(\rho - i a\rho) \pm i\pi) \qquad \ldots\ldots\ldots \text{(B11)}$$

as $li(e^{-x.e^{\pm i\pi}}) = Ei(x) \pm i\pi$

where $Ei(x) = \gamma + \ln(x) + \sum_1^\infty \frac{x^n}{n.n!}$ $\ldots\ldots\ldots$ (B12)

(Ref. 117, p.229, Eq.5.1.10)

(where γ = Euler's Constant)

Letting

$$Ei(\rho - i a\rho) + i\pi = = P + iQ\,, \qquad \ldots\ldots\ldots \text{(B12a)}$$

$$J' = \mathrm{Im}\; e^{-\rho}(\cos\rho a + i\sin\rho a)(P+iQ)$$

$$= e^{-\rho}[P\sin\rho a + Q\cos\rho a] \qquad \ldots\ldots\ldots \text{(B13)}$$

where

$$P = \gamma + \ln\rho + \sum_{n=1}^{\infty} \frac{\rho^n}{n.n!} \cdot \cos n\phi$$

$$Q = \pi - \phi - \sum_{n=1}^{\infty} \frac{\rho^n}{n.n!} \cdot \sin n\phi \qquad \ldots\ldots\ldots (B14)$$

$$a = \alpha/\sqrt{\beta\rho}$$

where $\rho^2 = r^2 + r\alpha^2/\beta$, $\tan\phi = \alpha/\sqrt{\beta.\rho}$, $\alpha = K_0.x$, $\beta = K_0.z$, $\rho = K_0.z\sec^2\theta$

(Equations (B.14) are derived using the result

$$\beta - i\alpha = re^{i\phi}, \quad r^2 = \alpha^2 + \beta^2, \quad \tan\phi = \alpha/\beta$$

in conjunction with equations (B12), (B12a) and De Moivre's Theorem).

Values for J' were calculated from equations (B13) and (B14) for discrete values of θ and, when multiplied by sec θ, the integrand had the form shown in fig. B5.

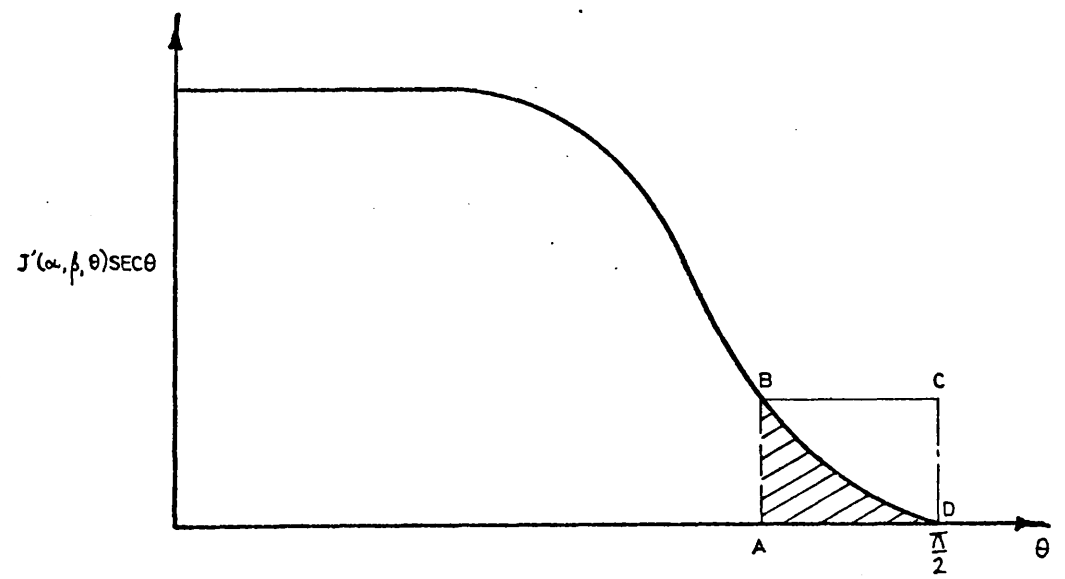

FIG. B5

Unfortunately the series (B14) became unstable at θ values near π/2. The series required many terms for convergence as θ approached π/2, which resulted in the calculation of cos nβ and sin nβ becoming unstable in the computer. Calculation of J' sec θ was therefore terminated at some value of θ (shown by point A in figure B5.). The remaining contribution to the integral, represented by the shaded area ABD in figure B5, was evaluated

as some fraction γ_θ of the rectangle ABCD.

The fraction γ_θ was determined by inspection, and was in general close to 1/3. Over most of the range of x and z the angle ($\pi/2$ - A) was small, and values of J, calculated by equation (B8) using Simpson's Rule, were accurate to ± 0.0005.

B.3.2. Calculation for the range $25 \leq Ko.x \leq 100$, $0 \leq Ko.z \leq 5$

Unfortunately the above method of calculation of J(Ko.x,Ko.z) became very inaccurate for Ko.x>10 so for the range $25 \leq Ko.x \leq 100$, $0 \leq Ko.z \leq 5$ the following procedure was adopted.

By use of the substitution $m = -m' K_o \sec^2\theta$ the equation for $C_{pl}(x,o,z)$ becomes

$$C_{pl}(x,o,z) = -\frac{4K_o^2}{\pi^2}\int_0^{2l(z)} \frac{\partial M}{\partial h}\,dh \int_0^{d(x)} df \int_0^{\frac{\pi}{2}} \sec^3\theta\, d\theta \int_0^{\infty} \frac{e^{-m'K_o(f+z)\sec^2\theta}\, \sin[K_o m'(x-h)\sec\theta]\, m'\, dm'}{1+m'} \quad \ldots\ldots\ldots \text{(B15)}$$

Integration with respect to f gives equation (B6) with the following expression for J(Ko.x,Ko.z):

$$J(K_o.x, K_o.z) = \int_0^{\frac{\pi}{2}} \sec\theta\, d\theta \int_0^{\infty} \frac{e^{-K_o m' z \sec^2\theta}\, \sin[K_o.x\, m' \sec\theta]\, dm'}{1+m'} \quad \ldots\ldots\ldots \text{(B16)}$$

When Ko.z = o, i.e. in the free surface, equation (B16) reduces to the known form (12, p.352)

$$J(K_o.x, o) = \int_0^{\frac{\pi}{2}} \sec\theta\, d\theta \int_0^{\infty} \frac{\sin[K_o.x.m'\sec\theta]\, dm'}{1+m'} = \frac{\pi^2}{4}[H_o(K_o x) - Y_o(K_o x)] \quad \ldots\ldots\ldots \text{(B17)}$$

where $H_o(x)$ is the Struve function of zero order and $Y_o(x)$ is the Bessel Function of the second kind and zero order.

Evaluation of equation (B.16) proceeds as follows:

The exponential $e^{-m'K_o z \sec^2\theta}$ may be expanded as an infinite series to give

$$J(\kappa_{ox}, \kappa_{oz}) = \sum_{m=0}^{\infty} \frac{(-)^m (\kappa_{oz})^m}{m!} \int_0^{\frac{\pi}{2}} \sec^{1+2m}\theta \, d\theta \int_0^{\infty} \frac{\sin[\kappa_{ox} \cdot m' \sec\theta] (m')^m}{1+m} \, dm' \qquad \ldots\ldots\ldots \text{(B18)}$$

the problem is now reduced to the evaluation of integrals of the type

$$\int_0^{\frac{\pi}{2}} \sec^{1+2m}\theta \, d\theta \int_0^{\infty} \frac{\sin[\kappa_{ox} m \sec\theta] m^m}{1+m} \, dm$$

which may be written as

$$\int_0^{\infty} \left\{ \int_0^{\frac{\pi}{2}} \sec^{1+2m}\theta \sin[\kappa_{o.x} m \sec\theta] \, d\theta \right\} \frac{m^m}{1+m} \, dm \qquad \ldots\ldots\ldots \text{(B19)}$$

where we have assumed that we may change the order of integration without loss of generality.

First, consider the integral

$$Q_\nu(\xi) = \int_0^{\frac{\pi}{2}} \cos^\nu\theta \cos\left(\xi \sec\theta - \frac{\nu\pi}{2}\right) d\theta \qquad \nu < 0 \qquad \ldots\ldots\ldots \text{(B20)}$$

It is readily seen that

$$Q_\nu(\xi) = \frac{\partial}{\partial\xi} Q_{\nu+1}(\xi) \qquad \ldots\ldots\ldots \text{(B21)}$$

$$Q_{-1}(\xi) = -\frac{\pi}{2} J_0(\xi) \qquad \ldots\ldots\ldots \text{(B22)}$$

Repeated application of the recurrence relation (B21) to the result (B22), in conjunction with the known result (91, p.18, eq.9):

$$2^r \frac{d^r J_m(z)}{dz^r} = \sum_{m=0}^{r} (-)^m \binom{r}{m} J_{m-r+2m}(z) \qquad \ldots\ldots\ldots \text{(B23)}$$

where $J_n(z)$ is the Bessel Function of the First Kind of order n, gives, for even values of ν,

$$Q_{-(\nu+1)}(x) = -\frac{\pi}{2.2^{\nu}}\left[2J_{\nu}(x) - 2\nu J_{\nu-2}(x) + \frac{2\nu(\nu-1)}{2!} J_{\nu-4}(x) - \cdots \right.$$

$$\left. \cdots\cdots \frac{(-)^{\frac{\nu}{2}}.\nu!}{\frac{\nu}{2}!\ \frac{\nu}{2}!} J_0(x) \right]$$

..... (B24)

where we have used

$$J_{-\nu}(x) = J_{\nu}(x) \qquad (\nu \text{ EVEN})$$

Substituting $\nu = 2n$ into equation (B24) gives

$$Q_{-(1+2n)}(x) = -\frac{\pi}{2.2^{2n}}\left[2J_{2n}(x) - 2.2nJ_{2n-2}(x) + \frac{2.2n.(2n-1)}{2!} J_{2n-4}(x) \cdots \right.$$

$$\left. \cdots + \frac{(-)^{k}\,2n!}{(2n-k)!\,k!} J_{2n-k}(x) \cdots\cdots \frac{(-)^{n}\,2n!}{n!\,n!} J_0(x) \right]$$

..... (B25)

Equation (B25) therefore represents a finite series involving Bessel Functions of the First Kind which may be substituted into equation (B18) to give

$$J(K_0x, K_0z) = \sum_{n=0}^{\infty} \frac{(K_0z)^n}{n!} \int_0^{\infty} \frac{Q_{-(1+2n)}(K_0mx)\, m^n}{1+m}\, dm \qquad \text{..... (B26)}$$

Evaluation of (B26) is accomplished by expanding $Q_{-(1+2n)}(K_0.mx)$ into the finite series (B25) for each n, multiplying each term by $m^n/(1+m)$ and integrating term by term from o to ∞. This involves integrals of the type

$$\int_0^{\infty} \frac{J_{\nu}(mx)\, m^{\mu}}{1+m}\, dm \ , \qquad \int_0^{\infty} J_{\nu}(mx)\, m^{\mu}\, dm$$

..... (B27)

which have the following values for certain ν and μ :

$$\int_0^\infty \frac{J_0(mx)}{1+m}\,dm = \frac{\pi}{2}\left[H_0(x) - Y_0(x)\right] \qquad \ldots\ldots\ldots \text{(B28a)}$$

$$\int_0^\infty \frac{J_1(mx)}{1+m}\,dm = \frac{1}{x} - \frac{\pi}{2}\left[H_1(x) - Y_1(x) - 2/\pi\right] \qquad \ldots\ldots\ldots \text{(B28b)}$$

$$\int_0^\infty J_\nu(mx)\,m^\mu\,dm = \frac{2^\mu\,\Gamma\left(\frac{1}{2}+\frac{1}{2}\mu+\frac{1}{2}\nu\right)}{x^{\mu+1}\,\Gamma\left(\frac{1}{2}-\frac{1}{2}\mu+\frac{1}{2}\nu\right)}\,,\quad |\mu| < |\nu+1| \qquad \ldots\ldots\ldots \text{(B28c)}$$

$$\int_0^\infty J_\nu(mx)\,dm = \frac{1}{x} \qquad \ldots\ldots\ldots \text{(B28d)}$$

Where $H_1(x)$ is the Struve Function of first order, $Y_1(x)$ is the Bessel Function of the second kind and first order and $\Gamma(x)$ is the Gamma Function.

The integrals (B.27) were computed for integer values of ν and μ by a recursive procedure I (n,m,a,x) written in KDF 9 Algol and given in figure B6. They were evaluated using reduction formulae of the type :

$$\int_0^\infty \frac{J_\nu(mx)\,m^\mu}{1+m}\,dm = \int_0^\infty J_\nu(mx)\,m^{\mu-1}\,dm - \int_0^\infty \frac{J_\nu(mx)\,m^{\mu-1}}{1+m}\,dm \qquad \ldots\ldots\ldots \text{(B29)}$$

in conjunction with the well-known Bessel Function recurrence relation :

$$J_\nu(x) = \frac{2(\nu-1)}{x}\,J_{\nu-1}(x) - J_{\nu-2}(x) \qquad \ldots\ldots\ldots \text{(B30)}$$

In procedure I (n,m,a,x) the second integral in equation (B29) was tested to see if it corresponded to one of the standard forms (B28) and if so, it was evaluated. If not, it was again reduced as in equation (B29) and the process repeated.

FIG. B6

```
real procedure I(n,m,a,x);   value n,m,a,x;
real x;  integer n,m,a;
begin comment Recursive Algol procedure to calculate
      infinite integrals involving Bessel functions of
      the first kind.  When a = 2 the Weber-Schafheitlin
      integral is referred to and when a = 1 an integral
      of this type with a 1+K denominator in the integrand
      is referred to.  In all cases n is the order of the
      Bessel Function Jn and m is the power of K in the
      numerator, x is the argument of the integral.  This
      procedure must be used in conjunction with procedure
      G(x), the gamma function procedure, and the Bessel
      Function procedures Yo(x), Y1(x), Ho(x) and H1(x);
      real d, e, f, g, h, i;
      if m = 0 and n = 0 and a = 1 then
      begin I:= 1.570796x(Ho(x)-Yo(x));   goto L; end;
      if m = 0 and n = 1 and a = 1 then
      begin I:= 1/x-1.570796x(H1(x)-Y1(x)-0.636620);
            goto L;
      end;
      if m = 0 and a = 2 then begin I:= 1/x; goto L; end;
      if a = 2 then
      begin if m = -1 and n = 1 then
            begin I:= 1.000000; goto L;  end;
            if abs(m) < abs(n+1) then
            begin d:= 0.50 + n/2;  e := m/2;
                  f:= d + e;  g := d - e;
                  h:= G(f);  i:= G(g);
                  I:= 2 ↑m x h/(x↑(m+1)xi); goto L;
            end
            else
            I:= 2x(n+1)x(I(n+1, m-1, 2, x))/x+I(n+2, m, 2, x);
      end;
      if m = 0 and a = 1 then
      begin I:= 2x(n-1)x(I(n-1,-1,2,x) -I(n-1,0,1,x)) / x
                  -I(n-2, 0, 1, x); goto L;
      end;
      if a = 1 then
      begin if m > 0 then I:= I(n, m-1, 2, x) -I(n, m-1, 1, x)
            else I:= I(n, m, 2, x) - I(n, m+1, 1, x);
      end;
L: end I;
```

NOTE :

$$I(m, m, 1, x) \equiv \int_0^\infty \frac{J_m(kx)\, k^m}{1+k}\, dk ,$$

$$I(m, m, 2, x) \equiv \int_0^\infty J_m(kx)\, k^m\, dk .$$

PROCEDURE I(n,m,a,x)

Care was necessary when using procedure I (n,m,a,x) to avoid numerical instability. This arose when large μ values occurred in conjunction with small x values in equation (B28 c) : this generally was the case when many terms were required in the exponential series in (B26) for convergence. It is known that the exponential series converges slowly, but for Ko.x>25 it was found that between four and eight terms gave adequate accuracy.

Expression (B26) was used to obtain J (Ko.x, Ko.z) values in the range $25 \leq$ Ko.x ≤ 100, $0 \leq$ Ko.z ≤ 5, as shown in figure B7.

As direct use of equations (B8) and (B26) gave rise to prohibitively long program run times when C_{P2} was calculated, a two-dimensional polynomial was fitted to the J (Ko.x, Ko.z) surface forming a machine table of coefficients.

Values of J (Ko.x, Ko.z) outside the range covered by the machine table were obtained in program L3 by application of equations (B8) and (B26), but their use was kept to a minimum.

The integrals in equation (B6) were evaluated in program L3 for the region Ko.x ≥ 0, Ko.z ≥ 0 (i.e. over the plane y = o excepting the free surface z = o) using Simpson's rule, there being no singular integrands in this region. The convention J (-Ko.x, Ko.z) = -J (Ko.x, Ko.z) was adopted (cf. ref. 12.p.358).

An abridged table of J (Ko.x, Ko.z) values, formed from the polynomial surface, is given in table B2 and values of C_{P2} calculated by program L3 at a Froude Number of 0.300 are shown in figure B8.

FIG. B7.

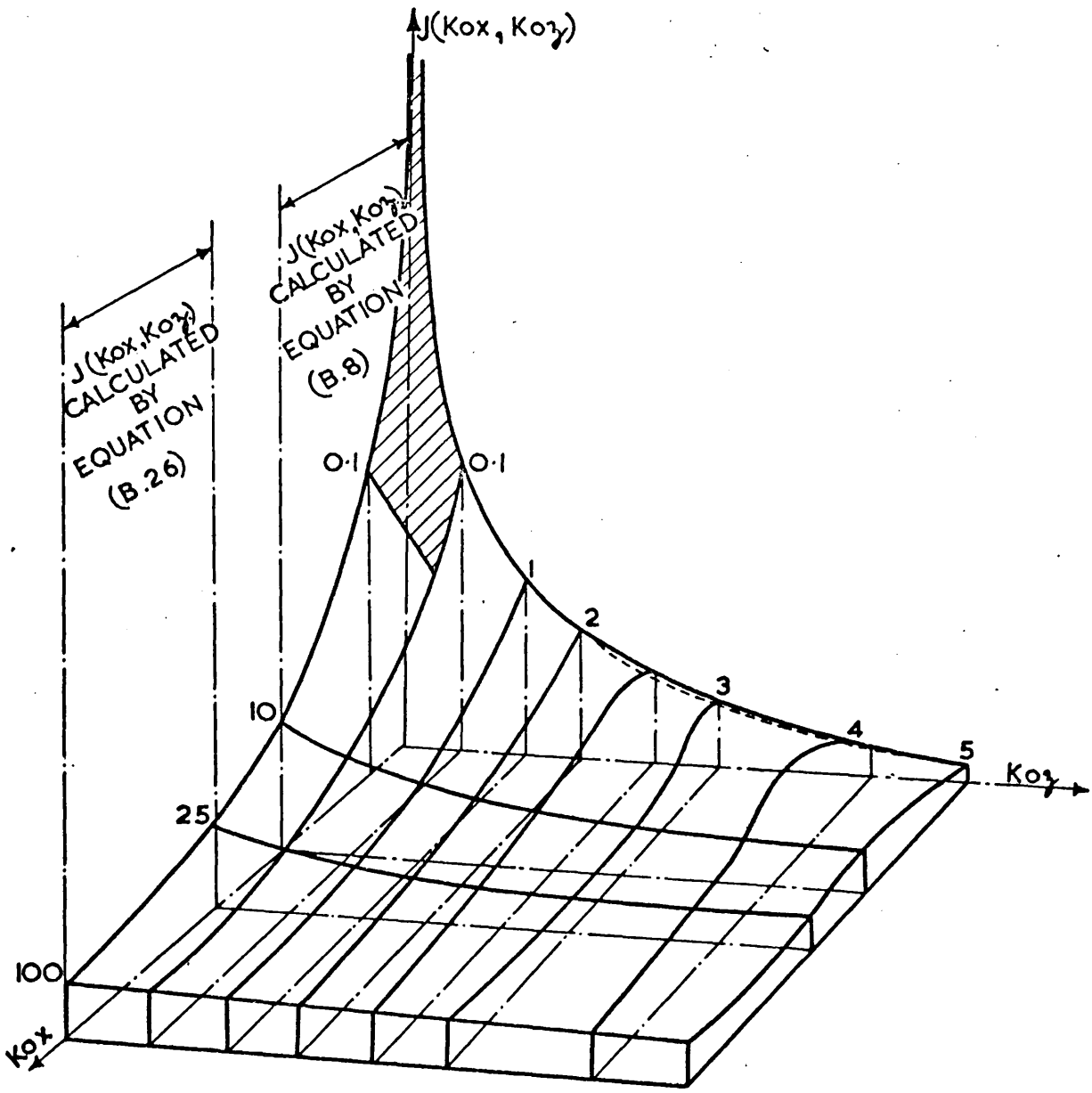

UNSHADED SURFACE STORED AS 2-D POLYNOMIAL IN PROGRAM L3.
SHADED SURFACE CALCULATED FROM EQUATION (B8) IN PROGRAM L3.

DIAGRAM NOT TO SCALE.

REPRESENTATION OF J (Kox, Koz.) SURFACE.

Ko.x \ Ko.z	0	0.1	0.2	0.3	0.4	0.6	0.8	1.0
0	+ ∞	4.660	3.449	2.745	2.254	1.597	1.174	0.881
0.5	1.861	1.788	1.689	1.575	1.456	1.221	1.011	0.832
1.0	1.181	1.140	1.106	1.062	1.012	0.909	0.805	0.707
1.5	0.877	0.848	0.833	0.807	0.774	0.716	0.653	0.593
2.0	0.690	0.666	0.660	0.645	0.624	0.587	0.546	0.506
2.5	0.571	0.548	0.546	0.538	0.524	0.497	0.468	0.440
3.0	0.488	0.466	0.466	0.462	0.452	0.431	0.409	0.387
3.5	0.425	0.405	0.406	0.404	0.397	0.379	0.363	0.345
4.0	0.376	0.357	0.358	0.357	0.351	0.338	0.325	0.311
4.5	0.336	0.318	0.319	0.318	0.313	0.304	0.295	0.282
5.0	0.303	0.286	0.286	0.285	0.281	0.276	0.269	0.258
5.5	0.277	0.260	0.259	0.258	0.256	0.253	0.247	0.237
6.0	0.255	0.240	0.237	0.236	0.235	0.233	0.229	0.220
6.5	0.237	0.222	0.219	0.219	0.218	0.217	0.213	0.205
7.0	0.222	0.207	0.205	0.204	0.204	0.202	0.199	0.192
7.5	0.207	0.193	0.192	0.192	0.191	0.189	0.187	0.181
8.0	0.193	0.180	0.180	0.180	0.179	0.177	0.175	0.172
8.5	0.181	0.168	0.169	0.169	0.168	0.167	0.165	0.163
9.0	0.172	0.159	0.159	0.159	0.158	0.158	0.156	0.156
9.5	0.165	0.152	0.150	0.150	0.150	0.150	0.148	0.149
10.0	0.154	0.143	0.144	0.145	0.143	0.142	0.142	0.143

COUPLED VALUES OF $J(K_{o.x}, K_{o.z})$

Range : $0 \leq K_{o.x} \leq 10.0$, $0 \leq K_{o.z} \leq 1.0$

Table B2

Ko.x \ Ko.z	1.0	1.5	2.0	2.5	3.0	3.5	4.0	4.5	5.0
0	0.881	0.453	0.243	0.134	0.075	0.042	0.025	0.014	0.008
0.5	0.832	0.512	0.319	0.203	0.133	0.089	0.061	0.043	0.031
1.0	0.707	0.496	0.344	0.240	0.170	0.122	0.089	0.067	0.052
1.5	0.593	0.454	0.341	0.254	0.191	0.144	0.111	0.086	0.068
2.0	0.506	0.409	0.325	0.255	0.200	0.156	0.125	0.101	0.082
2.5	0.440	0.368	0.304	0.249	0.202	0.164	0.134	0.110	0.092
3.0	0.387	0.334	0.283	0.238	0.199	0.167	0.139	0.117	0.099
3.5	0.345	0.304	0.264	0.227	0.194	0.166	0.141	0.121	0.104
4.0	0.311	0.278	0.246	0.215	0.188	0.163	0.141	0.123	0.107
4.5	0.282	0.256	0.229	0.204	0.180	0.159	0.140	0.123	0.108
5.0	0.258	0.237	0.215	0.193	0.173	0.154	0.138	0.122	0.109
5.5	0.237	0.220	0.202	0.183	0.166	0.150	0.135	0.121	0.109
6.0	0.220	0.206	0.190	0.174	0.159	0.145	0.131	0.119	0.108
6.5	0.205	0.193	0.180	0.165	0.152	0.140	0.128	0.117	0.106
7.0	0.192	0.182	0.170	0.158	0.146	0.135	0.124	0.114	0.105
7.5	0.181	0.172	0.162	0.151	0.140	0.130	0.120	0.111	0.103
8.0	0.172	0.163	0.154	0.144	0.134	0.126	0.117	0.109	0.101
8.5	0.163	0.155	0.146	0.137	0.129	0.121	0.113	0.106	0.099
9.0	0.156	0.148	0.140	0.131	0.124	0.117	0.110	0.103	0.097
9.5	0.149	0.142	0.133	0.126	0.120	0.113	0.107	0.100	0.095
10.0	0.143	0.136	0.128	0.122	0.116	0.110	0.104	0.098	0.092

Range : $0 \leq Ko.x \leq 10.0$, $1.0 \leq Ko.z \leq 5.0$

Table B2 Cont.

Ko.x \ Ko.z	0	0.5	1.0	1.5	2.0	2.5	3.0	3.5	4.0	4.5	5.0
10	0.154	0.143	0.143	0.136	0.128	0.122	0.116	0.110	0.104	0.098	0.092
15	0.105	0.102	0.101	0.097	0.093	0.091	0.089	0.086	0.081	0.078	0.076
20	0.078	0.078	0.078	0.076	0.075	0.075	0.074	0.072	0.068	0.065	0.065
25	0.062	0.063	0.064	0.064	0.064	0.065	0.064	0.062	0.059	0.057	0.057
30	0.052	0.053	0.054	0.055	0.056	0.057	0.056	0.054	0.053	0.052	0.051
35	0.045	0.046	0.046	0.048	0.049	0.049	0.049	0.048	0.047	0.047	0.046
40	0.040	0.040	0.040	0.041	0.042	0.042	0.042	0.042	0.042	0.042	0.042
45	0.035	0.035	0.035	0.036	0.036	0.037	0.037	0.037	0.038	0.038	0.038
50	0.031	0.031	0.031	0.032	0.032	0.032	0.033	0.033	0.034	0.034	0.034
55	0.028	0.028	0.028	0.029	0.029	0.029	0.029	0.030	0.031	0.031	0.031
60	0.026	0.026	0.026	0.027	0.027	0.027	0.027	0.028	0.028	0.028	0.028
65	0.024	0.025	0.025	0.025	0.025	0.025	0.025	0.026	0.026	0.026	0.026
70	0.023	0.023	0.023	0.023	0.024	0.024	0.024	0.024	0.024	0.024	0.024
75	0.021	0.021	0.021	0.022	0.022	0.022	0.022	0.022	0.022	0.022	0.022
80	0.019	0.020	0.020	0.020	0.020	0.020	0.020	0.020	0.021	0.021	0.021
85	0.018	0.019	0.019	0.018	0.018	0.018	0.019	0.019	0.019	0.019	0.020
90	0.017	0.018	0.018	0.018	0.018	0.018	0.018	0.018	0.018	0.018	0.018
95	0.017	0.017	0.017	0.018	0.018	0.018	0.017	0.017	0.017	0.017	0.017
100	0.016	0.016	0.016	0.016	0.016	0.016	0.016	0.016	0.016	0.016	0.016

Range : $10 \leq Ko.x \leq 100$, $0 \leq Ko.z \leq 5.0$

Table B2 Cont.

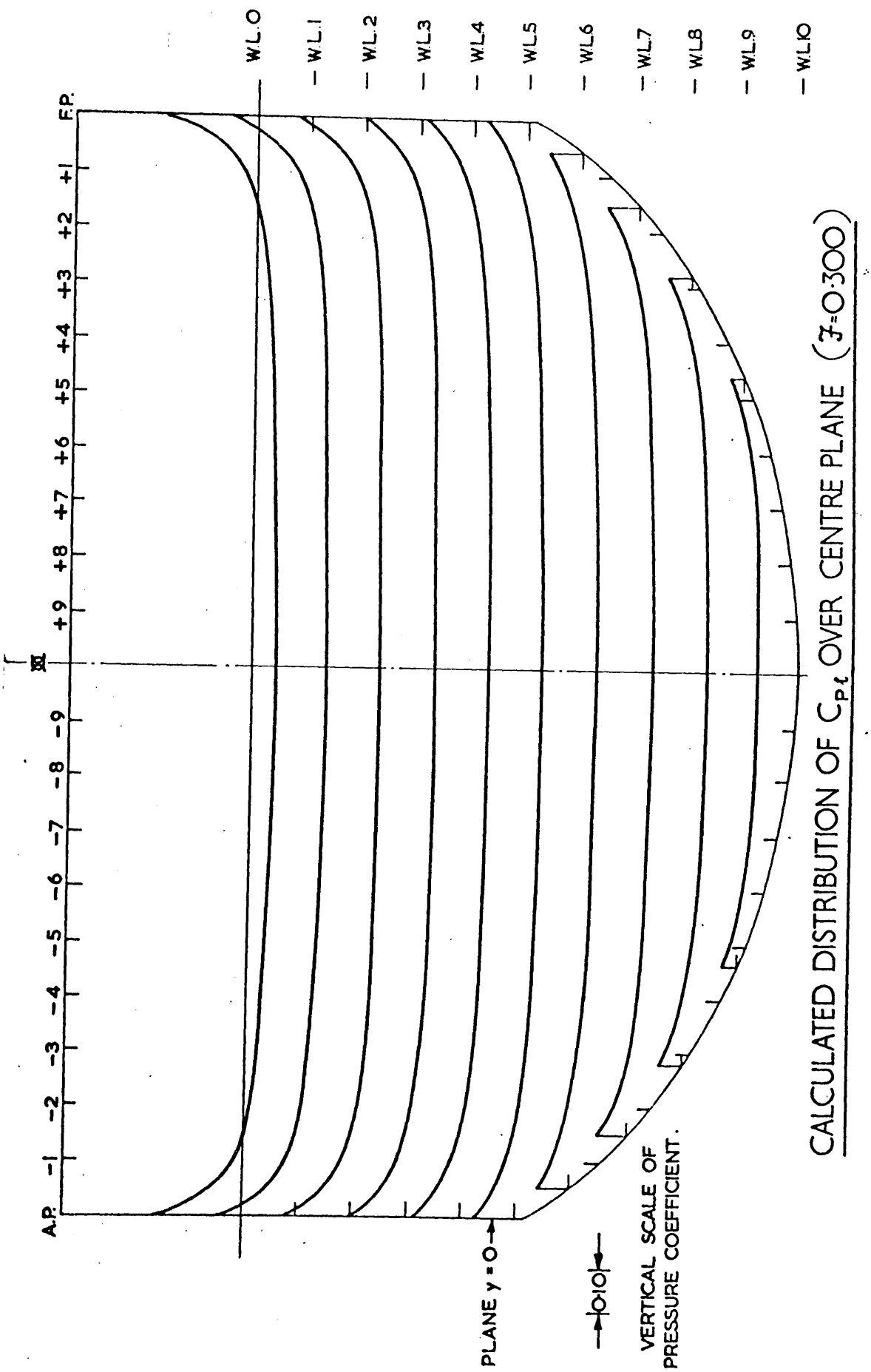

CALCULATED DISTRIBUTION OF C_{pl} OVER CENTRE PLANE ($\mathcal{F}$=0·300)

FIG. B8.

B.4. CALCULATION OF $C_{PW}(x,o,z)$. COMPUTER PROGRAM W2.

Letting z = -z for convenience and changing the origin to the bow,

$$C_{Pw}(x,0,z) = \frac{4K_o^2}{\pi}\int_0^{2l(\zeta)} \frac{\partial y}{\partial l}\, dl \int_0^{d(x)} df \int_0^{\frac{\pi}{2}} e^{-K_o(f+z)\sec^2\theta} \cos[K_o(x-l)\sec\theta]\sec^3\theta\, d\theta$$

which becomes, after integration with respect to f,

$$C_{Pw}(x,0,z) = \frac{4K_o}{\pi}\left\{\int_0^{2l(\zeta)} \frac{\partial y}{\partial l}\left[\int_0^{\frac{\pi}{2}} e^{-K_o z\sec^2\theta}\cos[K_o(x-l)\sec\theta]\sec\theta\, d\theta - \int_0^{\frac{\pi}{2}} e^{-K_o(d+z)\sec^2\theta}\cos[K_o(x-l)\sec\theta]\sec\theta\, d\theta\right.\right. \quad \ldots\ldots\ldots \text{(B31)}$$

Equation (B31) may be re-written in terms of known functions tabulated in reference (121). Using the notation of ref. (121) and adopting the convention that $M_1 \cos\phi_1 = o$ for x-h<o, (12,p.357) we have

$$C_{Pw}(x,0,z) = \frac{4K_o}{\pi}\left\{\int_0^{2l(\zeta)} \frac{\partial y}{\partial l} M_1(\sqrt{K_o z}, K_o(x-l))\cos\phi_1(\sqrt{K_o z}, K_o(x-l))\, dl\right.$$

$$\left. - \int_0^{2l(\zeta)} \frac{\partial y}{\partial l} M_1(\sqrt{K_o(d+z)}, K_o(x-l))\cos\phi_1(\sqrt{K_o(d+z)}, K_o(x-l))\, dl\right\} \quad \ldots\ldots\ldots \text{(B32)}$$

Values of the modulus $M_1(\alpha,\beta)$ and the phase $\phi_1(\alpha,\beta)$ were stored in program W2 in the form of a machine table accurate to ± 0.0005 and valid for the range $0.2 \leq \alpha \leq 2.4$, $0 \leq \beta \leq \infty$. The limitation on α gave rise to the following restrictions on the calculations for Inuid S201 :

$$0.18 \leq F \leq 1.80$$

$$0.04 \leq K_o.z \leq 4.17 \text{ and } 0.04 \leq K_o(d+z) \leq 4.17$$

$$0 \leq K_o(x-h) \leq +\infty$$

Values of M_1 and ϕ_1 were calculated at each Froude Number over the plane y=o (except for points on the free surface z=o) and the integrals in equation (B32) were evaluated by means of Simpson's Rule for $(x-h) < o$, $z > o$, there being no singular integrands in this range.

Values of C_{PW} obtained at a Froude Number of 0.300 are shown in figure B9.

FIG. B9.

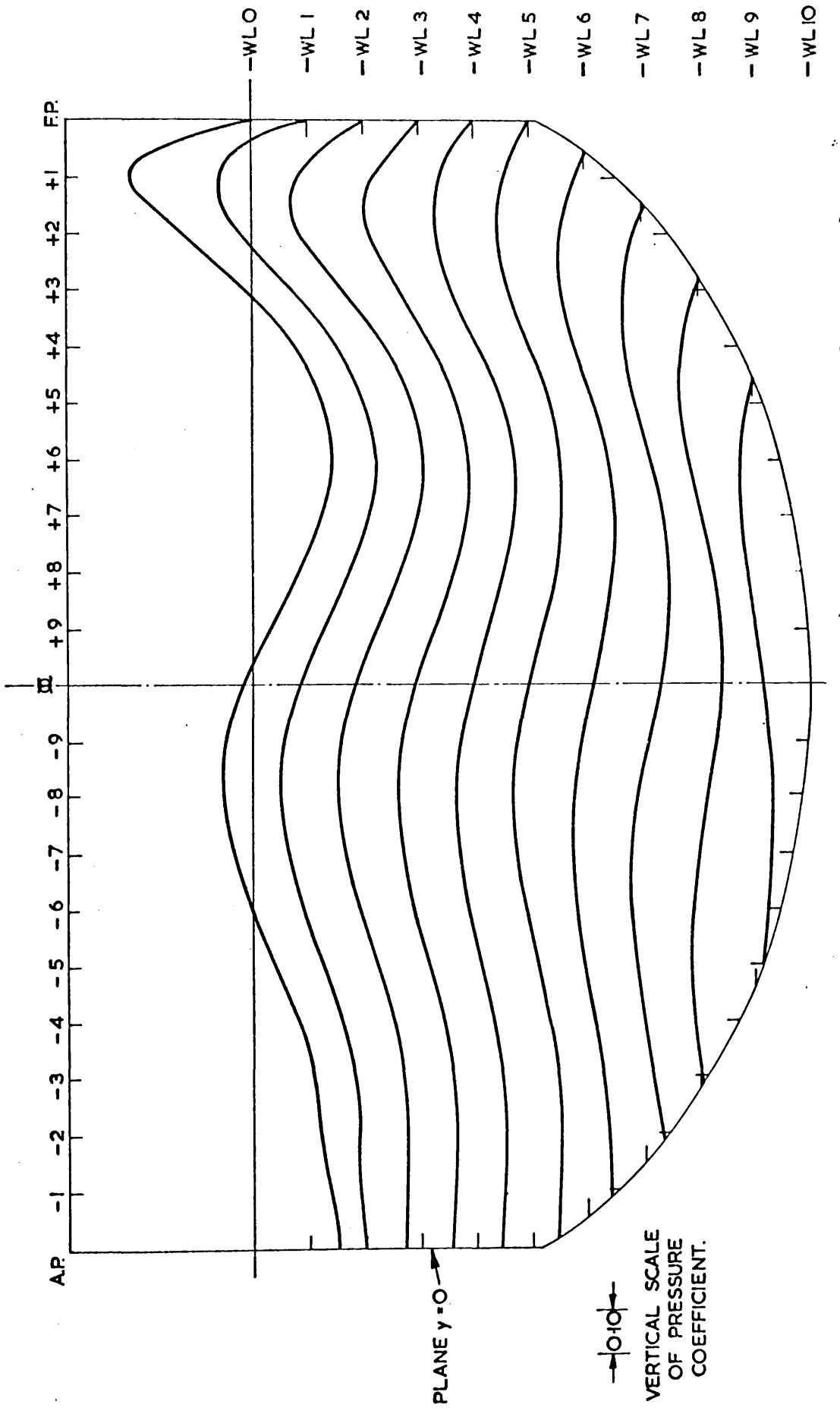

CALCULATED DISTRIBUTION OF C_{pw} OVER CENTREPLANE ($\bar{z}$=0·300)

B.5. CALCULATION OF $C_{PW}^{\circ}(x,o,o)$ and $C_{Pz}^{\circ}(x,o,o)$. COMPUTER PROGRAM WS.

Due to limitations in computer storage space, it was not possible to calculate parts of the free surface pressures in programs I3 and W2. These calculations involved singular integrands which were dealt with separately in program WS.

B.5.1. Calculation of $C_{PW}^{\circ}(x,o,o)$ values.

The first term in equation (B31) becomes, when z=o,

$$C_{Pw}^{\circ}(x,0,0) = \frac{4K_0}{\pi}\int_0^{2l(\frac{y}{l})} \frac{\partial \eta}{\partial l}\left\{\int_0^{\frac{\pi}{2}} \cos[K_0(x-l)\sec\theta]\sec\theta\, d\theta\right\} dl \qquad \ldots\ldots\ldots (B33)$$

This may be written, making use of the integral representation of the Bessel Function of the Second Kind,

$$C_{Pw}^{\circ}(x,0,0) = -\frac{4K_0}{\pi}\int_0^{2l(\frac{y}{l})} \frac{\partial \eta}{\partial l}\cdot\frac{\pi}{2}\, Y_0(K_0\xi)\, dl\,,\ \xi = x-l;\ Y_0(K_0\xi)=0\Big|_{\xi<0} \qquad \ldots\ldots\ldots (B34)$$

The function $Y_0(K_0\xi)$ is singular at $\xi = o$, tending to infinity like $\ln(K_0.\xi)$. It was integrated over the range $o \leq \xi \leq \epsilon$ by the approximate formula:

$$\int_0^{\epsilon} f(u)\ln(u)\,du = -\frac{\epsilon}{6}\left[(17/6-\ln\epsilon)f_0 + (20/6-4\ln\epsilon)f_1 - (\ln\epsilon+1/6)f_2\right] \qquad \ldots\ldots\ldots (B35)$$

where

$$f_{0,1,2} = \left[\frac{\partial \eta}{\partial l}[\xi,o].\frac{Y_0(K_0\xi)}{\ln(K_0\xi)}\right]_{\xi=o,\frac{\epsilon}{2},\epsilon} \qquad \ldots\ldots\ldots (B36)$$

(See refs. 122 and 123.)

Over the remainder of the range of ξ, Simpson's Rule was used with ordinate spacings shown in table B3. The integrand was well-behaved at points remote from the singularity as shown in figure B 10.

Range	No. of Intervals	Integration Rule
0 - 0.025 ξ	2	Eqtn. (B35)
0.025ξ - 0.050ξ	2	Simpson
0.050ξ - 0.10ξ	2	Simpson
0.10ξ - ξ	20	Simpson

Table B3

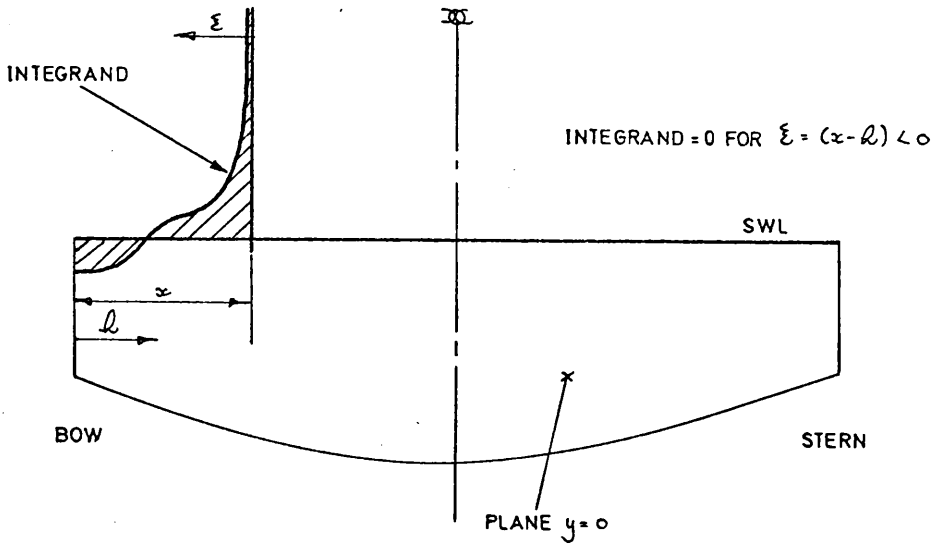

FIG. B10

B.5.2. Calculation of $C_{Pl}^{\circ}(x,0,0)$ Values

Equations (B17) and (B6) give the following expression for $C_{Pl}^{\circ}(x,0,0)$ represented by the first term of equation (B6) when $z = 0$

$$C_{Pl}^{\circ}(x,0,0) = \frac{-4K_0}{\pi^2}\int_0^{2l(x)} \frac{\partial y}{\partial l}\cdot\frac{\pi^2}{4}\left[H_0(K_0\xi) - Y_0(K_0\xi)\right] dl \qquad \ldots\ldots\ldots (B37)$$

where $\xi = x-h$ and we adopt the convention that

$$\left[H_0(-\xi) - Y_0(-\xi)\right] = -\left[H_0(\xi) - Y_0(\xi)\right]$$

The function $\left[H_0(K_0\xi) - Y_0(K_0\xi)\right]$ tends to infinity like $-\ln(K_0.\xi)$ as $K_0.\xi$ tends to zero. The integral in equation (B37) was therefore evaluated using equation (B35) with

$$f_{0,1,2} = \left[\frac{\partial \eta}{\partial \lambda} [\xi, 0] \cdot \frac{[H_0(k_0\xi) - Y_0(k_0\xi)]}{\ell_w(k_0\xi)} \right]_{\xi = 0, \frac{\epsilon}{2}, \epsilon}$$

Numerical integration was performed over the same ranges, using the same integration rules as shown in table B3. The integrand had the same general shape as shown in figure B2.

B.6. CALCULATION OF FORCES AND MOMENTS. SUMMARY PROGRAM WF.

Pressure coefficients calculated for a range of speeds by programs W0, W3, W2 and WS were read into a summary program WF. This evaluated the force and moment coefficients C_W, C_Z, C_M from equations (2.3.5.). The calculated pressure distribution over the plane y=o was obtained both in coefficient form as $C_{PTOT}(x,o,z)$ from equation (2.3.4.) and as pressure heads in inches of water obtained from equation (2.1.38 b.).

The following results were also calculated :

i) The ratio C_Z/C_W

ii) Percentage velocity increment, $(\delta V/V).100$ from equation (2.4.12).

iii) Percentage form factor, $K_{ff} = r_{ff} \times 100$ where r_{ff} is defined by equation (2.7.2). Use was made of equations (2.7.1), (2.4.4b) and (2.4.5b) for this.

iv) Mean sinkage coefficient, C_s, (which is equivalent to the mean sinkage as a percentage of the length L) from equations (2.3.5b) and (2.3.8.).

v) Trim coefficient, C_t, obtained from equation (2.3.7).

vi) The value of d^1 from equation (2.3.7) expressed as a percentage of the length L.

vii) Vertical distributions of both horizontal and vertical force components.

A typical output from program WF for a Froude Number of 0.300 is shown in Figure B11 and a flow diagram for all programs is shown in figure B12.

FIG. B11

WAVE FORCES

FROUDE NUMBER 0.3000; SPEED LENGTH RATIO 1.0080;

NON-DIMENSIONAL PRESSURES FREE + LOCAL + ZERO TERMS

WL ST	0	1	2	3	4	5	6	7	8	9
FP 0.0	0.211	-0.479	-0.558	-0.585	-0.543	-0.358	-0.253	-0.225	-0.228	-0.160
0.1	0.305	0.256	0.199	0.161	0.124	0.082	0.059	0.046	0.034	0.012
0.2	0.152	0.174	0.155	0.131	0.109	0.085	0.070	0.060	0.047	0.028
0.3	-0.006	0.032	0.045	0.049	0.049	0.046	0.044	0.044	0.040	0.031
0.4	-0.125	-0.084	-0.061	-0.041	-0.023	-0.010	0.002	0.012	0.024	0.027
0.5	-0.197	-0.157	-0.132	-0.107	-0.082	-0.061	-0.041	-0.022	-0.001	0.018
0.6	-0.222	-0.182	-0.160	-0.136	-0.113	-0.091	-0.072	-0.053	-0.023	0.008
0.7	-0.205	-0.170	-0.151	-0.132	-0.115	-0.097	-0.084	-0.070	-0.046	-0.004
0.8	-0.156	-0.126	-0.112	-0.099	-0.090	-0.079	-0.078	-0.078	-0.062	-0.018
0.9	-0.096	-0.069	-0.062	-0.057	-0.052	-0.051	-0.061	-0.073	-0.070	-0.029
1.0	-0.037	-0.014	-0.017	-0.016	-0.017	-0.021	-0.039	-0.060	-0.071	-0.041
1.1	0.004	0.023	0.018	0.014	0.011	0.003	-0.013	-0.037	-0.062	-0.046
1.2	0.017	0.033	0.027	0.024	0.019	0.013	0.004	-0.015	-0.049	-0.051
1.3	-0.003	0.017	0.014	0.011	0.009	0.007	0.011	0.002	-0.032	-0.051
1.4	-0.044	-0.018	-0.015	-0.013	-0.009	-0.006	0.006	0.010	-0.014	-0.048
1.5	-0.094	-0.063	-0.051	-0.043	-0.033	-0.025	-0.004	0.013	0.001	-0.043
1.6	-0.138	-0.098	-0.083	-0.068	-0.055	-0.042	-0.018	0.008	0.013	-0.034
1.7	-0.164	-0.118	-0.098	-0.079	-0.064	-0.050	-0.028	0.003	0.022	-0.025
1.8	-0.166	-0.104	-0.086	-0.067	-0.053	-0.044	-0.032	-0.005	0.026	-0.018
1.9	-0.148	-0.059	-0.040	-0.023	-0.020	-0.026	-0.036	-0.020	0.016	-0.020
2.0	-0.018	-0.599	-0.653	-0.660	-0.600	-0.399	-0.305	-0.276	-0.237	-0.196

PRESSURES IN INCHES OF WATER
STAGNATION PRESSURE 4.647 INCHES WATER

WL ST	0	1	2	3	4	5	6	7	8	9
FP 0.0	1.960	-4.440	-5.183	-5.433	-5.043	-3.325	-2.350	-2.090	-2.118	-1.672
0.1	2.833	2.375	1.848	1.495	1.152	0.762	0.548	0.446	0.316	0.111
0.2	1.412	1.616	1.440	1.217	1.012	0.789	0.650	0.557	0.437	0.260
0.3	-0.056	0.297	0.418	0.455	0.455	0.427	0.409	0.409	0.375	0.288
0.4	-1.161	-0.780	-0.587	-0.381	-0.214	-0.093	0.019	0.111	0.223	0.251
0.5	-1.830	-1.458	-1.226	-0.994	-0.762	-0.567	-0.391	-0.204	0.009	0.167
0.6	-2.062	-1.690	-1.486	-1.263	-1.050	-0.845	-0.669	-0.492	-0.214	0.074
0.7	-1.904	-1.579	-1.402	-1.226	-1.068	-0.901	-0.780	-0.650	-0.427	-0.037
0.8	-1.449	-1.170	-1.040	-0.920	-0.836	-0.734	-0.724	-0.724	-0.576	-0.167
0.9	-0.592	-0.641	-0.576	-0.529	-0.483	-0.474	-0.567	-0.678	-0.650	-0.269
1.0	-0.344	-0.130	-0.158	-0.149	-0.158	-0.195	-0.362	-0.557	-0.659	-0.381
1.1	0.037	0.214	0.167	0.130	0.102	0.028	-0.121	-0.344	-0.576	-0.427
1.2	0.158	0.307	0.251	0.223	0.176	0.121	0.037	-0.139	-0.455	-0.474
1.3	-0.028	0.158	0.130	0.102	0.084	0.065	0.102	0.019	-0.297	-0.474
1.4	-0.409	-0.167	-0.139	-0.121	-0.084	-0.056	0.056	0.093	-0.130	-0.446
1.5	-0.873	-0.576	-0.474	-0.399	-0.307	-0.232	-0.037	0.121	0.009	-0.399
1.6	-1.282	-0.910	-0.771	-0.632	-0.511	-0.393	-0.167	0.074	0.121	-0.316
1.7	-1.523	-1.096	-0.910	-0.734	-0.594	-0.464	-0.260	0.028	0.204	-0.232
1.8	-1.542	-0.985	-0.799	-0.622	-0.492	-0.409	-0.297	-0.046	0.241	-0.167
1.9	-1.375	-0.548	-0.372	-0.214	-0.186	-0.241	-0.334	-0.186	0.149	-0.186
2.0	-0.139	-5.564	-6.065	-6.130	-5.573	-3.706	-2.833	-2.563	-2.201	-1.820

FORCE DISTRIBUTIONS WITH DEPTH

WL	HORIZONTAL COMPONENT	VERTICAL COMPONENT
0	2.618e -2;	0.000 ;
1	1.819e -2;	-4.802e -3;
2	1.427e -2;	-6.689e -3;
3	1.093e -2;	-1.131e -2;
4	8.391e -3;	-1.260e -2;
5	5.989e -3;	-1.447e -2;
6	4.180e -3;	-4.976e -2;
7	2.319e -3;	-4.725e -2;
8	7.243e -4;	-3.505e -2;
9	1.756e -3;	-4.573e -2;
10	0.000 ;	0.000 ;

SUMMARY AT FROUDE NUMBER 0.3000;

WAVE RESISTANCE COEFFICIENT CW 6.623e -3;
TRIMMING MOMENT COEFFICIENT CM 2.396e -3;
VERTICAL FORCE COEFFICIENT CZ -2.077e -2;
RATIO OF CZ TO CW 3.044e 0;
PERCENT VELOCITY INCREMENT 1.087;
PERCENT FORM FACTOR K 2.012; RELATIVE TO HUGHES 1954 LINE
PERCENT MEAN SINKAGE -0.222;
PERCENT TRIM BY BOW 0.457;
WAVE RESISTANCE ACTS AT 2.679; PERCENT LBP BELOW LWL

TYPICAL OUTPUT FROM PROGRAM WF

FIG. B12

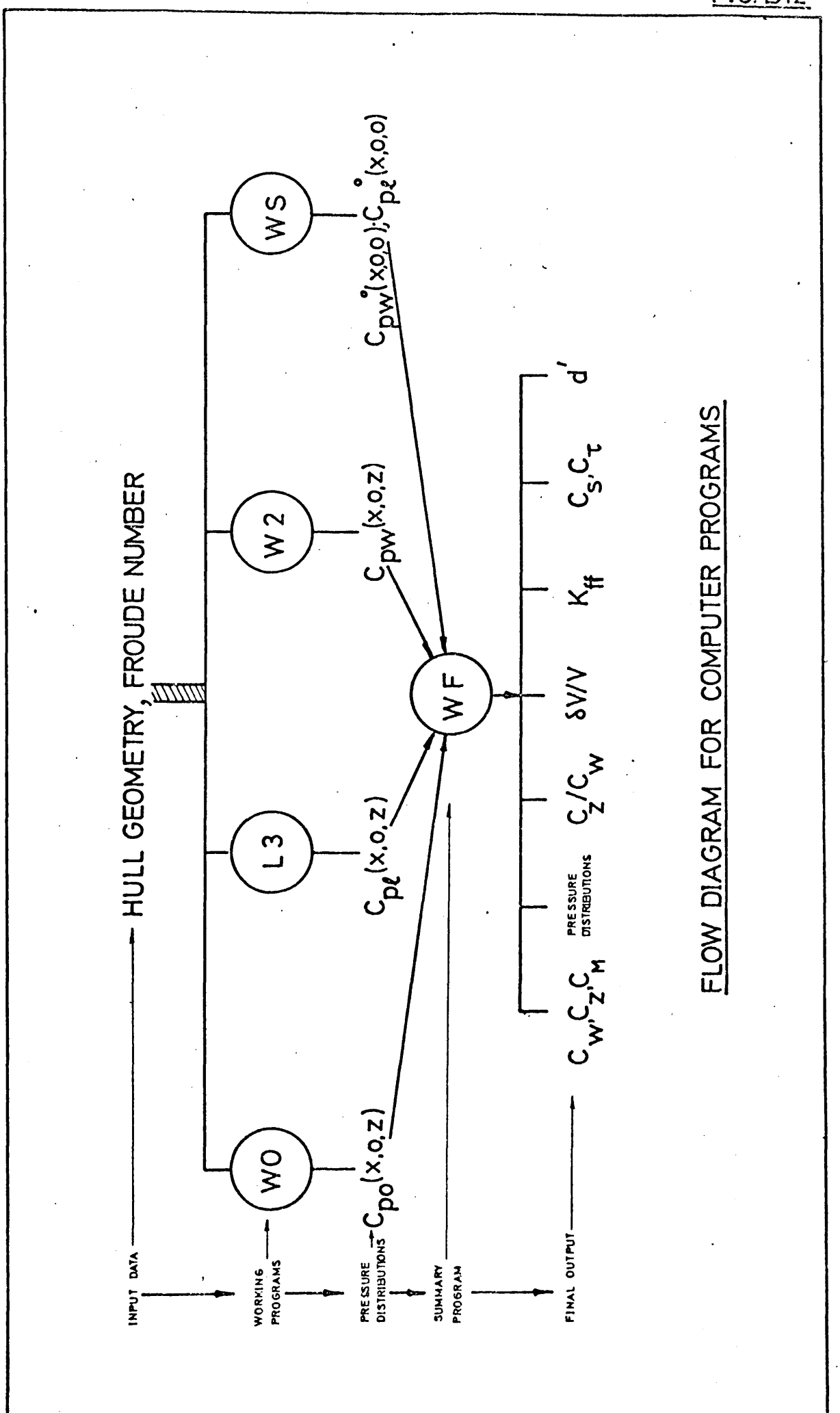

FLOW DIAGRAM FOR COMPUTER PROGRAMS

APPENDIX C

INVESTIGATION OF CROSS-COUPLING BETWEEN MEASURED VERTICAL FORCES AND TOTAL RESISTANCE

C.1. Elimination of Cross Coupling between measured Vertical Forces

Calibration of the proving rings at bow and stern with known weights showed that by loading the bow ring a small loading was applied to the stern ring and vice-versa. This cross-coupling is indicated in the calibration chart, figure C1.

The following notation is adopted :

δ_B : proving ring deflection corresponding to a vertical force Z_{BOW} acting at the bow before correction for the effect of total restrained resistance R_T'.

δ_S : proving ring deflection corresponding to a vertical force Z_{STERN} acting at the stern before correction for the effect of total restrained resistance, R_T'.

δ_{B_m} : measured bow proving ring deflection.

δ_{S_m} : measured stern proving ring deflection.

${}_S\delta_B$: bow proving ring deflection due to loading stern ring.

${}_B\delta_S$: stern proving ring deflection due to loading bow ring.

$\delta_{B_{ACT.}}$, $\delta_{S_{ACT.}}$: δ_B and δ_S corrected for the effect of R_T'.

The elimination of cross-coupling proceeded as follows:

$$\delta_{B_m} = \delta_B + {}_S\delta_B$$

$$\delta_{S_m} = \delta_S + {}_B\delta_S \qquad \ldots\ldots (C1)$$

But, due to the linearity of the calibration curves, figure C1.,

$$\left.\frac{{}_S\delta_B}{\delta_B}\right|_{Z_{BOW}=CONST.} = CONSTANT = K_1 \quad ; \quad \left.\frac{{}_B\delta_S}{\delta_S}\right|_{Z_{STERN}=CONST.} = CONSTANT = K_2 \quad ; \qquad \ldots\ldots (C2)$$

Substitution of equations (C2) into equations (C1) gives, after re-arranging,

$$\delta_B = \frac{\delta_{B_m}}{1+K_1} \quad ; \quad \delta_S = \frac{\delta_{S_m}}{1+K_2}$$

FIG. C1.

CALIBRATION CURVES FOR BOW AND STERN PROVING RINGS.

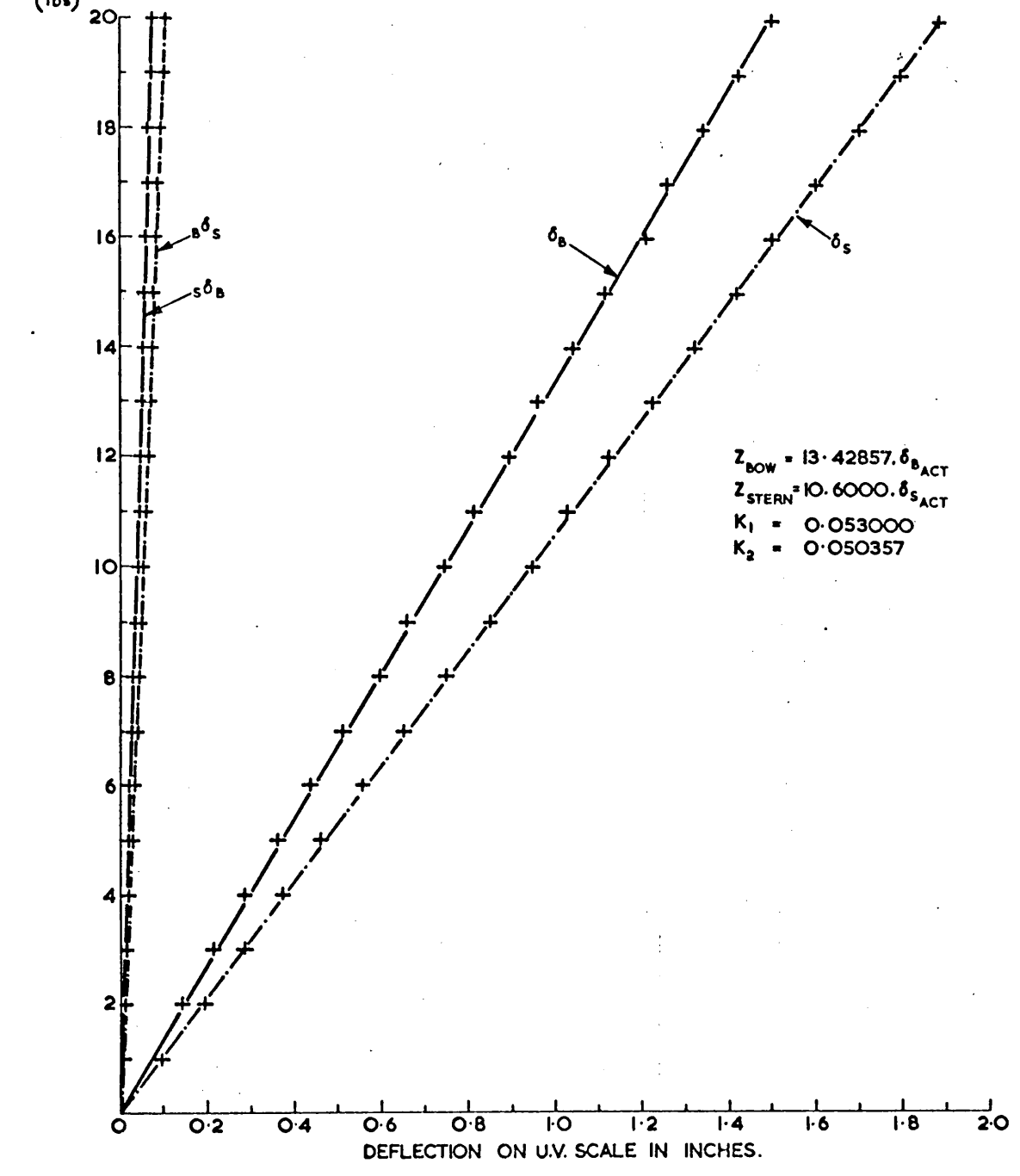

The deflections δ_B and δ_S are then further corrected for the effect of total resistance as detailed below. As an example, values of Z_{BOW} and Z_{STERN} before and after correction for vertical cross-coupling are given below

	BEFORE CORRECTION	AFTER CORRECTION
Z_{BOW}	7.36 lb.	11.29 lb.
Z_{STERN}	6.96 lb.	11.00 lb.

C.2. Elimination of total resistance/vertical force cross-coupling

The application of the total restrained resistance force, R_T', to the model at speed gave rise to small deflections of the proving rings. These deflections varied uniformly over part of the R_T' range until a maximum value was reached, denoting that all slackness in the system had been taken up. This has been demonstrated in figure 21 and is also shown in figure C3 below.

Calibration was effected by applying a horizontal force T to the model to represent R_T'. The towing wire was led round an auxiliary wheel on the towing space frame and attached to a rigid bar mounted to a **bulkhead** on the model. This bulkhead was forward of the towing frame so that any weights on the dynamometer scale pan applied a force to the model acting in the direction of R_T! The vertical position of T was arranged to coincide with that of the towing link as shown in figure C2.

It was then assumed that the vector $\underset{\sim}{R_T'}$ was equal to the vector $\underset{\sim}{T}$ or

$$\underset{\sim}{R_T'} = \underset{\sim}{T} \qquad \ldots\ldots\ldots (C4)$$

Calibration curves obtained with this arrangement are shown in figure C3. A mean curve through the experimental points was used for analysis purposes.

Values of $\delta_{B.ACT}$ and $\delta_{S.ACT}$ were then obtained from

FIG. C2

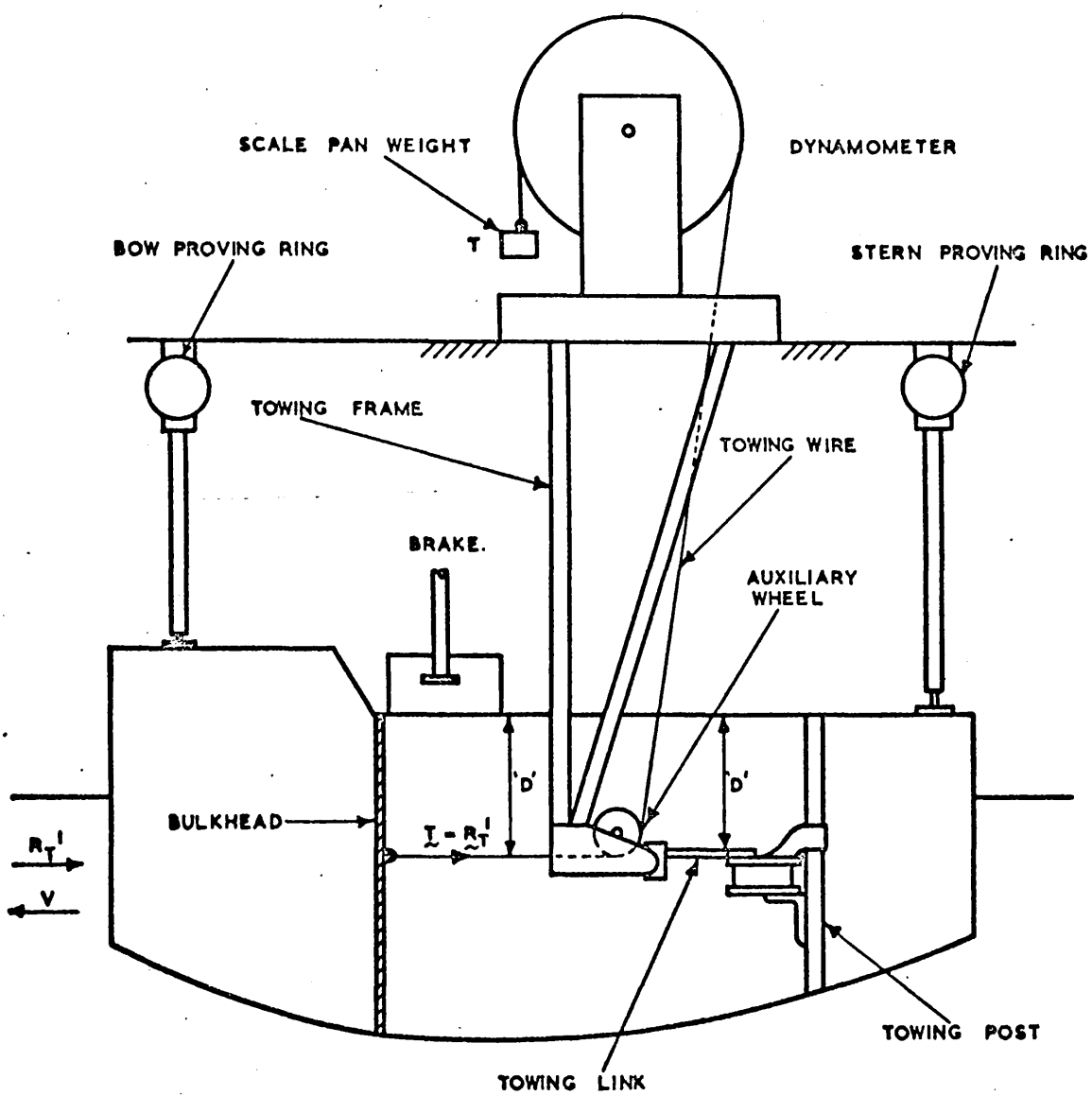

DRAWING NOT TO SCALE.

FOR DEFINITION OF 'D' SEE FIG. 22.

CALIBRATION APPARATUS FOR R_T' CROSS-COUPLING.

$$\delta_{B.Act} = \delta_B - \delta_{BR}$$

$$\delta_{S.Act} = \delta_S - \delta_{SR}$$

where δ_{BR} = deflection of bow ring by R_T'

δ_{SR} = deflection of stern ring by R_T'

Values of Z_{BOW} and Z_{STERN} were then calculated from the calibration factors given in figure C1.

A computer program was written to perform the above analysis on the vertical force results. Machine tables were compiled from the calibration curves in figure C2 and the restrained resistance/speed curve. Values of forces, moments and force and moment coefficients were thus obtained after correction for blockage, tide, temperature (density correction) and cross-coupling.

FIG. C3.

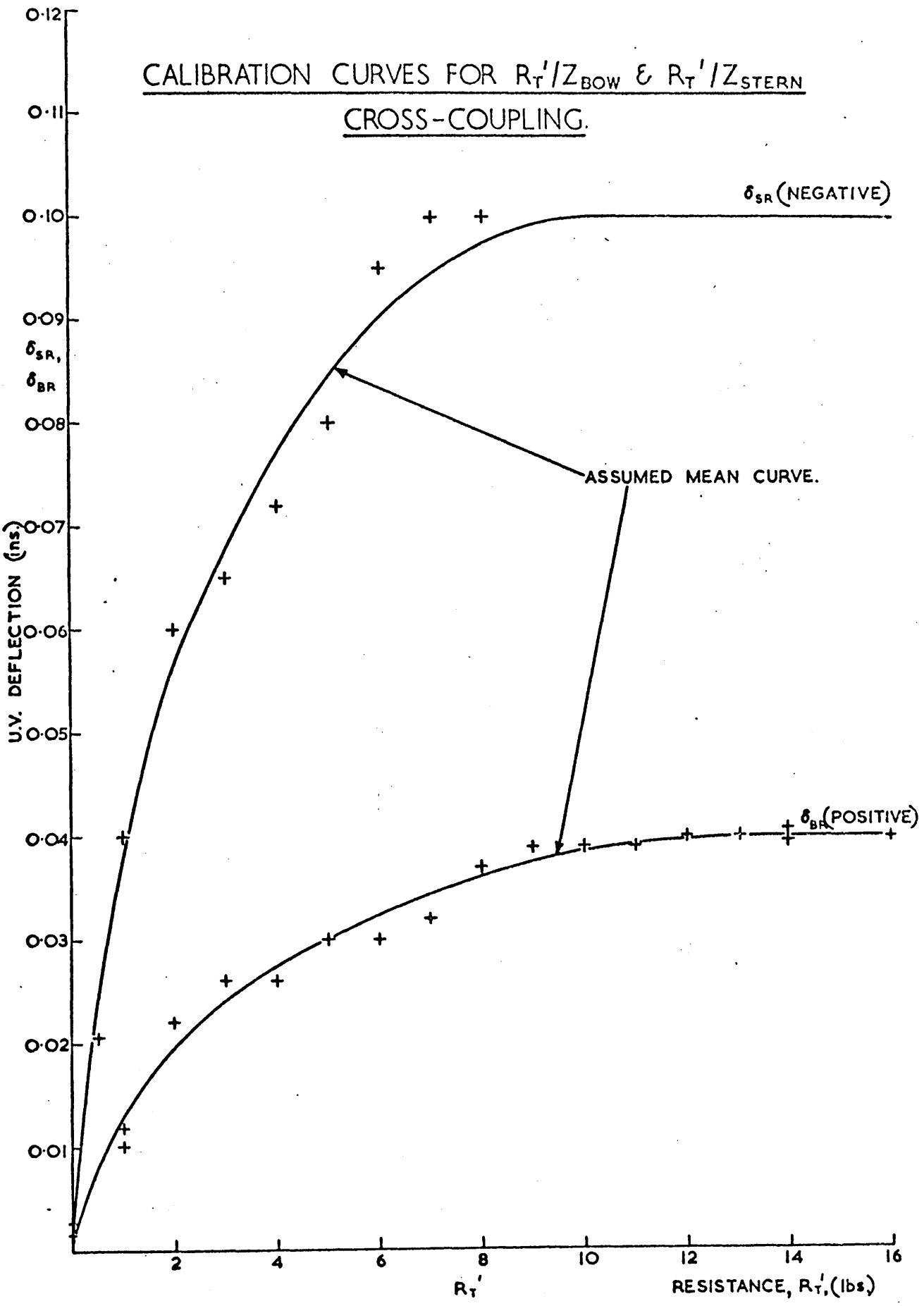
CALIBRATION CURVES FOR R_T'/Z_{BOW} & R_T'/Z_{STERN} CROSS-COUPLING.
δ_{SR} (NEGATIVE)
ASSUMED MEAN CURVE.
δ_{BR} (POSITIVE)
U.V. DEFLECTION (ins.)
δ_{SR}, δ_{BR}
0·12
0·11
0·10
0·09
0·08
0·07
0·06
0·05
0·04
0·03
0·02
0·01
2
4
6
8
10
12
14
16
R_T'
RESISTANCE, R_T', (lbs.)